Author:
Kim, Seung Chan

Title:
The roles of FUS in neurodegenerative disease

The roles of FUS in neurodegenerative disease

Seung Chan Kim

A dissertation submitted to the University of Bristol in accordance with the requirements for award of the degree of Doctor of Philosophy in the Faculty of Translational Health Sciences.

December 2019

Word Count: 28,876

Abstract

Fused in sarcoma (FUS) is a DNA/RNA-binding protein that modulates gene expression by associating with a wide range of transcription-related factors in the nucleus and/or cytoplasm of neurons. Abnormal expression of FUS or mutant forms of FUS were reported to be involved in the pathologies of amyotrophic lateral sclerosis (ALS) and frontotemporal lobar degeneration (FTLD). Since both ALS and FTLD include neurodegeneration, the synapse weakening process might be exhibited prior to the neuronal death. However, there are many missing gaps and mechanisms not well explained.

In this PhD study, the nature and consequence of abnormal FUS were investigated in terms of the potential pathology that would be involved in ALS, FTLD and other possible neurodegenerative diseases. By utilising main pathogenic factors of FUS (nuclear localisation signal (NLS) mutation and hypomethylation), both morphological and neurophysiological alterations by abnormal expression and propagation of FUS were investigated.

First, cytosolic accumulation of FUS was investigated using FUS-P525L mutant form, which has mutation on NLS region that is required for nuclear internalisation of FUS. FUS-P525L was shown to have quicker translocation though the dendrites than that of FUS-WT and this difference resulted in the reduction of spine density in the apical dendrites of FUS-P525L cells. FUS-P525L cells were shown to have increased synaptic conductance and intrinsic excitability and the excitability was returned to the control level when Calcium-permeable AMPA receptor (CP-AMPAR) blocker IEM-1460 was applied. And had decreased basal synaptic transmission and inhibited induction of both long-term potentiation (LTP) and long-term depression (LTD).

Second, FUS mutant with enhanced cation-π interaction was investigated by using FUS-16R mutant form, which has 16 additional arginine residues therefore increases the chance of hypomethylation. The spine density of FUS-16R cells were shown to be reduced in both basal and apical dendrites compared to FUS-WT cells. In addition, intrinsic excitability and basal synaptic transmissions were reduced in FUS-16R cells.

Together, the results suggest that abnormal expression of FUS mutant is widely involved in the morphological, electrophysiological synapse weakening and it is related to the neuronal activity and excitability.

Acknowledgements

Everyone knows PhD study is challenging and difficult. But the real value of PhD study is not just about studying, but also about interacting with other researchers to develop scientific point of view. I would not be able to make this far without magnificent people who gave me the advices, supports, inspirations and motivations on true science.

First, I want to show gratitude to my supervisors who have never stopped instructing me and showing me the way to be a good scientist. I would like to sincerely appreciate Professor Kei Cho for giving enormous amount of advices to inspire and motivate me. His passion on high quality science and keen sense of true science have never been dried out and he always has eagerness towards the knowledge on neuroscience. I also want to appreciate the great efforts from Dr. Daniel Whitcomb who gave me the insights of critical thinking as a scientist and guided me whenever I need help for the experiments and PhD studies.

And I thank the former senior postdocs in the lab, Dr. Jee Hyun Yi who instructed and cheered me up to make my PhD experience in Bristol much smoother and Dr. Philip Regan who gave me numerous tips for the experiments. I also want to thank my friends, Miriam Durazo, Celia Martinez, and Tom Steward, who shared the PhD experiences together. And my colleagues in King's College London, Dr. Scott Mitchell, Dr. Saviana Barbati and Dr. Seyed Rasooli-Nejad, I want to say thank you for helping and supporting me as a great team.

This project was supported by the UK Dementia Research Institute which receives its funding from UK DRI Ltd, funded by the UK Medical Research Council, Alzheimer's Society and Alzheimer's Research UK.

I also want to present my great appreciation on Gachon Gil medical center in Korea and Chairperson Gil Ya Lee for supporting me this amazing opportunity and funding my PhD study in this leading university in the field of neuroscience research. And I also appreciate Professor Seong Soo An and Professor Hyon Lee who made this opportunity available.

And I give my love to my family who gave me the strength to move forward whenever I felt overwhelmed by many difficult situations during my study.

Author’s declaration

I declare that the work in this dissertation was carried out in accordance with the requirements of the University's Regulations and Code of Practice for Research Degree Programmes and that it has not been submitted for any other academic award. Except where indicated by specific reference in the text, the work is the candidate's own work. Work done in collaboration with, or with the assistance of, others, is indicated as such. Any views expressed in the dissertation are those of the author.

SIGNED: ..... DATE:.....

Table of contents

List of figures

List of tables

Abbreviations

ACSF	Artificial cerebrospinal fluid
ADAR2	Adenosine deaminase type 2
ADMA	Asymmetric dimethylated arginine
ALS	Amyotrophic lateral sclerosis
AMPAR	α-amino-3-hydroxy-5-methyl-4-isoxazolepropionic acid receptor
CA1-3	cornu Ammonis1-3
CP-AMPAR	Calcium-permeable AMPA receptors
DAT	Day After Transfection
DIV	Day In Vitro
EPSC	Excitatory postsynaptic currents
FET	FUS, EWSR1 and TAF15
FTD	Frontotemporal dementia
FTLD	Frontotemporal lobar degeneration
FUS	Fused in sarcoma
LC	Low-complexity
LLPS	Liquid-liquid phase separation
LTD	Long-term depression
LTP	Long-term potentiation
mEPSC	miniature EPSC
MMA	Monomethylated arginine
NMDAR	N-methyl-D-aspartate receptor
ROI	Regions of interest
SG	Stress granule
SOD1	Superoxide dismutase 1
TDP-43	TAR DNA-binding protein 43
TRN-1	Transportin-1
UMA	Unmethylated arginine

CHAPTER 1

General Introduction

1.1. Pathophysiology and neurodegenerative disease

Neurodegenerative disease refers to the progressive condition that neurons losses their functions and results in neuronal degeneration or death. This progression is accompanied by atrophy or lesions in various brain or central nervous system (CNS) regions and causes significant clinical phenotypes.

In the most cases, neurodegenerative diseases are symptomized to be dementia and motor neuron diseases, such as Alzheimer's disease (AD), Parkinson's disease (PD), frontotemporal dementia (FTD, or frontotemporal lobar degeneration (FTLD)) and amyotrophic lateral sclerosis (ALS). These diseases damage the abilities to memorise, think, behave, move and eventually, ruin the everyday life. Briefly introducing each disease, AD is known to present atrophy in wide range of cortex, thought to be affected from medial temporal lobe in the early stage and accompanied by cognitive impairment, PD shows neuronal loss in substantia nigra and mainly impairs motor and non-motor functions. FTD expressed with neuronal loss in frontotemporal lobe and alteration of behaviour and dysfunction of language skills, ALS is characterised by loss of motor neurons and showing dysfunction of voluntary muscles.

They are mainly regarded and expressed to be age-dependent, however, environments, genetic mutations, lifestyle or various factors also have been identified and/or expected to trigger early onset form of the diseases (Erkkinen et al., 2019). Accurate understanding of those factors will make early and accurate diagnoses easier and give clues for therapeutic or preventive approaches toward those diseases. Considering the progression of those diseases are slow and accumulative than acute, the number of patients is exponentially growing to result in high demand of social care resources and it gives burdens to the responsible family members. Therefore, early and accurate diagnosis of the diseases gaining attentions worldwide and the importance of them are growing.

The most dominant neurodegenerative disease, AD, takes about 60-80 % of dementia worldwide, estimated to be 24 million (Mayeux and Stern, 2012).

The prevalence of AD was 701 cases per 100,000 in 2016 (Nichols et al., 2019). PD is the second common neurodegenerative disease and comes with the motor symptoms. The prevalence of PD is generally known to be 100-200 cases per 100,000 (Von Campenhausen et al., 2005) and prevalence of dementia within PD cases is thought to be 30 % (Hely et al., 2008). FTD is also one of the major dementia and it is mostly expressed to be early onset, takes 12 % of dementia before 65 years and 2 % of dementia from 65 years and older cases (Van Der Flier and Scheltens, 2005). The prevalence of FTD is estimated for 0.01-4.6 cases per 1000 people (Hogan et al., 2016). And ALS is the most common motor neuron disease and the prevalence is about 6 cases per 100,000 (Talbott et al., 2016). Overall, these diseases are expressed in the older age groups and the population of aged group is increasing, therefore, the worldwide economic cost of dementia was reported to be $1 trillion (USD) in 2018, according to the world Alzheimer report 2018.

The progression of diseases primarily damage distinct neural areas, for instance, cerebral cortex is affected in AD and FTD, basal ganglia and thalamus are affected in AD, PD and FTD, hippocampus is affected in AD, brain stem and spinal cord are affected in ALS (Gan et al., 2018). When those neural regions are damaged, then, clinical phenotypes appear such as behavioural, cognitive, primary motor, extrapyramidal symptoms and metabolism and they are overlapped in AD, FTD, ALS and PD (Ahmed et al., 2016). For instance, behavioural symptoms and metabolism issues are expressed in all 4 different diseases, whereas cognitive symptoms are prominent in AD and FTD, motor (primary motor, extrapyramidal) symptoms are expressed in ALS, PD and FTD. Because of that heterogeneity in the clinical phenotypes, there were efforts to find the connections between neurodegeneration and molecular pathology (or proteinopathy) (Golde and Miller, 2009; Pievani et al., 2014).

1.2. Proteinopathies – distinct diseases with shared pathophysiology

Proteinopathy (or proteopathy) is a category of disease with malfunction of proteins. Common mechanism of proteinopathy is generally characterised by misfolding of certain proteins that can act as seeding molecules to recruit multiple functioning proteins and form bigger complexes (widely referred as oligomers, inclusions or aggregates), which in turn, disrupt cellular functions and cause cell death. This concept has been applied to neuronal degenerations to explain progression of the diseases (Jucker and Walker, 2011).

As the known molecules in the inclusions or aggregates of the proteinopathy, amyloid β (Aβ) and Tau are mainly identified in AD, α-synuclein in PD, TAR DNA-binding protein 43 (TDP-43) and fused in sarcoma (FUS) are mainly found in FTD and ALS (Fu et al., 2018). These proteins are normally expressed in the various range of cells in the healthy conditions and have their basic roles. However, in the pathological condition, those molecules are prone to aggregate like prion protein (Goedert et al., 2010). The aggregates are known to be misfolded into β-sheet structure and propagate by seeding to recruit other proteins into the aggregates (Soto and Estrada, 2008). These aggregates are deposited in the wide range area of the brain and CNS regions and interfere the neuronal functions and induce neurodegenerations. Interestingly, each protein has the predominant area that is deposited and induces neuronal toxicity, therefore, it results in the distinct neuronal degeneration patterns and likely correlates with the clinically affected brain regions as mentioned above (Gan et al., 2018).

For the further aspects to the neural dysfunctions and clinical phenotypes, those pathologies also have been investigated in the further smaller level, neurons. Therefore, neurodegeneration is also referred to be a series of phenomena that describes the progressive loss of neuronal structure and function (Haass and Selkoe, 2007). In that sense, those proteinopathy is not just neural region-specific, but also neuron-specific and gene-specific that contribute the selective vulnerability of the neurons (Fu et al., 2018).

Obviously, the mutations on the genes of the main pathological proteins (e.g. Aβ, α-synuclein, TDP-43 and FUS) in each neurodegenerative disease and the other genes that accelerate the neuronal pathologies are largely involved. Mentioning few major genes for each disease, APP, PSEN1 and PSEN2 are involved in AD pathology, SNCA, LRRK2 are involved in the PD pathology, TARDBP, superoxide dismutase 1 (SOD1), FUS are involved in ALS pathology, GRN, microtubule-associated protein Tau (MAPT) are involved in FTD and C9orf72 is involved in both ALS and FTD (Fu et al., 2018). These pathogenic gene and protein expression result in the alterations of neuronal homeostasis (Gan et al., 2018). For instance, protein quality control mechanism and autophagy and lysosome pathway are dysregulated, therefore, it accelerates accumulation of misfolded proteins (Gomez-Pastor et al., 2017; Taylor et al., 2016). In addition, adenosine triphosphate (ATP) production of mitochondria can be also less efficient by aging and eventually impaired by neurodegenerative diseases (Golpich et al., 2017). And adding up to those disruption of neuronal homeostasis, those pathogenic proteins can propagate to the other adjacent neurons via seeding (Braak and Braak, 1991; Luk et al., 2012) or interfere the normal function of stress granules (Aulas and Velde, 2015) to spread out the neuronal toxicity intracellular or cell-to-cell manner. Overall, neurodegenerative diseases can cause the alteration of neuronal dynamics and result in neuronal death eventually.

1.3. Memory as a cognitive function

The brain is a key organ for learning and memory that consists of the neuronal dynamics through connections among nerve cells. The brain receives sensory inputs from the environment and coordinates various information through different brain regions. As described previously, various neurodegenerative diseases damage different compartments of the brain, therefore, disable their normal functions. Since the functionality of learning and memory is widely affected from synaptic level, it has been monitored in many neurodegenerative diseases. Although it is distinct in certain disease,

brain region, neuron and major pathogenic protein types, however, the principle neuronal dynamics of learning and memory is shared throughout CNS. In addition, the proteinopathy of neurodegenerative diseases not just stay in the main area of disease, but also spread through CNS, therefore, those well-characterised neuronal models for learning and memory also can be utilised to study diverse range of neurodegenerative diseases, such as ALS and FTD. To understand the function of memory, the most common theory postulated was Hebb's rule "neurons fire together and wire together" (Hebb, 1949) and this theory was previously suggested by Cajal (Cajal, 1894). Therefore, neuronal activity and neuronal circuit from various brain regions process information and store the encoded information as a memory (Squire, 2009).

1.3.1. Definitions of memory

Memory has long been thought of as a process in which sensory information is encoded, stored and made accessible for retrieval (Nadel and Hardt, 2011). It has long been established (Waugh and Norman, 1965) that memory does not occur via a single process but various subtypes. Broadly, there are three different types of memory; sensory memory, short-term memory and long-term memory depend on the duration of the memory and how the memory is produced and processed. The memory types are drawn as a diagram in Fig. 1-1.

Sensory memory refers to the sensed information from the outside world such as iconic memory from visual stimuli, echoic memory from auditory stimuli and haptic memory from tactile stimuli. Among them, iconic memory is dominantly used and to be relied on (Atkinson and Shiffrin, 1968). For the formation of the memory, visual stimuli need to be processed by retinal receptors and cells and occipital lobes (Camina and Güell, 2017). For the further conversion and consolidation, the information goes through ventral route to inferior temporal cortex (Camina and Güell, 2017).

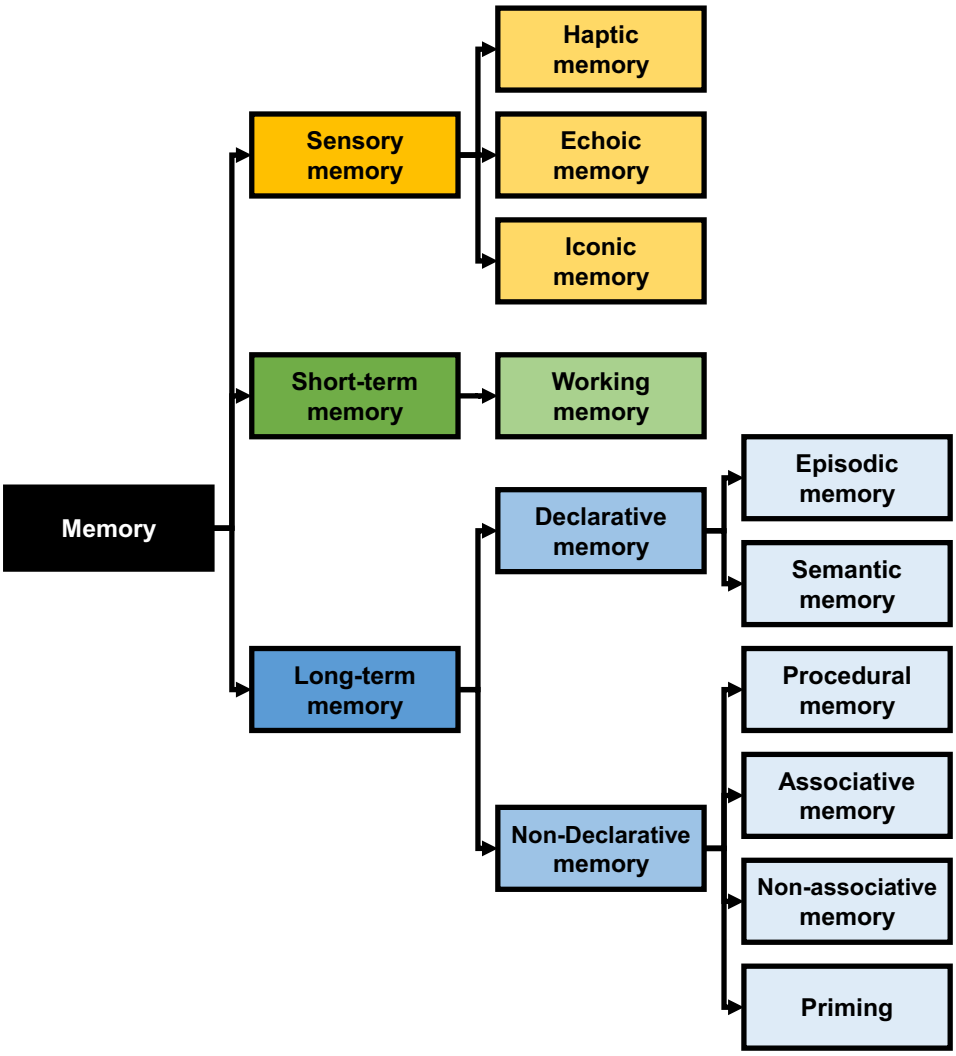

Figure 1-1 Classification of memory types.

The diagram of memory types was adapted from (Camina and Güell, 2017).

Short-term memory (working memory) is the processed information for a short period of time (Baddeley and Hitch, 1974), therefore, short-term memory can work as an independent memory or work as a prior stage of long-term memory to be processed. The first example of short-term memory can be seen from Miller's 1956 study in which participants were required to study a sheet of numbers and subsequently list them without refereeing to the original reference. The information processing capacity (or working memory) of the participant can be proposed from the amount of correct

numbers repeated. It has been suggested that working memory has the central executive, visuospatial sketchpad, phonological buffer, episodic buffering components, all of which interact each other (Baddeley and Hitch, 1974). **The central executive** has roles to focus on attention, to separate attention from multiple tasks, to access to long-term memory (Baddeley and Hitch, 1974) and requires frontal lobe activity. **Visuospatial sketchpad** is specialised to the formation and maintenance of the visual and spatial contents of short-term memory. It has been suggested to be mainly held in the right hemisphere of the brain. **Phonological buffer** (or phonological loop) is specialised to the formation and maintenance of the auditory information by storing short-term acoustic contents and rehearsing subvocal articulatory contents. This has found to be on the left hemisphere of the posterior superior temporal gyrus (Buchsbaum et al., 2001). **Episodic buffer** is able to store memories in a short-term and can integrate information from different sources (Baddeley, 2000). There are no specific brain area(s) proven to do this role, thus, episodic buffer is often hypothesised as short-term memory (Baddeley, 2000). Overall, working memory can give attention and integrate information to form short-term information for the further consolidation of the memory to be stored.

Long-term memory is the information to be stored for long and/or permanent period of time and can be recalled. It is categorised into two different types; declarative memory and non-declarative (procedural) memory.

Declarative memory is the information which can be recalled consciously. It was further categorised to episodic memory and semantic memory by Tulving in 1972 (Tulving, 1972). Episodic memory represents the information about personal experiences or specific events related to the time and place. Therefore, these declarative memory forms are important for the cognitive functions of the brain. This type of memories is known to be processed mainly in the hippocampus and cortices near hippocampus (Allen and Fortin, 2013; Irish and Piguet, 2013). **Episodic memory** is unique as it consists of

personal experiences in terms of temporal and spatial context. Episodic memory has been thought to be one of the major neurocognitive memory systems (Schacter and Tulving, 1994). Episodic memory is thought to be exclusive for the humans because it is difficult to define and convert the concept of the personal experience to the nonhuman species (Templer and Hampton, 2013). But there are still approaches to define episodic-like memory from animal studies (Clayton and Dickinson, 1998; Easton et al., 2012). In addition, episodic memory is more vulnerable to the neuronal dysfunction compared to the other memory systems (Tulving, 2002). Hippocampus and adjacent cortices participate in the process of episodic memory. **Semantic memory** represents the understandings and thinking of the common knowledge and concepts. The exact brain regions required for semantic memory are still debated but temporal and inferior parietal lobes are known to be broadly related (Binder and Desai, 2011). However, two main hypotheses exist, 1) memory is processed in the temporal lobe and hippocampal formation as episodic memory, 2) memory can be associated with the wide-range of sensory and motor cortices and converged in the inferior parietal lobe and temporal lobe in the brain (Binder and Desai, 2011).

Non-declarative memory is commonly explained as the memory of skill learning, where on has the ability to repeatedly complete a motor task (e.g. tying shoelaces) that is recalled unconsciously. Non-declarative memory is further categorised to procedural memory, associative memory, non-associative memory and priming (Camina and Güell, 2017). **Procedural memory** is related to physical skills and habits. This still requires the conscious learning process to be associated, but once acquired, it becomes automated and does not require conscious thinking. For the acquisition, the striatum of the basal ganglia is required and for the execution, motor neuronal regions such as cerebellum are needed. **Associative memory** is a process that storing and retrieving information to associate multiple different types of the information. Or, this process can do simply associating the existing information than generating new information (classical conditioning) (Pavlov, 1927) or association of information to affect positively or negatively

to the further behaviour (operant conditioning) (Skinner, 1938). **Non-associative** memory represents alterations of the responses toward the repetitive stimulations that result in either decreased response (habituation) or increased response (sensitisation) (Kandel, 1976). This is process in the reflex pathways and related to acetylcholine and serotonin. **Priming** is the process that certain stimulation affects the responses towards other stimulations in the future. This is known to be related to neocortex (Baars et al., 2010). Overall, these different long-term memory types have different functions and associated with the different brain regions.

1.3.2. Neuroanatomy of memory

Then how are memories are obtained, processed and stored? At the beginning, information from outside world needs to be received via sensory organs and then converted via sensory cortices as sensory memory. Sensory memory is delivered to association areas such as frontal, temporal and parietal lobes and processed to the short-term memory. At this stage, spatial type (potential episodic memory) and non-spatial type memories (potential semantic memory) are handled separately. And both types of the memories enter the parahippocampal region but go through the different sub regions. Spatial type memories mainly go through parahippocampal cortex and postrhinal cortex and then they are transferred to medial entorhinal cortex. Meanwhile, non-spatial type memories go through perirhinal cortex and then transferred to lateral entorhinal cortex. Both spatial and non-spatial type memories enter the hippocampus for the consolidation process and the process can be done either separately or associatively. Then, the memories are encoded to declarative memory, either episodic memory or semantic memory and amygdala can add emotional context for the episodic memory. Those encoded memories are thought to be stored in the associative cortices and when the memories are needed to be retrieved or executed, prefrontal cortex receives the information and then delivers it to the relevant cortices or regions of the brain to take actions. Overall, these connected compartments

for the memory circuit are all necessary, however, for the declarative long-term memory, hippocampus conducts the core process of the consolidation. In that context, many studies have been done with the hippocampus to dissect the process of learning and memory and it has been reported that the deficit of hippocampal functionality caused cognitive impairment and deficit in learning and memory (Broadbent et al., 2004; Eichenbaum, 2004; Jarrard, 1993). Therefore, it is important to know the basic structure and what is happening in the hippocampus during the learning and memory process.

Hippocampus is known to consist of dentate gyrus, cornu Ammonis (CA)1~3 and subiculum (Fig. 1-2). These brain regions form the neural circuit to receive the information from x, process and forward to y. CA1 is considered as the main spot of the memory circuit in the hippocampus. Each CA1 pyramidal neuron has two distinct dendritic branches (e.g., apical dendrite and basal dendrite) and receives distinct inputs from different brain regions. The layers of CA1 area match with the dendritic region and soma of each CA1 neuron; proximal apical dendrite in stratum radiatum (SR), distal apical dendrite in stratum lacunosum moleculare (SLM), basal dendrite in stratum oriens (SO) and soma in stratum pyramidale (SP). The main excitatory input CA1 neurons receive is via the Schaffer-collateral pathway that originates at CA3 neurons and terminates at proximal apical dendrite of CA1 (Masurkar, 2018). Proceeded this, the dentate gyrus receives input from entorhinal cortex, process it, then gives input to CA3, which is mossy fibre pathway. CA1 can also receive direct input from entorhinal cortex to distal apical dendrite. And distal apical dendrite also receives inputs from prefrontal cortex via nucleus reunions of thalamus. Meanwhile, basal dendrite receives input from CA2 directly and also contralateral CA3 gives input to the region (associational commissural pathway) (Masurkar, 2018). CA1 itself has different functions and neuronal features dependent on the anatomical location within the hippocampus. CA1 neurons can be located either in the dorsal or ventral area, proximal or distal area and deep or superficial area of the hippocampus. The main area of the CA1 responsible for processing spatial declarative memory is proximal area in dorsal hippocampus

(Henriksen et al., 2010; Jung et al., 1994). The ventral area has broader roles related to anxiety, motivation, fear and others (Okuyama et al., 2016; Zhu et al., 2014). The inhibitory drive within the CA1 is mainly provided by GABA (γ-aminobutyric acid)-ergic interneurons which deliver inputs in the dynamic manner (Klausberger and Somogyi, 2008).

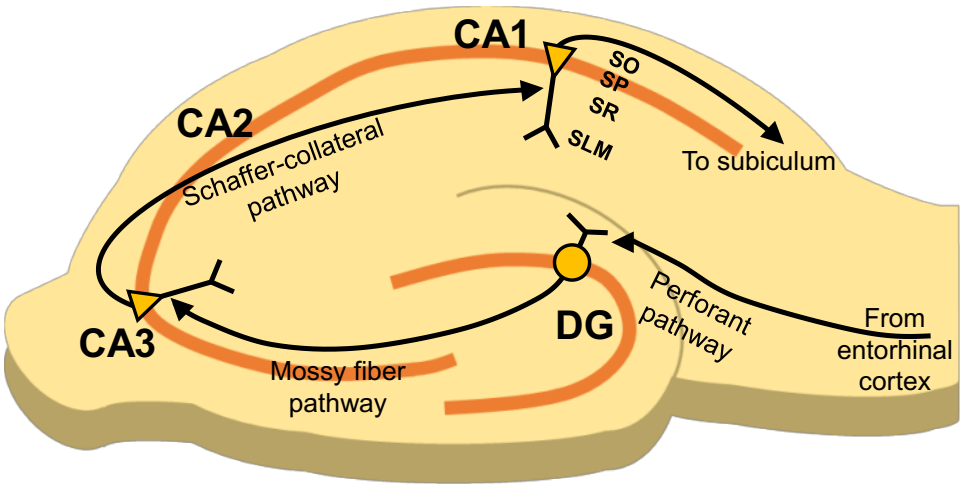

Figure 1-2 Hippocampal circuitry.

The basic circuitry of hippocampus was illustrated. Entorhinal cortex delivers inputs to the granule cells dentate gyrus (DG) via performant pathway. Axons of granule cells deliver the signal to cornu Ammonis (CA)3 pyramidal cells via mossy fibre pathway. And axons of CA3 delivers signal to CA1 pyramidal cells via Schaffer-collateral pathway. Those 3 pathways also referred as trysynaptic circuit. The processed signals are mainly delivered back to entorhinal cortex via subiculum.

In addition to the hippocampus itself, the input from **entorhinal cortex** also has major roles for the formation of the declarative memory, especially spatial memory (Parron et al., 2006), and consolidation of the memory (Takehara-Nishiuchi, 2014). The entorhinal cortex basically works as a bridge between neocortex and hippocampus closely communicate with hippocampus. The entorhinal neurons process spatial context by forming hexagonal grid patterns (known as grid cells) as the response to the surrounding spatial environment. And then, grid cells deliver the information to the place cells in the hippocampus for the further process to generate the spatial memory, which is a type of episodic memory (Moser et al., 2015).

In short, the hippocampus has a highly aligned and organised circuit that can perform dynamic process of the memory in the coordination with the adjacent brain regions such as entorhinal cortex. However, the studies on this process have been further dissected to the smaller level; synapse and neurotransmission.

1.4. Molecular mechanisms of memory

1.4.1. The synapse

Neuronal circuits described above coordinate the information and the store memory through the creation and strengthening of synapses (Südhof and Malenka, 2008). A synapse is the junction between cells and transfers signals from the presynaptic neurons to the postsynaptic neurons. Once a presynaptic neuron is excited enough to deliver action potentials, the intracellular Ca^{2+} level is increased and resulting in synaptic vesicles release via exocytosis into the synaptic cleft. These synaptic vesicles are filled with neurotransmitter. The postsynaptic neuron then detects the neurotransmitters with the diverse postsynaptic receptors. Upon, neurotransmitter binding the receptors either open the ion channels themselves to allow the flow of ions into the neuron or activate G proteins to send further intracellular signal cascades. Generally, especially in the case of ion channels, binding of neurotransmitters causes either excitatory and/or inhibitory function of neuron by allowing ions to flow through the channels. If Na^+ flows into the cell via ion channels, then, the cell is depolarised and shows excitatory postsynaptic response, on the other hand, if Cl^- flows into the cell or K^+ flows out via ion channels, then, the cell is hyperpolarised and shows inhibitory postsynaptic response. Thus, summation of those responses decides whether the signal would be delivered further or stopped and not to be sent.

Synaptic transmission can be categorised by the neurotransmitters that are involved in either excitatory and/or inhibitory function of neuron. There are

plenty of chemical molecule species capable of neurotransmission, for example, amino acids, amines and peptides. Among them, the most abundant molecules in the brain are two amino acid types, one is glutamate for the excitatory synapses and the other one is GABA for the inhibitory synapses. Furthermore, glutamatergic receptors have been intensively studied and put the importance on the roles in learning and memory and also involved in the synaptic changes (or synaptic plasticity) (Bliss and Collingridge, 1993). Due to the importance and predominance, glutamatergic receptors have been targeted as the main parameters for studying neuronal or synaptic changes by neurodegenerative diseases (Sheldon and Robinson, 2007).

1.4.2. Excitatory ionotropic glutamate receptors

Glutamate receptors are mainly expressed in the synaptic region of the neurons and have main roles in the glutamatergic neurotransmission of excitatory neurons. There are ionotropic glutamate receptors (iGluRs) and G-protein coupled metabotropic glutamate receptors (mGluRs). iGluRs are ligand gated ion channels which permit the influx of Na and Ca ions (See Traynelis et al., 2010 for review). On the other hand, metabotropic glutamate receptors are activated via G-protein coupled signal cascades and regulate neuronal function. In general, iGluRs are more likely participate in the fast responses and mGluRs is relatively slower response than iGluRs. The subtypes of glutamate receptors are displayed in the Fig. 1-3.

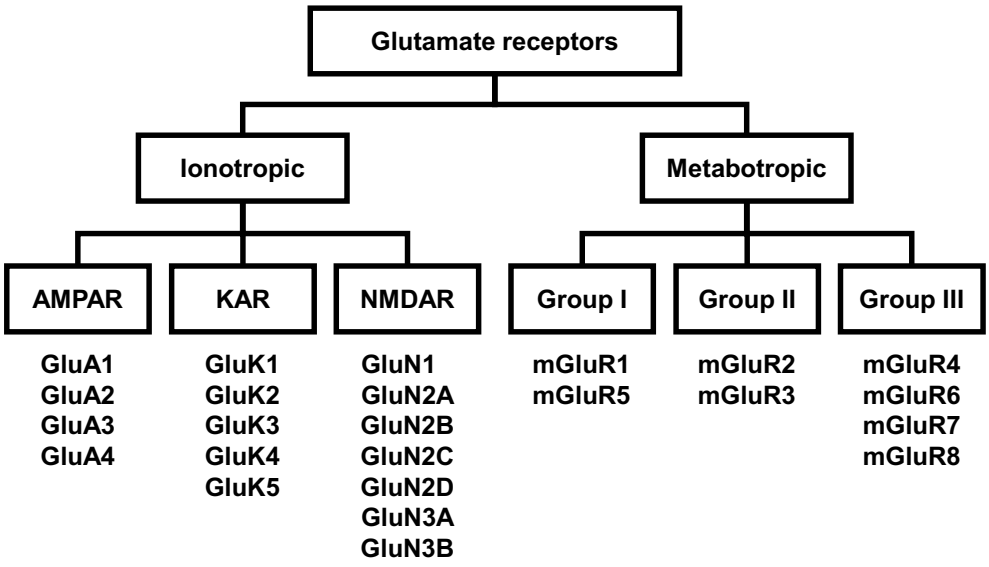

Figure 1-3 Classification of glutamate receptors and subunits.

Glutamate receptors are mainly classified to ionotropic and metabotropic receptors and further divided into AMPAR, KAR, NMDAR and group I, II, III mGluR. The subunits of each glutamate receptor type were also shown.

There are 3 different ionotropic receptor groups, each of them has high affinity with specific agonists such as α-amino-3-hydroxy-5-methyl-4-isoxazolepropionic acid (AMPA), N-methyl-D-aspartate (NMDA) and/or kainate, respectively. Those receptors are named as AMPA receptors, NMDA receptors and kainate receptors, since they were selectively bound with each agonist and activated in the pharmacologically analysis. AMPA receptors (AMPARs) and NMDA receptors (NMDARs) are the predominant types of the excitatory neurons in the brain and have main roles for synaptic transmission and are involved in learning and memory (Citri and Malenka, 2008).

Activation of **AMPAR**s causes the major component of fast excitatory synaptic transmission in the brain. AMPARs bind with glutamate (or other antagonists such as AMPA and 5-Fluorowillardiine) to allow the influx of Na^+ and efflux of K^+ and also influx of Ca^{2+} in some occasions (Zieglgänsberger et al., 2005). An important feature of AMPARs, is they can regulate synaptic efficacy through postsynaptic signalling cascades, which cause AMPARs to

be either recruited or removed from synaptic surface. AMPARs have 4 subunit types, which are GluA1, GluA2, GluA3 and GluA4 and form tetramers to make AMPARs functional (Greger et al., 2017). The combination and status of subunits make the different functionalities of AMPARs. Most of AMPARs are composed of 2 dimers and in the most cases, a dimer of GluA2 combined with a dimer of either GluA1, GluA3 or GluA4. Since GluA2 is included in almost all the AMPARs, the diverse functionality is usually determined by the status of GluA2. The mRNA of GluA2 usually goes through post-transcriptional modification at 607th residue by adenosine deaminase type 2 (ADAR2) and this change is related to Q/R editing site of GluA2 subunit that decides whether AMPAR is permeable to Ca^{2+} or not (Fig. 1-4).

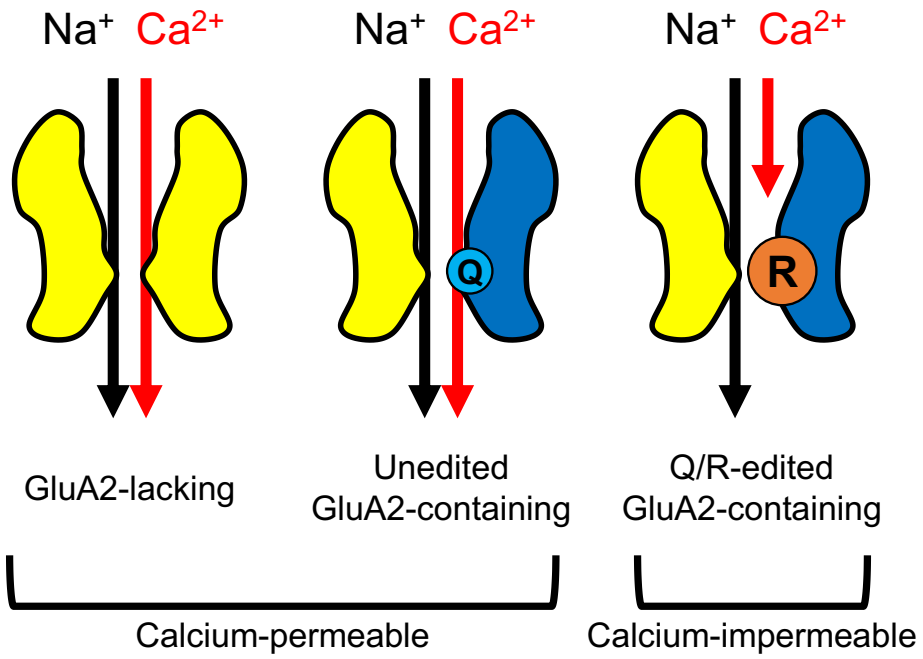

Figure 1-4 Calcium permeability of AMPARs.

Calcium permeability of AMPARs is mainly defined by the status of GluA2 subunit. If AMPAR is lacking GluA2 (left) or Q/R editing of GluA2 (centre), then, AMPAR is calcium permeable. However, predominant AMPARs contain Q/R-edited GluA2 subunit and they are calcium impermeable (right).

The Q/R site of GluA2 is predominantly edited to R and AMPARs are mostly impermeable to Ca^{2+}. Non-edited Q variant and GluA2-lacking AMPARs are Ca^{2+}-permeable, thus conductance is higher than that of R variant GluA2-containing AMPARs (Swanson et al., 1997). Considering the combination of those factors, AMPARs can be referred as either Ca^{2+}-permeable AMPARs (CP-AMPARs) or Ca^{2+}-impermeable AMPARs (CI-AMPARs) depends on the permeability of Ca^{2+} ions. Due to that difference, CP-AMPARs and CI-AMPARs have different current–voltage characteristics (or I-V curve). Since CP-AMPARs are not only permeable to Na^{+} and K^{+} but also Ca^{2+}, this causes stronger inward rectification of I-V curve (Bowie and Mayer, 1995; Washburn et al., 1997). Therefore, abnormal expression of Q variant and/or GluA2-lacking AMPARs are frequently found and implied in the neuronal pathologies, specifically those related to excitotoxicity (Kwak and Weiss, 2006; Liu et al., 2006, 2004; Noh et al., 2005). In addition to Q/R editing, other variation of AMPAR subunits can be edited in the different ways to change the kinetics of AMPARs (Dingledine et al., 1999). mRNAs of GluA2, GluA3, GluA4 also go through R/G editing to change the speed of recovery from non-conducting and desensitised state (Wright and Vissel, 2012). The other variation is FLIP/FLOP alternative splicing of all the GluA subunits to change the speed of desensitisation (Dingledine et al., 1999).

NMDARs also have important roles in synaptic plasticity, learning and memory (Collingridge, 1987). At the resting status, Mg^{2+} blocks the ion pore, therefore, no ion can pass through the NMDAR channel. Depolarisation of neuron (mainly by AMPAR) removes Mg^{2+} from the pore and allow the influx of Na^{+} and Ca^{2+}, efflux of K^{+}. NMDARs have various subunits, which are GluN1, GluN2A~D and GluN3A~B. The combination of subunits can be either di-heteromer or tri-heteromer and always forms tetramer. Di-heteromeric NMDARs are composed of two dimers, one GluN1 dimer and either one of GluN2A, GluN2B, GluN2C, GluN2D or GluN3A. Tri-heteromeric NMDARs are composed of two GluN1 and GluN2A/2B, GluN2A/2C, GluN2B/2D and GluN2B/3A. GluN2 subunits bind to glutamate and GluN1 and GluN3 can bind to glycine. The main combination of NMDAR subunits is

GluN1 and GluN2 (Predominantly GluN2A and 2B) di-heteromer (McKay et al., 2018; Miglio et al., 2005; Sanz-Clemente et al., 2013). Since GluN2B has longer deactivation time compared to GluN2A (Paoletti et al., 2013), the ratio of GluN2B is usually found to be higher when the neuron is more exciting condition such as in early developmental brain or under excitotoxic environment (Martel et al., 2009, 2012).

1.4.3. Synaptic plasticity in the hippocampus

The connectivity of synapses can be either strengthened or weakened, a process which highly depends on the patterns of the synaptic input and/or experience. This change of synaptic connective strength (or efficiency) is called synaptic plasticity and it is considered to be a key component of the cellular and molecular mechanism of learning and memory (Bliss and Collingridge, 1993). This concept was initially suggested by Donald Hebb, who stated “neurons fire together and wire together” (Hebb, 1949). If one cell’s axon is close to the other cell’s dendrites and can excite, then the repetitive stimulation can induce metabolic change of those cells and strengthen the connectivity to form neuronal assembly (or engram). Addition to that neuronal assembly, there was a closely-related idea that morphological changes at synaptic region is the substrate for the learning (Konorski, 1948). To prove the concept, it was demonstrated by application of high-frequency electric stimulation in the rabbit’s hippocampus that induced the stable and persistent potentiation of the neuronal responses (Bliss and Lomo, 1973), later named long-term potentiation (LTP) (Douglas and Goddard, 1975). The molecular profile underpinning the synaptic changes was discovered with the great advance in the development of selective agonists and antagonists for the receptors on the synaptic membranes of neurons (Watkins and Jane, 2006). The NMDAR was revealed as a key component as NMDAR-mediated synaptic plasticity was discovered and is important for the learning and memory process (Morris et al., 1986), which is sensitive to hippocampus (Bliss and Collingridge, 2013;

Morris et al., 1982). Therefore, synaptic plasticity happens between neurons to store information in the brain, which is basically learning and memory, and this concept has been postulated, demonstrated and proven for centuries and greatly improved in several decades with the advanced devices and techniques.

The diversity of synaptic plasticity has been discovered and it is not clear that how many types of synaptic plasticity exist and their potential relationship (Südhof and Malenka, 2008). However, the main types of synaptic plasticity can be categorised in terms of the tendency of either potentiating or depressing, time span either long or short, molecular or cellular specificity and so forth. Broadly, these are categorised into short-term synaptic plasticity (lasts several minutes or less) and long-term synaptic plasticity (few hours, days or more) by the length of the maintained time (Cowan, 2008). In most cases, short-term plasticity only requires the trafficking of synaptic components, while long-term plasticity requires changes in the molecular profile and also accompanied by translation of the synaptic structural proteins to sustain the altered synaptic strength and morphology of the dendritic spines (Mayford et al., 2012).

Short-term synaptic plasticity is transient changes that lasts very short period of time. It occurs predominantly at pre-synaptic neuron and is related to the change of the presynaptic level of Ca^{2+} to modify the dynamics of the release of synaptic vesicles (Zucker and Regehr, 2002). Paired-pulse facilitation (PPF) and depression (PPD) occurs when 2 pulses are delivered at short (less than 20 ms for PPD) or slightly long intervals (20~500 ms for PPF) (Citri and Malenka, 2008). This is mainly due to the probability (or readiness) of the release of synaptic vesicles from the presynaptic region. Trains of stimulations also induce longer transient changes (several seconds to minutes) such as augmentation, post-tetanic potentiation (PTP) and post-tetanic depression (PTD) that are also related to the probability of the synaptic vesicles in addition to the sensitivity of the ligand-gated receptors (Zucker and Regehr, 2002). The occupancy of the presynaptic receptors or

retrograde messengers also modulate the short-term synaptic plasticity, as well. Overall, short-term synaptic plasticity is mainly modulated by probability of synaptic vesicles, thus, this work as filter of high or low frequency input.

Long-term synaptic plasticity is characterised by sustained changes that lasts for long period as the activity dependent response. This change is often accompanied by morphological changes of spines and background molecular profiles at synapse (Ho et al., 2011). LTP has been studied in the various way, as mentioned earlier, by postulating concepts, proving the concept with electrophysiology, pharmacology, molecular biology, behaviour test and other methods. NMDAR-dependent LTP is the most studied type of synaptic plasticity and has numerous evidences that are demonstrated in the CA1 region of the hippocampus of various mammalian models (Martin et al., 2000; Zola-Morgan et al., 1993).

As stated earlier, NMDAR-dependent LTP first requires activation of AMPARs to depolarise the post-synaptic region, removing the Mg^{2+} block from NMDAR to open and allow the influx of Ca^{2+}. Once the concentration of Ca^{2+} increases to certain point by application of high-frequency stimulation (HFS), an intracellular cascade is triggered, and it is known to include Ca^{2+}/calmodulin-dependent protein kinase II (CaMKII) (Park et al., 2014). This cascade is mainly composed of protein kinases and eventually triggers AMPAR trafficking to the post-synaptic membrane and results in the increased synaptic transmission efficiency (Lüscher and Malenka, 2012). In addition to the recruitment of AMPAR to the synaptic membrane, LTP needs further process to maintain the potentiation. Local translation of synaptic and structural proteins and trafficking of mRNAs to dendrites often suggested as the requirements to sustain LTP. This process eventually enlarges the active synaptic region of both pre- and post-synaptic neuron and strengthen the synaptic transmission (Loebel et al., 2013). On the other hand, NMDAR-dependent long-term depression (LTD) also has been studied massively in the CA1 hippocampal neurons and known to be a counterpart of LTP in terms of the modulation of synaptic strength. NMDAR-Dependent LTD is typically

induced by application of low-frequency stimulation (LFS). Similar to LTP, this LTD requires depolarisation and increase of Ca^{2+} level in post-synaptic region but in the moderate level. In this case, this Ca^{2+} triggers different cascade that includes calcineurin and other phosphatases (Mulkey et al., 1994). This cascade results in the removal of AMPARs from synaptic region and decreases the efficiency of synaptic transmission and the size reduction or removal of synapse (Wiegert and Oertner, 2013). In addition to the post-synaptic changes in NMDAR-dependent LTP or LTD, presynaptic region can also undergo synaptic plasticity. Presynaptic LTP is often suggested as triggered by massive action potentials and increase of Ca^{2+} level in pre-synaptic region. These changes cause the increased release of neurotransmitter. There are several more different types of long-term synaptic plasticity types such as metabotropic glutamate receptor-dependent LTD, endocannabinoid-mediated LTD, metaplasticity, synaptic scaling and this is not the whole list of them (Citri and Malenka, 2008). Overall, these long-term plasticity types are activity-dependent and bidirectional regulation of the synaptic strength. Therefore, these activity-dependent synaptic changes are considered as the underlying mechanisms of encoding and saving of the information in the brain, which are implied in memory formation.

Then how important is the hippocampus for studying synaptic plasticity? The early findings of LTP and other forms of synaptic plasticity were mainly found and studied in the hippocampus and for the decades, connection between synaptic plasticity in the hippocampus and functionality of learning and memory have been repetitively proven and reviewed (Bliss et al., 2018; Lynch, 2004; Nicoll, 2017). Patients with deficit in the hippocampus have been reported to have memory deficits (Boyer et al., 2007; Nagy et al., 1996; Penfield and Milner, 1958) and in the rodent models (Altemus and Almli, 1997; Gallagher, 1997), inhibition of the major components of the hippocampal synaptic plasticity such as NMDAR has proven to damage the learning ability (Newcomer et al., 2000) and also, it was demonstrated that learning task could generate the activity patterns of hippocampal CA1 neuron and LTP (Whitlock et al., 2006). Therefore, the hippocampus became the

most important, well-established tool to study synaptic plasticity, thus, the hippocampus can be utilised for seeking either pathologies or therapies that are closely connected to the memory function of the brain.

1.4.4. Molecular mechanisms and protein interactions in synaptic plasticity

As described in the session 1.4.3., main components of synaptic plasticity are receptors of neurotransmitters and their trafficking is critical to reflect the efficiency of neurotransmission. Therefore, molecular and protein interactions mediating the trafficking and sustaining the altered state of those receptors also have critical roles in synaptic plasticity. This topic has been relatively well studied in Schaffer-Collateral pathway between hippocampal CA3 and CA1 neurons.

AMPAR is a main component of LTP and LTD studies and it has been known to be a major target of trafficking and expression in and out of the synaptic surface during synaptic plasticity (Collingridge et al., 2004). Basically, trafficking of AMPARs is categorised to exocytosis, endocytosis and lateral diffusion and many molecules are involved to mediate the trafficking. When AMPARs are on the synaptic membrane, GluA2 subunit is anchored to PDZ proteins such as AMPAR binding protein (ABP) and glutamate receptor-interacting protein (GRIP) (Dong et al., 1997; Osten et al., 2000). In addition, GluA2 is needed to be bound with N-ethylmaleimide-sensitive factor (NSF) to maintain AMPARs staying in the synaptic region (Nishimune et al., 1998). GluA2 subunit also can bind with protein interacting with C-kinase (PICK1) after phosphorylation at Serine 880 by protein kinase Cα (PKCα) to be dissociated from ABP/GRIP and become available for later diffusion (Hee Jung Chung et al., 2000; Perez et al., 2001). Or NSF can be substituted by AP2 adaptor complex and this causes the endocytosis of AMPARs (Lee et al., 2002). The endocytosed AMPARs can be recycled with the binding of GluA1 subunits to synapse-associated protein 97 (SAP97) and myosin-VI (Wu et al., 2002). Again, AMPARs can laterally diffuse and then once reach to the synaptic region, AMPARs can bind with postsynaptic density protein

95 (PSD-95) and this aids the anchoring at the synapse (Bredt and Nicoll, 2003).

In addition to the trafficking of AMPARs, the dynamics of cytoskeletons is also important for the changes on dendritic spines where synaptic plasticity happens. Mainly cytoskeletons in the dendritic spines are consist of actin proteins and highly dynamic during synaptic plasticity (Borovac et al., 2018), therefore, regulating their dynamics is important for the structural alteration of dendritic spines. The dynamics of actin proteins is often described as a balance between globular (G)-actin (monomer) and filamentous (F)-actin (polymer). F-actin is the functioning component of cytoskeleton to support the spine structure, thus, bundled F-actin is stabilised in the basal state (Hotulainen and Hoogenraad, 2010). Induction of synaptic plasticity (e.g. LTP), active CaMKII detaches F-actin bundles and then Cofilin/actin depolymerizing factor (ADF) dissociates F-actins into free F-actins and G-actins (Bamburg and Bernstein, 2010). Afterwards, Aip1 and Arp2/3 bind to F-actin and mediate F-actin assembly, which results in the growth of the spines (Ichetovkin et al., 2002; Okreglak and Drubin, 2010). Finally, Drebrin, α-actinin and inactivated CaMKII stabilise the newly formed F-actin bundles and maintain the structure (Djinovic-Carugo et al., 1999; Koganezawa et al., 2017; Okamoto et al., 2007).

Overall, these molecular mechanisms and protein interactions are involved in the synaptic plasticity and interruption or dysfunction of those molecular mechanism can be important starting point of studying neurodegenerative diseases.

1.4.5. Synaptic dysfunction and neurodegeneration

As articulated in the previous sections, synapse is the very fundamental element that comprises neuronal activity, memory and cognition. Therefore, synapse has been suggested to be highly vulnerable and sensitive when it comes to the neurodegeneration. Synapses are often reported to be altered

before expression of symptoms or neuronal degeneration (Wishart et al., 2006). Therefore, a loss or impairment of neuronal regulatory dynamics for the connectivity in synapses can be the origin or the initiative mechanism of pathophysiology of neurodegenerative diseases. This pathological process is widely involved in the synaptic plasticity, which is a change in synaptic communication weight between neurons and thought to be a cellular mechanism of learning and memory (Neves et al., 2008). Therefore, its main categories, LTP and LTD, have been studied in the context of neurodegenerations and/or aging whether they are actually affected or not during the progression of the diseases. To investigate the changes, the efficiency of neurotransmission can be monitored by checking the population and activity of those glutamate receptors. As mentioned in the section 1.1.4., AMPA receptor is one of the most dominant and dynamic glutamate receptor in excitatory neurons (Bredt and Nicoll, 2003) and it is widely accepted that AMPA receptor internalisation from synaptic region is an underlying molecular mechanism of LTD (Beattie et al., 2000) and vice versa for LTP (Bliss and Collingridge, 2013). Among the disease model, AD was widely investigated to understand the dysfunction of those synaptic plasticity process. For instance, application of Aβ has been shown to induce rapid recruitment of AMPARs (Whitcomb et al., 2015) and inhibit the induction of NMDAR-mediated LTP (Palop and Mucke, 2010). Tau was also found to be hyperphosphorylated during AD pathology (Kosik and Finch, 1987), especially post synaptic region in the neurodegenerative condition where LTD-like pathways mainly occur (Tai et al., 2012). These synaptic changes are highly dependent on Ca^{2+} homeostasis of the neurons and its dysregulation in the neurodegenerative diseases is also known to contribute the neuronal vulnerability (Morrison et al., 1998). In addition, FUS-related diseases are also shown to have altered status of Ca^{2+} homeostasis (Leal and Gomes, 2015; Machamer et al., 2018; Tischbein et al., 2019) and the involvement to the regulation of AMPAR (Udagawa et al., 2015), it would be important to look into the roles of FUS in the regulatory dynamics of the synapses.

1.5. Proteinopathy and synaptic dysfunction: the role of Fused in sarcoma (FUS)

1.5.1. Structure and function of FUS

FUS is a DNA/RNA-binding protein in which mutations or abnormal expression have been implicated in the pathogenesis of ALS and FTLD patients (Kwiatkowski et al., 2009; Neumann et al., 2009). FUS is thought to modulate the expression of genes by association with a wide range of transcription-related factors in different types of neurons in the nucleus and/or cytosol (Dormann and Haass, 2013; Fujioka et al., 2013). However, the pathological mechanisms of mutated FUS on neuronal physiology are not well understood.

FUS is expressed on chromosome 16 and is a part of FET-family (or FET proteins), a group of DNA/RNA-binding proteins that include FUS, EWSR1 and TAF15 (FET) (Crozat et al., 1993; Law et al., 2006). These proteins have common structural domains, which include N-terminal low-complexity (LC) domain, Arg-Gly-Gly (RGG) domains, a zinc finger (ZnF) domain, RNA recognition motif (RRM) and nuclear localisation signal (NLS) (Schwartz et al., 2015). Each domain has specific roles (Sama et al., 2014): RRM is an RNA binding site; RGG and ZnF contribute to FET-RNA binding and diversify binding RNA partners; LC and RGG domains promote self-assembly of FET proteins; NLS contributes to the localisation of FUS into nucleus (Fig. 1-5).

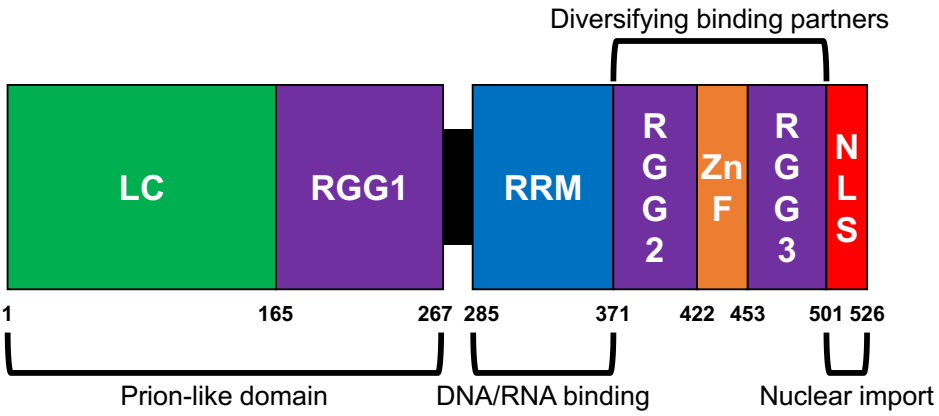

Figure 1-5 Schematic structure of FUS protein.

As a family of FET protein, FUS is consist of LC, RGG1-3, RRM, ZnF and NLS domains.

The major role of FUS is thought to be DNA/RNA processes such as DNA repair, transcription, miRNA processing, splicing, RNA transport and local translation (Dormann and Haass, 2013; Lagier-Tourenne et al., 2010). These regulatory roles are known to be done with direct binding with DNA/RNA or indirect interaction through intermediate molecules. For DNA repair, FUS is recruited to DNA double-strand breaks and interact with histone deacetylase 1 (HDAC1) or poly-ADP-ribose polymerase (PARP) (Mastrocola et al., 2013; Wang et al., 2013). For the transcription of RNA, FUS binds to the C-terminal domain of RNA polymerase II and RNA is thought to assist that binding (Kwon et al., 2013; Schwartz et al., 2012). FUS is also involved in RNA splicing by directly/indirectly binding with pre-mRNA or being a part of the spliceosome machinery (Kameoka et al., 2004; Wu and Green, 1997; Zhou et al., 2002). Relationship with miRNA is also indirectly done by binding with a protein, which is involved in miRNA maturation (Gregory et al., 2004). RNA transport and local translation has been suggested to be dependent on various neuronal activity and its mechanism has been proposed as the binding of FUS with RNA and transported via microtubule proteins (Belly et al., 2005; Fujii et al., 2005; Kanai et al., 2004). Although FUS has some preferences for binding with certain sequence or motifs of DNA/RNA,

however, binding tendency depends more likely on overall affinity than well-defined specificity of the sequence (Wang et al., 2015).

1.5.2. Potential roles of FUS in neurons

The distribution of FUS in either the nucleus or cytoplasm differs from cell type to type (Andersson et al., 2008). In neurons, FUS is mainly located in the nucleus and it can move between nucleus and cytoplasm by nucleo-cytoplasmic shuttling (Zinszner et al., 1997). The intracellular trafficking of FUS was further discussed in the section 3.1.1., Chapter 3. This trafficking of FUS is known to be involved in the transportation of various essential mRNAs to the synaptic region and possibly mediated and accelerated by mGluR5 activation (Fujii and Takumi, 2005). Those target mRNAs are related to the components of the synapse such as actin-related proteins, therefore, knock out of FUS caused abnormal morphology of dendritic spines (Fujii and Takumi, 2005), indicating FUS activity is related to synaptic morphology, as well. The roles of cytosolic FUS in the morphologic changes were further discussed in the section 3.1.2., Chapter 3. In addition, FUS is involved in various RNA processing and regulation, such as, RNA splicing and polyadenylation (Fujioka et al., 2013; Masuda et al., 2016) and local translation in the soma and neurites like axons and dendritic branches (Kamelgarn et al., 2018; López-Erauskin et al., 2018; Yasuda et al., 2013). In the postsynaptic dendrites and spines, FUS stabilises mRNA of GluA1 to regulate AMPAR function (Udagawa et al., 2015) and also associates with NMDAR to regulate the expression of the other mRNAs (Belly et al., 2005), thus, synaptic activity can be affected by FUS. Also, FUS can directly bind to Tau RNA and get involved in the alternative splicing of the mRNA and expression of the protein (Ishigaki et al., 2017). Knockdown of FUS increased the expression of Tau exon 3 and 10, which in turn, increase of the longest isoform of Tau 2N4R that is more likely to be aggregated in Alzheimer's disease pathology compared to the other isoforms of Tau (Orozco et al., 2012). Therefore, it can be suggested that FUS might have roles in dendritic

spine dynamics by transporting and processing of RNAs at the dendritic spines which in turn, affect the stability and the morphology of dendritic spines. These dynamic, morphological, structural and translational changes at dendritic spines by FUS can be related to the synaptic plasticity, but it needs to be investigated further.

FUS is assembled to form either homogenous or heterogeneous aggregates to respond to cellular changes (Fig. 1-6). In cellular stress conditions (e.g. Osmotic stress, irradiation) cytoplasmic FUS protein is recruited into stress granules (SGs) (Higelin et al., 2016; Sama et al., 2013). The roles of SGs are not clearly understood, but thought to be related to the protection of mRNAs against cellular stress by storing mRNAs into the granules, processing, splicing and translation of RNA by recruiting RNA and RNA-binding proteins (RBPs) (Nover et al., 1989; Protter and Parker, 2016; Schwartz et al., 2015). After the stress is resolved, these granules are disassembled and FUS protein can return to be transportable between cytoplasm and nucleus (Deng et al., 2014; Niu et al., 2012). This kind of SGs or SG-like aggregates consist of various RBPs (e.g. FUS, TDP-43, TIA1) (Lagier-Tourenne et al., 2010; Wolozin, 2012) to form hydrogel-like structures, which is stable and reversible in the cells (Murakami et al., 2015). The concentration of FUS in the cytoplasm also affects the formation of SGs and high cytoplasmic concentration by either overexpression or NLS mutation can increase the formation of SGs in the presence of stress conditions (Andersson et al., 2008; Li et al., 2013; Sama et al., 2013). In addition, increased cytosolic FUS and cation-π interaction between FUS proteins also involved in FUS condensations and phase separations and it is regulated by post-translational methylation of arginine residues in FUS (Dormann et al., 2012; Rappsilber et al., 2003). The FUS-FUS interaction and the relationship between hypomethylation and enhanced cation-π interaction were further discussed in the section 5.1.1. and 5.1.2., Chapter 5.

Overall, FUS can translocate from nucleus to cytoplasm and dendritic spines with the abilities to bind to various RNA and ribonucleoprotein particle (RNP)

targets to form granules. If these mechanisms have disrupted or overdriven by mutations in FUS, deleterious pathology will be initiated.

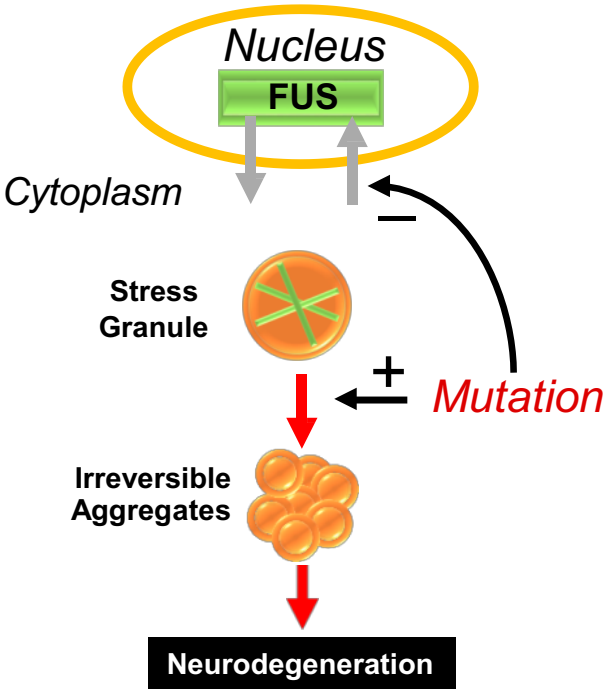

Figure 1-6 Schematic model of the FUS pathology through the formation of stress granule.

FUS is predominantly localised in the nucleus and shuttles between cytosol and nucleus. In the cytosol, FUS can be recruited to stress granules (SGs) as a part of cellular response to the cellular stress. Mutations on FUS inhibit the nuclear localisation of FUS and accelerate irreversible aggregation of FUS and eventually induce neurodegeneration.

1.5.3. Mutations in FUS and neurodegenerative diseases

Several mutant forms of FUS were found in subtypes of ALS and FTLD cases, accompanying deposition of insoluble FUS in motor neurons and neurodegeneration (Deng et al., 2014; Higelin et al., 2016). The effects of the mutations were dependent on the domain of the sites. The mutations at LC domain abolishes binding of transcription factors or impairs the assembly of FUS, either abolition of reversible hydrogel formation or acceleration of fibrilisation (Murakami et al., 2015). The mutations at NLS impairs the

localisation of FUS into the nucleus and enhances the accumulation of FUS in the cytoplasm (Dormann et al., 2010; Higelin et al., 2016). The mutations in RGG2, ZnF, RGG3 domains can impair the affinity of FUS towards RNAs or SGs, formed in response to cellular stress (Schwartz et al., 2015). As a whole, mutations of FUS could result in accumulation of cytoplasmic portion of FUS proteins and make them recruited into SGs, SG-like aggregates or irreversible fibrils. Eventually, those cytoplasmic FUS induce DNA damage, impair DNA-repairing and apoptosis (Higelin et al., 2016; Scekic-Zahirovic et al., 2016). Therefore, the mutations in FUS gene cause either gain of function or loss of function.

As stated above, the concentration of cytosolic FUS is related to the increased formation of SG and mutation at NLS domain promotes the accumulation of FUS in cytoplasm. In other words, FUS-containing irreversible aggregates or SGs were found in FUS-ALS or FUS-FTLD patients (Mackenzie et al., 2010a; Vance et al., 2013) and FUS with NLS mutant accelerated the pathologies in the neuronal cytoplasm (Deng et al., 2010; Kwiatkowski et al., 2009). Thus, cytoplasmic aggregates of FUS, especially NLS mutant forms, have been investigated to find out the mechanisms of FUS pathology (Blokhuis et al., 2013; Vance et al., 2013).

1.5.4. Implied mechanism and importance of FUS

ALS (also known as Lou Gehrig's disease) is a neurodegenerative disease that characterised by the loss of motor neurons in the cerebral cortex, brain stem and spinal cord (Van Langenhove et al., 2012; Ling et al., 2013). This neuronal loss causes atrophy and dysfunction of voluntary muscles and most patients die within few years from the onset of the first symptom. The causes of the disease are still being characterised, though mutations in C9orf72, SOD1, TARDBP and FUS/TLS genes have been found in ALS patients, along with pathological inclusions of TDP-43, SOD1 and FUS proteins (Ling et al., 2013).

FTLD (or referred as FTD in clinical practice) is another neurodegenerative disease that neuronal loss happens in the frontal and temporal lobe (Van Langenhove et al., 2012; Ling et al., 2013). This leads to behavioural change and dysfunction of language skills. From FTLD patients, mutations of MAPT and progranulin (PGRN) were mainly found and TDP-43, Tau, FUS and ubiquitin-proteasome system (UPS) pathologies were also found (Ling et al., 2013).

Both ALS and FTLD share several pathologies related to RNA processing and protein regulatory dynamics especially, such as TDP-43 and FUS DNA/RNA binding proteins (Lagier-Tourenne et al., 2010; Ling et al., 2013). Mutations or aggregations of TDP-43 and FUS can develop DNA/RNA and protein dynamics-related pathologies for example, malfunction of DNA repairing mechanism, alternative splicing and abnormal changes of mRNA expression to protein, which will cause disruption of cellular homeostasis and degeneration, eventually. Therefore, investigating common pathologies of FUS or TDP-43 would be needed to find the shared pathophysiological changes in both ALS and FTLD in addition to the other major targets from other neurodegenerative diseases.

1.6. Aims and summary

As articulated, FUS has the various roles to regulate the dynamics of DNA/RNA and also involved in the deleterious pathologies of ALS/FTLD. Since both ALS and FTLD includes neurodegeneration, the synapse weakening process might be done prior to the neuronal death. However, there are many missing gaps and mechanisms not well explained. The aim of this thesis is to investigate the early physiological and morphological alterations by the abnormal expression of FUS that eventually forms cytosolic inclusions throughout the dendrites. By biolistically transfecting 2 different mutant forms, 2 major pathologies found in the FUS-opathy were tested in the organotypic hippocampal slices model to utilise well-characterised neuronal circuit of neurotransmission and synaptic plasticity.

First, cytosolic accumulation of FUS was investigated using FUS-P525L mutant form, which has mutation on NLS region that is required for nuclear internalisation of FUS. In the Chapter 3, the intracellular trafficking and morphological changes by FUS-P525L expressions were discussed. FUS-P525L was shown to have quicker translocation though the dendrites than that of FUS-WT and this difference resulted in the reduction of spine density in the distal part of the apical dendrites in FUS-P525L neurons. In the Chapter 4, the electrophysiological changes by FUS-P525L expressions were discussed. FUS-P525L was shown to have increased synaptic conductance and intrinsic excitability and the excitability was returned to the control level when CP-AMPAR blocker IEM-1460 was applied. And had decreased basal synaptic transmission and inhibited induction of both LTP and LTD.

Second, FUS mutant with enhanced cation-π interaction was investigated by using FUS-16R mutant form, which has 16 additional arginine residues therefore increases the affinity between FUS proteins to form inclusions in the cytosol. In the Chapter 5, both morphological and electrophysiological changes by FUS-16R were discussed. The spine density of FUS-16R cells were shown to be reduced in both basal and apical dendrites compared to FUS-WT cells. In addition, intrinsic excitability and basal synaptic transmissions were reduced in FUS-16R cells.

Together, the results suggest that abnormal expression of FUS mutant is widely involved in the morphological, electrophysiological synapse weakening and it is related to the neuronal activity and excitability.

CHAPTER 2

Materials and methods

2.1. Animal-derived materials

2.1.1. Animals

All procedures involving animals were performed in accordance with the UK Scientific Procedures Act, 1986. Male Wistar Han rats of postnatal 6-8 days (P6-P8) were used to prepare organotypic slice culture on the day of delivery.

2.1.2. Organotypic hippocampal slice culture preparation

Animals were sacrificed by cervical dislocation (Schedule 1) and then decapitated. The upper skin and then the skull of the head was cut sagittally from the middle back of the head. Frontal bone was cut coronally and the upper skull was opened with forceps. The whole brain of rat was quickly transferred to the ice-cold cutting solution (238 mM sucrose, 2.5 mM KCl, 26 mM $NaHCO_3$, 1 mM NaH_2PO_4, 11 mM D-glucose, 5 mM $MgCl_2$ and 1 mM $CaCl_2$). Hippocampi were dissected and cut into 350 µm coronal slices with McIlwain tissue chopper. The hippocampi were transferred to culture medium (78.8% minimum essential medium (MEM), 20% horse serum (heat-inactivated), 30 mM HEPES, 26 mM D-glucose, 5.8 mM $NaHCO_3$, 2 mM $CaCl_2$, 2 mM $MgSO_4$, 70 µM Ascorbic Acid, 0.1% 1 mg/ml Insulin, pH 7.3 and 320–330 mOsm) and separated into individual slices. Hippocampal slices were washed by transferring slices into the 35 ml petri dishes with fresh culture medium for 4 times. The washed slices were placed onto a semi-permeable membrane inserts (Millipore, PICM0RG50) in a 6-well plate with culture medium. The slices were stored in an incubator at 35 ºC 5% CO_2 and medium was changed every 2-3 days.

2.2. Biolistic transfection

2.2.1. Genes of interest

Neurons were transfected with plasmids that contain gene of interest. Plasmid DNA constructs were kindly provided from Professor Peter St

George-Hyslop (Clinical neurosciences, Cambridge Institute for Medical Research, UK). Information of the plasmid constructs were shown as a Table 2-1. For the mutations, FUS-P525L has only mutation of P525L, on the other hand, FUS-16R mutation has mutations on G167R, G170R, G173R, G202R, S205R, S221R, G225R, G228R, G230R, M254R, G379R, N381G, insert387G, G398R, G401R, S402G, G404R, G456R, M464R, therefore, FUS-16R has 16 additional arginine residues.

FUS genes were loaded to 2 different types of plasmid vectors to tag either EYFP or mCherry as displayed in Fig. 2-1. Later for the transfection, those plasmid DNA constructs were loaded to gold microcarriers with the amount as shown on Table 2-1 and the procedure is explained in the chapter 2.2.4. Venus, mCherry and TdTomato are types of structural fluorescence marker protein and Venus is further used as transfection control.

Name	Backbone	Insert	Species	Tag	bacteria resistance	Amount used (µg)
YFP_FUS-FL-P525L	peYFP-C1	FUS-P525L	Human	N-term YFP	Kanamycin	20
YFP_FUS-FL-WT	peYFP-C1	FUS	Human	N-term YFP	Kanamycin	20 or 40
YFP_FUS-FL-16R	peYFP-C1	FUS-16R	Human	N-term YFP	Kanamycin	20 or 40
mCherry_FUS-FL-WT	pmCherry-C1	FUS	Human	N-term mCherry	Kanamycin	20 or 40
mCherry_FUS-FL-16R	pmCherry-C1	FUS-16R	Human	N-term mCherry	Kanamycin	20 or 40
Venus	-	-	Jellyfish	-	Ampicillin	10
mCherry	-	-	Discosoma	-	Ampicillin	60
TdTomato	-	-	Discosoma	-	Ampicillin	10

Table 2-1 Information of DNA plasmid constructs used in the study.

Basic information of DNA genes of interest and used amount were displayed.

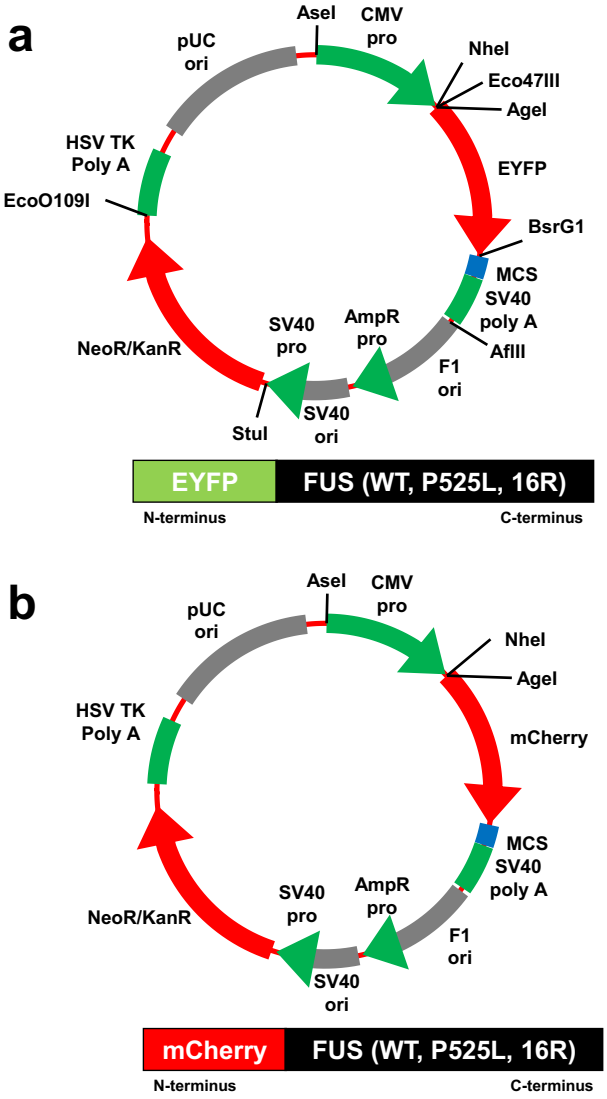

Figure 2-1 Plasmid vectors used for tagging FUS proteins.

Plasmid vectors were utilised to add either EYFP or mCherry at the N-terminus of FUS proteins. (a) peYFP-C1 vector was used and as a result, N-terminus of each type of FUS protein was tagged. (b) pmCherry-C1 vector was used and as a result, N-terminus of each type of FUS protein was tagged.

2.2.2. Plasmid amplification

The whole process of this amplification takes 3 consecutive days. DH5α (Invitrogen, 18265-017) E.coli strain was used for the amplification of the plasmids.

First day was to transform DH5α with the target plasmid. 50 µl of DH5α (expected to yield >1 x 10^6 transformants / µg) was aliquoted to a 1.5 ml tube from thawed stock on the ice. 1-10 ng of target plasmid was added and gently mixed, then, incubated on ice for 30 minutes. Next, 20 seconds of heat shock at 42 °C was applied on a heat block and then placed on ice for 2 minutes. 950 µl of SOC medium (Invitrogen, 15544-034) was added to maximise the transformation efficiency of the plasmid and then the tube was incubated in the 37 °C shaker for 1 hour. 120 µl of media with transformed E.coli was plated on the premade agarose gel plate with the antibiotics either 50 µg/ml of kanamycin (Sigma-Aldrich, K0254) or 100 µg/ml ampicillin (Sigma-Aldrich, A9518) for the target plasmid. After 10 minutes, the agarose plate was incubated overnight in the 37 °C oven.

Second day was to prepare for the starter culture. The agarose plate was checked whether transformed E.coli with target plasmid formed colonies. One of the colonies was transferred into a 1.5 ml tube with 1ml of LB Broth and 1 µl of appropriate antibiotic. The tube was incubated in the 37 °C shaker for 6-7 hours as the starter culture. The starter culture was transferred into an autoclaved glass flask with 80ml LB broth and 80 µl of appropriate antibiotic and then incubated overnight in the 37 °C shaker.

Third day was to purify the target plasmids with Plasmid midi kit (QIAGEN, 12943) and it was conducted based on the product manual with few minor variations. The incubated flask from the previous day was checked whether the broth was cloudy, indicating amplified E.coli cells. The broth was split into two 50 ml falcon tubes, then, centrifuged at 2800 rpm for 15 min. The supernatant was discarded. 2 ml of buffer P1 was added into each tube to resuspend the pellets and then the contents were mixed into one tube. 4 ml of buffer P2 was added, gently mixed and then incubated at RT for 3 minutes to lyse the E.coli cells. 4 ml of buffer S3 was added and mixed to precipitate cell debris. The mixture was centrifuged at 2800 rpm for 5 minutes and

filtered into a new tube to remove precipitant. 2 ml of buffer BB (binding buffer) was added and gently mixed together. To separate the target plasmid, the mixed buffer was gone through the QIAGEN plasmid plus midi spin column with suction from a vacuum pump. The column with target plasmid was washed with 0.7 ml of buffer ETR by centrifuging at 13,000 rpm for 45 seconds and the flow-through was discarded. The washing step was repeated for twice with 0.7 ml of buffer PE. Further spinning at 10,000 rpm for 2 minutes to remove the remaining buffer. Then, the column was placed on the new 1.5 ml tube. 110 µl of buffer EB buffer (elution buffer) was added on the column and incubated at RT for 3 minutes and then, the column and the tube were spun at 13,000 rpm for 45 seconds. The flow-through was transferred again on the column and incubated at RT for 2 minutes, then, they were spun at 13,000 rpm for 1 minute. The flow-through was again, transferred on the column and incubated for 1 minutes, it then, spun at 13,000 rpm for 1 minute. The concentration of the eluted plasmid was defined by using NanoPhotometer (Implen, P300).

2.2.3. Concept of biolistic transfection: Gene gun

Biolistic transfection (biological and ballistic transfection) is a technique to deliver DNA into target cells by using small-sized carriers such as gold particles. This is mechanical method, therefore, versatile and simple to be used on diverse kinds of cells and tissues that includes hippocampal organotypic culture slices. The big advantage of biolistic transfection is that this method physically delivers genes, therefore, it can be reliably applied to a variety of neuron and tissue types with higher success rate and less limitations compared to the other transfection methods (McAllister, 2000). In addition, it is also easy to combine and deliver few different DNAs together, thus, easier to express target genes with different visual markers (e.g. fluorescence proteins). The core component of this technic is gene gun, which is designed to release pressurised inert gas flow to shoot DNA-containing carrier particles into the cells. Those carrier particles are usually

prepared to be bound with target genes using spermidine, then, loaded in the plastic Tefzel cartridge, so called bullets. Once carrier particles are shot from the gene gun, then, the particles penetrate through the tissues and cell membranes and release plasmid that contains target gene to be expressed. The concept summary of biolistic transfection is shown in Fig. 2-2.

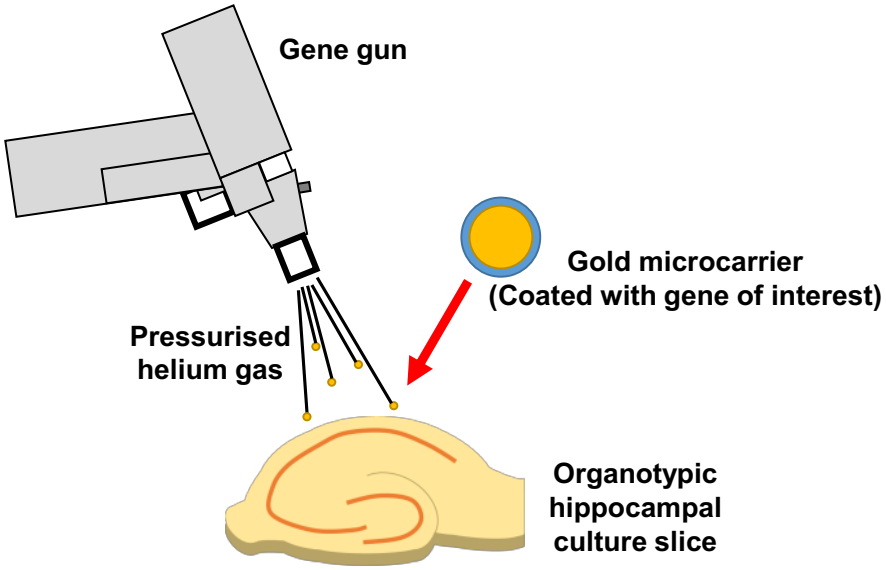

Figure 2-2 Biolistic transfection.

Organotypic hippocampal slices were biolistically transfected by using Helios gene gun system (Bio-Rad). Gold microcarriers were coated with gene of interest (DNA plasmids), loaded on gene gun and pressurised helium gas propels microcarriers just enough to penetrate cell membrane and transfect the cell. Usually, target genes are tagged with fluorescence tags, therefore, transfected cells can be identified.

2.2.4. Microcarrier preparation

Tefzel tubing (Bio-Rad, 1652441) was inserted into the tubing prep station (Bio-Rad) and dried with nitrogen gas, while rotating, for minimum 30 minutes. To prepare the DNA/RNA construct solutions, constructs of interest were mixed at the desired ratio (total volume 100 µl, maximum DNA/RNA content 100 µg). A 100 µl of 50 mM spermidine was added to 10 mg of gold microcarriers (1.6 µm) (Bio-Rad, 1652264), vortexed for 10 seconds and then bath-sonicated for 10 seconds. Then DNA/RNA construct solution was

added and the mixture was vortexed together for 10 seconds. Calcium chloride (100 µl of 1 M) was added dropwise while the mixture was gently vortexed. The mixture was left at RT for 10 minutes to precipitate the solution. The mixture was mini-centrifuged for -15 seconds and then supernatant was removed. The pellet was resuspended and washed with 1 ml of 100 % ethanol for 3 times (mini-centrifuged for 5 seconds and the supernatants removed every time). After the last wash, the supernatant was removed and remaining gold microcarrier mixture was resuspended and mixed with 3 ml 20 µg/ml polyvinylpyrrolidone in 100 % ethanol. The mixture was aspirated into 10 ml syringe with 3-5 cm silicone tubing attachment. The aspirated mixture was loaded into the Tefzel tubing on the prep station and held in place for 2 minutes. The solution was slowly aspirated, and the tubing was turned 180º and left for 30 seconds. The tubing was rotated for 1 minute followed by, an additional 5 minutes of rotation with a nitrogen gas flow to dry out the remaining liquids inside the tubing. The tubing was cut into 0.5'' cartridge (gene gun bullets), desiccated and stored for the further experiments.

2.2.5. Gene transfection

Hippocampal neurons were transfected with a gene gun (Helios gene gun system, Bio-Rad). Each gene gun bullet cartridge contains DNA/RNA constructs bound to 1.6 µm gold microcarriers. To shoot the gene gun, bullets were loaded into the cartridge holder and assembled to the gene gun. The gene gun was connected to the helium cylinder at the pressure of 140-180 psi. Once gene gun was ready, 6-well culture plates with hippocampal slices were taken out of the incubator. The culture membranes were aimed with the gene gun (distance between the front tip of the gene gun's barrel liner and the membrane was 1 cm), then the gene gun was triggered to shoot the gold microcarriers to the culture tissues. Once the process was done, the culture plates were returned to the incubator.

Transfection was done at Day In Vitro (DIV) 3-5 to let organotypic hippocampal slices stabilise on the membrane before the transfection process. Once the transfection was done, hippocampal slices were left in the incubator for Day After Transfection (DAT) 2-7 depends on the experiment type. For the electrophysiology experiments, DAT 3-4 time window was used for early stage, DAT 5-7 time window was used for late stage. The summary of the timetable is shown in Table 2-2. DAT 5-7 time window was mainly selected to make sure the pathogenic inclusions translocated through dendrites, which will be described in the results chapters. To be clear, these different time windows represent the progression of pathology, however, they are relatively early progression before neuronal death, therefore, those time points are not directly matched with early onset or late onset of the real disease and patients.

Day In Vitro (DIV)	0	1	2	3	4	5	6	7	8	9	10
Day After Transfection (DAT)				0	1	2	3	4	5	6	7
Slice culture preparation											
Transfection											
Experiments (Early)											
Experiments (Late)											

Table 2-2 Summary of transfection timetable.

Time course of Days in vitro (DIV) and Day After Transfection (DAT) were displayed with the critical steps of the experiments with blue boxes.

2.3. Electrophysiology

2.3.1. Electrophysiology rig setup

The recording chamber for the electrophysiology experiments (Warner Instruments, RC-26G) was attached on a glass coverslip (Warner Instruments, CS-22/40) with the sealing of vacuum grease (Dow Corning).

Perfusion of artificial cerebrospinal fluid (ACSF) (119 mM NaCl, 2.5 mM KCl, 26 mM $NaHCO_3$, 1 mM NaH_2PO_4, 11 mM D-glucose, 4 mM $CaCl_2$, 4 mM $MgCl_2$, 0.02 mM picrotoxin, 0.01 mM 2-chloroadenosine) was supplied from a glass bottle with 95 % O_2 / 5 % CO_2, perfused by peristaltic pump (Watson-Marlow, 323S/D) at about the flow rate of 2-3 ml / min through polythene tubing (Fisher Scientific, 800/100/460), Norprene tubing (Cole-Parmer, 06410-01) and PTFE tubing (Cole-Parmer, 06417-31). The bottle with ACSF was heated to 37 °C in a water bath (Nickel-Electro, Clifton NE1-4) and perfusion tubing was heated with a pen heater (ALA Scientific Instruments, HPT-2A) and a control unit (npi electronic, TC-10) to adjust the temperature to 28-30 °C when the perfusion enters the recording chamber. A syringe needle with a suction pump (Charles Austen, Dymax 5) was placed to remove the excessive ACSF from the recording chamber. To visualise the recording chamber, a microscope (Nikon, Eclipse E600FN) and a camera (Hitachi, KP-M1AP) were used. The X-, Y- movement of the table was adjusted by an in-house built X-, Y-plate and Z- movement was adjusted by automated motor unit (Prior, Optiscan) attached to the microscope. To reduce the recording noise from vibrations, the whole microscope and X-, Y-plate were placed on the air table (Newport, VH3036W-OPT) and the air was supplied by an air compressor (Bambi, 35 / 20). An in-house built Faraday cage was used to cover the whole unit above the air table and to shield the inside from electrical fields. For the stimulation, two-strand-twisted Nickel80 / Cromium20 wire (Advent Research Materials, NI653514) and the wire was inserted through a glass capillary and fixed and it was prepared as a pair of stimulating electrodes. The pair of stimulating electrodes were held by a pair of manipulators (Scientifica, LBM-7). The end of the wire was soldered to general electric wires and connected to a pair of constant voltage isolated stimulators (Digitimer, DS2A – Mk.II) that generate 0.1 ms square-wave constant voltage pulses as triggered by commands. For making recording glass electrodes, Flaming/Brown micropipette puller (Sutter Instruments, P-1000) was used to pull the glass capillaries (Harvard Apparatus, 30-0057) to

the pipette resistance of 4-7 MΩ (Ideally about 5.5 MΩ). The electrodes were then filled with internal filling solution (see chapter 2.3.2.) and fixed to an electrode holder (Molecular Devices, 1-HL-U) that is connected to a headstage (Molecular Devices, CV-7B) and the headstage was connected to an amplifier (Molecular Devices, Axon multiclamp 700B). A 0.2 mm silver wire (Advent Research Materials, AG548815) was coated with chloride in advance and fixed to the electrode holder to touch the filling solution inside the glass electrodes. The back of the headstage was connected to another long silver wire, which was also coated with chloride in advance and then the coated part was submerged inside the recording chamber to be a ground reference. The whole electrode on headstage unit was mounted on the automated micromanipulator (Scientifica, PatchStar).

The data acquisition was done at 20 kHz with Multiclamp 700B amplifier and a CA-1000 data acquisition device (National Instruments) and filtered at 2 kHz. For the recording and saving of the data from electrophysiology experiments, WinLTP version 2.10 software (Anderson and Collingridge, 2007) was used.

A cultured hippocampal slice was placed in the recording chamber and an in-house built mesh net was placed to surround the slice and prevent the movement by the flow of ACSF. For the experiments requiring preincubation, cultured hippocampal slices were placed in 5 ml of ACSF (room temperature, bubbled with 95 % O_2 / 5 % CO_2) with the drugs of interest (e.g. IEM-1460). Concentration and incubation time are described in the results chapters as the drugs used. The preincubated slice was transferred to the recording chamber perfused with ACSF containing the same drugs.

2.3.2. Whole-cell patch and recording

For whole-cell patch clamp, hippocampal slice was placed in the recording chamber with ACSF perfusion of the consistent flow rate and temperature as described in the chapter 2.3.1. One each stimulating electrode was placed

on the Schaffer-collateral pathway (experimental pathway) and subiculum-CA1 pathway (reference pathway) when required.

For voltage clamp experiments, the recording electrode was filled with Cs methanesulfonate filling solution (130 mM Cs methanesulfonate, 10 mM HEPES, 0.5 mM EGTA, 4 mM Mg-ATP, 0.3 mM Na-GTP, 6 mM QX-314 chloride, 8 mM NaCl, pH 7.2 and 285-290 mOsm). For current clamp experiments, K-Gluconate filling solution (135 mM K-Gluconate, 10 mM HEPES, 0.5 mM EGTA, 2 mM Mg-ATP, 0.3 mM Na-GTP, 8 mM NaCl, pH 7.2 and 275-290 mOsm) was used.

The recording electrode was positively pressurised to prevent blockage of the tip of the electrode by using a 1 ml syringe connected to the electrode holder via Tygon lab tube (RS components, ACF00002-C). Once the electrode pipette dipped into the solution in the recording chamber, the resultant current through the tip was set to zero by using the software Multiclamp 700B. Pipette resistance was also checked whether that was within the ideal range (4-7 MΩ) with WinLTP by applying 10 mV square-wave pulse of 100 ms through the headstage. Target CA1 cell in the pyramidal cell layer was identified by Venus or YFP (yellow fluorescence protein) fluorescence with a blue light source (CoolLED, pE-300) for the transfected cells or in-built bright-field of the microscope for untransfected cells. Once target cell was identified, the tip of the electrode was approached carefully. When the tip of the electrode was close enough to show a dent on the target cell by the positive pressure from the tip, the pressure was released (and gentle negative pressure applied if needed) to make a giga-seal (GΩ) between pipette tip and the membrane of the cell body. Once giga-seal was accomplished, holding voltage was set to -30 mV and gradually changed to -70 mV. Then, capacitive transient of pipette was compensated. Negative pressure was applied to break the cell membrane between pipette internal solution and cytosol of the cell. If the patch was successful, test pulse (generated by 10 mV square-wave) on WinLTP should show capacitive transient pattern that the peak would be calculated to the series resistance

(Rs) and current difference would be calculated to the membrane resistance (Rm) (Fig. 2-3). For Rs, only patched cells under 23 MΩ with the change of max 20 % were used for analysis not to record signals with blockage of the recording pipette. For Rm, only cells over 50 MΩ were further recorded and used to ensure stable attachment of the tip on the cellular membrane without rupturing excessively (Finkel et al., 2006; Ionescu-Zanetti et al., 2005).

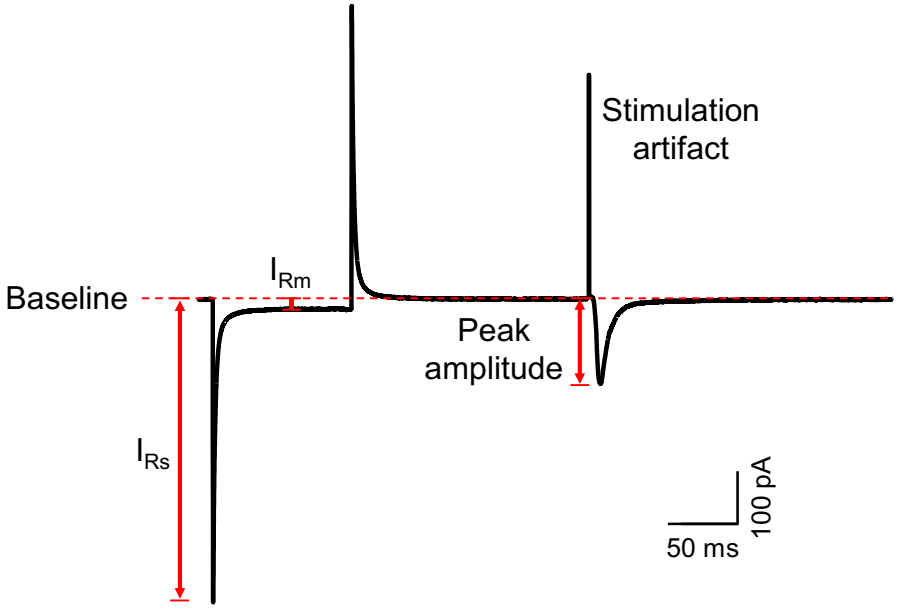

Figure 2-3 Parameters of whole-cell patch recording.

An example single trace of whole-cell recording. Series resistance (Rs), membrane resistance (Rm) and peak amplitude were measured from each single trace.

After each cell was patched, resting membrane potential (RMP) was also checked by temporarily removing voltage holding of the recording pipette. Only cells with RMP hyperpolarised than -40 mV because less polarised cells easily showed epilepsy upon electric stimulations. These passive properties of patched cells (Rs, Rm and RMP) are supposed to evaluate the quality of the whole-cell patch. Therefore, once the passive properties of the patched cells met the proper condition as stated above, difference between groups should not significantly influence the actual data sets of the electrophysiological recordings. To confirm the quality of the whole-cell patch recording, example passive properties from each major transfection groups

were plotted as a supplementary data (Fig. 2-4). The recorded data sets are part of AMPA/NMDA current tests in Chapter 4 and 5. From each cell, RMP values were acquired right after whole-cell patch and for Rs and Rm values, 10 sweeps of test pulses per 30 seconds were recorded and averaged. Most of transfected cells were paired with untransfected cells, thus n-number of untransfected cell group is bigger than other FUS transfected cell groups. The data set was shown as Mean ± SEM. From multiple neurons from different groups (Untransfected: 49 cells, FUS-WT: 12 cells, FUS-P525L: 15 cells, FUS-16R: 15 cells), recorded RMP (Untransfected: -58.65 ± 1.03 mV, FUS-WT: -61.42 ± 2.91 mV, FUS-P525L: -56.67 ± 1.08 mV, FUS-16R: -63.68 ± 1.60 mV, $F = 3.378$, $p = 0.0217$), Rs (Untransfected: 14.45 ± 0.45 MΩ, FUS-WT: 17.08 ± 1.07 MΩ, FUS-P525L: 16.19 ± 0.87 MΩ, FUS-16R: 14.64 ± 0.76 MΩ, $F = 2.727$, $p = 0.0486$) and Rm (Untransfected: 177.45 ± 10.10 MΩ, FUS-WT: 158.40 ± 25.20 MΩ, FUS-P525L: 237.58 ± 40.27 MΩ, FUS-16R: 101.12 ± 9.40 MΩ, $F = 7.117$, $p = 0.0002$) distributed within the proper range of whole-cell patch to be used as electrophysiology data sets.

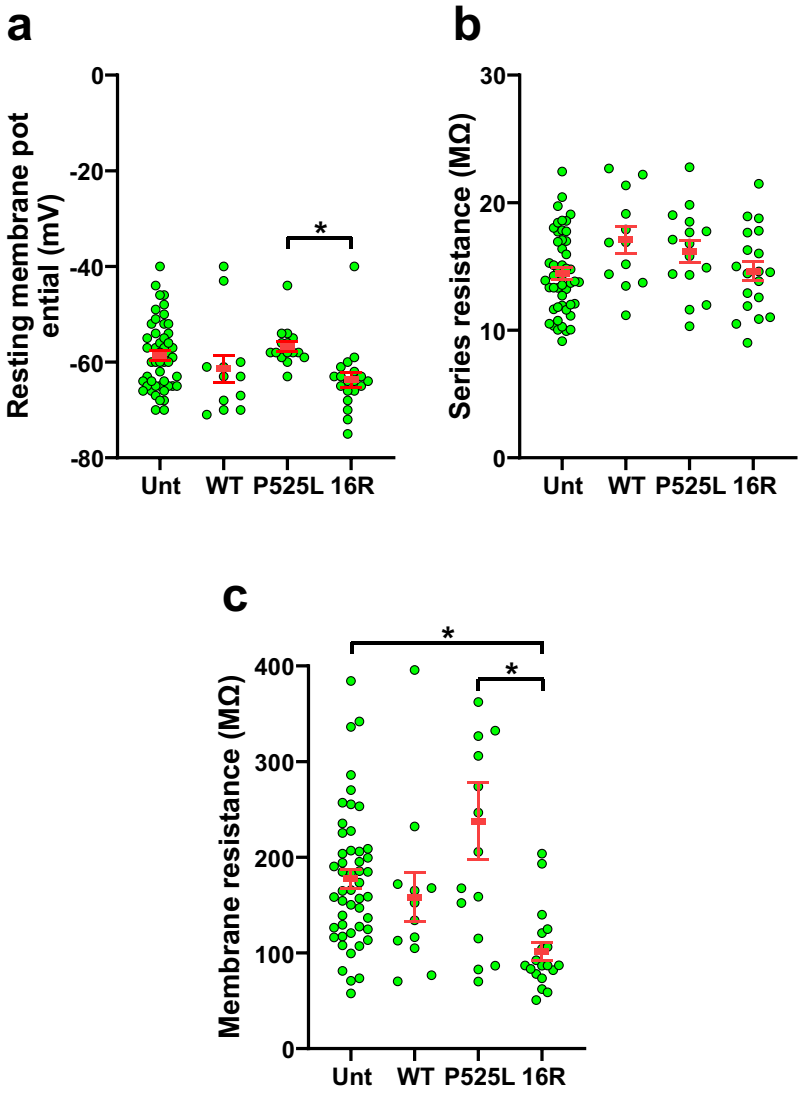

Figure 2-4 Example passive properties of neurons during whole-cell patch recording.

Passive properties were recorded to confirm the quality of whole-cell patch. (a) Resting membrane potential (RMP). (b) Series resistance (Rs). (c) Membrane resistance (Rm).

2.3.2.1. EPSCs

Excitatory postsynaptic currents (EPSCs) were generated by stimulating electrodes previously placed on Schaffer-collateral pathway (experimental

pathway) and subiculum-CA1 pathway (reference pathway) at a holding voltage of -70 mV. Two pathways were stimulated alternately at 15 seconds interval. Only cells show fast rise / decay kinetics with monosynaptic responses were used. The peak amplitude was used for the parameter of the synaptic efficacy. For $EPSC_{NMDA}$, the peak at 90-100 ms after stimulation artefact was measured. Rm, Rs, DC were also measured to monitor the quality of the whole-cell patch.

For AMPA/NMDA current tests, 10 $EPSC_{AMPA}$ recorded at -70 mV voltage and changed to +40 mV voltage holding, waited for > 2 minutes and further 10 $EPSC_{NMDA}$ were recorded. Total 20 EPSC per one experiment were recorded. One transfected cell and the other untransfected cell in one slice were always recorded as a pair.

2.3.2.2. mEPSCs

For miniature EPSCs (mEPSCs) experiments, target cells were voltage clamped at -70 mV, then, ACSF with 500 nM tetrodotoxin, 50 μM D-AP5 and 20 μM bicuculline was perfused for 7 minutes. The perfusion was to remove the EPSCs induced by excitation of presynaptic neuron. Therefore, this procedure makes the presynaptic neurons to release neurotransmitters without any contamination of action potential-mediated release of synaptic vesicles. After the perfusion, then mEPSCs were continuously recorded without any electrical stimulation for 6 minutes.

2.3.2.3. LTP / LTD

For the baseline recording, two stimulating electrodes were alternately delivered stimulations every 15 seconds. For LTP experiments, a stable baseline was recorded for 5 minutes and then, 200 pulses of 2 Hz stimulation at the holding voltage of 0 mV (Kullmann and Nicoll, 1992; Malinow and Tsien, 1990) were delivered to the Schaffer-collateral pathway. EPSCs were further

recorded for 35 minutes at the holding voltage of -70 mV. For LTD experiments, a stable baseline was recorded for 10 minutes and then, 200 pulses of 1 Hz stimulation at the holding voltage of -40 mV (Hjelmstad et al., 1997; Lüthi et al., 1999) were delivered to the Schaffer-collateral pathway. EPSCs were further recorded for 40 minutes at the holding voltage of -70 mV. Only one cell per hippocampal slice was recorded due to the irreversible stimulations were applied, therefore, transfected cells and untransfected cells were recorded from separated slices. To increase the comparability between control vs transfected cells, always one cell from each group was recorded from same animal and same preparation.

2.3.2.4. Firing activities

For firing activity experiments, target cells were current clamped, then 500 ms of square-wave current was injected to the cells from -50 to 450 pA in 50 pA steps. Between each step, the interval was 15-20 seconds to avoid overstimulation.

2.3.3. Data analysis and statistics

For the EPSCs, those measured peak amplitude, Rm, Rs and DC were used for the analysis as acquired from WinLTP. For mEPSCs, single trace files were imported to Clampfit 10.7 (Molecular Devices) and EPSC events over 15 pA from baseline were detected to exclude contamination from the baseline noise and then, peak amplitude, rise time 10% to 90% and decay time 90% to 10% were measured from each event. All the peaks were manually checked and false events were rejected. For firing activity experiments, single trace files were imported to Clampfit and number of firing events were counted with the threshold of 20 mV. And the frequency was calculated from inter-event interval.

For AMPA/NMDA experiments, the mean values of 10 AMPA EPSCs and 10 NMDA EPSCs were used for the unpaired t-test comparison between transfected and untransfected cells.

For LTP / LTD experiments, each time point was normalised with the average of the baseline (all the time points before LTP / LTD induction protocols) therefore, baseline was converted to 100 %. The change by LTP / LTD induction protocols was calculated by comparing the 5 time points prior to the induction protocol and 5 time points at the end of recording. Initially, to verify the magnitude of LTP / LTD from each neuron, a paired t-test was used to compare the pre- and post-induction protocols. An unpaired t-test was applied to analyse differences between groups.

For mEPSC experiments, rise time and decay time were compared between transfected and untransfected cells via the Mann-Whitney test, due to a none-standard distribution. However, due to a standard distribution, the mEPSC event frequency of transfected and untransfected cells was compared using an unpaired t-test.

For firing activity experiments, the frequency and the number of firing events were compared at each excitatory input point by using an unpaired t-test. The difference between groups were compared with a repeated measures analysis of variance (RM-ANOVA).

The data sets were analysed with Sigmaplot 12 software (Systat Software) and displayed as the mean value ± standard error of the mean (SEM). Significant difference between groups indicates a p-value of less than 0.05 ($p < 0.05$) for all the statistical tests.

2.4. Multi-photon and confocal imaging

2.4.1. Optic parameters

Multi-photon imaging was performed in either the Wolfson Bioimaging Facility (WBFLM) of University of Bristol or Wohl Cellular Imaging Centre

(WCIC) of King's College London. In WBFLM, Leica Application Suite X (LAS X) software with SP8 AOBS (Leica) confocal laser scanning microscope mounted on dm6000 (Leica) microscope was operated with 25X HC Fluotar water dipping objective (Working distance: 2.5 mm, Numeric aperture: 0.95). In WCIC, NIS-Elements software on A1R Multiphoton system (Nikon) was operated with 25X CFI75 Apochromat 25XC water dipping objective (Working distance: 2.0 mm, Numeric aperture: 1.10) was used. Additional digital magnification (0.75X-6X) was applied depending on the experiment.

Spinning disk confocal imaging was performed from Prof. Kei Cho's lab in King's College London Dementia Research Institute (KCL-DRI). In KCL-DRI, NIS-Elements software on A1R Multiphoton system (Nikon) was operated with Plan 100X/1.10 W water dipping objective (Working distance: 2.5 mm, Numeric aperture: 1.10) was used.

Transfected hippocampal slices were placed in a 35 ml petri dish, containing HEPES buffer (30 mM glucose, 25 mM HEPES, 5 mM KCl, 119 mM NaCl, 500 nM picrotoxin, 1μM glycine, 2 mM $MgCl_2$, 2 mM $CaCl_2$). For the filters, I3 (Excitation: 450-490 nm, Emission: 515 nm) (for Venus) and/or N21 (Excitation: 515-560 nm, Emission: 590 nm) (for mCherry) filters were used for each target protein. Image were acquired as z-stacks with 1 μm intervals with 3 averages at each plane.

2.4.2. Image process and assay parameters

Taken images from section 2.4.3. were further processed and analysed with ImageJ software. Regions of interest (ROIs) are categorised into 3 groups (apical dendrites at 0-100 μm and 100-200 μm, basal dendrites at 0-100 μm) and some groups were not taken if it was not available to find any secondary, tertiary or more branched dendrites and/or bright ROIs in that area. Within the categories, 15 μm X 15 μm sized 3 ROIs were randomly picked and cropped among dendrites with spines. Since morphological analysis was part of broad screening of neuronal change by FUS rather than heavily focused

on morphology, 2D analysis was utilised over 3D analysis to make the analysis simple, quick and no requirement of specialised paid software, though, 2D slightly sacrifices accuracy. The cropped ROI images were z-projected (Max brightness), converted to 8-bit and the contrast and brightness were optimised. Within the ROIs, spine densities were manually counted only when the spine has neck where spine head can be defined and the length of the whole spine was shorter than 5 μm to exclude filopodia. Since manual analysis can be easily biased without blinding and randomisation, those multiple data sets were crosschecked with other lab members to confirm that the tendency to be same. By drawing straight line with measuring function of ImageJ, spine head widths, spine head lengths, spine neck width and spine length were measured within ROIs and then, spine head / neck width ratio and spine head area were calculated from measured values. Based on the measured values, spines were categorised to 3 different shapes (stubby, thin, and mushroom) according to the length, head / neck width ratio. Stubby spines were defined as length < 1 μm and head width / neck width ratio < 1.5. Thin spines were defined as length 1 – 5 μm and head width / neck width ratio < 1.5. Mushroom spines were defined as length < 5 μm and head width/neck width ratio > 1.5. If a spine length was longer than 5 μm, the spine was regarded as filopodium and not used for the analysis. The parameters and criteria for analysing dendritic spines are summarised in the Fig. 2-5.

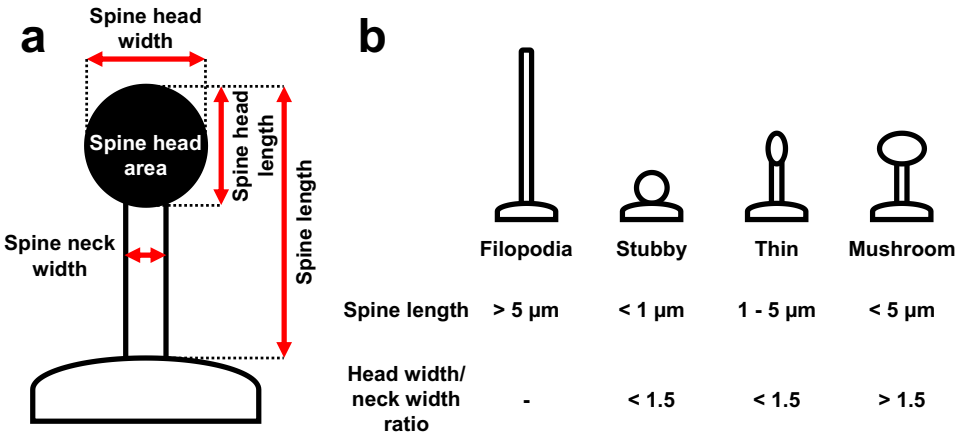

Figure 2-5 Parameters of spine morphology classification.

(a) Parameters of spine morphology were measured as displayed. (b) Based on the measured parameters, shapes of dendritic spines were categorised into filopodia, stubby, thin and mushroom shapes.

2.4.3. Data analysis and statistics

For all the morphology analyses, basal dendrites or apical dendrites were separately analysed, thus, they were not directly compared with any statistical analysis.

For the spine density comparisons, measured values of different groups were compared by using unpaired t-test.

For the shape of the dendritic spines, the ratio of spines in different shapes was calculated per each cell and then, those ratios of each shape type were pooled together. Within each shape type, the differences between groups were compared by using unpaired t-test.

Those backup parameters (spine head width, spine head length, spine neck width, spine length, Spine head width / spine neck width, Spine head area) were plotted and compared by using unpaired t-test.

The data sets were analysed with Sigmaplot 12 software (Systat Software) and displayed as the mean value ± SEM. Significant difference between

groups indicates a p-value of less than 0.05 ($p < 0.05$) for all the statistical tests.

2.5. Pharmacological reagents

See Table 2-3 for the details of the pharmacological reagents used for this study.

Pharmacological reagents	Description	Company and Cat. No.	Concentration	Solvent
2-chloroadenosine	Adenosine receptor agonist	Abcam ab120037	10 μM	ddH_2O
Bicuculline	$GABA_AR$ antagonist	Abcam ab120107	20 μM	DMSO
D-AP5	NMDAR antagonist	Abcam ab120003	50 μM	ddH_2O
IEM-1460	CP-AMPAR antagonist	Abcam ab141507	50-100 μM	DMSO
Picrotoxin	$GABA_AR$ antagonist	Abcam ab120315	20 μM	ddH_2O
TTX	Voltage-gated Na^+ channel blocker	Abcam ab120054	500 nM	ddH_2O

Table 2-3 Pharmacological reagents used in the study.

Information of the reagents and the usage of them were shown.

CHAPTER 3

Effect of FUS inclusions on dendritic spine morphology

3.1. Introduction

3.1.1. Imbalance of trafficking of FUS in neurodegenerative disease

FUS is nuclear protein and dominantly localised in the nucleus about 90 % or more (Hock et al., 2018), however, many cases from ALS, FTLD and other neurodegenerative diseases found mutation of FUS caused an imbalance of FUS level between nucleus and cytosol (Deng et al., 2010; Neumann et al., 2009; Svetoni et al., 2016). This imbalance of FUS trafficking was often suggested to be the cause of either/both the depletion of FUS in the nucleus and/or accumulation of cytosolic FUS (Ederle and Dormann, 2017; Ishigaki and Sobue, 2018). This different degree of the formation of FUS inclusions is suggested to be potentially due to the environmental differences between the nucleus and the cytosol such as different pool of DNA/RNAs (Chen, 2009; Yang et al., 2015) and proteins (Burke et al., 2015; Hofweber et al., 2018) that can interact with FUS either in the nucleus or in the cytosol. Those interaction may accelerate the formation of inclusions in the cytosol by recruiting FUS proteins into the aggregates (e.g. abnormally long mRNA can bind with multiple FUS proteins to accelerate cytosolic localisation of FUS (Tyzack et al., 2019)) or dissociate the FUS inclusions into individual FUS proteins by chaperoning the conformation of FUS to be less aggregative and import FUS into the nucleus (Guo et al., 2018). The depletion of FUS in the nucleus is often considered as loss-of-function because FUS is known to regulate the dynamics of DNA/RNA in the nucleus. Therefore, reduced expression or knockdown of FUS resulted in the decreased viability, impaired cellular proliferation and increased histone H3 phosphorylation (mitotic arrest), altered gene expression (either up or downregulation), loss of Gems (compact protein structure in the nucleus) that form complex with survival motor neuron (SMN) proteins and regulate small nuclear RNPs (snRNPs) for the splicing of RNAs, and so on (Kino et al., 2015; Ward et al., 2014; Yamazaki et al., 2012). While, the accumulation of FUS in the cytosol is frequently considered as gain-of-function because high level of cytosolic FUS can propagate from soma to dendrites, forms inclusions, which can

either accelerate or block the normal function of FUS (Kryndushkin et al., 2011; Shelkovnikova et al., 2014) and induce neurodegeneration (Dormann and Haass, 2011; Naumann et al., 2018). Both depletion of FUS and cytosolic accumulation of FUS alter and interfere the normal roles of FUS, however, cytosolic accumulation of FUS is thought to be more deleterious to the neurons (Dormann, 2016; Scekic-Zahirovic et al., 2016) and cellular stress (e.g. hyperosmolar stress, irradiation and thermal stress) has been demonstrated to boost the effect (Higelin et al., 2016; Murakami et al., 2012).

Then what can cause the imbalance of FUS trafficking? There are several possibilities but the well-characterised cause of the FUS mislocalisation is the mutation on the NLS domain. FUS mutations are mainly clustered in the NLS domain where nuclear-trafficking protein Transportin-1 (TRN-1) binds to (Dormann et al., 2012; Mackenzie et al., 2010b). Since FUS protein is initially translated in the cytoplasm, thus, once nuclear localisation mechanism is inhibited by NLS domain mutation, then, FUS accumulates in the cytosolic area and subject to form increased SG or non-SG inclusions. Therefore, patients with NLS mutations often show young-onset progressive clinical phenotypes (Shang and Huang, 2016) and NLS mutants of FUS have well-characterised pathologic progression (e.g. mislocalisation) than the other mutants (Ederle and Dormann, 2017; Mackenzie et al., 2010b), therefore, frequently utilised as experimental models of FUS pathology. Simply, neuronal aging (Higelin et al., 2016) or overexpression of FUS (Mitchell et al., 2013) can also cause cytosolic FUS and FUS inclusions. Or, expression of RNAs with abnormally extended introns can also alter the normal nucleo-cytosolic balance of FUS (Tyzack et al., 2019) as FUS can translocate from nucleus to the cytosol when bound with RNA (Zinszner et al., 1997). In that aspect, if the binding affinity between FUS and RNA is abnormally high or if RNA can be bound with multiple FUS proteins due to the expression of abnormal RNA species (e.g. mutation or abnormally increased expression), then FUS can be accumulated in the cytosol together with RNA. Overall, any mechanism that causes mislocalisation and cytosolic aggregation of FUS can have similar pathologic progression in the neurons.

3.1.2. Cytosolic FUS and morphologic changes of neurons

Propagation and imbalanced level of cytosolic FUS will be problematic, in addition, FUS also has roles in the neuronal trajectories such as dendrites and axons. Therefore, the roles of FUS in both physiological and pathological situations need to be discussed.

Even though FUS is predominantly nuclear protein, FUS is also located in the cytosolic space, mainly bound with mRNA, and propagate through dendrites and axons in the physiological conditions (Belly et al., 2005; Schoen et al., 2016; Yasuda et al., 2013). Therefore, FUS functions as cargo ship for mRNAs in the cytosolic area and through neurites (Fujii et al., 2005; Sahoo et al., 2018). In addition, FUS is involved in the stability of mRNAs (Colombrita et al., 2012) and the local translation of proteins in the axonal and dendritic region (López-Erauskin et al., 2018; Sahoo et al., 2018; Shiihashi et al., 2017). This local translation includes the essential structural and synaptic proteins (Fujii and Takumi, 2005; Udagawa et al., 2015; Yokoi et al., 2017), therefore, FUS is closely related to the neuronal morphology.

Then, what happens to the neuronal morphology when FUS expression is altered? Overexpression of both wildtype and NLS mutant forms of FUS can cause dendritic morphologies to be less branches and spines and abnormal branching of axon. Overexpression of wildtype FUS and Caz (homolog of FUS in Drosophila), NLS mutants FUS-P525L and Caz-P398L caused simplified dendritic branching and altered axonal and synaptic transport (Machamer et al., 2018). Mice model with FUS-R521C overexpression reduced dendritic spine number, maturity and dendritic length, which were also moderately impaired in wildtype FUS overexpression (Qiu et al., 2014). In other transgenic mice model with ΔNLS-FUS had phenotypes of reduced dendritic spines and synaptic marker proteins such as postsynaptic density 95 (PSD95) and vesicular glutamate transporter 1 (VGLUT1) (Shiihashi et al., 2017). Expression of FUS-H517D and FUS-P525L mutants in human-induced pluripotent stem cell (hiPSCs)-derived motor neurons showed abnormal axon branching (Akiyama et al., 2019) and reduced neurite length

(Ichiyanagi et al., 2016). In other study, overexpression of wildtype FUS doesn't show morphological changes from transgenic mice while FUS-R521G mice showed dendritic defects (Sephton et al., 2014), therefore, cytosolic FUS level is more important than total FUS regardless of FUS variants. In addition, depletion or knockout of FUS in the mice model also caused deleterious effects to the morphology such as the reduced number of total spines and mature spines in the dendrites (Yokoi et al., 2017), outlength of neurite was reduced (Ishigaki et al., 2017). Therefore, cytosolic level of FUS needs to be maintained to the optimal range to sustain the normal morphology of neurites.

3.1.3. NLS mutant FUS-P525L as a tool to investigate cytosolic FUS

FUS protein is composed of total 526 amino acids and FUS-P525L (Proline at 525 is substituted to Leucine) is a type of NLS mutant at C-terminus of FUS protein that impairs the internalisation of FUS proteins into the nucleus by interfering the binding between nuclear transport receptor Transportin-1 (TRN-1) and FUS (Dormann et al., 2010). NLS mutants are dominant among FUS mutants that causes ALS and FUS-P525L mutation has been found and identified from ALS patients (Deng et al., 2014; Naumann et al., 2019). In a cohort study showed that among ALS cases, the percentage of FUS-P525L cases was 1.37 % but when it comes to the cases within FUS mutant group, FUS-P525L cases took about 8.44 %, therefore, it is one of the most common form of FUS-NLS mutants together with FUS-R521 mutants (Shang and Huang, 2016). The cases have been reported to express very progressive and early onset ALS phenotypes compared to the other FUS mutants (Lattante et al., 2012; Naumann et al., 2019), reported to be found more from female patients (Huang et al., 2010; Mochizuki et al., 2012).

Because of this fast progression of pathology, FUS-P525L has been utilised and studied to investigate the mechanisms of abnormal trafficking / accumulation of FUS in the cytosolic compartment of neurons and consequential pathologies. For instance, FUS-P525L was demonstrated to

show abnormally reduced interaction with TRN-1 and mislocalisation of FUS (Neumann et al., 2012), association with stress granules (Lenzi et al., 2015), increased tendency to form aggregates and irreversible hydrogels (Marrone et al., 2020; Murakami et al., 2015), abnormal fission of mitochondria (Deng et al., 2015), impaired DNA damage response and repair (Wang et al., 2013) and altered synaptic calcium transients (Machamer et al., 2018). Like other FUS mutant forms, FUS-P525L doesn't seem to be investigated intensively for synaptic physiology or morphology and most of studies were conducted with motor neurons since ALS is basically motor neurons disease. Therefore, it would be useful to combine FUS-P525L and hippocampal neurons to investigate how FUS can alter the synaptic physiology and dynamics.

Considering previous studies, abnormal FUS translocation will alter the physiology of the neurons from the synapse level in the early stage before the neuron is progressed to cell death and this pathologic process does not necessarily require the alteration of FUS in the nucleus. Thus, by utilising NLS mutant FUS-P525L, morphology of dendritic spines was investigated to check the translocation pattern of cytosolic FUS through the dendrites and affects the morphology of dendritic spines.

3.2. Results

3.2.1. FUS-P525L mutant causes cytosolic inclusions

As articulated previously, the NLS mutant FUS (FUS-P525L) has impaired trafficking ability and accumulates in the cytosolic area (Vance et al., 2013). To confirm that this mislocalisation of FUS occurs in our model, YFP-tagged wildtype FUS (FUS-WT) and FUS-P525L were overexpressed in the hippocampal CA1 neurons and imaged on the multiphoton microscope system (Fig. 3-1). FUS-WT was predominantly localised in the somatic area (thought to be locked in the nucleus) at 5 days after transfection (Fig. 3-1a), whereas FUS-P525L propagated through the dendrites and formed inclusions in the somatic cytosol and dendritic cytosols at 5 days after

transfection, which is the minimum stabilising time point after using biolistic transfection method (Fig. 3-1b).

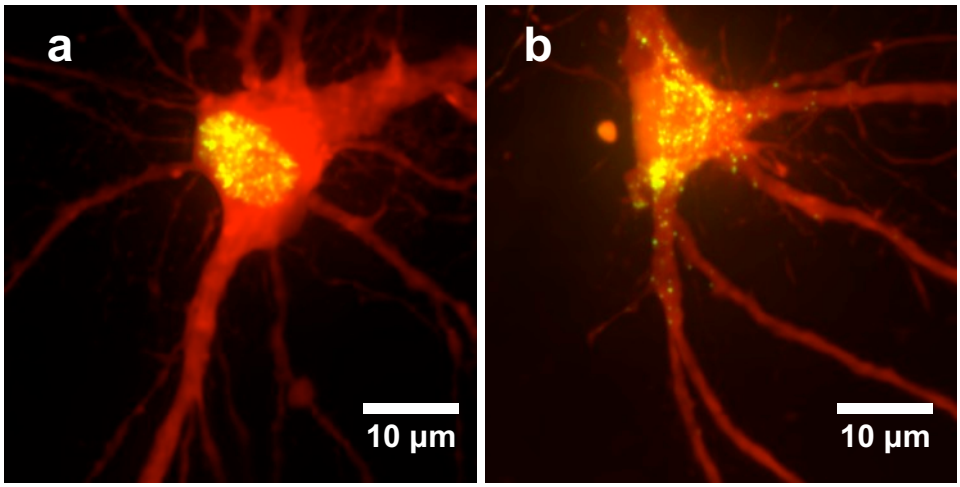

Figure 3-1 Confocal images of CA1 neurons with FUS-WT and FUS-P525L transfection.

Each YFP-tagged FUS was imaged at DAT5 with red fluorescence structural marker, TdTomato on confocal spinning disk. (a) YFP-tagged FUS-WT was predominantly locked in the somatic region. (b) YFP-tagged FUS-P525L translocated through dendrites and multiple inclusions were found. The spinning disk confocal images were acquired from Prof. Kei Cho's lab in King's College London Dementia Research Institute (KCL-DRI).

Propagation of FUS-P525L at different time points after transfection were also observed with FUS-P525L transfected CA1 neurons (Fig. 3-2). This was to investigate how quickly FUS-P525L can translocate from soma to the dendrites, therefore, electrophysiological changes can be compared and crosschecked in the later chapters. Two days after transfection (Fig. 3-2a), FUS-P525L already accumulated in somatic cytosol and formed inclusions. Comparing with the different cells at the same time point (Fig. 3-1b), dendritic propagation of FUS-P525L was variable at this stage. FUS-P525L inclusions (Fig. 3-2b) were formed in soma and widespread through the dendrites around three days after transfection, a trend that was at five (Fig. 3-2c) and six days (Fig. 3-2d) post transfection. In brief, cytosolic propagation of FUS-P525L inclusions occurs at very early time point of transfection (2 days). In

contrast to FUS-P525L mutation, no FUS-WT was visible in the cytosol as it was still locked in the nucleus (Fig. 3-1a).

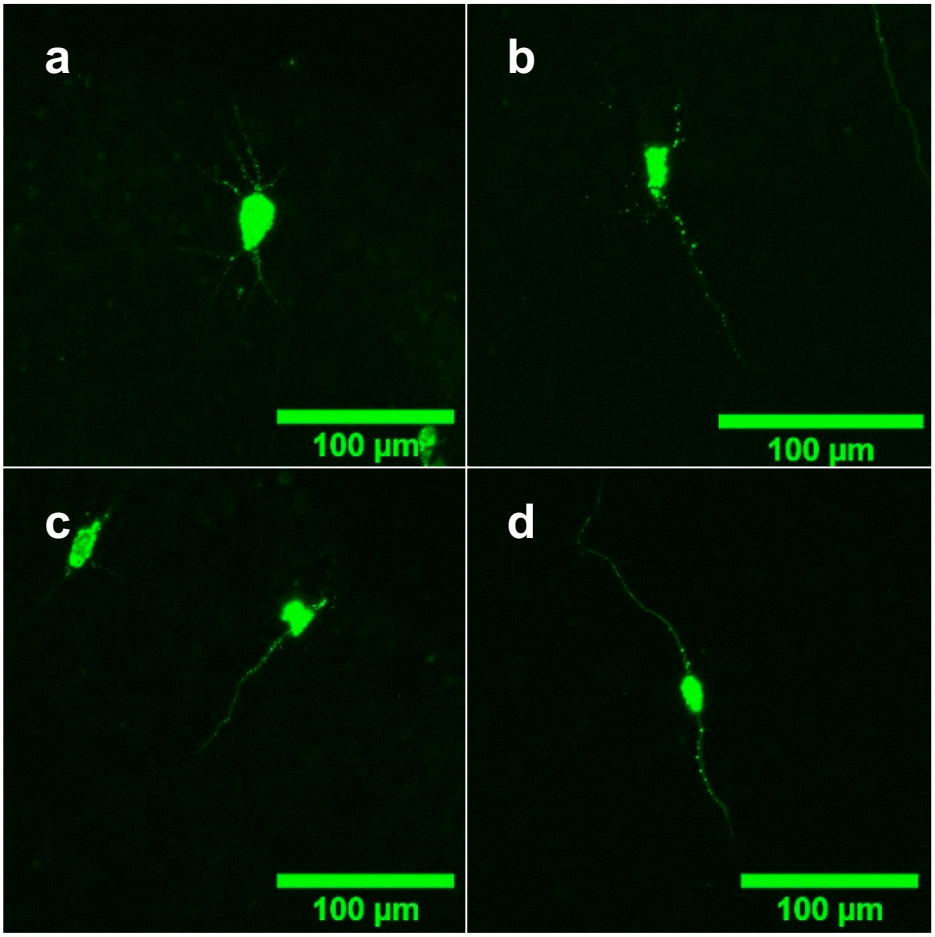

Figure 3-2 Translocation of FUS-P525L in different time points through dendrites.

Multiphoton images of FUS-P525L were taken at (a) DAT2, (b) DAT3, (c) DAT5, (d) DAT6. From DAT2 to DAT6, YFP-tagged FUS-P525L proteins were all highly expressed in the cytosolic area and translocated through dendrites with significant FUS inclusions.

Overall, within the time window for the optimal biolistic transfection method, FUS-WT was confined in the nucleus whereas FUS-P525L caused cytosolic inclusions. Due to the variability of cytosolic expression at early post transfection days, 5-7 days post transfection was selected further experiments. This post transfection time point will ensure that FUS-P525L propagation is consistent and saturated, while, FUS-WT is predominantly

confined in the nucleus. Therefore, FUS-P525L and FUS-WT would show the maximised differential phenotypes of pathophysiology in terms of different FUS distribution.

3.2.2. Dendritic spine density is reduced in FUS-P525L expressing neurons

Since overexpression of cytosolic FUS was suggested to reduce the dendritic spines by trapping essential mRNAs needed for maintaining the structure of dendritic spines (Machamer et al., 2018; Shiihashi et al., 2017), it was needed to be investigated whether FUS inclusions affect the synapse morphology. Especially, spine density of neurons represents the connectivity between neurons and efficiency of synaptic transmission, therefore, spine density was thought to be decreased if cytosolic FUS weakens or destroys the synaptic connections.

Hippocampal CA1 neurons were transfected with Venus (FUS negative), FUS-WT (wildtype overexpression) and FUS-P525L either with Venus or mCherry co-transfection, then dendritic spine density was measured from both basal or apical dendrites of CA1 neurons (Fig. 3-3 and Table 3-1). Due to the different circuitry between basal and apical dendrites as articulated in the section 1.3.2. (Masurkar, 2018), they were analysed separately. The data set was shown as Mean ± Standard Error of Mean (SEM). Hippocampal slices from 6 animals for Venus, 5 animals for FUS-WT and 7 animals for FUS-P525L were used for the results in Chapter 3 dendritic spine analysis.

The spine density of the basal dendrites was not affected by either FUS-P525L or FUS-WT expression (Fig. 3-3a). However, at apical dendritic regions, FUS-P525L induced a significant decrease in spine density (Fig. 3-3b).

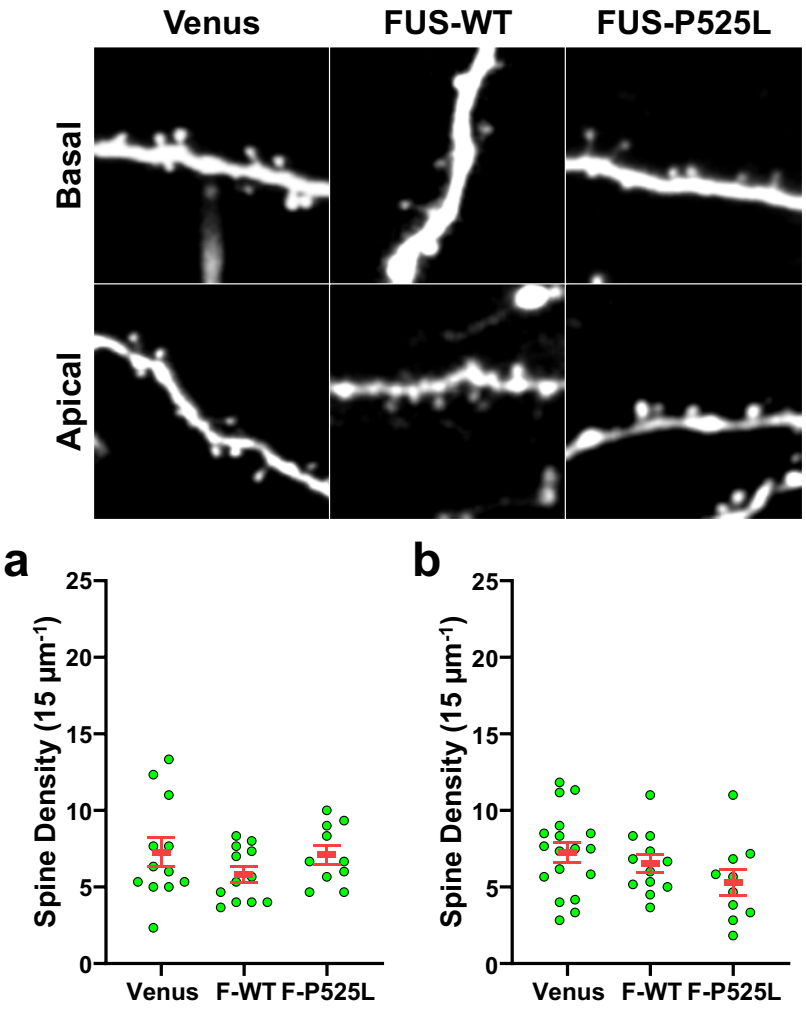

Figure 3-3 Spine density of apical dendrites was reduced in FUS-P525L expressing neurons.

CA1 cells were transfected with Venus, FUS-WT and FUS-P525L and the dendritic spines were imaged at DAT5-7. Example ROI (15 µm x 15 µm) images were taken from each group. (a) In the basal dendritic region, spine densities did not show significant differences between groups. (b) Also in the apical dendritic region, spine density was not different.

Basal dendrites	Venus (V)	FUS-WT (W)	FUS-P525L (P)
n-number (Cell)	12	12	10
Spine density ($15\ \mu m^{-1}$)	7.27 ± 0.95	5.80 ± 0.50	7.10 ± 0.61
***p*-value** ANOVA, (W vs P), (V vs W), (V vs P)	0.3027		0.4487
	0.3251		0.9849

Apical dendrites	Venus (V)	FUS-WT (W)	FUS-P525L (P)
n-number (Cell)	18	12	10
Spine density ($15\ \mu m^{-1}$)	7.25 ± 0.62	6.51 ± 0.58	5.29 ± 0.83
***p*-value** ANOVA, (W vs P), (V vs W), (V vs P)	0.1514		0.4976
	0.7039		0.1281

Table 3-1 Statistical summary of spine density of basal and apical dendrites in Venus, FUS-WT and FUS-P525L expressing neurons.

Statistics of Fig. 3-3 was summarised as tables.

Overall, FUS-P525L transfection specifically reduced the number of spines in the apical dendrites, not in the basal dendrites whereas FUS-WT did not alter significant dendritic spine numbers in either region. Therefore, this data suggests that cytosolic inclusion of FUS induces a synapse weakening process through the reduction of available synapses and this may be variable to the different regions of dendrites.

3.2.3. Effects of FUS-P525L on dendritic spine morphology

Neuronal morphology, in particular the shape of dendritic spine is highly coupled to function (Bourne and Harris, 2008). The morphology of a spine represents the maturation, health and strength of the spines, in a manner governed by neuronal activity, and therefore it indicates the fate of the synapse (Bourne and Harris, 2008; Tønnesen and Nägerl, 2016). The most popular and common categories of spine morphology are filopodia, stubby, thin and mushroom shapes (Hering and Sheng, 2001; Rochefort and

Konnerth, 2012). With the idea, it was of interest that whether expression of mutant FUS can alter the morphology of the dendritic spines because FUS is required for the maturation of the spines (Yokoi et al., 2017).

The standard morphological categorisation was used as the criteria for this study except for the filopodia because it is often considered as immature, non-functional spine and was therefore excluded from the analysis. The mushroom shaped spines are considered to be most mature, followed by thin shaped and then stubby shaped spines (Ebrahimi and Okabe, 2014; Rochefort and Konnerth, 2012). Representative ROIs (15 µm in length) were extracted from basal and apical dendrites and all the spines found were categorised into stubby, thin and mushroom based on the length and width ratio (see section 2.4.2. for the criteria), then, the percentage was calculated for each neuron (Fig. 3-4 and Table 3-2). And measured parameters for the spine shape categorisation (Spine head width, Spine head length, Spine neck width, Spine length, Spine head width / spine head length and Spine head area) were also displayed as the supplementary data for basal (Fig. 3-5 and Table 3-3) and apical (Fig. 3-6 and Table 3-4) dendritic spines. The data set was shown as Mean ± SEM.

In the basal dendrites (Fig 3-4a), the percentage of stubby spines were higher in FUS-WT, whereas thin spines and mushroom spines did not show any significant differences. In apical dendrites (Fig. 3-4b), stubby spines and thin spines did not show significant differences but in mushroom shape, FUS-WT was lesser than the other groups.

Overall, although FUS-P525L expressing neurons exhibit a general reduction in spine density (**see section 3.2.2.**), they did not exhibit a change in the distribution of spine morphology. Surprisingly, the FUS-WT expressing cells had an increased percentage of stubby basal dendritic spines and decreased mushroom apical dendritic spines. Therefore, overall maturation level of dendritic spines is reduced in FUS-WT expressing cells.

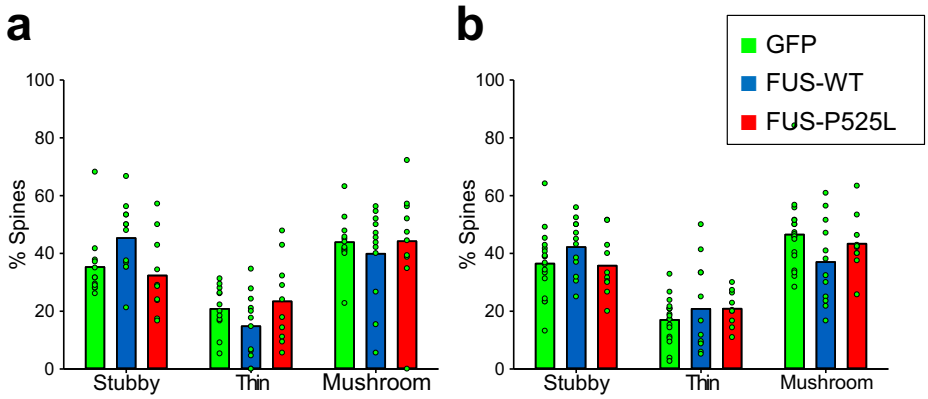

Figure 3-4 Dendritic spine shape was not altered in FUS expressing neurons.

(a) In basal dendrites, the ratio of different shapes of spines was not altered by FUS transfected neurons compared to Venus transfected neurons. (b) In apical dendrites, the ratio of spine shapes was not altered in FUS neurons.

Basal dendrites	Venus (V)	FUS-WT (W)	FUS-P525L (P)
n-number (Cell)	12	12	10
Stubby (% Spines)	35.29 ± 3.28	45.31 ± 3.55	32.37 ± 4.32 %
***p*-value** ANOVA, (W vs P),	**0.0464 (F = 3.396)**		0.0530
(V vs W), (V vs P)	0.1347		0.8475
Thin (% Spines)	20.82 ± 2.32	14.79 ± 3.26	23.40 ± 4.55
***p*-value** ANOVA, (W vs P),	0.1973 (F = 1.711)		0.1945
(V vs W), (V vs P)	0.4041		0.8560
Mushroom (% Spines)	43.88 ± 2.69	39.89 ± 4.59	44.22 ± 6.02
***p*-value** ANOVA, (W vs P),	0.7461 (F = 0.296)		0.7817
(V vs W), (V vs P)	0.7939		0.9985

Apical dendrites	Venus (V)	FUS-WT (W)	FUS-P525L (P)
n-number (Cell)	18	12	10
Stubby (% Spines)	36.47 ± 2.67	42.18 ± 2.79	35.77 ± 3.30
***p*-value** ANOVA, (W vs P),	0.2779 (F = 1.326)		0.3491
(V vs W), (V vs P)	0.3331		0.9847
Thin (% Spines)	17.01 ± 1.80	20.81 ± 4.42	20.87 ± 1.88
***p*-value** ANOVA, (W vs P),	0.5074 (F = 0.6910)		0.9999
(V vs W), (V vs P)	0.5844		0.6092
Mushroom (% Spines)	46.51 ± 2.94	37.01 ± 4.19	43.36 ± 3.12
***p*-value** ANOVA, (W vs P),	0.1408 (F = 2.068)		0.4731
(V vs W), (V vs P)	0.1194		0.8005

Table 3-2 Statistical summary of dendritic spine shape of basal and apical dendrites in Venus, FUS-WT and FUS-P525L expressing neurons.

Statistics of Fig. 3-4 was summarised as tables.

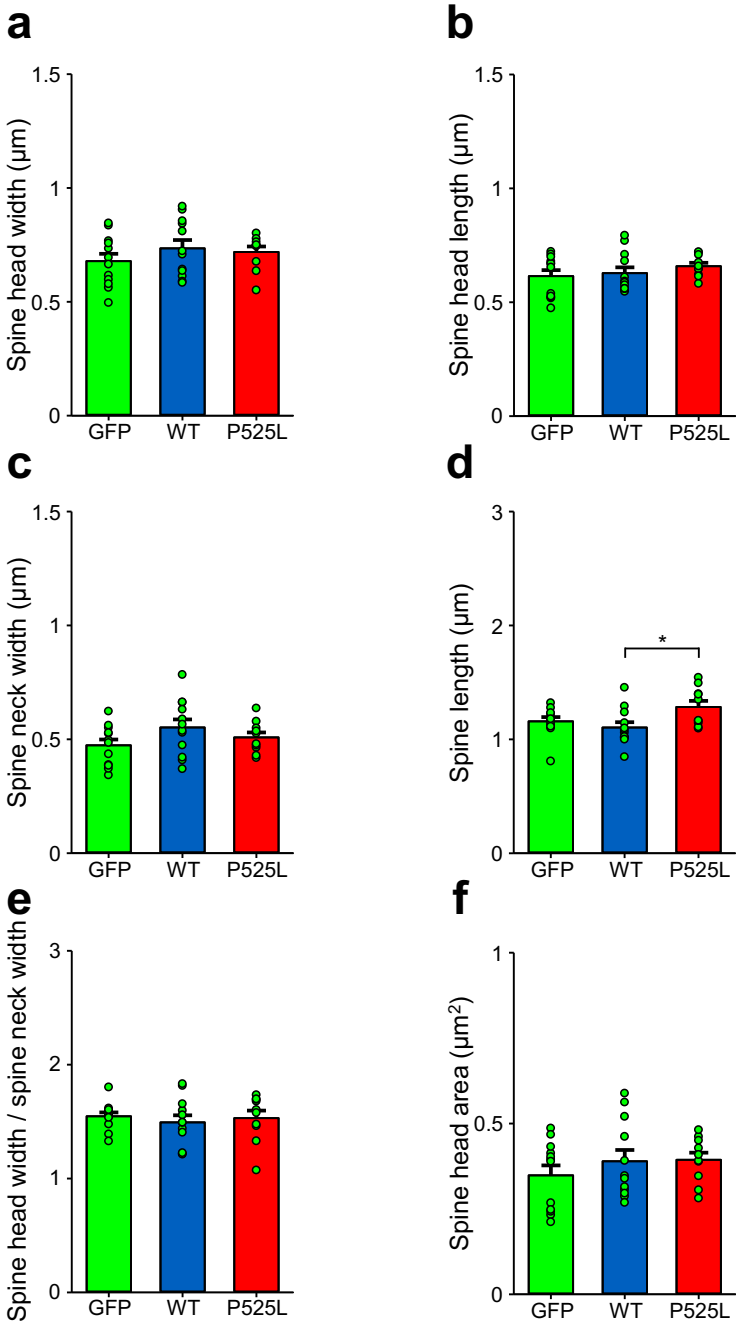

Figure 3-5 Parameters of the spine shapes were measured in basal dendritic spines.

(a) Spine head width was all similar between groups. (b) Spine head length was similar between groups. (c) Spine neck width was similar between groups. (d) Spine length was longer in FUS-P525L cells. (e) Spine head width / spine neck width ratio did not show any difference between groups. (f) Spine head area also did not show any difference between groups.

Basal dendrites	Venus (V)	FUS-WT (W)	FUS-P525L (P)
n-number (Cell)	12	12	10
Spine head width (µm)	0.6787 ± 0.0322	0.7353 ± 0.0361	0.7192 ± 0.0241
***p*-value** ANOVA, (W vs P), (V vs W), (V vs P)	0.4297 (F = 0.8681)		0.9359
	0.4153		0.6592
Spine head length (µm)	0.6148 ± 0.0262	0.6282 ± 0.0251	0.6584 ± 0.0148
***p*-value** ANOVA, (W vs P), (V vs W), (V vs P)	0.4360 (F = 0.8528)		0.6505
	0.9094		0.4132
Spine neck width (µm)	0.4738 ± 0.0256	0.5524 ± 0.0351	0.5086 ± 0.0217
***p*-value** ANOVA, (W vs P), (V vs W), (V vs P)	0.1564 (F = 1.971)		0.5496
	0.1337		0.6838
Spine length (µm)	1.1589 ± 0.0370	1.1049 ± 0.0460	1.2847 ± 0.0532
***p*-value** ANOVA, (W vs P), (V vs W), (V vs P)	**0.0298 (F = 3.941)**		**0.0253**
	0.6631		0.1467
Spine head width / spine head length	1.5475 ± 0.0341	1.4942 ± 0.0613	1.5317 ± 0.0652
***p*-value** ANOVA, (W vs P), (V vs W), (V vs P)	0.7661 (F = 0.2688)		0.8811
	0.7560		0.9777
Spine head area (μm^2)	0.3486 ± 0.0290	0.3898 ± 0.0328	0.3938 ± 0.0210
***p*-value** ANOVA, (W vs P), (V vs W), (V vs P)	0.4745 (F = 0.7638)		0.9948
	0.5599		0.5298

Table 3-3 Statistical summary of parameters measured for the differentiation of basal dendritic spine shapes in Venus, FUS-WT and FUS-P525L expressing neurons.

Statistics of Fig. 3-5 was summarised as a table.

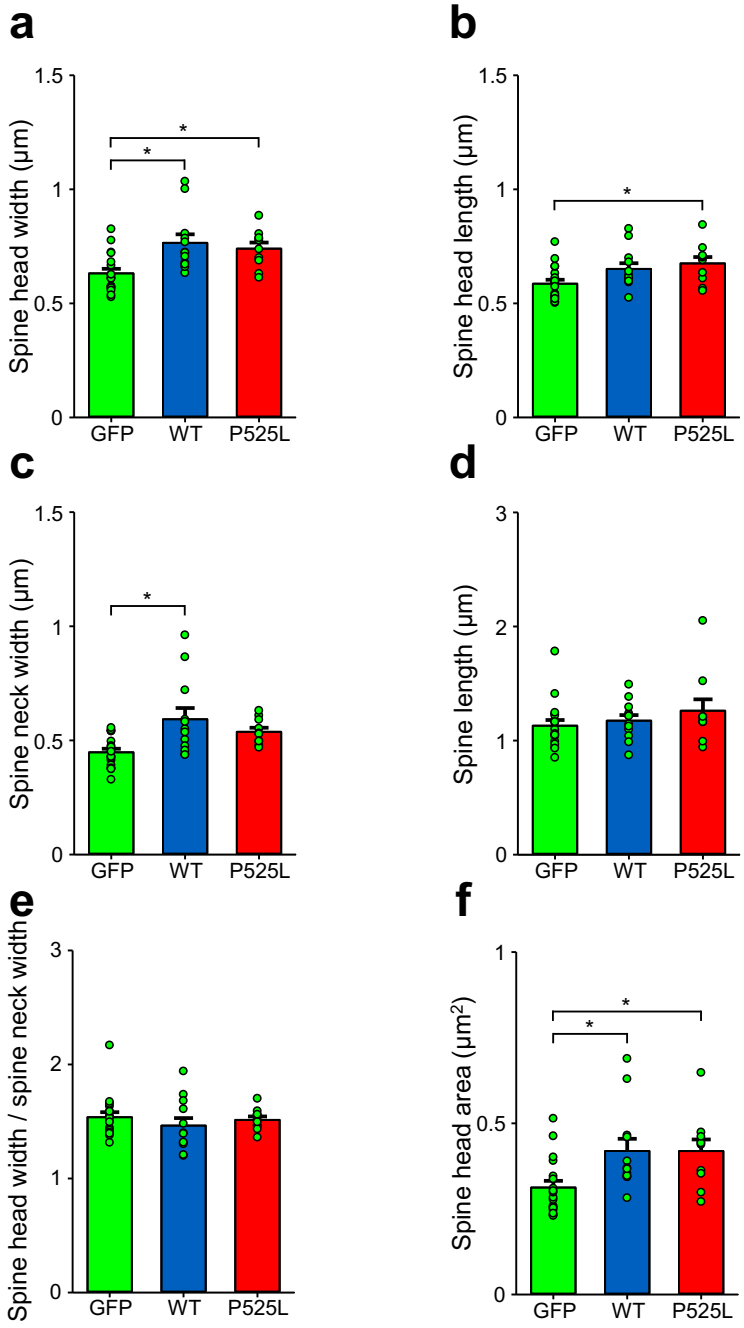

Figure 3-6 Parameters of the spine shapes were measured in apical dendritic spines.

(a) Spine head width was wider in FUS-WT and FUS-P525L cells. (b) Spine head length was longer in FUS-P525L cells. (c) Spine neck width was wider in FUS-WT cells. (d) Spine length was all similar between groups. (e) Spine head width / spine neck width ratio did not show any difference between groups. (f) Spine head area was bigger in FUS-WT and FUS-P525L cells.

Apical dendrites	Venus (V)	FUS-WT (W)	FUS-P525L (P)
n-number (Cell)	18	12	10
Spine head width (µm)	0.6321 ± 0.0198	0.7655 ± 0.0372	0.7404 ± 0.0264
***p*-value** ANOVA, (W vs P), (V vs W), (V vs P)	**0.0017 (F = 7.611)**		0.8267
	0.0026		**0.0238**
Spine head length (µm)	0.5867 ± 0.0174	0.6513 ± 0.0250	0.6757 ± 0.0276
***p*-value** ANOVA, (W vs P), (V vs W), (V vs P)	**0.0174 (F = 4.531)**		0.7651
	0.0972		**0.0229**
Spine neck width (µm)	0.4480 ± 0.0159	0.5929 ± 0.0492	0.5380 ± 0.0178
***p*-value** ANOVA, (W vs P), (V vs W), (V vs P)	**0.0028 (F = 6.913)**		0.4636
	0.0024		0.0976
Spine length (µm)	1.1309 ± 0.0499	1.1748 ± 0.0492	1.2619 ± 0.1002
***p*-value** ANOVA, (W vs P), (V vs W), (V vs P)	0.3681 (F = 1.027)		0.6579
	0.8678		0.3349
Spine head width / spine head length	1.5379 ± 0.0442	1.4643 ± 0.0665	1.5146 ± 0.0300
***p*-value** ANOVA, (W vs P), (V vs W), (V vs P)	0.5675 (F = 0.5753)		0.8013
	0.5391		0.9454
Spine head area (μm^2)	0.3126 ± 0.0193	0.4194 ± 0.0355	0.4190 ± 0.0338
***p*-value** ANOVA, (W vs P), (V vs W), (V vs P)	**0.0087 (F = 5.416)**		>0.9999
	0.0210		**0.0311**

Table 3-4 Statistical summary of parameters measured for the differentiation of apical dendritic spine shapes in Venus, FUS-WT and FUS-P525L expressing neurons.

Statistics of Fig. 3-6 was summarised as a table.

3.2.4. Local vulnerability of apical dendritic spines in FUS-P525L expressing neurons

Overall spine density and shape of either basal or apical dendrites were not different between groups but FUS (FUS-WT and FUS-P525L) transfected neurons had bigger head width and area only in apical dendrites, therefore, still there is a possibility that spine dynamics has been locally altered in apical region. Due to the complex and branched structure of dendrites, they have difference (or gradient) of molecular and ionic dynamics between proximal vs distal dendrites from where dendritic branch starts (Weber et al., 2016). This difference may cause different degree of vulnerability caused by FUS expression, thus, it was of interest to further investigate whether proximal vs distal dendrites have different spine density upon FUS transfections.

Raw images for spine density assay (Fig. 3-3, randomly selected ROIs) were re-cropped from proximal and distal part of same dendrites as pairs to investigate the possible local synaptic changes (Fig. 3-7 and Table 3-5). Counted spine density of proximal and distal dendrites were compared within group (Fig. 3-7a~c) and the ratio of either distal / proximal or proximal / distal dendritic spine density from all three groups were compared (Fig. 3-7d, e). The data set was shown as Mean ± SEM.

The comparisons of proximal vs distal spines did not show any difference from Venus (Fig. 3-7a) and FUS-WT (Fig. 3-7b) transfected neurons, whereas, FUS-P525L neurons (Fig. 3-7c) showed the reduction of spine density in distal part. As FUS-P525L has difference between proximal vs distal spine density, the ratio of that also showed different trends compared to Venus and FUS-WT (Fig. 3-7d, e). Within ANOVA comparison (multiple comparison), only proximal / distal showed significance and it was not quite significant in distal / proximal ratio, however, T-test comparison between Venus vs FUS-P525L showed significance (p = 0.0407, Power: 0.552). This is possibly due to the relatively small size of n-number of each group.

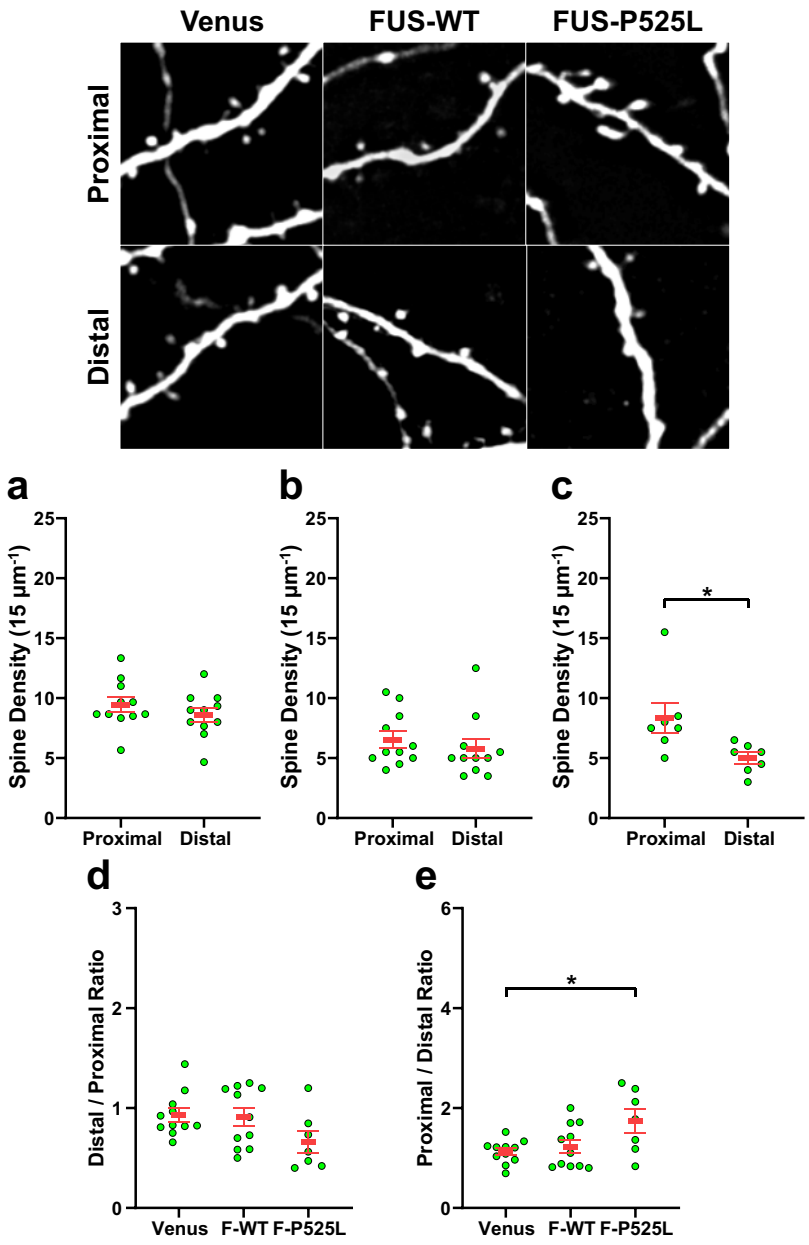

Figure 3-7 Spine density and the ratio of proximal vs distal apical dendrites were altered in FUS-P525L expressing neurons.

Dendritic spine images from Fig. 3-3 were re-cropped from proximal vs distal region. Example ROI (15 µm x 15 µm) images were taken from each group. (a) Venus neurons had similar number of proximal and distal dendritic spines. (b) FUS-WT neurons also had similar number of proximal and distal dendritic spines. (c) FUS-P525L neurons had reduced distal dendritic spines than proximal dendrites. (d) Distal / Proximal ratio was slightly reduced in FUS-P525L neurons. (e) Proximal / Distal ratio was significantly increased in FUS-P525L neurons.

	Venus (V)	FUS-WT (W)	FUS-P525L (P)
n-number (Cell)	11	11	7
Proximal S.D. ($15\ \mu m^{-1}$)	9.43 ± 0.60	6.55 ± 0.68	8.35 ± 1.26
Distal S.D. ($15\ \mu m^{-1}$)	8.60 ± 0.57	5.77 ± 0.79	5.00 ± 0.46
***p*-value** (T-test) (Proximal vs Distal)	0.330	0.466	**0.0284 (Power: 0.628)**
Distal / Proximal Ratio	0.93 ± 0.07	0.91 ± 0.09	0.66 ± 0.11
***p*-value** ANOVA, (W vs P), (V vs W), (V vs P)	0.1045 (F = 2.466)		0.1564
	0.9828		0.1170
Proximal / Distal Ratio	1.12 ± 0.07	1.23 ± 0.13	1.74 ± 0.24
***p*-value** ANOVA, (W vs P), (V vs W), (V vs P)	**0.0188 (F = 4.650)**		0.0543
	0.8445		**0.0182**

Table 3-5 Statistical summary of spine density of proximal and distal region of apical dendrites in Venus, FUS-WT and FUS-P525L expressing neurons.

Statistics of Fig. 3-7 was summarised as a table.

Overall, only FUS-P525L (not FUS-WT) transfection caused local reduction of spine density in distal part of dendrites rather than proximal dendritic spines. As discussed in the session 3.2.2., this reduction was not found when whole dendritic spine density was compared. Therefore, cytosolic accumulation of FUS inclusion may cause more deleterious results to the distal dendrites and make distal synapses more vulnerable.

3.3. Discussion

3.3.1. FUS-P525L is a proper experimental tool to investigate progressive cytosolic FUS proteinopathy

This chapter investigated the effect of FUS inclusions on the morphology of dendritic spines of CA1 neurons. As demonstrated, NLS mutant FUS formed inclusions in the cytosol and fully translocated from soma to the tip of the dendrites at the early stage of the transfection (2 days) and it did not show significant difference with the spreading patterns at 4, 5 days after transfection. DAT 2 (2 days after transfection) is earlier than the general use of transfected hippocampal neurons for the electrophysiology experiments, which usually requires more than 2 days of stabilisation of cells and expression of the target genes after biolistic transfection of organotypic hippocampal culture slices. This progressive feature of FUS-P525L is consistent with the early and progressive clinical phenotypes from familiar patients with the NLS FUS mutants (Shang and Huang, 2016). This massive cytosolic translocation was not observed from FUS-WT expressing CA1 neurons. FUS pathology is mainly defined by FUS containing inclusions in the neurons and these inclusions are predominantly localised in the cytosol, in FUS mutations both with and without the NLS mutants. Therefore, utilising the NLS mutant FUS (FUS-P525L) is a good tool for investigating the downstream pathology of cytosolic FUS inclusions.

3.3.2. Different vulnerability of dendritic spines against FUS-P525L expression in different compartment of dendrites of CA1 neurons

Expression of FUS-P525L did not induce massive alterations of spines on both basal and apical dendrites, however, it did reduce the spine density at the distal part of the apical dendrites. In addition, overall apical dendritic spine density of FUS-P525L neurons were reduced if individual ROIs were not averaged (data not shown). Then, why and how do FUS inclusions cause a region dependent pathology even though FUS inclusions are present in all

the way through the dendrites? The difference between apical and basal dendrites in terms of changes in spine density may arise from physiological consequences. For instance, apical dendrites receive the major excitatory input to CA1 neurons via the Schaffer-collateral pathway (Jarsky et al., 2005), which is ipsilateral pathway from CA3 neurons, whereas basal dendrites mainly receive inputs from CA2 in this hippocampal slice model. In addition, majority of excitatory inputs to CA1 are delivered to apical dendrites, whereas inhibitory inputs to CA1 are mainly delivered to basal dendrites (Olypher et al., 2012). Therefore, more excitatory input can accelerate neural activity of apical dendrites (rather than basal dendrites) and may affect the pathology of dendritic FUS inclusions (Tischbein et al., 2019). Furthermore, FUS inclusion may interfere molecule trafficking (Soo et al., 2015; Sundaramoorthy et al., 2015), therefore, FUS can trap the essential molecular resources (e.g. structural mRNAs, proteins), required to sustain the spine structure and activity, not to be delivered to the dendritic spines and eventually destroy the spines by stopping the synaptic dynamics and depletion of resources. In addition, the reduction of spines is very distinct in the distal area compared to the proximal area of dendrites. This might be closely related to the translocation of FUS because translocation of RNP is thought to depend on the microtubule mediated (Fujii and Takumi, 2005). The direction of RNP movement via microtubule is either unipolar or bipolar and it is bipolar in proximal, unipolar in distal dendrites (Hirokawa and Takemura, 2005), therefore, this polarity might have contributed the accumulation of FUS in the distal dendrites rather than proximal dendrites. Due to the complex nature of neurons, it is likely that all the hypothesis described above may play a synergistic part in exacerbating the pathology, and thereby warrant further investigation of the mechanism and clarification of the cause of the spine reduction whether it is due to the inhibition of spine formation or elimination of formed spines.

3.3.3. Abnormal expression of FUS is involved in the morphological alteration of dendritic spines

FUS-P525L expressing neurons did not exhibit any change in spine shape compared to Venus expressing cells. This means cytosolic FUS did not significantly altered the overall maturity of the spines. Although, the head size of apical dendritic spines was bigger in both FUS-WT and FUS-P525L, thus, overexpression of FUS in general seem to affect dynamics of dendritic spines in some way. And FUS-P525L transfected cells showed distal vulnerability, still there is marginal chance for cytosolic FUS-P525L to translocate to distal part of apical dendrites and accelerate the overall growth of the spine size. If this growth of spine size is a part of maturation, this might have caused the increase of postsynaptic excitatory receptors, resulted in excitotoxicity to be destroyed from distal dendrites eventually. However, the major changes in the dendritic spine would be much complicated than it actually looks like. FUS is basically RNA binding protein, therefore, NLS variants (or mutants) of FUS can cause the alteration of the dynamics of mRNAs related to the spine morphology. Expression of NLS-truncated FUS (ΔNLS-FUS) showed the decrease of spine density in cortical neurons and also had no change of the portion of mature spines (Shiihashi et al., 2017), the tendency is consistent with this thesis study. Further investigation in that study also demonstrated the expression of ΔNLS-FUS reduced the expression of AMPA receptor subunits, trapped other mRNAs and RNPs and reduced local translation in the dendrites. In addition, in other study with FUS-R521C mutant showed that expression of that NLS mutant FUS exhibited the interference of DNA damage repair and reduced expression of brain-derived neurotrophic factor (BDNF), which is related to the generation and maintenance of synapses and dendrites (Qiu et al., 2014). Therefore, this reduced spine density can be started with the interruption of the spinogenesis and then co-progression with the degeneration of existing spines without changing the ratio of mature spines. On the other hand, overall dendritic spine size of FUS-WT expressing cells was increased without changing the number of spines. Considering the normal function of cytosolic FUS that is

required for the maturation of dendritic spines (Fujii and Takumi, 2005; Udagawa et al., 2015; Yokoi et al., 2017), FUS-WT may have slightly boosted the function. However, overexpressed FUS-WT was predominantly locked in the nucleus, the pathologic mechanism is more likely started from the inside of the nucleus. In addition, endogenous FUS was not knocked out, therefore, it is possible that FUS-WT could have boosted the leakage of FUS into the cytosol and caused the moderate effect similar to FUS-P525L. However, there is a possibility that overexpression of FUS-WT can cause opposite effects like autoregulation of the mRNA level of FUS, reducing the total level of endogenous FUS (Zhou et al., 2013). Though, the morphology of dendritic spines are highly dynamic and transient (Hering and Sheng, 2001), it needs to be careful to tell the actual status of the spines and further study would be required.

In summary, NLS mutant form FUS-P525L rapidly propagated to cytosol, formed dendritic FUS inclusions and cause synapse weakening in the distal part of the apical dendrites in CA1 neurons. To investigate the further pathophysiological alterations of cytosolic FUS, electrophysiological changes were also monitored in the further studies in the next chapter.

CHAPTER 4

Consequences of dendritic FUS inclusions on hippocampal neurophysiology

4.1. Introduction

4.1.1. Physiological alteration in the neurons with cytosolic FUS

By utilising NLS mutant FUS, Chapter 3 found that propagation of cytosolic FUS caused weakening of synapse structure in CA1 neurons. Therefore, it is of interest whether the aberrant inclusions of FUS result in functional modifications. As articulated in the Chapter 1, it is known that FUS plays a key role in neuronal homeostasis, synaptic regulation of dendritic spine (Higelin et al., 2016). Both gain- and loss-of-function are associated with FUS-mediated pathologies in terms of cellular and neurophysiological aspects, such as alteration of gene expression, alternative splicing that are critical for the viability of neurons (Ishigaki and Sobue, 2018; Scekic-Zahirovic et al., 2016). In addition, NLS mutants of FUS are also involved in the dysregulation of intracellular transport of essential molecules (e.g. mRNA) through dendrites, organelle interaction (e.g. endoplasmic reticulum (ER)-mitochondria interaction) and maintenance of dendritic spines of the cell (Farg et al., 2013; Shiihashi et al., 2017; Zinszner et al., 1997). The NLS mutant also results in a disruption of ER-mitochondria tethering and Ca^{2+} exchange between them (Stoica et al., 2016) to perturb ATP production and activate GSK-3β. The activation of GSK-3β is involved in neurodegenerative pathologies such as Tau phosphorylation in AD pathology (Regan et al., 2017) and the activity of GSK-3β is also increased by mutant TDP-43 (Ambegaokar and Jackson, 2011), therefore, it suggests that FUS pathology shares common pathway with the other neurodegenerative pathologies (Stoica et al., 2016). Collectively, suggesting that cytoplasmic FUS aberrantly regulate cellular homeostasis, Ca^{2+} signalling, axonal trafficking, neurophysiological function. It is notable that the link between Ca^{2+} and neurodegenerative diseases has been suggested because Ca^{2+} is one of the most versatile and universal secondary messenger that participate in very basic functions of cells, such as growth, survival, apoptosis and regulation of excitability of cells (Mattson, 2007). Therefore, it is important to know how

dysregulation of Ca^{2+} kills the neurons as a significant risk factor in the neurodegenerative diseases (Pchitskaya et al., 2018).

4.1.2. Excitotoxicity in FUS pathology

Some evidences suggest that alteration of neuronal excitability could be the part of the pathophysiology during neurodegeneration (e.g. increased excitability can induce excitotoxicity). Specifically, dysregulation of calcium ion (Ca^{2+}) in both ALS and FTLD was found to exhibit abnormal increase of Ca^{2+} permeability or decreased buffering ability of Ca^{2+} (Imamura et al., 2016; Leal and Gomes, 2015). It has been suggested that Ca^{2+} permeability profile of AMPARs can be altered in the ALS cases by the altered mRNA expression (Hideyama and Kwak, 2011). For instance, the NLS mutant FUS was shown to downregulate Gria2 (gene of GluA2) in the rodent stem cell model (Capauto et al., 2018), therefore, it was assumed that the overall composition of the AMPAR will be altered (e.g. less GluA2). The GluA2 subunit of AMPAR is important because it regulates the Ca^{2+}-permeability of AMPARs (Geiger et al., 1995; Jonas and Burnashev, 1995; Washburn et al., 1997). The GluA2 subunit is Ca^{2+}-impermeable (Pachernegg et al., 2015) and included in the most of AMPARs (about 95% in CA1 neurons) (Lu et al., 2009). However, absence of the GluA2 subunit leads AMPARs which are Ca^{2+}-permeable AMPARs (CP-AMPARs). In addition to the GluA2-lacking AMPARs, reduction of post-transcription modification of GluA2 (Q/R editing site) also causes the increase of CP-AMPARs (Isaac et al., 2007). Therefore, changed AMPAR subtypes by FUS NLS mutation could alter the intrinsic excitability of the neuron and induced excitotoxicity, ultimately leading to cell death.

As articulated above, NLS mutant FUS has been reported to induce the excitotoxicity and neuronal death. Then, we also need to know how synapses are changed by NLS FUS in the cytosol before the neuron undergoes degeneration. The reason to investigate the electrophysiology is that these tools are sensitive enough to measure the electric responses from synapses, therefore, small alteration of the ion channel profile (e.g. ratio of subtypes or

number of AMPARs) on the neuronal membranes can be detected. In addition, the functionality of dendritic spines (e.g. local translation or trafficking of neurotransmitter receptors) can be tested by induction of synaptic plasticity (e.g. LTP and LTD). Thus, it was of interest that the electrophysiological patterns of synaptic changes caused by cytosolic NLS mutant FUS (FUS-P525L).

4.2. Results

4.2.1. Expression of FUS-P525L mutant regulates the kinetics of mEPSCs

mEPSC represent a type of spontaneous responses caused by the release of a neurotransmitter vesicles from the presynaptic region (in the absence of action potential) and responses by receiving the neurotransmitters at the post-synaptic neurotransmitter receptors. Assays of mEPSC can determine modification of pre- and/or postsynaptic function.

In this section, mEPSCs from FUS-P525L and FUS-WT were compared with those from untransfected cells to investigate whether presynaptic release of neurotransmitter vesicles and the profile of postsynaptic receptors was changed by overexpression of wildtype and/or cytosolic FUS. To monitor the presynaptic profile, number of mEPSC event (inter-event interval) was counted and to monitor the postsynaptic profile, peak amplitude, rise time (10% to 90% of the maximum amplitude) and decay time (90% to 10% of the maximum amplitude) so amount and kinetics of postsynaptic receptors can be calculated. Peak amplitude is strongly correlate with the number of synaptic neurotransmitter receptors, meanwhile, rise and decay times are likely to be changed by the traits or kinetic alteration of each receptor. Therefore, comparing peak amplitude of mEPSC with rise and decay time would be a good start to look at how number of receptors and kinetics are altered and have any correlation for those alterations. To do so, first, mEPSCs from each group were plotted for the comparison of peak amplitude vs rise time (Fig. 4-1) and peak amplitude vs decay time (Fig. 4-2) to get the

brief idea of the correlation between peak amplitude and the kinetics of mEPSC events. Hippocampal slices from 9 animals for Control, 3 animals for FUS-WT and 4 animals for FUS-P525L were used during the mEPSC experiments.

The distribution of amplitude overlapped entire ranges of mEPSCs between untransfected control and FUS-P525L transfected neurons. However, FUS-P525L expressing neurons were more widely distributed in terms of the rise time of mEPSCs (Fig. 4-1c) compared to untransfected (Fig. 4-1a) and FUS-WT (Fig. 4-1b) groups. The trend was similar in the decay time of FUS-P525L (Fig. 4-2c) when compared to untransfected (Fig. 4-2a) and FUS-WT (Fig. 4-2b) groups. These graphs did not show any no significant correlation between peak amplitude and kinetics of mEPSC events.

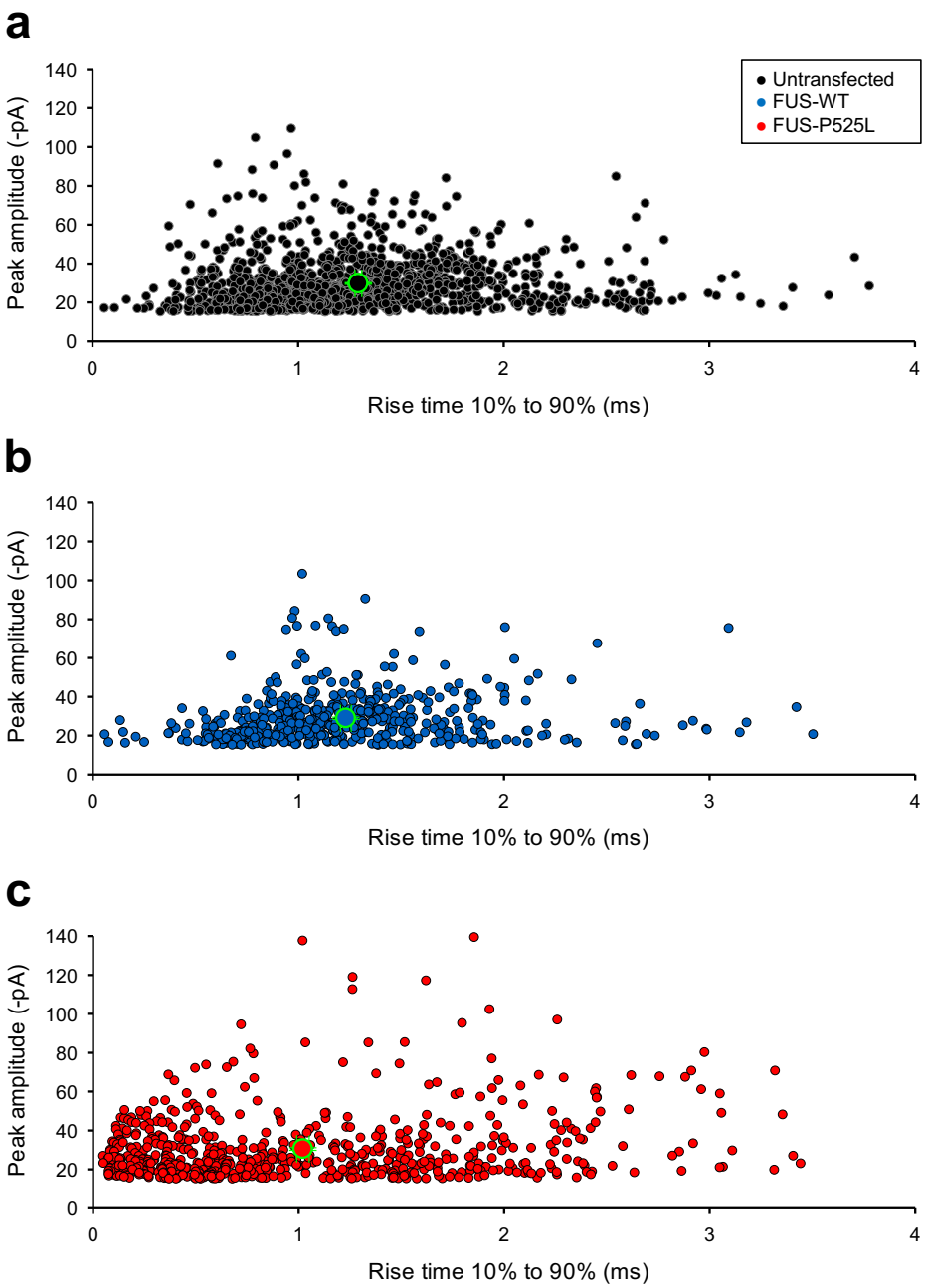

Figure 4-1 mEPSC comparison of peak amplitude vs rise time (10% to 90%)

Peak amplitude vs rise time of mEPSC from (a) untransfected, (b) FUS-WT, (c) FUS-P525L cells were plotted to check the difference of populated tendency. FUS-P525L showed notable decrease of rise time compared to the other groups.

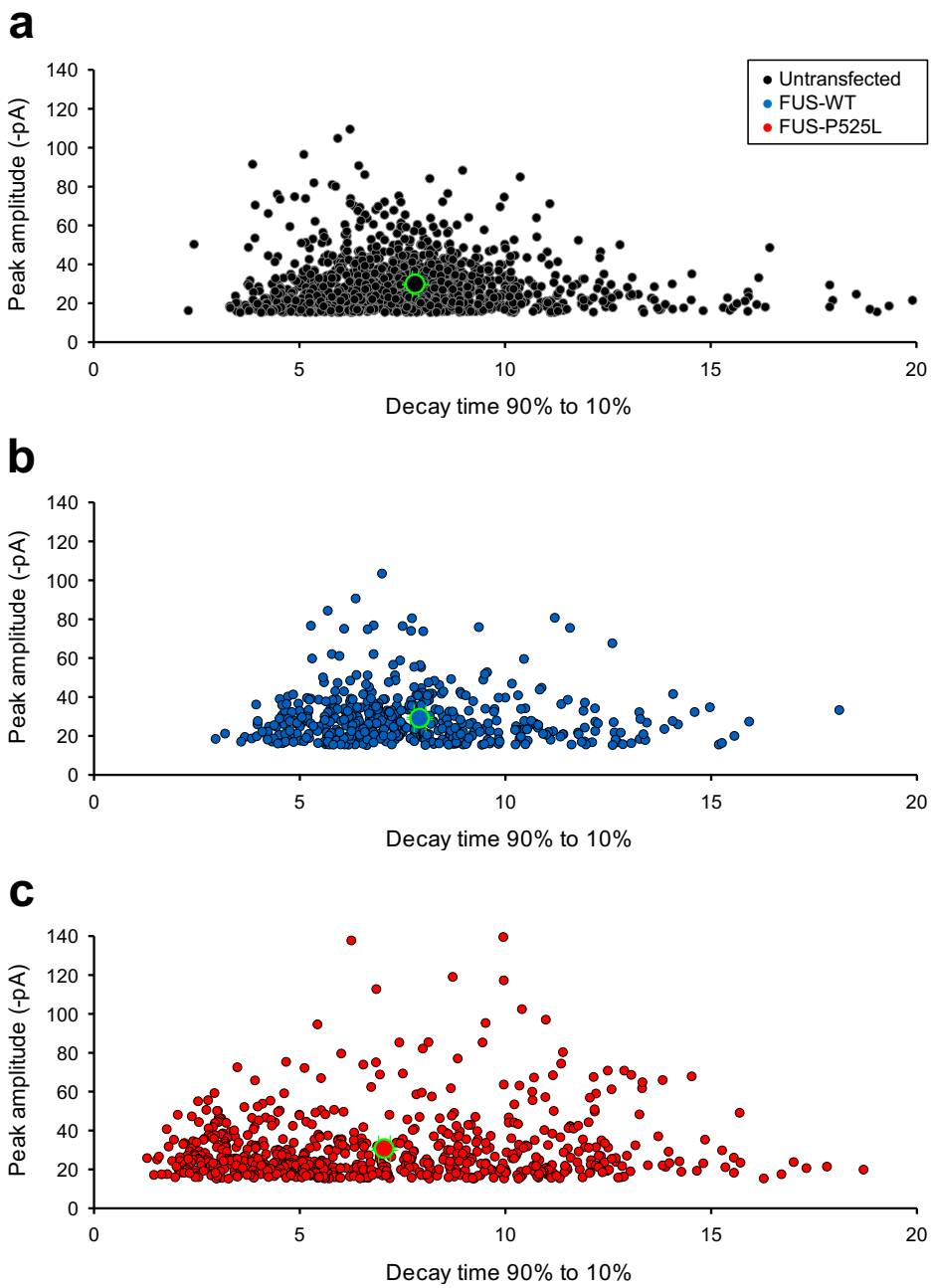

Figure 4-2 mEPSC comparison of peak amplitude vs decay time (90% to 10%)

Peak amplitude vs decay time of mEPSC from (a) untransfected, (b) FUS-WT, (c) FUS-P525L cells were plotted to check the difference of populated tendency. FUS-P525L showed notable decrease of decay time compared to the other groups.

Next, those mEPSC events from Fig. 4-1 and Fig. 4-2 were statistically analysed for each parameter to investigate any alterations by FUS-P525L or FUS-WT expressions (Fig. 4-3, 4) (Untransfected: n = 1147 events, 20 cells, FUS-WT: n = 498 events, 12 cells, FUS-P525L: n = 651 events, 11 cells). Events from each cell were averaged for the comparison between groups. The data set was shown as Mean ± Standard Error of Mean (SEM). The amplitude of events from each group (Fig. 4-3b) did not show any statistic differences and distributions were similar in cumulative curves (Untransfected: 27.663 ± 1.217 -pA, FUS-WT: 26.612 ± 1.645 -pA, FUS-P525L: 31.613 ± 2.327 -pA) (One-way ANOVA: p = 0.130, F = 2.148). The frequency of mEPSC (Fig. 4-3c) also had no statistical differences between groups (Untransfected: 1.1651 ± 0.2867 Hz, FUS-WT: 1.1836 ± 0.3248 Hz, FUS-P525L: 1.1304 ± 0.2897 Hz) (One-way ANOVA: p = 0.994, F = 0.00616). The rise time of mEPSC events (Fig. 4-4a) did not show any significant differences between groups (Untransfected: 1.337 ± 0.071 Hz, FUS-WT: 1.315 ± 0.105 Hz, FUS-P525L: 1.269 ± 0.162 Hz) (One-way ANOVA: p = 0.901, F = 0.104). The mEPSC event decay time (Fig. 4-4b), was also did not show statistical differences (Untransfected: 8.116 ± 0.307 ms, FUS-WT: 8.275 ± 0.447 ms, FUS-P525L: 8.515 ± 0.752 ms) (One-way ANOVA: p = 0.835, F = 0.181). Although there were no statistical differences in rise and decay time of mEPSC between groups, the cumulative curves with individual events showed shifted rise and decay time in FUS-P525L neurons that indicates the marginal chance of alteration by overexpression. Overall, FUS-P525L overexpression did not show any alteration of the properties of mEPSC. This suggests that FUS-P525L expression did not alter the conductance of mEPSC events significantly in CA1 neurons.

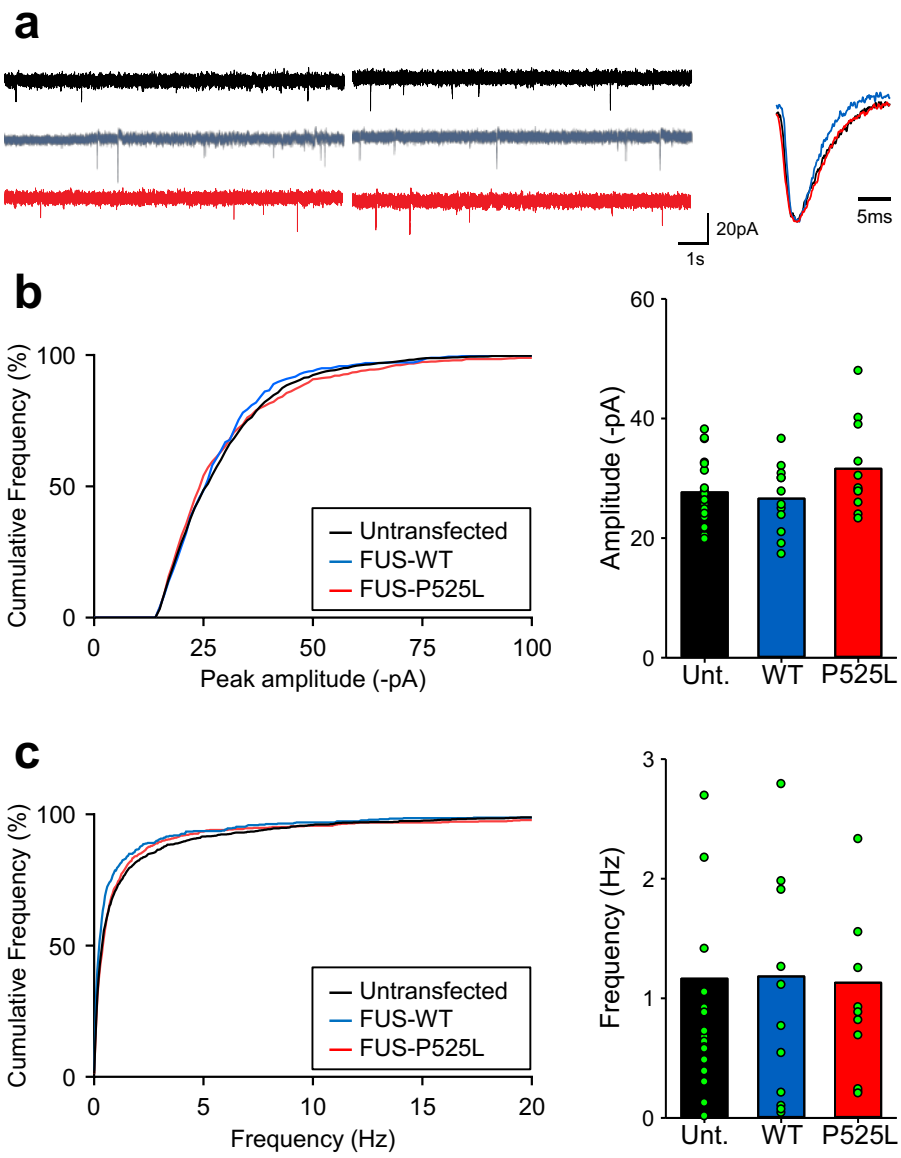

Figure 4-3 Peak amplitude and frequency of mEPSC did not show statistical difference between untransfected and FUS-WT and FUS-P525L expressing neurons.

mEPSC events from Fig. 4-1 and Fig. 4-2 were statistically compared. (a) Example recordings from untransfected (black), FUS-WT (blue) and FUS-P525L (red). Averaged mEPSC single traces were taken and the peak scale was fitted from each group's one example cell. (b) Peak amplitude of mEPSC events did not show any statistic difference between groups. (c) Frequency of mEPSC events was not significantly different between groups.

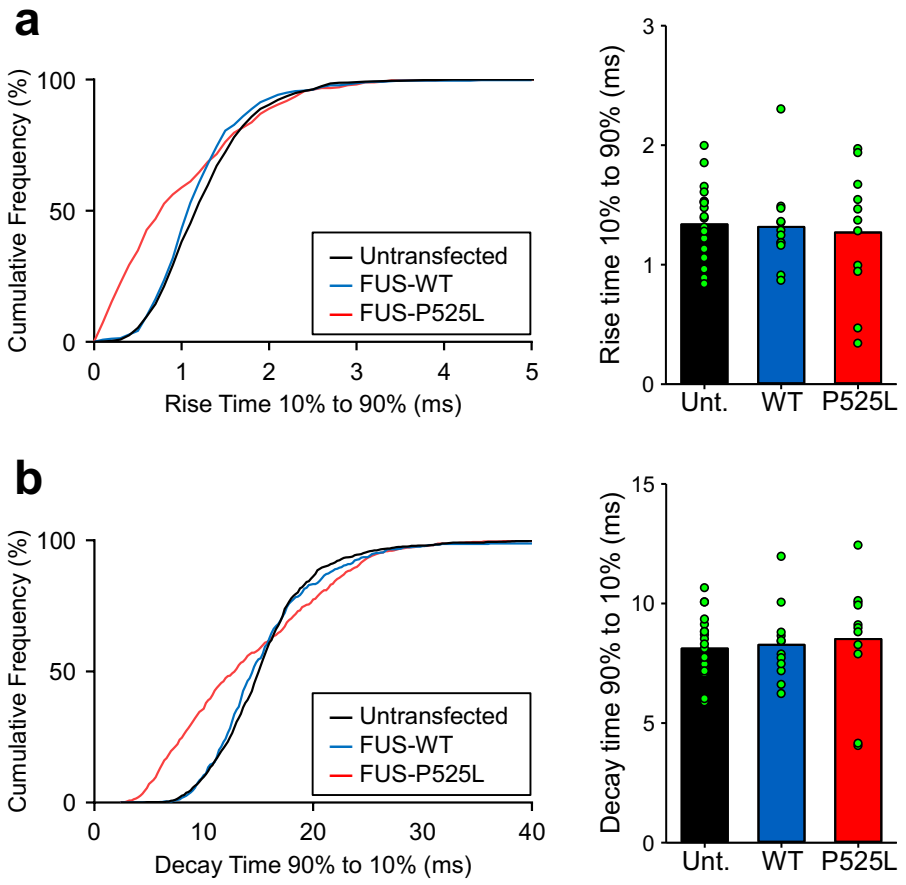

Figure 4-4 Kinetics of mEPSC was faster in FUS-P525L expressing neurons.

mEPSC events from Fig. 4-1 and Fig. 4-2 were statistically compared. (a) Cumulative comparison of the rise time (10% to 90%) was reduced in FUS-WT and the reduction was bigger in FUS-P525L cells, however, averaged values from each cell did not show any difference between groups. (b) Cumulative comparison of the decay time (90% to 10%) was significantly decreased in FUS-P525L cells, not in FUS-WT cells, however, averaged values from each cell did not show any difference between groups. Overall, FUS-P525L had events with decreased rise and decay time compared to untransfected and FUS-WT cells but it was not great enough to show difference in averaged comparison between groups.

4.2.2. Intrinsic excitability is increased in FUS-P525L expressing neurons

The intrinsic excitability indicates how neurons are depolarised to fire action potentials. This property depends on the resting membrane potential and ion exchange through ion channels and receptor profile of the neuron. Therefore,

intrinsic excitability is related to the input-output of the neuron (Nelson and Turrigiano, 2008; Zhang and Linden, 2003). Since excitotoxicity has been reported in various ALS studies (Van Damme et al., 2005; King et al., 2016), it is important to investigate whether inclusions of FUS affect intrinsic excitability of the neuron.

Firing activity experiments were conducted with CA1 neurons in the presence or absence of FUS-P525L or FUS-WT transfection. Transfected and adjacent untransfected neurons were recorded and analysed by a pair-wise assay within the same hippocampal slices. The main comparison parameters were frequency (calculated from inter-event interval) and number of firing activity events. The resting membrane potentials and threshold of action potentials were also measured for the additional profiles of cells. The data set was shown as Mean ± SEM for each X-axis point. Hippocampal slices from 7 animals for FUS-P525L, 9 animals for FUS-WT were used during the firing activity experiments.

First, the intrinsic excitability of FUS-P525L expressing cells were compared with paired untransfected neurons (Fig. 4-5). FUS-P525L cells required a smaller current input (about 100 pA) to be fired when compared to the untransfected counterparts (about 200 pA) (Fig. 4-5a). In addition, FUS-P525L cells had increased firing frequency overall (degree of freedom (DF) = 1, F = 6.141, p = 0.022, n = 22 cells each) (Fig. 4-5b) when compared with untransfected cells. The number of events increased until an input of 200 pA (DF = 1, F = 7.749, p = 0.011, n = 22 cells each) (Fig. 4-5c), when the input goes over 250 pA and higher, the number of events of FUS-P525L was saturated due to the desensitisation of the neurons and overtaken by that of untransfected cells, thus, overall comparison from -50 to 450 pA did not show the significant differences (DF = 1, F = 0.0101, p = 0.921, n = 22 cells each).

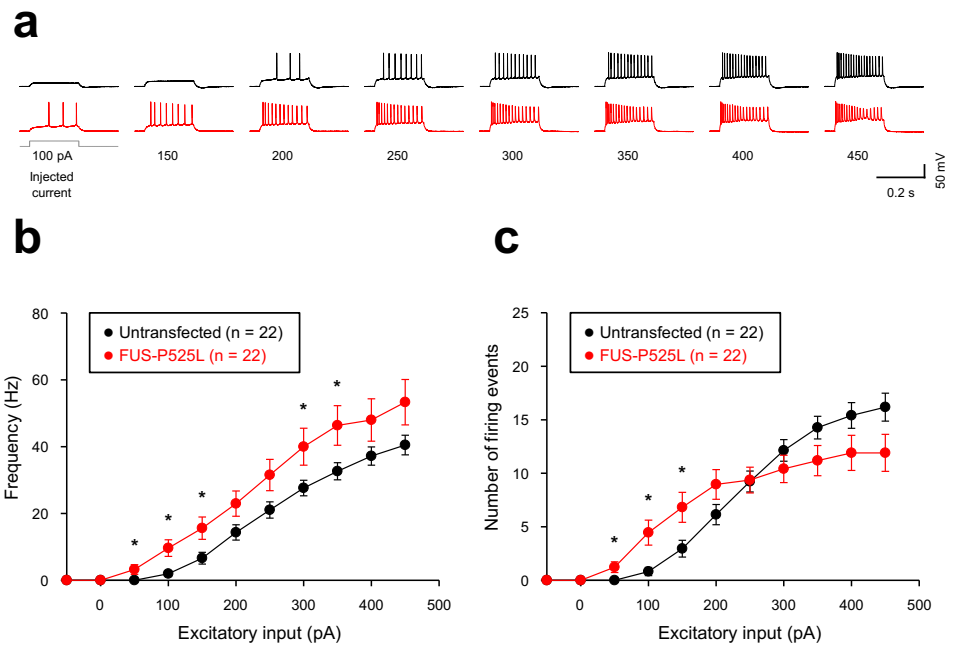

Figure 4-5 Intrinsic excitability was increased in FUS-P525L expressing neurons.

(a) Example firing activity patterns by current injection of 100-450 pA in control neuron (black) and FUS-P525L neuron (red). (b) Frequency of firing activity in FUS-P525L was higher at 50, 100, 150, 300, 350 pA injection and overall comparison with untransfected group also showed the increase of the frequency. (c) Number of firing event of firing activity was increased in FUS-P525L until the input of 200 pA, however the number of the events was saturated from 250 pA injection, therefore, overall comparison between groups did not show the significant difference.

Next, the intrinsic excitability of FUS-WT cells was compared with untransfected neurons (Fig. 4-6). FUS-WT cells showed very similar firing pattern when compared to untransfected cells (Fig. 4-6a). Also, firing frequency (DF = 1, F = 2.457, p = 0.135, n = 18 cells each) (Fig. 4-6b) of FUS-WT showed no statistical differences from untransfected cells but the number of events were decreased (DF = 1, F = 5.642, p = 0.030, n = 18 cells each) (Fig. 4-6c).

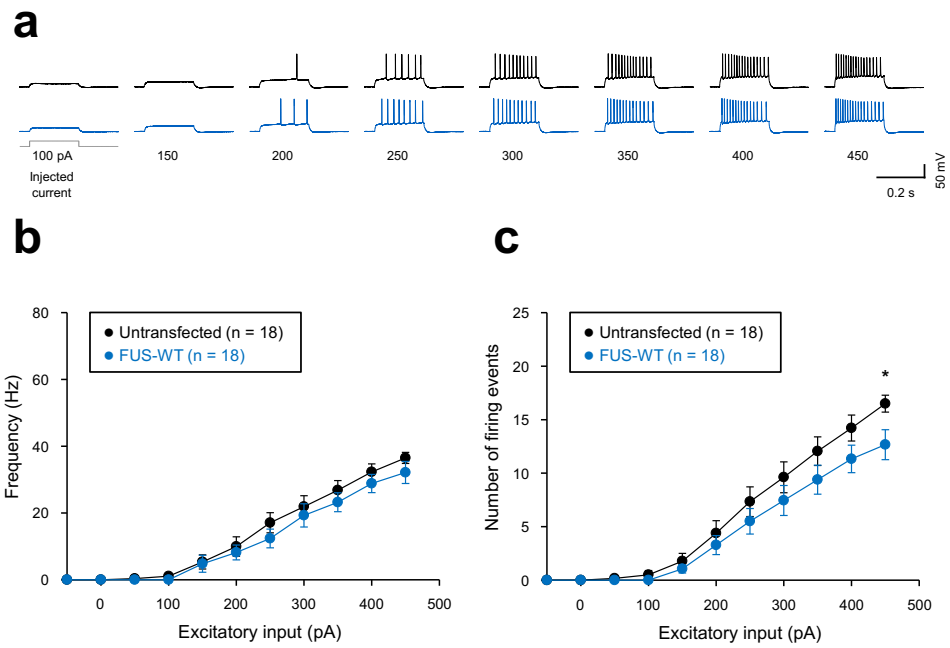

Figure 4-6 Intrinsic excitability was slightly decreased in FUS-WT expressing neurons.

(a) Example firing activity patterns by current injection of 100-450 pA in control neuron (black) and FUS-WT neuron (blue). (b) Frequency of firing activity in FUS-WT did not show any significant differences from untransfected group. (c) Number of firing event of firing activity was decreased at the current injection of 450 pA in FUS-WT cells and overall comparison with untransfected group reveals slight decrease in FUS-WT cells.

Overall, FUS-P525L showed an increased intrinsic excitability however, FUS-WT did show no statistical differences in firing frequency when compared with untransfected counterpart but decrease in the number of events. This suggests that FUS can cause hyper-excitability and it leads the neuron to be more susceptible to the excitotoxicity in synapse. In addition, overexpression of wildtype FUS altered the intrinsic excitability but in the opposite direction and a milder manner when compared to the FUS-P525L cells.

4.2.3. Evoked basal synaptic transmission is reduced in FUS-P525L expressing neurons

Evoked basal synaptic transmission to CA1 through Schaffer-collateral synapses are involved in cellular mechanism of learning and memory in the hippocampus. Since Chapter 3 showed a selective decrease of apical dendritic spines in FUS-P525L expressing neurons, it is of interest whether evoked basal synaptic transmission is affected by inclusions of FUS in CA1. Electrically evoked AMPAR and NMDAR-induced synaptic currents through Schaffer-collateral pathway were analysed to determine any alteration in the basal synaptic transmission of the pathway. This is essential as the AMPARs and NMDARs are the main synaptic components of the excitatory neurons in the pathway (SC to CA1). The data set was shown as Mean ± SEM. Hippocampal slices from 10 animals for FUS-P525L, 5 animals for FUS-WT were used for the basal synaptic transmission experiments.

Both $EPSC_{AMPA}$ and $EPSC_{NMDA}$ of FUS-P525L and FUS-WT cells were paired and compared with adjacent untransfected cells (Fig 4-7). In the comparison of FUS-P525L vs untransfected cells (Fig. 4-7b, c), both $EPSC_{AMPA}$ (FUS-P525L: -158.8 ± 13.0 pA, untransfected: -214.9 ± 13.5 pA, p = 0.004 (power: 0.836), n = 25) and $EPSC_{NMDA}$ (FUS-P525L: 136.5 ± 16.8 pA, untransfected: 254.8 ± 29.7 pA, p = 0.001 (power: 0.920), n = 18) were significantly reduced in FUS-P525L cells compared with control untransfected cells. However, in the FUS-WT vs untransfected cells (Fig. 4-7e, f), there were no statistical differences in terms of $EPSC_{AMPA}$ (FUS-WT: -151.0 ± 9.7 pA, untransfected: -187.8 ± 28.7 pA, p = 0.236, n = 13) and $EPSC_{NMDA}$ (FUS-WT: 128.5 ± 22.4 pA, untransfected: 167.5 ± 31.8 pA, p = 0.327, n = 13).

Overall, basal synaptic transmission was altered in FUS-P525L cells but not in FUS-WT cells. This means the postsynaptic profile of the main two excitatory glutamatergic receptors were altered, which may represent a change in the number and/or conductance of glutamate receptors.

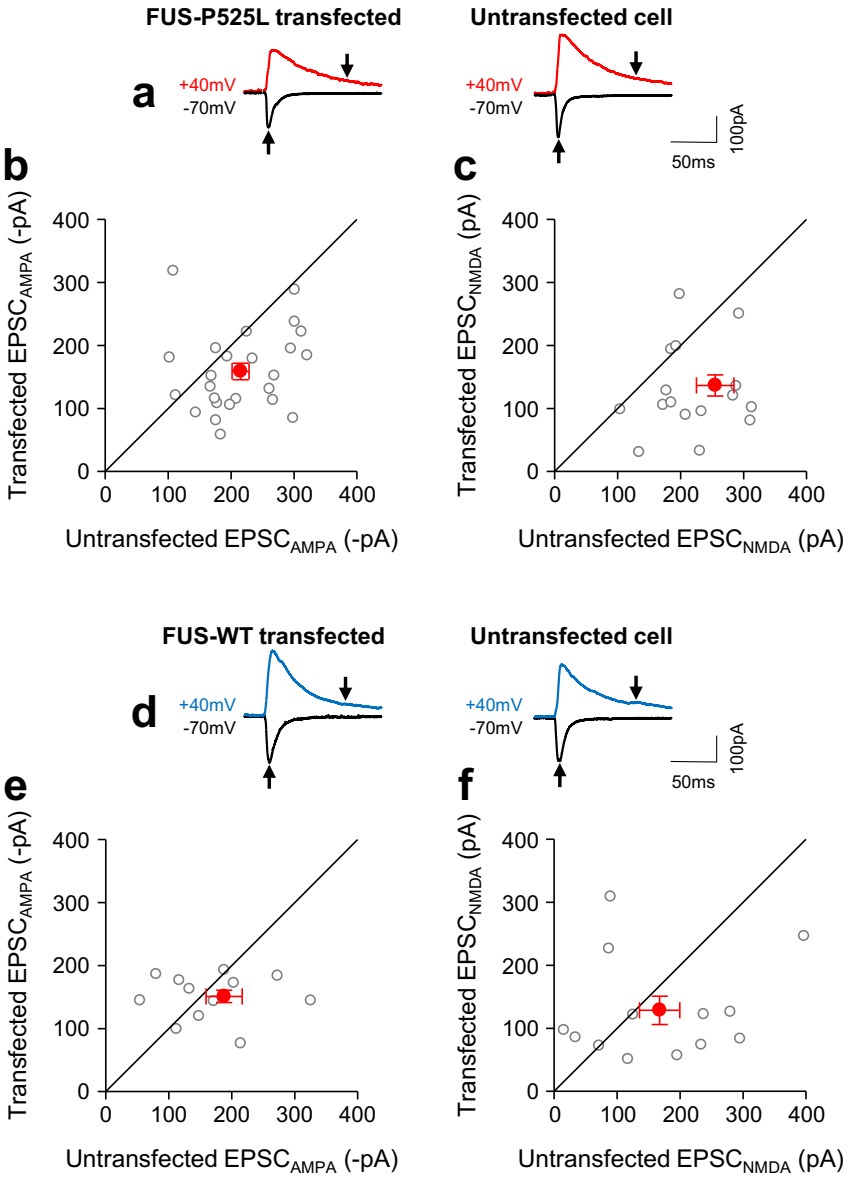

Figure 4-7 Amplitudes of AMPAR and NMDAR mediated currents were smaller in FUS-P525L expressing neurons, not in FUS-WT expressing neurons.

(a) Example single traces of AMPAR and NMDAR mediated currents from FUS-P525L cell and a paired untransfected cell was displayed. (b) Average amplitudes of AMPAR mediated currents were smaller in FUS-P525L cells. (c) Average amplitudes of NMDAR mediated currents were smaller in FUS-P525L cells. (d) Example single traces of AMPAR and NMDAR mediated currents from FUS-WT cell and a paired untransfected cell was displayed. (e) Average amplitudes of AMPAR mediated currents did not show any significant differences between FUS-WT cells and paired untransfected cells. (f) Average amplitudes of NMDAR mediated currents did not show any significant differences between FUS-WT cells and paired untransfected cells.

4.2.4. CP-AMPAR blocker IEM-1460 attenuated the increased excitability of FUS-P525L mutant neurons

The FUS-P525L induced alteration to the mEPSCs kinetics and firing activity suggested changes in postsynaptic function. Therefore, this chapter also investigates whether FUS-P525L expression dysregulates the postsynaptic receptor profile, specifically glutamate receptor. Since AMPAR are involved in generating the fast component of EPSC, a conductance change of AMPAR may regulate kinetics of mEPSC and increased intrinsic excitability. AMPAR conductance changes are mainly due to the Ca^{2+} permeability profile dictated by the GluA2 subunit (Swanson et al., 1997) (also see section 1.1.4). Furthermore, an increase in CP-AMPARs can directly cause increased neuronal excitability (Li et al., 2012). Therefore, this chapter investigated whether inclusion of FUS regulates CP-AMPAR and affect the intrinsic excitability of the neuron. The competitive, voltage-dependent open channel CP-AMPAR blocker IEM-1460, which blocks both GluA2-lacking and unedited GluA2 containing AMPARs (Schlesinger et al., 2005), was tested on firing activity experiments with FUS-P525L and FUS-WT transfected CA1 cells (Fig. 4-8, 9). The data set was shown as Mean ± SEM for each X-axis point. Hippocampal slices from 7 animals for FUS-P525L, 5 animals for FUS-WT were used for the firing activity experiments with IEM-1460.

FUS-P525L cells with IEM treatment did not show the increased firing frequency ($F = 3.296$, $p = 0.091$, n = 15) (Fig. 4-8b) and number of events ($F = 3.604$, $p = 0.078$, n = 15) (Fig. 4-8c) when compared with IEM-treated untransfected cells. Crosschecking with FUS-WT with IEM treatment also did not show any alterations of firing frequency ($F = 0.0216$, $p = 0.886$, n = 12) (Fig. 4-9b) and number of events ($F = 0.164$, $p = 0.694$, n = 12) (Fig. 4-9c).

Therefore, the increased intrinsic excitability caused by cytosolic FUS (FUS-P525L) (Fig. 4-5) may have occurred due to the CP-AMPARs and this is consistent with the increased conductance of mEPSC (Fig. 4-1~4). However, it is not clear if the CP-AMPARs consist of GluA2-lacking AMPARs and/or

unedited GluA2-containing AMPARs, therefore, this requires further studies in the future.

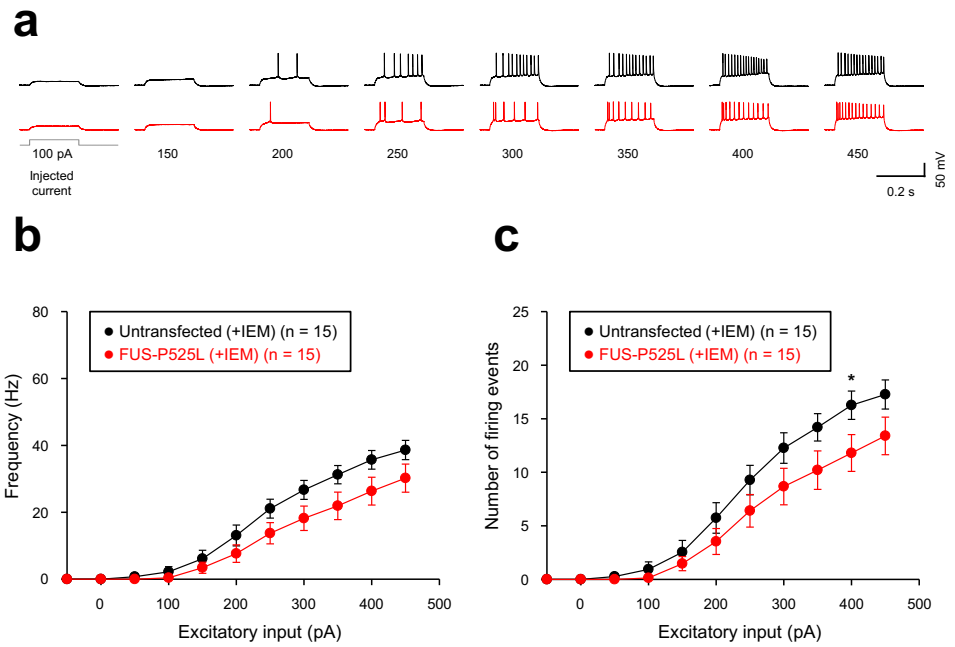

Figure 4-8 Increased intrinsic excitability in FUS-P525L expressing neurons was attenuated by CP-AMPAR blocker, IEM-1460.

(a) Example firing activity patterns by current injection of 100-450 pA in control neuron (black) and FUS-P525L neuron (red). (b) Frequency of firing activity with IEM-1460 in FUS-P525L cells did not show any differences with untransfected counterparts. (c) Number of firing event of firing activity with IEM-1460 in FUS-P525L cells showed decrease at 400 pA current injection but overall comparison with untransfected cells did not show statistical differences.

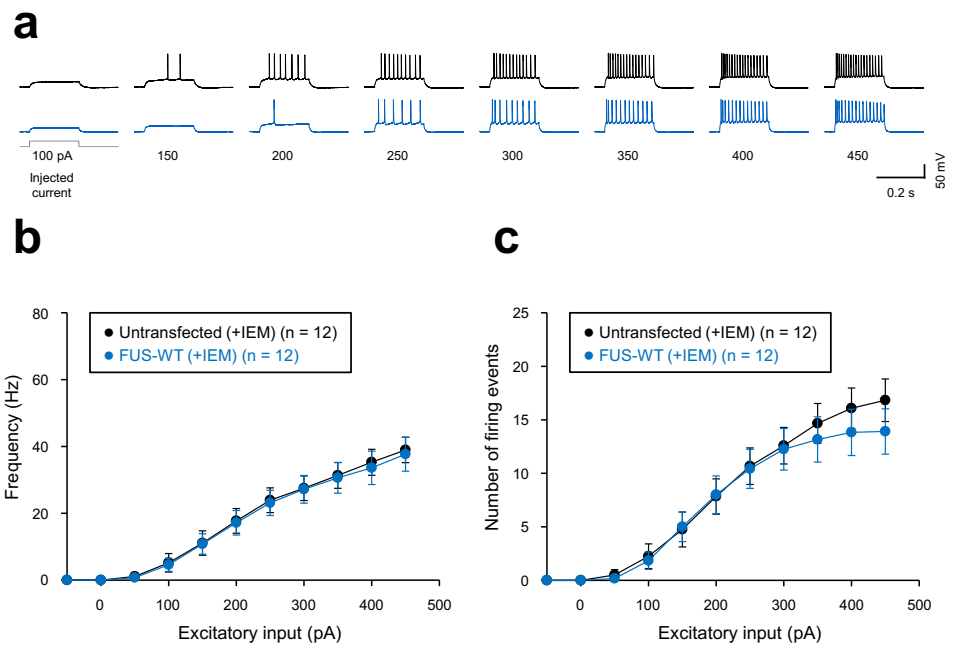

Figure 4-9 Intrinsic excitability did not show any difference between FUS-WT expressing neurons and untransfected neurons in the presence of CP-AMPAR blocker, IEM-1460.

(a) Example firing activity patterns by current injection of 100-450 pA in control neuron (black) and FUS-WT neuron (blue). (b) Frequency of firing activity in FUS-WT cells did not show any difference with untransfected counterparts. (c) Number of firing event of firing activity also did not show any significant difference between FUS-WT and untransfected cells.

4.2.5. Induction of long-term synaptic plasticity was inhibited in FUS-P525L expressing neurons

As articulated in the general introduction chapter 1, LTP and LTD are fundamental types of synaptic plasticity that regulate the efficacy of synaptic plasticity. For this process, neuronal input from the presynaptic neuron to the postsynaptic neuron needs to be delivered in the specific patterns, such as HFS for LTP and LFS for LTD. They are accompanied by the trafficking of postsynaptic surface AMPARs (Malenka and Bear, 2004).

The experiments were performed 3-4 days after FUS-P525L transfection. The data set was shown as Mean ± SEM for the comparison of the post-

LTP/LTD induction EPSC. Hippocampal slices from 7 animals for LTP, 11 animals for LTD experiments were used. Induction of LTP (2 Hz, 200 pulses at 0 mV) (Conducted by Dr. Jee Hyun Yi) was inhibited in FUS-P525L transfected hippocampal CA1 cells (100.9 ± 9.4 %, n = 12) and it was significantly different (p = 0.00564 (power = 0.894)) from control CA1 cells (166.2 ± 17.5 %, n = 11) (Fig. 4-10). Induction of LTD (1 Hz, 200 pulses at -40 mV) was inhibited in FUS-P525L transfected hippocampal CA1 cells (90.37 ± 7.46 %, n = 13) and it was significantly different (p = 0.00201 (power = 0.910)) from control CA1 cells (58.00 ± 5.93 %, n = 15) (Fig. 4-11).

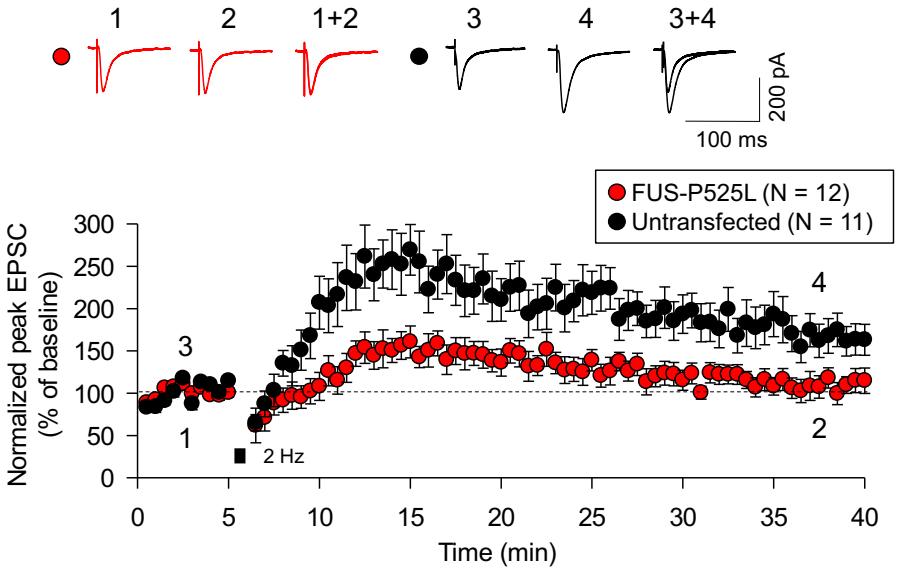

Figure 4-10 LTP induction was inhibited in FUS-P525L neurons.

LTP was induced by 200 pulses of 2 Hz stimulation at the holding voltage of 0 mV. In FUS-P525L cells, LTP induction was inhibited, whereas untransfected cells exhibited induction of LTP.

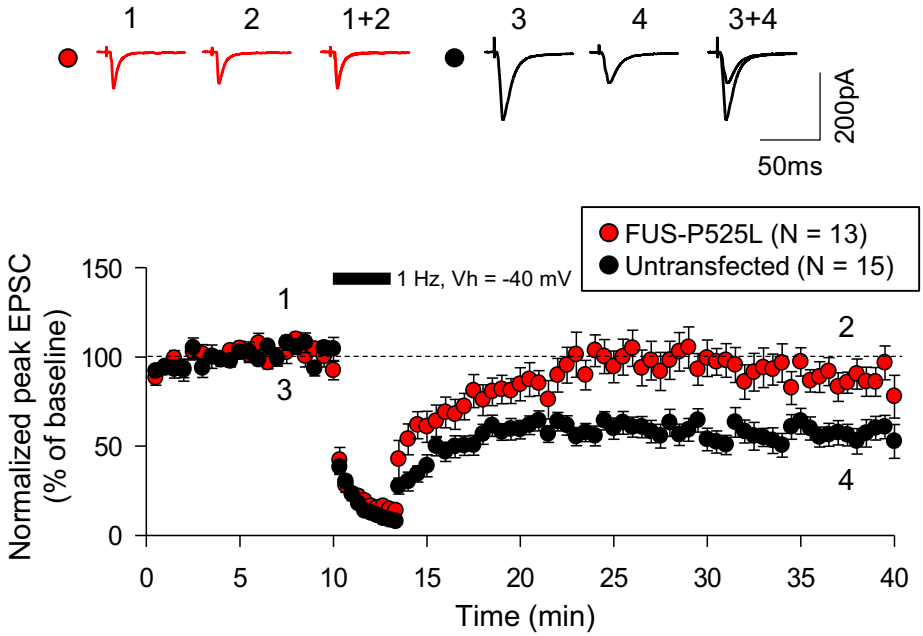

Figure 4-11 LTD induction was inhibited in FUS-P525L neurons.

LTD was induced by 200 pulses of 1 Hz stimulation at the holding voltage of -40 mV. In FUS-P525L cells, LTD induction was inhibited, whereas untransfected cells exhibited induction of LTD.

Overall, both LTP and LTD were inhibited by dendritic inclusions of FUS in CA1 neurons. This implies that pathology of cytosolic FUS is not biased to one direction of synaptic plasticity and it impairs the whole mechanism of synaptic plasticity possibly by interrupting local translation of proteins or mRNA trafficking into the dendrites or binding with machinery signalling proteins near dendritic spines, which will require further studies. This may explain how FUS affects learning and memory by inclusions of FUS in neurodegenerative disease.

4.3. Discussion

4.3.1. FUS-P525L alters neurophysiology of CA1 neurons

In this chapter, physiological alterations of hippocampal neurons by NLS mutant form of FUS (FUS-P525L) were investigated in the comparison with FUS-WT. FUS-P525L expression did not alter the amplitude and frequency of mEPSC because single AMPAR current is about -7.2 pA (Amin et al., 2017) and the difference of averaged peak mEPSC amplitude from each synapse was only 1-2 pA, which is not enough to represent the altered number of AMPARs in each synapse. Rise time and decay time kinetics of mEPSC correlate with synaptic conductance and they were massively changed in the comparison of mEPSC events, however, when it comes to the averaged value of each cell, difference was not significant. Taking together, this would be more likely postsynaptic alteration of the composition of the neurotransmitter receptors than the total amount change of those receptors and these changes would be occurred only in the certain local population of the dendritic spines. This would be the reason why the reduction of dendritic spines did not correlate with the peak amplitude, frequency nor averaged values of synaptic kinetics. In addition, FUS-P525L expressing neurons had increased intrinsic excitability whereas FUS-WT neurons had decreased intrinsic excitability, which suggests the regulatory roles of FUS that cytosolic FUS boosts the excitability and nuclear FUS reduces the excitability. This can be multiple mechanisms but one possible scenario is the interaction between FUS-P525L and mitochondria that induces mitochondrial damage and ROS production (Deng et al., 2015) that causes the increased excitability of cells (Zsurka and Kunz, 2015). It is not clear how FUS-WT reduced the excitability but ALS mutant FUS can be related to the hypoexcitability by the imbalance of ion balance, specifically reduction of Na^+/K^+ ratio by increased expression of potassium channel subtypes and decreased expression of sodium channel subtypes (Naujock et al., 2016). It is because sodium channels are responsible for depolarisation to let neuron exhibit action potentials and then potassium channels are responsible for repolarisation to

let neurons to terminate the action potential and be ready for the next action potentials. However, further mechanism needs to be studied for more accurate explanations. Evoked basal synaptic transmission was decreased in FUS-P525L neurons and this represents the reduction of the total amount of AMPARs and NMDARs in the apical dendrites. Since apical dendrites of CA1 neuron are the main receiver of the input via Schaffer-collateral (Jarsky et al., 2005), these synaptic alterations by FUS-P525L expression would be site specific. The spine densities of overall basal or apical dendrites were not significantly different between FUS-P525L and other groups (Venus and FUS-WT), however, within apical dendrites of FUS-P525L neurons, there were lesser spines at the distal than proximal dendritic region. Distal components of dendrites are known to be more sensitive to synaptic Ca^{2+} signalling and synaptic plasticity compared to proximal dendrites (Weber et al., 2016), therefore, lesser spines in specific populations could be consistent with the reduced AMPAR- and NMDAR-mediated EPSC and it may not correlate with mEPSC, since mEPSC is coming from all different kinds of dendritic spines from proximal to distal, basal to apical dendrites. Then, collected data suggested the change of postsynaptic profile by cytosolic FUS and the relationship between FUS pathology and excitotoxicity has been reported in other studies (Aizawa et al., 2016; King et al., 2016; Tischbein et al., 2019), thus, the intrinsic excitability was examined again with CP-AMPAR blocker IEM-1460. As demonstrated, the increased excitability of FUS-P525L expressing neurons was attenuated by IEM-1460, indicating that this response originated from CP-AMPAR. Thus, FUS-P525L altered the receptor composition increasing the CP-AMPARs. And then, synaptic plasticity induction was tested and FUS-P525L neurons showed the inhibited LTP and LTD induction. As synaptic plasticity requires the local translation of new proteins (Costa-Mattioli et al., 2009), there would be possibilities that FUS-P525L may have interrupted the machinery. Or, FUS-P525L already could have boosted the maturation of dendritic spines by massively accelerating local translation of synaptic proteins such as GluA1 subunits, therefore, further induction of synaptic plasticity was not available. Still there

is a caveat that the transfection itself had slightly interfered those mechanism, thus, there is a room to further cross-confirm LTP and LTD results with FUS-WT or Venus transfected neurons.

Overall, the neurophysiology of CA1 cells, from the basal synaptic transmission to the intrinsic excitability and synaptic plasticity, were all altered by FUS-P525L expression.

4.3.2. Increase of CP-AMPAR is part of FUS pathology

It has previously been demonstrated that ALS related FUS mutation caused a decreased expression of Gria2 (Capauto et al., 2018). Thereby, implying a reduction of GluA2 subunit in total AMPARs, which would increase the proportion of AMPARs permeable to Ca^{2+}. In addition, from sporadic ALS patients, mRNA of ADAR2 was downregulated and this caused decrease of GluA2 Q/R editing (target of ADAR2 activity) to increase the proportion of Ca^{2+}-permeable GluA2-containing AMPARs (Yamashita and Kwak, 2014). The ADAR2 downregulation has been co-occurred with the fragmentation and aggregation of TDP-43 in TDP-43 pathology, thus, one of them could be considered as the upstream of the counterpart (Aizawa et al., 2010). Then, increase of Ca^{2+} by increased CP-AMPAR and the activation of a protease calpain were suggested as the upstream of TDP-43 cleavage and aggregation (Yamashita et al., 2012). Furthermore, an ALS patient with FUS mutant (P525L, in NLS region) showed deficiency of ADAR2 and GluA2 Q/R editing (Aizawa et al., 2016), therefore, FUS pathology can be closely linked to the increase of CP-AMPAR and Ca^{2+} dysregulation in the neurons. As articulated above, abnormal expression of FUS is responsible for the altered AMPAR profile by altering gene expression and/or modification of GluA2. This altered GluA2 expression in ALS has been suggested as one of the underlain mechanisms of motor neuron vulnerability, hyperexcitability and excitotoxicity of ALS neurons (King et al., 2016; Vandenberghe et al., 2000), therefore, altered ratio of AMPAR subtypes by FUS NLS mutation might have changed intrinsic excitability and induced excitotoxicity to cell death.

In addition to the roles in excitability, CP-AMPAR also has roles in other essential functions of neurons and possibly altered CP-AMPAR may cause the change of those functions during pathology. CP-AMPAR is known to participate in synaptic plasticity, which is different from conventional NMDAR-dependent LTP (Jia et al., 1996; Park et al., 2019). It has been shown to be involved in two steps, 1. activation of protein kinase A (PKA) for the phosphorylation of GluA1 at S845 to induce CP-AMPAR exocytosis and 2. recruit peripheral CP-AMPARs into the synaptic region (Park et al., 2018). Step 2 is thought to be NMDAR-independent LTP and does not necessarily need to be consecutive to step 1 (Jia et al., 1996; Whitehead et al., 2013). These have been mainly demonstrated by GluA2 KO, antagonising GluA2 or inhibition of GluA2 editing (Okada et al., 2001). In addition, high calcium permeability of neuron is required for synaptogenesis and that mechanism is crucial during developmental period of immature brain, therefore, the composition of CP-AMPAR (mainly by regulating expression of GluA1:2 ratio) is increased during that period (Kumar et al., 2002). CP-AMPAR-mediated synaptic plasticity also has roles during rapid response to the neuronal condition such as acute stress and oligomeric Aβ treatment (Whitcomb et al., 2015; Whitehead et al., 2013).

Considering the roles of CP-AMPAR in the synaptic region, it would be plausible to think that the altered expression of CP-AMPAR by abnormal FUS expression would interfere synaptic plasticity. Still, this aspect requires further investigations and evidences to prove the direct mechanism between the expression of NLS mutant FUS and increased level of CP-AMPARs by increasing GluA2-lacking AMPARs, Q/R-unedited GluA2-containing AMPARs or other unidentified mechanisms.

Chapter 5

Enhanced cation-π interaction of FUS and synaptic changes

5.1. Introduction

5.1.1. FUS-FUS protein interaction

FUS and other RBPs are prone to be assembled into either heterogeneous SGs or non-SG aggregates that consist of predominantly FUS (Shelkovnikova et al., 2014). The molecular interactions of FUS are mediated by LC domain (Murakami et al., 2015; Murthy et al., 2019) and RGG-rich domains (Burke et al., 2015) and these interactions include very basic molecular interactions such as hydrogen bonding and hydrophobic interactions (Murthy et al., 2019) and also, cation-π interaction that modulated by arginine methylations (Fig. 5-1), which can affect the FUS-FUS protein interactions (Dormann et al., 2012; Rappsilber et al., 2003). This attractive interaction induces aggregation of FUS proteins to form liquid-liquid phase separation (LLPS) that can constitute membrane-free organelles to participate in the cellular functions such as local translation or transport of RNA (Sephton and Yu, 2015; Weber and Brangwynne, 2012). Though LLPS is involved in the cellular functions, it can be an initiative process of FUS proteinopathy in the neurons (Murthy et al., 2019). LLPS state of FUS can be progressed to irreversible fibrils under certain conditions, such as low concentration of salt, low level of methylation (hypomethylation) on arginine residues (Qamar et al., 2018) or disease specific mutations on FUS (Murakami et al., 2015; Patel et al., 2015). And LLPS can be dissociated by interaction with TRN-1, ATP and single-stranded DNA (ssDNA) (Hofweber et al., 2018; Kang et al., 2019). Therefore, formation and dynamics of LLPS have been regarded as an important mechanism of FUS proteinopathy.

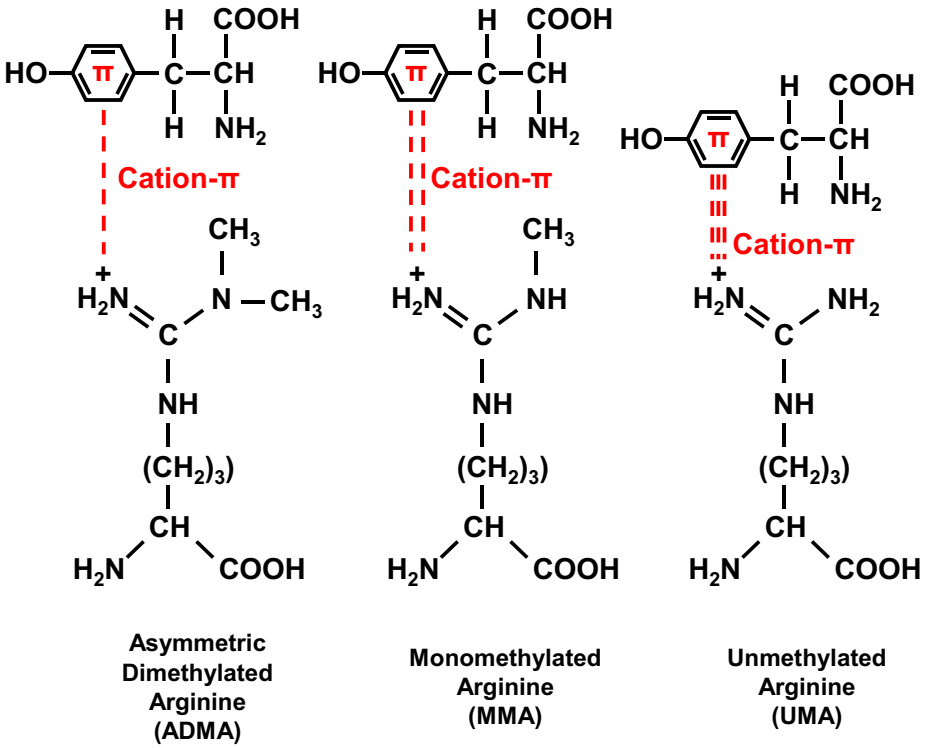

Figure 5-1 Different arginine methylation species have different strength of cation-π interaction with tyrosine residues.

The schematics was adapted from (Qamar et al., 2018). Cation-A interaction between tyrosine and arginine residues is weak when it comes to (a) asymmetric dimethylated arginine (ADMA). Cation-A interaction has intermediate interaction when it is (b) monomethylated arginine (MMA). Cation-A interaction is strong when it is (c) unmethylated arginine (UMA). Therefore, increased number of arginine residues and hypomethylation of arginine residues cause stronger cation-A interaction between molecules.

5.1.2. Pathology of hypomethylated FUS

Aberrant aggregation of FUS, especially homogeneous self-aggregation caused by environmental stress or mutation on FUS itself is implicated in ALS, FTLD and other neurodegenerative diseases (Deng et al., 2014; Ling et al., 2013; Sun et al., 2011). There are similarities of FUS aggregation between different neurodegenerative diseases, the mechanism of

aggregation can be variable and excusive for the specific disease type. For instance, the hypomethethylation of arginine residues was found in FTLD-FUS, which resulted in enhanced cation-π interaction, formation of LLPS and aggregation of FUS protein (Dormann et al., 2012; Neumann et al., 2012). This was further demonstrated by using the variant FUS proteins that have additional 6 to 21 arginine residues under the condition of hypomethylation (e.g. usage of arginine methyltransferase inhibitor), showing strengthened cation-π interaction between FUS proteins to enhanced the formation of hydrogel or fibrillary gel, which in turn, impaired the known functions of SGs (Qamar et al., 2018). Thus, it is of interest whether hypomethylated FUS without any mutation on NLS region results in synaptic dysfunction.

This chapter investigated the effect of a FUS mutant (FUS-16R) with enhanced cation-π interaction (mimicking hypomethylating condition of FUS) on neuronal function and structure. With additional 16 arginine residues, FUS-16R may exhibit different pathological traits from FUS-P525L because FUS-P525L is predominantly localised in the cytosol and propagates through the neurites very quickly with the intact molecular interactions, on the other hand, FUS-16R can easily form inclusions and shows LLPS than FUS-P525L in both inside and outside of the nucleus (Qamar et al., 2018) and exhibits a slower nucleus-to-cytosol propagation speed than FUS-P525L, yet still much faster than FUS-WT. Therefore, FUS-16R will show the different aspects of FUS pathology especially focused on the LLPS nature of FUS.

5.2. Results

5.2.1. FUS-16R exhibits slow cytosolic translocation

The translocation speed of FUS-16R was investigated to compare that with FUS-WT and/or FUS-P525L expression (Fig. 5-2). As FUS-16R has intact NLS region, FUS-16R at DAT5 still showed the predominant localisation in the somatic area (thought to be inside the nucleus), massively formed granules there with leakage into the cytosolic region through the dendrites.

Therefore, the granule size and the translocation speed of FUS-16R is possibly different from those of FUS-P525L.

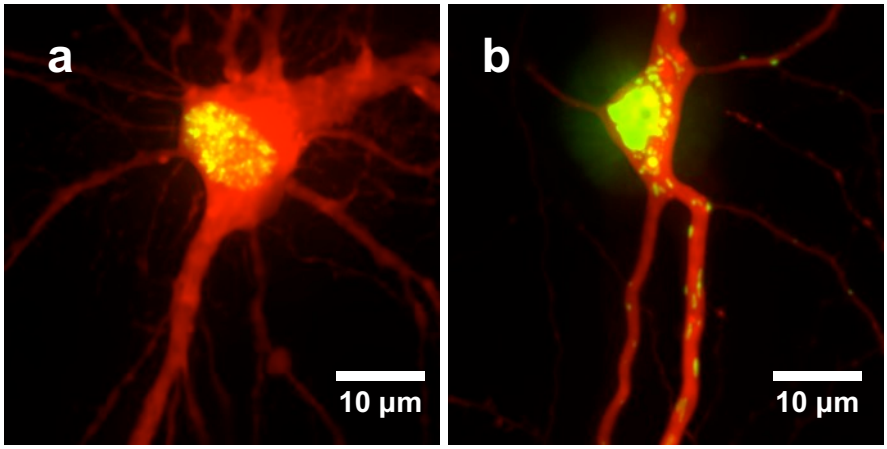

Figure 5-2 Confocal images of CA1 neurons with FUS-WT and FUS-16R transfection.

Each YFP-tagged FUS was imaged at DAT5 with red fluorescence structural marker, TdTomato on confocal spinning disk. (a) YFP-tagged FUS-WT was predominantly locked in the somatic region. (b) YFP-tagged FUS-16R formed granules in the somatic area and translocated through dendrites. The spinning disk confocal images were acquired from Prof. Kei Cho's lab in King's College London Dementia Research Institute (KCL-DRI).

5.2.2. Dendritic spine density is reduced at dendrites of FUS-16R mutant neurons

As articulated in the section 3.2.2., cytosolic FUS was suggested to reduce the dendritic spines by trapping essential mRNAs needed for maintaining the structure of dendritic spines (Machamer et al., 2018; Shiihashi et al., 2017). Since FUS-16R variant is more aggregative form compared to FUS-P525L, this trapping effect can be more deleterious.

To investigate any alteration of synaptic connectivity between neurons, the number of dendritic spines was observed in FUS-16R expressing CA1 neurons and compared with Venus and FUS-WT expressing neurons (Fig. 5-3 and Table 5-1). FUS-16R cells showed lower spine density at basal dendrites when compared to Venus and FUS-WT cells (Fig. 5-3a). In addition, spine density in apical dendrites (Fig. 5-3b) also showed lower spine density

in FUS-16R cells. The data set was shown as Mean ± Standard Error of Mean (SEM). Hippocampal slices from 6 animals for Venus, 5 animals for FUS-WT and 4 animals for FUS-16R were used for the results in Chapter 5 dendritic spine analysis.

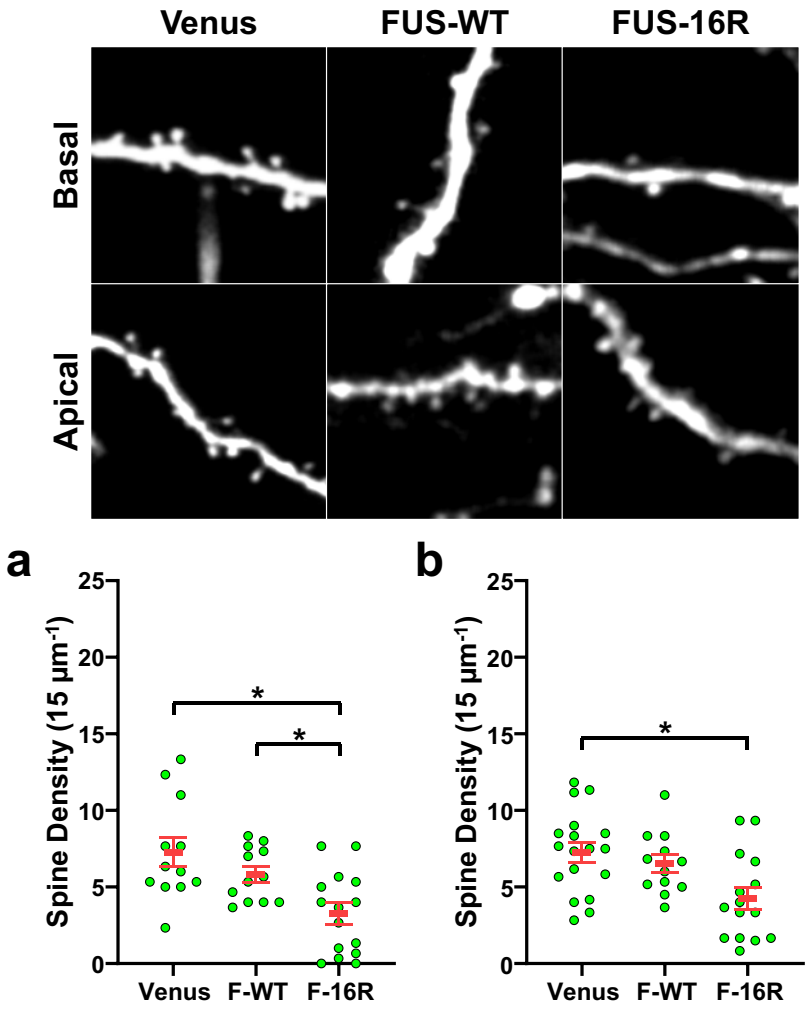

Figure 5-3 Spine density of both basal and apical dendrites were reduced in FUS-16R expressing neurons.

In addition to Venus and FUS-WT in Fig. 3-3, CA1 cells were also transfected with FUS-16R and the dendritic spines were imaged at DAT5-7. Example ROI (15 µm x 15 µm) images were taken from each group. FUS-16R expressing neurons showed the reduced spine density both (a) in the basal dendritic region and (b) in the apical dendritic region.

Basal dendrites	Venus (V)	FUS-WT (W)	FUS-16R (R)
n-number (Cell)	12	12	13
Spine density ($15\ \mu m^{-1}$)	7.27 ± 0.95	5.80 ± 0.50	3.260 ± 0.68
***p*-value** ANOVA, (W vs R), (V vs W), (V vs R)	**0.0014 (F = 7.913)**		**0.0478**
	0.3750		**0.0012**

Apical dendrites	Venus (V)	FUS-WT (W)	FUS-16R (R)
n-number (Cell)	18	12	15
Spine density ($15\ \mu m^{-1}$)	7.25 ± 0.62	6.51 ± 0.58	4.46 ± 0.38
***p*-value** ANOVA, (W vs R), (V vs W), (V vs R)	**0.0058 (F = 5.844)**		0.0719
	0.7162		**0.0049**

Table 5-1 Statistical summary of spine density of basal and apical dendrites in Venus, FUS-WT and FUS-16R expressing neurons.

Statistics of Fig. 5-3 was summarised as tables.

Overall, spine density was reduced at both basal and apical dendrites of FUS-16R cells. This suggests that expression of FUS with enhanced cation-π interaction (FUS-16R) induces synapse weakening process possibly by trapping essential mRNA molecules for the dendritic spine structure.

5.2.3. Effects of FUS-16R mutant on dendritic spine morphology

The shape of dendritic spine is related to the functionality and maturation status of the synapse as articulated in the section 3.2.3. To find out whether FUS with enhanced cation-π interaction would alter or inhibit the maturation of the spines or not, the shape of dendritic spine was compared among FUS-16R, Venus and FUS-WT expressing neurons. As same as the previous chapters, the ROIs were separated into basal and apical dendrites and the spines were categorised into stubby, thin and mushroom then percentage was calculated for each neuron (Fig. 5-4 and Table 5-2) with the same method as used in the chapter 3. And measured parameters for the spine

shape categorisation (Spine head width, Spine head length, Spine neck width, Spine length, Spine head width / spine head length and Spine head area) were also displayed as the supplementary data for basal (Fig. 5-5 and Table 5-3) and apical (Fig. 5-6 and Table 5-4) dendritic spines. The data set was shown as Mean ± SEM.

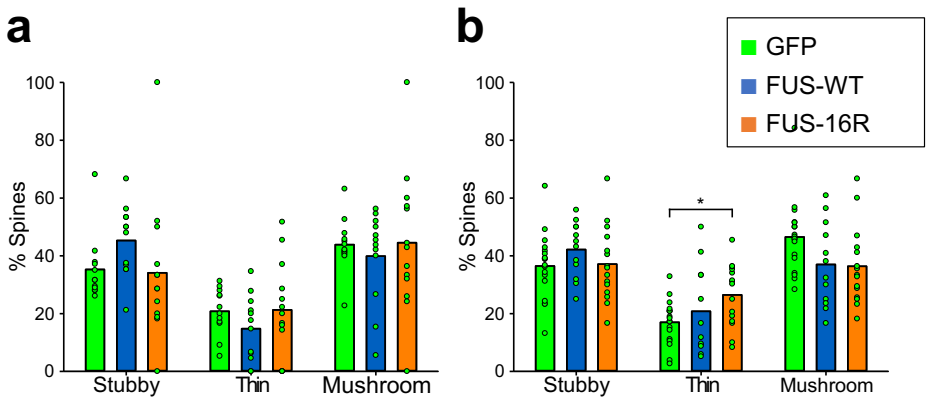

Figure 5-4 Apical dendritic spine shape was altered in FUS-16R and FUS-WT expressing neurons.

(a) In basal dendrites, the ratio of spine shapes did not show any alterations. (b) In apical dendrites, the ratio of thin spines was increased in FUS-16R expressing neurons.

In the basal dendrites (Fig 5-4a), the percentage of stubby spines were statistically similar in all the cell types and it was same for thin spines and mushroom spines that all did not show any significant differences between groups.

In apical dendrites (Fig. 5-4b), stubby spines did not show significant differences but there were more thin shape spines in FUS-16R cells. And mushroom-shaped spines were lesser in FUS-WT and FUS-16R when compared to Venus cells.

Overall, FUS-16R cells did not change the shape of the dendritic spines in basal dendrites but in apical dendrites, there were more thin spines and less mushroom spines. This data suggests that FUS with enhanced cation-π interaction (FUS-16R) interfered the maturation of spines possibly by

trapping mRNAs required for the expression of proteins for the spine structure.

Basal dendrites	Venus (V)	FUS-WT (W)	FUS-16R (R)
n-number (Cell)	12	12	13
Stubby (% Spines)	35.29 ± 3.28	45.31 ± 3.55	34.14 ± 6.66
***p*-value** ANOVA, (W vs R), (V vs W), (V vs R)	0.2244 (F = 1.562)		0.2497
	0.3377		0.9849
Thin (% Spines)	20.82 ± 2.32	14.79 ± 3.26	21.30 ± 4.58
***p*-value** ANOVA, (W vs R), (V vs W), (V vs R)	0.3745 (F = 1.011)		0.4101
	0.4778		0.9950
Mushroom (% Spines)	43.88 ± 2.69	39.89 ± 4.59	44.54 ± 6.79
***p*-value** ANOVA, (W vs R), (V vs W), (V vs R)	0.7874 (F = 0.2407)		0.7950
	0.8499		0.9953

Apical dendrites	Venus (V)	FUS-WT (W)	FUS-16R (R)
n-number (Cell)	18	12	15
Stubby (% Spines)	36.47 ± 2.67	42.18 ± 2.79	37.13 ± 3.32
***p*-value** ANOVA, (W vs R), (V vs W), (V vs R)	0.3808 (F = 0.9880)		0.4988
	0.3852		0.9852
Thin (% Spines)	17.01 ± 1.80	20.81 ± 4.42	26.47 ± 2.77
***p*-value** ANOVA, (W vs R), (V vs W), (V vs R)	0.0617 (F = 2.979)		0.3940
	0.6320		**0.0491**
Mushroom (% Spines)	46.51 ± 2.94	37.01 ± 4.19	36.38 ± 3.47
***p*-value** ANOVA, (W vs R), (V vs W), (V vs R)	0.0636 (F = 2.943)		0.9919
	0.1488		0.0885

Table 5-2 Statistical summary of dendritic spine shape of basal and apical dendrites in Venus, FUS-WT and FUS-16R expressing neurons.

Statistics of Fig. 5-4 was summarised as tables.

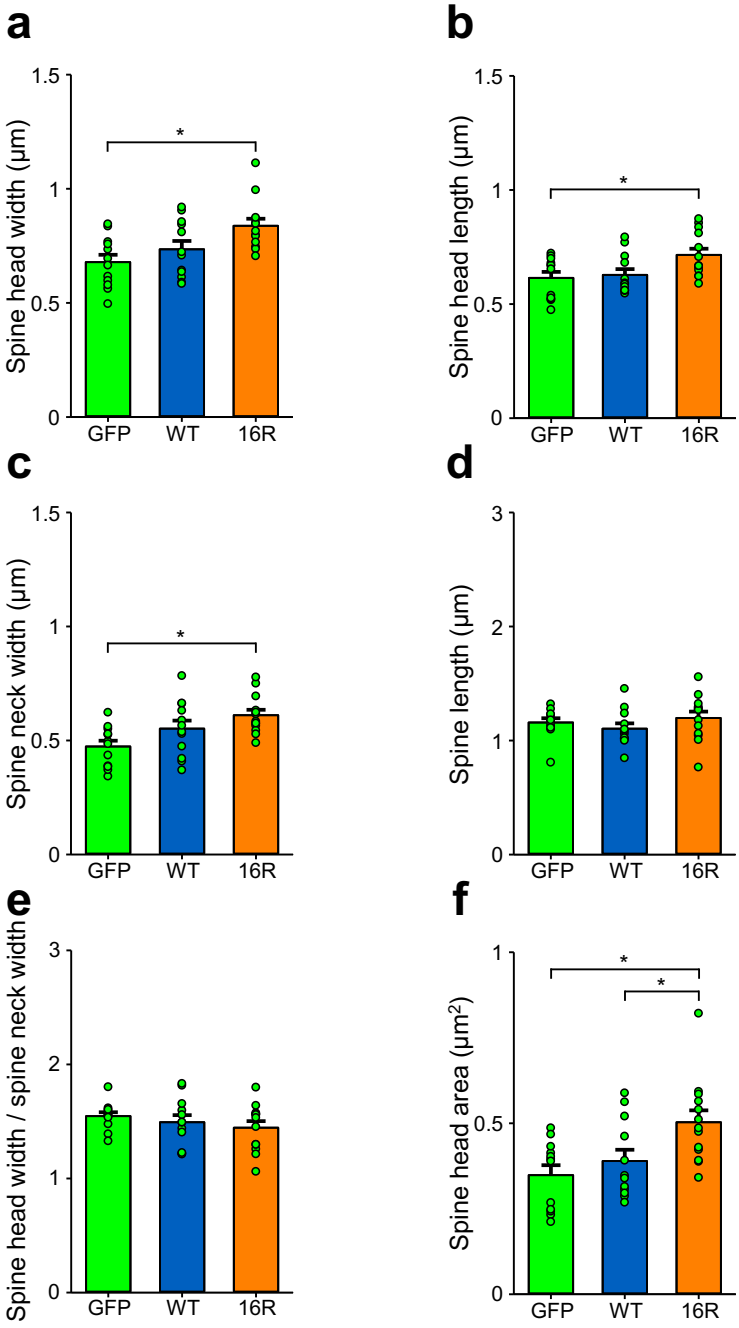

Figure 5-5 Parameters of the spine shapes were measured in basal dendritic spines.

(a) Spine head width was wider in FUS-16R cells. (b) Spine head length was longer in FUS-16R cells. (c) Spine neck width was wider in FUS-WT cells, the widest in FUS-16R cells. (d) Spine length did not show any difference between groups. (e) Spine head width / spine neck width ratio was not different between groups. (f) Spine head area was bigger in FUS-16R cells.

Basal dendrites	Venus (V)	FUS-WT (W)	FUS-16R (R)
n-number (Cell)	12	12	13
Spine head width (μm)	0.6787 ± 0.0322	0.7353 ± 0.0361	0.8382 ± 0.0308
***p*-value** ANOVA, (W vs R), (V vs W), (V vs R)	**0.0055 (F = 6.094)**		0.0834
	0.4643		**0.0044**
Spine head length (μm)	0.6148 ± 0.0262	0.6282 ± 0.0251	0.7156 ± 0.0272
***p*-value** ANOVA, (W vs R), (V vs W), (V vs R)	**0.0194 (F = 4.438)**		0.0607
	0.9323		**0.0265**
Spine neck width (μm)	0.4738 ± 0.0256	0.5524 ± 0.0351	0.6113 ± 0.0235
***p*-value** ANOVA, (W vs R), (V vs W), (V vs R)	**0.0059 (F = 5.987)**		0.3127
	0.1443		**0.0042**
Spine length (μm)	1.1589 ± 0.0370	1.1049 ± 0.0460	1.1985 ± 0.0558
***p*-value** ANOVA, (W vs R), (V vs W), (V vs R)	0.3835 (F = 0.9860)		0.3515
	0.7102		0.8247
Spine head width / spine head length	1.5475 ± 0.0341	1.4942 ± 0.0613	1.4459 ± 0.0571
***p*-value** ANOVA, (W vs R), (V vs W), (V vs R)	0.3983 (F = 0.9460)		0.7917
	0.7604		0.3647
Spine head area (μm^2)	0.3486 ± 0.0290	0.3898 ± 0.0328	0.5032 ± 0.0345
***p*-value** ANOVA, (W vs R), (V vs W), (V vs R)	**0.0049 (F = 6.251)**		**0.0456**
	0.6521		**0.0049**

Table 5-3 Statistical summary of parameters measured for the differentiation of basal dendritic spine shapes in Venus, FUS-WT and FUS-16R expressing neurons.

Statistics of Fig. 5-5 was summarised as a table.

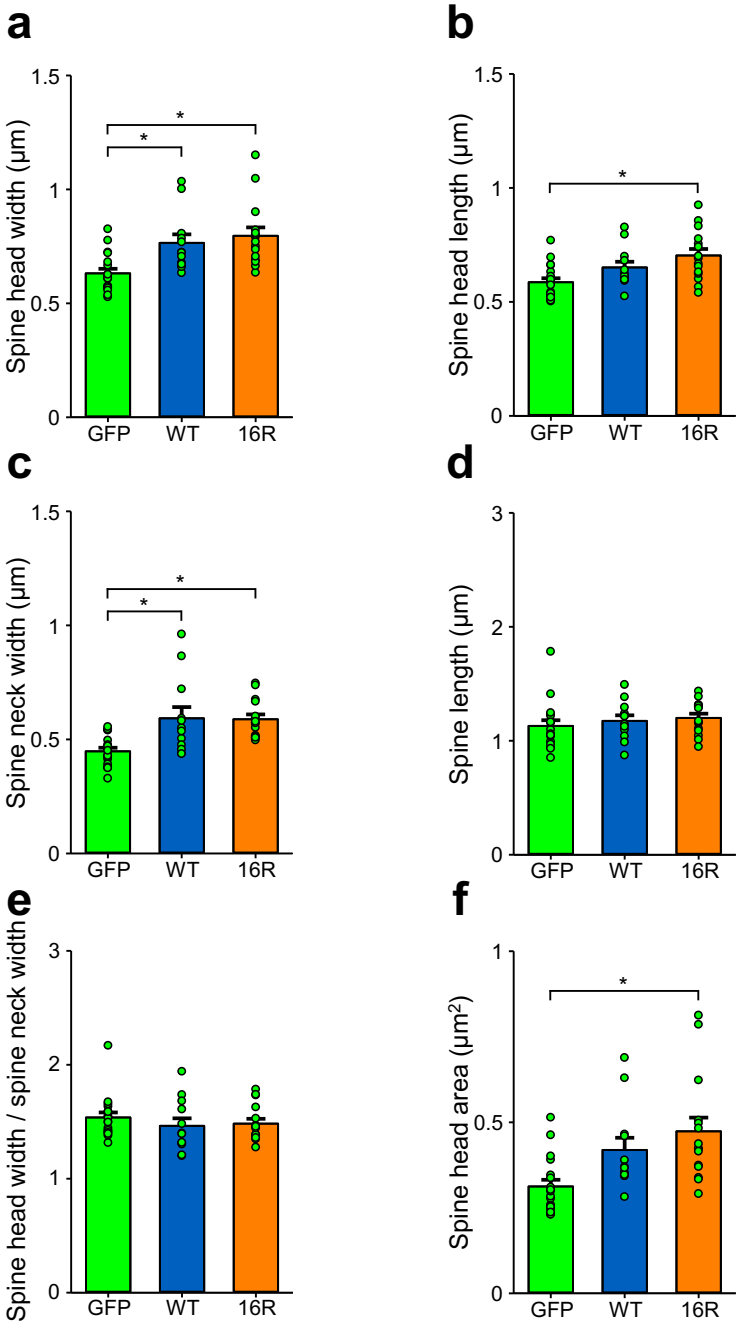

Figure 5-6 Parameters of the spine shapes were measured in apical dendritic spines.

(a) Spine head width was wider in FUS-WT and FUS-16R cells. (b) Spine head length was longer in FUS-16R cells. (c) Spine neck width was wider in FUS-WT and FUS-16R cells. (d) Spine length was similar in all the 3 groups. (e) Spine head width / spine neck width ratio was not different between groups. (f) Spine head area was significantly bigger in FUS-16R cells.

Apical dendrites	Venus (V)	FUS-WT (W)	FUS-16R (R)
n-number (Cell)	18	12	15
Spine head width (μm)	0.6321 ± 0.0198	0.7655 ± 0.0372	0.7966 ± 0.0367
***p*-value** ANOVA, (W vs R), (V vs W), (V vs R)	**0.0006 (F = 9.015)**		0.7764
	0.0114		**0.0008**
Spine head length (μm)	0.5867 ± 0.0174	0.6513 ± 0.0250	0.7037 ± 0.0284
***p*-value** ANOVA, (W vs R), (V vs W), (V vs R)	**0.0026 (F = 6.876)**		0.3052
	0.1481		**0.0018**
Spine neck width (μm)	0.4480 ± 0.0159	0.5929 ± 0.0492	0.5885 ± 0.0214
***p*-value** ANOVA, (W vs R), (V vs W), (V vs R)	**0.0004 (F = 9.354)**		0.9941
	0.0024		**0.0017**
Spine length (μm)	1.1309 ± 0.0499	1.1748 ± 0.0492	1.2009 ± 0.0373
***p*-value** ANOVA, (W vs R), (V vs W), (V vs R)	0.5375 (F = 0.6301)		0.9270
	0.7930		0.5164
Spine head width / spine head length	1.5379 ± 0.0442	1.4643 ± 0.0665	1.4842 ± 0.0417
***p*-value** ANOVA, (W vs R), (V vs W), (V vs R)	0.5484 (F = 0.6095)		0.9613
	0.5629		0.7048
Spine head area (μm^2)	0.3126 ± 0.0193	0.4194 ± 0.0355	0.4736 ± 0.0401
***p*-value** ANOVA, (W vs R), (V vs W), (V vs R)	**0.0016 (F = 7.523)**		0.4873
	0.0587		**0.0013**

Table 5-4 Statistical summary of parameters measured for the differentiation of apical dendritic spine shapes in Venus, FUS-WT and FUS-16R expressing neurons.

Statistics of Fig. 5-6 was summarised as a table.

5.2.4. Apical dendritic spines in FUS-16R expressing neurons does not exhibit local vulnerability

FUS-16R transfected neurons showed the reduction of spine density both in basal and apical dendrites and also showed bigger head area compared to other groups. Therefore, FUS-16R transfected neurons may exhibit much deleterious phenotypes compared to FUS-WT or even FUS-P525L. As cytosolic accumulation of FUS-P525L in the neurons showed local reduction of spine densities at the distal region, it could be worth to check whether stronger FUS-FUS interaction would exhibit similar patterns or not. With the same criteria, spines of proximal vs distal dendrites were investigated for FUS-16R transfected neurons.

Raw images for spine density assay (Fig. 5-3, randomly selected ROIs) were re-cropped from proximal and distal part of same dendrites as pairs to investigate the possible local synaptic changes (Fig. 5-7 and Table 5-5). Counted spine density of proximal and distal dendrites were compared within group (Fig. 5-7a~c) and the ratio of either distal / proximal or proximal / distal dendritic spine density from all three groups were compared (Fig. 5-7d, e). The data set was shown as Mean ± SEM.

The proximal vs distal spine density of FUS-16R expressing neurons (Fig. 5-7c) did not show any difference but the distribution of data points were quite scattered to exhibit bigger error bars compared to Venus (Fig. 5-7a) and FUS-WT (Fig. 5-7b) neurons. The ratio of proximal vs distal spine density from FUS-16R also did not show any difference when compared to Venus and FUS-WT (Fig. 5-7d, e) by ANOVA tests. Those data points of FUS-16R were again more variable than the other groups and caused bigger error bars.

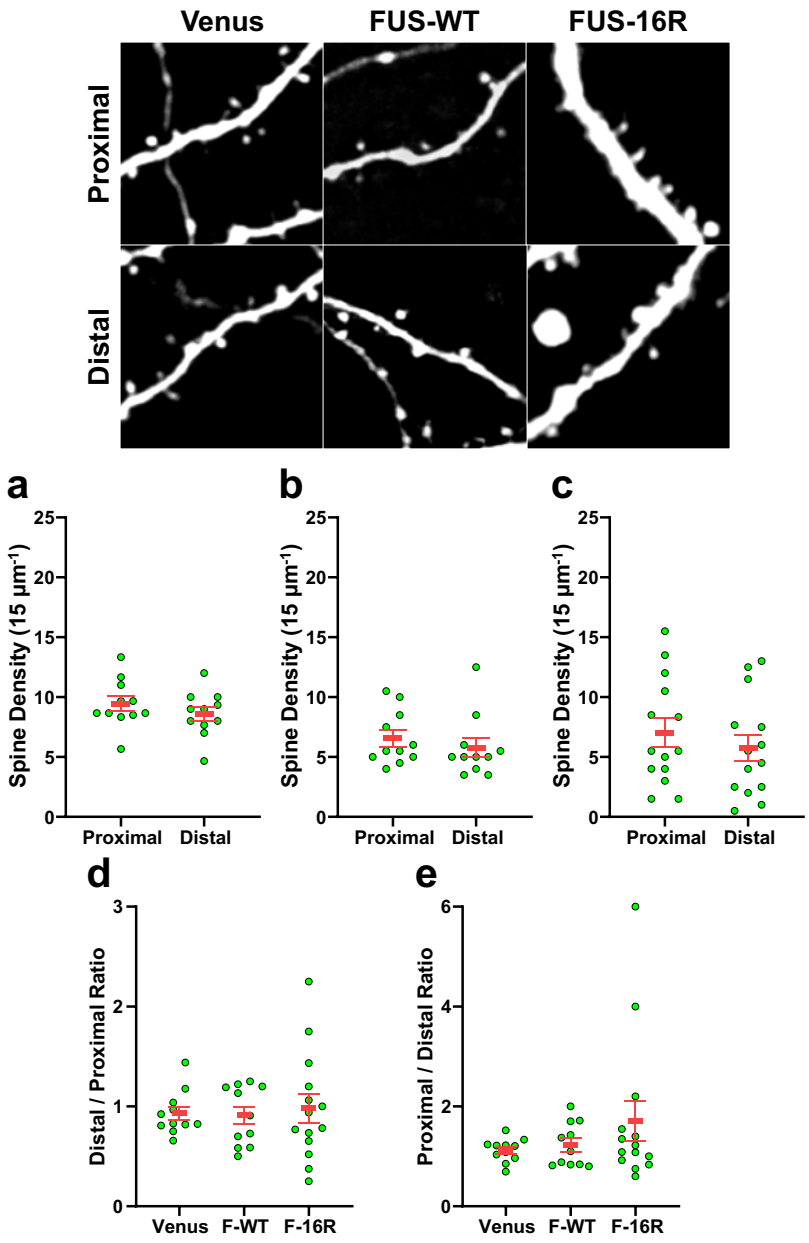

Figure 5-7 Spine density and the ratio of proximal vs distal dendrites were not altered in FUS-16R expressing neurons.

Dendritic spine images from Fig. 5-3 were re-cropped from proximal vs distal region. Example ROI (15 µm x 15 µm) images were taken from each group. (a) Venus neurons had similar number of proximal and distal dendritic spines. (b) FUS-WT neurons also had similar number of proximal and distal dendritic spines. (c) FUS-16R neurons also had similar number of proximal and distal dendritic spines. (d) Distal / Proximal ratio was all similar in all the groups. (e) Proximal / Distal ratio was also all similar in all the groups.

	Venus (V)	FUS-WT (W)	FUS-16R (R)
n-number (Cell)	11	11	14
Proximal S.D. ($15\ \mu m^{-1}$)	9.43 ± 0.60	6.55 ± 0.68	7.02 ± 1.19
Distal S.D. ($15\ \mu m^{-1}$)	8.60 ± 0.57	5.77 ± 0.79	5.76 ± 1.19
***p*-value** (T-test) (Proximal vs Distal)	0.330	0.466	0.447
Distal / Proximal Ratio	0.93 ± 0.07	0.91 ± 0.09	0.85 ± 0.11
***p*-value** ANOVA, (W vs R), (V vs W), (V vs R)	0.8235 (F = 0.1954)		0.8996
	0.9884		0.8249
Proximal / Distal Ratio	1.12 ± 0.07	1.23 ± 0.13	1.71 ± 0.40
***p*-value** ANOVA, (W vs R), (V vs W), (V vs R)	0.2804 (F = 1.322)		0.4420
	0.9674		0.3069

Table 5-5 Statistical summary of spine density of proximal and distal region of apical dendrites in Venus, FUS-WT and FUS-16R expressing neurons.

Statistics of Fig. 5-7 was summarised as a table.

Overall, FUS-16R expression did not induce local reduction of spine density, rather caused global reduction throughout the dendrites. The trend was relatively variable in FUS-16R, which indicates the effects might be acute than gradual pattern once deleterious mechanism is triggered by inclusions. Since FUS-FUS interaction is much stronger with FUS-16R than FUS-P525L, the nature of FUS-16R inclusions may cause more global dysfunction of neurons rather than infiltrate to the very local part of the dendrites.

5.2.5. Intrinsic excitability is decreased in FUS-16R mutant neurons

Intrinsic excitability was investigated by testing the input-output efficiency of neuron that is triggered by current injection and exhibited as action potentials as articulated in the section 4.2.2. To compare the intrinsic excitability of FUS-16R CA1 cells with untransfected control cells, firing activity experiments were conducted (Fig. 5-8). The data set was shown as Mean ± SEM for each X-axis point. Hippocampal slices from 7 animals for FUS-16R were used for the firing activity experiments. Firing pattern of FUS-16R cells generally required a similar current input to fire when compared to the untransfected counterpart but tend to fire slightly less with the higher current inputs (Fig. 5-8a). Firing frequency of FUS-16R cells were similar to untransfected cells (DF = 1, F = 2.975, p = 0.110, n = 13 cells each) (Fig. 5-8b) but the number of events was fewer with the higher current input over 250 pA (Fig. 5-8c) and there was significant differences in overall group comparison (DF = 1, F = 10.927, p = 0.006, n = 13 cells each) when compared with untransfected cells.

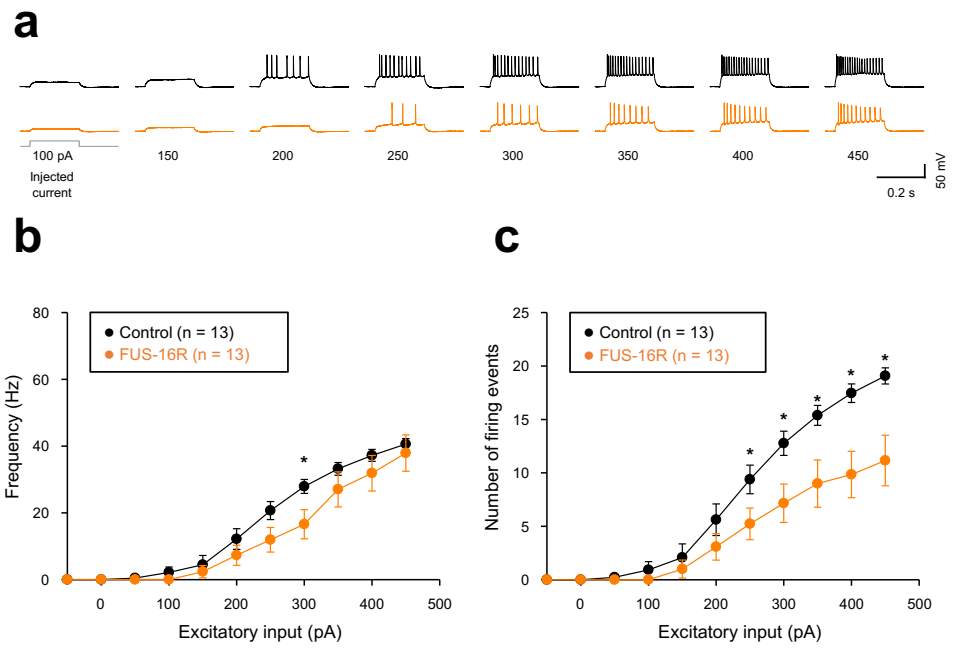

Figure 5-8 Intrinsic excitability was decreased in FUS-16R expressing neurons.

(a) Example firing activity patterns by current injection of 100-450 pA in control neuron (black) and FUS-16R neuron (orange). (b) Frequency of firing activity in FUS-16R was slightly smaller at 300 pA injection but had no difference as a whole comparison. (c) Number of firing event of firing activity was decreased in FUS-16R.

Overall, intrinsic excitability of FUS-16R cells was decreased in FUS-16R cells in the comparison with untransfected control cells. This suggests that the pathologic mechanism of FUS-16R would be more likely related to the hypoexcitability than excitotoxicity.

5.2.6. Evoked basal synaptic transmission is reduced in FUS-16R expressing neurons

Evoked basal synaptic transmission via AMPA/NMDA receptors is a parameter of synaptic efficacy through Schaffer-collateral pathway as articulated in the section 4.2.3. Therefore, to check the potential synaptic efficiency changes by FUS with enhanced cation-π interaction, AMPA and NMDA receptor mediated EPSCs were analysed in FUS-16R expressing neurons and compares with untransfected control neurons. The data set was shown as Mean ± SEM. Hippocampal slices from 9 animals for FUS-16R were used for the basal synaptic transmission experiments. Both $EPSC_{AMPA}$ and $EPSC_{NMDA}$ of FUS-16R cells were compared with paired untransfected cells (Fig. 5-9). When FUS-16R transfected cells and untransfected cells were compared in terms of $EPSC_{AMPA}$ (FUS-16R: - 164.5 ± 10.3 pA, untransfected: - 278.0 ± 37.6 pA, p = 0.006 (power: 0.807), n = 20) and $EPSC_{NMDA}$ (FUS-16R: 113.1 ± 12.8 pA, untransfected: 226.0 ± 42.0 pA, p = 0.01 (power: 0.705), n = 20), both $EPSC_{AMPA}$ and $EPSC_{NMDA}$ were reduced in FUS-16R transfected cells.

Overall, basal synaptic transmission was decreased in FUS-16R cells when compared to untransfected cells. This suggests that expression of FUS-16R weakened the synaptic strength of Schaffer-collateral pathway, which is consistent with the reduced spine density of apical dendrites as shown in the section 5.2.2.

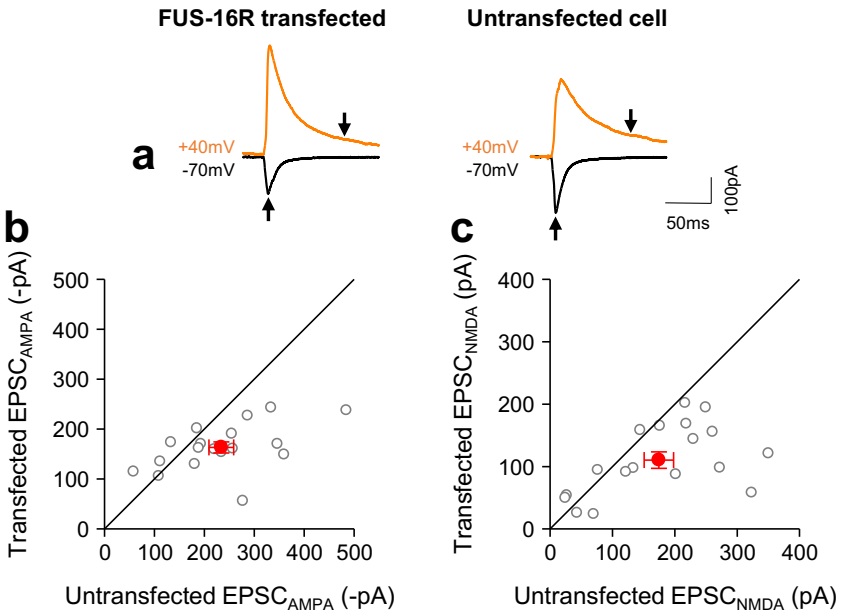

Figure 5-9 Amplitudes of AMPAR and NMDAR mediated currents were smaller in FUS-16R expressing neurons.

(a) Example single traces of AMPAR and NMDAR mediated currents from FUS-16R cell and a paired untransfected cell was displayed. (b) Average amplitudes of AMPAR mediated currents were smaller in FUS-16R cells. (c) Average amplitudes of NMDAR mediated currents were smaller in FUS-16R cells.

5.3. Discussion

5.3.1. Enhanced cation-π interaction of FUS weakens the overall synaptic strength of CA1 neurons

The FUS with enhanced cation-π interaction, FUS-16R, represents the enhanced cation-π interaction of FUS proteins by adding additional arginine residues to boost LLPS process as shown in the neurodegenerative diseases (Qamar et al., 2018). In terms of the expression of the FUS protein variant, FUS-16R did not show massive translocation through the dendrites as shown for the FUS-P525L in the section 3.2.1. This would be mainly due to the intact NLS region of FUS-16R. But still, FUS-16R shows more cytosolic diffusion compared to FUS-WT, which could be due to the milder impairment of nuclear localisation by interfering the interaction between FUS protein and TRN-1 with the hypomethylation (Hofweber et al., 2018). In terms of dendritic spine morphology and dynamics, FUS-16R CA1 cells showed a reduced spine density in both basal and apical dendrites and consistent with that, the glutamatergic receptor mediated basal synaptic transmission was reduced. As observed in the experiments, global reduction of spine density in FUS-16R cells was different tendency from FUS-P525L cells that showed the local reduction of spines at the distal part of apical dendrites. Considering the aggregative nature of hypomethylated arginine residues, it is plausible that FUS-16R forms inclusions much quicker than FUS-P525L, therefore, average size of FUS-16R inclusions would be bigger than FUS-P525L inclusions that would slow down the speed of diffusion in the cytosol. In addition, NLS domain is intact in FUS-16R, therefore, it may start to form inclusions from the inside of the nucleus, disrupt the homeostasis of the neuron and affect the whole dendrites, rather than translocate to the dendrites, form the inclusions, then, alter the RNA/DNA and/or protein dynamics on-site as FUS-P525L would do. With the accordance to that, FUS-16R may autoregulate the expression of endogenous FUS to reduce the total level of endogenous FUS and also aggregative nature of FUS-16R is more likely to trap other FUS proteins or essential mRNAs required for the spine

maturation. Thus, FUS-16R may have similar pathologic mechanism with the overexpression of FUS-WT but FUS-WT may exhibit much milder phenotypes than that of progressive FUS-16R proteins.

5.3.2. FUS-16R alters neurophysiology of CA1 neurons

In addition to the significant molecular dynamics and the alteration of the dendritic spine morphology, FUS-16R expressing neurons exhibited the altered neurophysiology of CA1 neurons. First, the glutamatergic receptor mediated basal synaptic transmission was reduced. Similar to FUS-P525L results (Fig. 4-7b, c), postsynaptic profile of main two excitatory glutamatergic receptors were altered and it was also consistent with the reduction of dendritic spine density of CA1 cells (Fig. 5-2). Those changes on the synapses are rely more on the FUS species with enhanced cation-π interaction than total level of FUS expression as FUS-WT did not alter the basal synaptic transmission (Fig. 4-7e, f). Therefore, NLS mutant FUS and FUS with enhanced cation-π interaction both has deleterious effects to the synapse. In addition, intrinsic excitability was rather decreased than increased. This could be the altered expression of sodium and potassium channels therefore Na^+/K^+ ratio was reduced and caused hypoexcitability as once mentioned in section 4.3.1. for the results of FUS-WT.

Overall, these data suggest that both FUS-P525L, FUS-16R are deleterious to synaptic structure and function, however, the pathophysiological effects of the two FUS mutations likely occur via different a mechanism(s). FUS-16R is mainly locked in the nucleus like FUS-WT at the early stage of transfection but FUS-16R forms inclusions in the nucleus and then comes out of the nucleus and starts to diffuse and form inclusions in the cytosols. Therefore, it can be suggested that FUS-16R may interrupt the normal transcription, alternative splicing, trafficking of mRNAs in and out of the nucleus, translation in the cytosol and potentially weaken both basal and apical dendrites and also morphological maturation of apical dendritic spines, as well. However,

this needs further fine investigation to know the molecular mechanism of neuronal FUS-16R in the future.

CHAPTER 6

General discussion

6.1. The roles of FUS on synapse during the pathophysiology (Further discussion on findings)

6.2. Caveats and limitations of the study

6.3. Comparing with the other FUS mutant models and future possibilities

6.4. Linking FUS pathology models to neurodegenerative diseases

6.1. The roles of FUS on synapse during the pathophysiology

FUS was first identified as a novel RNA-binding protein in cancer pathology (Crozat et al., 1993; Rabbitts et al., 1993) and shown to be involved in the abnormal transcription. Furthermore, FUS is involved in the DNA repair (Hicks et al., 2000; Kuroda et al., 2000; Wang et al., 2013) and the gene expression by the association with diverse transcription factors (Riggi et al., 2007) and related proteins such as RNA polymerase II (Bertolotti et al., 1996, 1998). Arginine residues of FUS were reported to be dimethylated (Rappsilber et al., 2003) during post-translation modification and it has been implied to have regulatory function for FUS.

Recent studies found that FUS emerged as an aberrantly regulated protein in neurodegenerative disease, especially ALS and FTLD (Kwiatkowski et al., 2009; Lagier-Tourenne and Cleveland, 2009; Vance et al., 2009). The proceeding decade since its emergence, many roles of FUS in both physiological and pathological conditions have been found and articulated. Especially, FUS has been known to be recruited to the SG formation in the response to the diverse cellular stress such as hyperosmolar stress, heat shock stress, oxidative stress (Li et al., 2013; Wolozin, 2012). Since SGs are formed in the cytosol, NLS mutations of FUS were shown to accelerate the formation of cytosolic inclusions under stress conditions and disrupt normal functions of FUS as a DNA/RNA modulator and induce cellular toxicity. The NLS mutants were also demonstrated to impair fast axonal transport by phosphorylating and inhibiting kinesin-1 via activation of p38 mitogen-activated protein kinases (p38 MAPK) (Sama et al., 2017). Therefore, this would be a part of morphological alterations by NLS mutant FUS. Furthermore, another RNA metabolism regulator ataxin-2 was shown to be co-localised with FUS in the intracellular organelles (e.g. ER-Golgi) to induce fragmentation of Golgi and trigger apoptosis (Farg et al., 2013). This apoptosis was reported from ALS patients and demonstrated to be boosted by NLS mutant FUS, therefore, interaction with ataxin-2 can be another background mechanism of the physiological alterations by NLS mutant FUS

(Farg et al., 2013). Even though there are many interesting ideas have been reported, still it is difficult to draw a whole picture of the pathophysiology of NLS mutant FUS.

In this PhD study, the nature and consequence of abnormal FUS variants were investigated in terms of the potential pathology that would be involved in ALS, FTLD and other possible neurodegenerative diseases. As articulated above, the main pathogenic factors of FUS (NLS mutation and hypomethylation) were utilised to investigate both morphological and physiological alterations by abnormal expression, propagation and aggregation of FUS in the neuronal cytosols.

The key findings from the expression of NLS mutant cytosolic FUS (FUS-P525L) can be summarised into few points. First, the translocation through the dendrites and the formation of inclusions were highly accelerated in the FUS-P525L expressing neurons. Therefore, FUS-P525L expression can more directly alter the dynamics of dendritic spines, locally. This will be involved in the alteration of the local translation in the spines to inhibit the induction of synaptic plasticity. Second, dendritic spine loss was exclusively shown in the distal part of apical dendrites rather than global loss. This suggests that FUS-mediated alterations make synapses vulnerable from distal end of the dendrites, which is possibly due to the translocation of FUS inclusions towards distal dendrites and accumulation at the end. In addition, AMPA/NMDA mediated EPSCs were decreased to be consistent with the reduced spines at distal part of the apical dendrites. This synapse weakening process can be linked to the faster conductance of synapse and increased intrinsic excitability in FUS-P525L neurons. Therefore, this shows the potential link to the excitotoxicity and increased proportion of CP-AMPAR as they are implied in the FUS pathology (King et al., 2016). Still the mechanism is not quite clear whether it is destruction of existing spines or inhibition of spinogenesis in the combination of excitotoxicity. However, there is a potential clue that synaptic plasticity in distal compartment is prone to form clustered spines with GluA1 subunits of AMPARs upon sensory experience

while homeostatic enhancement (or scaling) by sensory deprivation is more likely global phenotype throughout the neuronal dendrites with GluA2 subunits in layer 2/3 pyramidal neurons (Makino and Malinow, 2011). Therefore, it would be worthwhile to check the local alteration of the composition and subtypes of AMPAR than the change of the whole cell in the future.

To further confirm the role(s) of dendritic inclusions of FUS on neuronal function, this study alternatively utilised abnormal expression of additional arginine mutant form FUS (FUS-16R). FUS-16R exhibited a similar but different pathological outcomes compared to FUS-P525L. FUS-16R was designed to investigate the effects of enhanced cation-π interaction and mimicked hypomethylation, therefore, it was mainly locked in the nucleus in the early stage of expression, and exhibits slower cytosolic translocation than that of FUS-P525L. However, FUS-16R formed inclusions quicker than FUS-WT due to the enhanced cation-π interaction. Thus, FUS-16R likely formed inclusions in the nucleus before getting accumulated in the cytosol. Thus, FUS-16R inclusion in the nucleus might have trapped essential transcription factors required for the survival of the neuron to alter the profile of gene expression. Furthermore, this nuclear aggregation will be less likely to release free FUS into the dendritic region even though the inclusions can translocate through the dendrites. Dendritic FUS is important for the local translation of structural proteins (Fujii and Takumi, 2005; Yokoi et al., 2017) and stability of GluA1 subunits of AMPARs (Udagawa et al., 2015), thus, trapping free FUS may have caused the reduction of synaptic AMPARs, reductions of spines in both apical and basal dendrites.

Overall, this study showed that both FUS-P525L and FUS-16R caused synaptic loss with the different alterations on the neuronal physiology. Still there would be molecular mechanisms to be discovered further to explain the pathology, this study demonstrated FUS can trigger either gain-of-toxicity or loss-of-function and both of them altered neuronal excitability and were able to cause the synapse weakening at the end.

6.2. Caveats and limitations of the study

The current PhD study found pathophysiological roles of FUS, but it also remains limitations to be address in the future.

The main target FUS construct in this study, FUS-P525L, is one of the most popular mutant forms to investigate the pathology of ALS, FTLD and FUS related pathologies and it does exist in the real familiar patients. However, FUS-P525L represents a very rare (1.37 % of 947 cases) (Shang and Huang, 2016) and progressive form of the disease, therefore, there would be possibilities that the pathologies won't directly fit into the general forms of neurodegenerative diseases. However, the inclusion of FUS without NLS mutation has been associated with certain pathological progress in the brain (Aoki et al., 2012; Armstrong et al., 2011; Deng et al., 2010). This raises the question that FUS could be modified to be aggregated without any NLS or disease related mutations and subsequently affected synaptic function. Therefore, FUS-16R form represents an alternative experimental model. Overall, those FUS mutant forms are good for investigating the nature of FUS pathology in some aspects, but it may need further conceptual justification and translation into the disease model.

Since FUS has various fundamental biological roles, I utilised an experimental approach to 'overexpress the FUS mutants' with endogenous FUS. Therefore, the main focus was the effects of cytosolic inclusions of FUS in CA1 neurons. The constructs in this study would be appropriate for investigating the effects of cytosolic FUS (FUS-P525L), FUS overexpression (FUS-WT) and enhanced FUS-FUS interactions (FUS-16R), as intended. Unfortunately, due to this design they won't directly show the loss-of-function by nuclear depletion of FUS by NLS mutation because endogenous FUS will be localised in the nucleus and exhibit the normal functions. But still, there is a possibility of nuclear depletion even with endogenous FUS because NLS mutant FUS can trap those endogenous FUS by co-aggregation in the cytosolic area (Vance et al., 2013).

The rodent hippocampal organotypic slice culture model is a well-established neuronal circuit model to investigate the physiology of neurons, however, the pathology of FUS is mainly exhibited in the motor neurons even though FUS pathology is also found in the hippocampal CA1 neurons (Armstrong et al., 2011; MacKenzie et al., 2011). Therefore, it is good to investigate the general neuronal pathology of FUS in the presence of input via natural synaptic connections and neuronal activities and ALS/FTLD cases with cognitive impairments (Ishigaki and Sobue, 2018) but there can be some differences from the pathophysiology of motor neuronal aspects.

6.3 Comparing with the other FUS mutant models and future possibilities

Cytosolic mislocalisation and aggregation are the most prominent features of FUS-mediated pathology. Therefore, experimental models of FUS have focused on many NLS mutant forms (R521C, P525L or truncation of NLS, etc) or FUS knockout models to investigate the loss-of-function. Hypomethylation of arginine was also mimicked and examined to simulate more aggregative forms of FUS mediated pathology by reducing protein arginine methyltransferase 1 (PRMT1) (Hofweber et al., 2018; Tradewell et al., 2012) or adding additional arginine residues (Qamar et al., 2018), as utilised in this thesis study.

Since expressing the FUS mutant leads to dendritic spine loss, it is of interest how this can be caused. To extend the study further and strengthen the direct connection to the pathology, it would be a good idea to utilise neuronal activity-dependent experimental models in the future. One of the most adaptable approach is utilisation of optogenetics such as channelrhodopsin-2 (ChR2) and cryptochrome 2 (CRY2). ChR2 is a light sensitive ion channel that is opened by blue wavelength light, causing the influx of Na^+, therefore, inducing action potentials. This approach may prove that additional neuronal activity can boost the FUS-mediated pathophysiology in CA1 neurons. Since hyperactivation of glutamate receptors causes neuronal excitotoxicity and

was mediated by Ca^{2+} (Tischbein et al., 2019), fine tuning of the neuronal activity can be tested by using ChR2. In terms of CRY2, it is activated by blue light to be clustered to quickly form SG-like inclusions. Therefore, tagging FUS with CRY2 and blue light activation can simulate the LLPS of FUS (Shin et al., 2017) to be utilised to investigate the toxic physiology of FUS inclusions under spatiotemporal control of FUS-FUS interaction.

Since a diverse range of animal models were utilised for the pathology of FUS from the past, it is hard to say which animal model is the best above all. In that sense, many different kinds of FUS models, such as yeast, fruit fly, nematode, zebra fish and rodent models were used to uncover the roles of FUS either by overexpressing or knocking out FUS-WT and/or mutant FUS (Lanson and Pandey, 2012). As utilised in this thesis study, rodent models are reliable and versatile tools to investigate the neurodegenerative diseases and have genetic similarities to human. It is also, there are many difficulties and ethical issues with using human tissues, however, it is always good to crosscheck with the neuronal models from human origin because there would be always unpredicted and possible differences between species that can result in misleading perspectives. One effort to challenge that difficulties is using induced pluripotent stem cells (iPSCs). One big advantage of iPSC is the source cells containing actual genes from diseased patients can be directly harvested and also, it is relatively free of the ethical issues. In addition, iPSCs can be differentiated into diverse range of cell types such as brain neurons and motor neurons (Rowe and Daley, 2019). However, those iPSC models have conceptual limitation since it does not form clustered and unidirectional circuits that delivers excitatory and inhibitory inputs and outputs, therefore, the rodent hippocampal circuit model approach is still valid and both iPSC and rodent models can be complimentary models for each other.

6.4. Extending the study in the future

There would be great opportunities to extend the study by utilising those ideas and experimental tools mentioned in section 6.3. in the future. Cry2 domain has been conjugated to neurodegenerative disease-related proteins (e.g. Aβ, TDP-43 and FUS) to investigate the aggregating nature of the proteins (Hsien et al., 2019; Shin et al., 2017; Zhang et al., 2018). Cry2 domain has been identified and utilised for decades, however, it is relatively recent for the optogenetic tool to be used for recruiting aggregative proteins to form inclusions. Therefore, the conjugated form of Cry2 and FUS, so-called OptoFUS, has a lot of potential for studying physiological changes during aging and FUS-mediated neurodegenerations. In this thesis, NLS mutant FUS and enhanced cation-π form of FUS have been utilised to simulate cytosolic accumulation of FUS and formation of inclusions but it was not available to control their aggregation in a spatiotemporal manner even though the main purpose of the study was to investigate the dendritic accumulation of FUS inclusions and measure the synaptic changes. With a fine local photostimulation of OptoFUS to either soma or dendrites near spines, it would be possible to know the direct effects of FUS inclusions in the local area and which compartment has more toxic phenotypes. This can be applied together with electrophysiology and morphological changes.

In addition to Cry2 domain, ChR2 or similar optogenetic domains would be utilised for the local induction of neuronal activity by photo-stimulation. The relationship between neuronal activity and translocation of FUS inclusions has been studies in some occasions, however, those studies mostly aimed to induce global excitotoxicity rather than local and physiological activation of neurons (Tischbein et al., 2019). Therefore, with ChR2, it would be available to investigate how physiological activity of neurons can cause translocation and accumulation of FUS through dendrites to result in excitotoxicity and/or neurodegeneration.

Overall, simulating physiological condition would give us better insights of the early pathophysiology of the neurodegenerative disease.

6.5. Linking FUS pathology models to neurodegenerative diseases

As mentioned before, FUS is implicated in the subtypes of ALS and FTLD. Since TDP-43 is also pathogenic inclusion factor in ALS and FTLD, they are overlapped in many ways with FUS-type ALS and FTLD in the clinical phenotypes. Both TDP-43 and FUS form the inclusions frequently reported with ubiquitination (Farrawell et al., 2015; Neumann et al., 2006; Seelaar et al., 2010), however, the progression and pathogenic features of neuronal pathology between FUS and TDP-43 are quite distinct (Nolan et al., 2016). For instance, FUS pathology is involved in the interaction with FET protein (MacKenzie et al., 2011), TRN-1 (Suárez-Calvet et al., 2016) and arginine methylation (Guerrero et al., 2016) whereas TDP-43 pathology is involved in the cleavage of TDP-43 itself (Ito and Suzuki, 2011; Neumann et al., 2006). Furthermore, FUS inclusions from ALS-FUS and FTLD-FUS have different features, such as FET and TRN-1 are only found from FUS inclusions of FTLD-FUS (MacKenzie et al., 2011; Suárez-Calvet et al., 2016). Also in terms of arginine methylations, ALS-FUS inclusions are dimethylated (ADMA), while FTLD-FUS is either unmethylated (UMA) or monomethylated (MMA) (Suárez-Calvet et al., 2016). FUS mutations, especially NLS forms are only obvious in ALS-FUS, not in FTLD-FUS (Nolan et al., 2016), therefore, it is plausible to say FUS-P525L model represents more likely the pathology of ALS-FUS, on the other hand, FUS-16R model represents more likely the pathology of FTLD-FUS.

With those distinguished pathologies in mind, fast accumulation of cytosolic FUS inclusions are more likely linked to ALS-FUS, therefore, most findings from NLS mutant form FUS-P525L might be categorised into this pathology. In addition, arginine methylation is mostly ADMA and NLS mutation inhibits TRN-1 binding, therefore, increased expression of cytosolic FUS protein itself is the core factor for the toxic alterations of local translations than what formation of irreversible inclusions do (Shiihashi et al., 2016) but still, those inclusions will trap the RNAs and translation related factors to accelerate the toxicity (Kamelgarn et al., 2018; Reber et al., 2016). Another point to be noted

here is that excitotoxicity has been reported in a greater number of ALS than FTLD cases (Starr and Sattler, 2018). These previous findings are closely related to the increased excitability in FUS-P525L expressing neurons, which was not shown in FUS-16R expressing neurons in this PhD study. Furthermore, this excitability change is thought to be related to the increased composition of CP-AMPARs and altered conductance, which ended up with the decreased apical dendritic spines that implies it is neuronal activity-dependent. Collecting the thoughts and data from previous studies and the current PhD study, high expression of cytosolic FUS (mainly FUS-P525L and other NLS mutant FUS) increased the synaptic component of CP-AMAPRs and this CP-AMPAR mediated excitotoxicity causes synaptic weakening and it is neuronal activity-dependent.

On the other hand, hypomethylated (UMA and MMA) FUS inclusions are more likely linked to FTLD-FUS, therefore, findings from arginine mutant form FUS-16R might be categorised into this pathology. Hypomethylation of FUS causes the formation of inclusions by LLPS (Hofweber et al., 2018) both in and out of the nucleus even without the mutations (Snowden et al., 2011) and also recruits other FET proteins and TRN-1 into the inclusions (Neumann et al., 2011, 2012; Suárez-Calvet et al., 2016). Collectively, therefore, it can interrupt the homeostasis of RNAs more severely both in the nucleus and cytosol.

Although distinction between ALS/FTLD-FUS pathologies, the main purpose of this study was to find how those dysfunctions of FUS affect the synapses and neuronal circuits, therefore, the aspects can be applied to any other types of neurons or circuits. Furthermore, the ALS/FTLD-FUS pathologies can show a comorbidity, and can co-exist in multiple neuron types in one diseased individual (Mochizuki et al., 2012) and also, other pathology-related proteins (e.g. TDP-43) can interact with FUS (Honda et al., 2014; Ishigaki et al., 2017; Ling et al., 2010). This coexpression results in numerous pathophysiological scenarios and eventually, it would be important to draw possible connections between neurodegenerative diseases in the future.

References

Ahmed, R.M., Devenney, E.M., Irish, M., Ittner, A., Naismith, S., Ittner, L.M., Rohrer, J.D., Halliday, G.M., Eisen, A., Hodges, J.R., et al. (2016). Neuronal network disintegration: Common pathways linking neurodegenerative diseases. J. Neurol. Neurosurg. Psychiatry *87*, 1234–1241.

Aizawa, H., Sawada, J., Hideyama, T., Yamashita, T., Katayama, T., Hasebe, N., Kimura, T., Yahara, O., and Kwak, S. (2010). TDP-43 pathology in sporadic ALS occurs in motor neurons lacking the RNA editing enzyme ADAR2. Acta Neuropathol. *120*, 75–84.

Aizawa, H., Hideyama, T., Yamashita, T., Kimura, T., Suzuki, N., Aoki, M., and Kwak, S. (2016). Deficient RNA-editing enzyme ADAR2 in an amyotrophic lateral sclerosis patient with a FUS(P525L) mutation. J. Clin. Neurosci. *32*, 128–129.

Akiyama, T., Suzuki, N., Ishikawa, M., Fujimori, K., Sone, T., Kawada, J., Funayama, R., Fujishima, F., Mitsuzawa, S., Ikeda, K., et al. (2019). Aberrant axon branching via Fos-B dysregulation in FUS-ALS motor neurons. EBioMedicine *45*, 362–378.

Allen, T.A., and Fortin, N.J. (2013). The evolution of episodic memory. Proc. Natl. Acad. Sci. U. S. A. *110*, 10379–10386.

Altemus, K.L., and Almli, C.R. (1997). Neonatal hippocampal damage in rats: Long-term spatial memory deficits and associations with magnitude of hippocampal damage. Hippocampus *7*, 403–415.

Ambegaokar, S.S., and Jackson, G.R. (2011). Functional genomic screen and network analysis reveal novel modifiers of tauopathy dissociated from tau phosphorylation. Hum. Mol. Genet. *20*, 4947–4977.

Amin, J.B., Salussolia, C.L., Chan, K., Regan, M.C., Dai, J., Zhou, H.X., Furukawa, H., Bowen, M.E., and Wollmuth, L.P. (2017). Divergent roles of a peripheral transmembrane segment in AMPA and NMDA receptors. J. Gen. Physiol. *149*, 661–680.

Anderson, W.W., and Collingridge, G.L. (2007). Capabilities of the WinLTP data acquisition program extending beyond basic LTP experimental functions. J. Neurosci. Methods *162*, 346–356.

Andersson, M.K., Ståhlberg, A., Arvidsson, Y., Olofsson, A., Semb, H., Stenman, G., Nilsson, O., and Aman, P. (2008). The multifunctional FUS, EWS and TAF15 proto-oncoproteins show cell type-specific expression patterns and involvement in cell spreading and stress response. BMC Cell Biol. *9*, 37.

Aoki, N., Higashi, S., Kawakami, I., Kobayashi, Z., Hosokawa, M., Katsuse, O., Togo, T., Hirayasu, Y., and Akiyama, H. (2012). Localization of fused in sarcoma (FUS) protein to the post-synaptic density in the brain. Acta Neuropathol. *124*, 383–394.

Armstrong, R.A., Gearing, M., Bigio, E.H., Cruz-Sanchez, F.F., Duyckaerts, C., MacKenzie, I.R.A., Perry, R.H., Skullerud, K., Yokoo, H., and Cairns, N.J. (2011). The spectrum and severity of FUS-immunoreactive inclusions in the frontal and temporal lobes of ten cases of neuronal intermediate filament inclusion disease. Acta Neuropathol. *121*, 219–228.

Atkinson, R.C., and Shiffrin, R.M. (1968). Human Memory: A Proposed System and its Control Processes. Psychol. Learn. Motiv. *2*, 89–195.

Aulas, A., and Velde, C. Vande (2015). Alterations in stress granule dynamics driven by TDP-43 and FUS: A link to pathological inclusions in ALS? Front. Cell. Neurosci. *9*, 1–13.

Baars, B.J., Gage, N.M., Baars, B.J., and Gage, N.M. (2010). Learning and memory. Cogn. Brain, Conscious. 304–343.

Baddeley, A. (2000). The episodic buffer: a new component of working memory? Trends Cogn. Sci. *4*, 417–423.

Baddeley, A.D., and Hitch, G. (1974). Working Memory. Psychol. Learn. Motiv. *8*, 47–89.

Bamburg, J.R., and Bernstein, B.W. (2010). Roles of ADF/cofilin in actin polymerization and beyond. F1000 Biol. Rep. *2*, 1–7.

Beattie, E.C., Carroll, R.C., Yu, X., Morishita, W., Yasuda, H., von Zastrow, M., and Malenka, R.C. (2000). Regulation of AMPA receptor endocytosis by a signaling mechanism shared with LTD. Nat. Neurosci. *3*, 1291–1300.

Belly, A., Moreau-Gachelin, F., Sadoul, R., and Goldberg, Y. (2005). Delocalization of the multifunctional RNA splicing factor TLS/FUS in hippocampal neurones: Exclusion from the nucleus and accumulation in dendritic granules and spine heads. Neurosci. Lett. *379*, 152–157.

Bertolotti, A., Lutz, Y., Heard, D.J., Chambon, P., and Tora, L. (1996). hTAF(II)68, a novel RNA/ssDNA-binding protein with homology to the pro-oncoproteins TLS/FUS and EWS is associated with both TFIID and RNA polymerase II. EMBO J. *15*, 5022–5031.

Bertolotti, A., Melot, T., Acker, J., Vigneron, M., Delattre, O., and Tora, L. (1998). EWS, but Not EWS-FLI-1, Is Associated with Both TFIID and RNA Polymerase II: Interactions between Two Members of the TET Family, EWS and hTAF II 68, and Subunits of TFIID and RNA Polymerase II Complexes . Mol. Cell. Biol. *18*, 1489–1497.

Binder, J.R., and Desai, R.H. (2011). The neurobiology of semantic memory. Trends Cogn. Sci. *15*, 527–536.

Bliss, T. V, and Lomo, T. (1973). Long-lasting potentiation of synaptic transmission in the dentate area of the anaesthetized rabbit following stimulation of the perforant path. J. Physiol. *232*, 331–356.

Bliss, T.V.P., and Collingridge, G.L. (1993). A synaptic model of memory: long-term potentiation in the hippocampus. Nature *361*, 31–39.

Bliss, T.V.P., and Collingridge, G.L. (2013). Expression of NMDA receptor-dependent LTP in the hippocampus: bridging the divide. Mol. Brain *6*, 1–14.

Bliss, T.V.P., Collingridge, G.L., Morris, R.G.M., and Reymann, K.G. (2018).

Long-term potentiation in the hippocampus: Discovery, mechanisms and function. Neuroforum *24*, A103–A120.

Blokhuis, A.M., Groen, E.J.N., Koppers, M., Van Den Berg, L.H., and Pasterkamp, R.J. (2013). Protein aggregation in amyotrophic lateral sclerosis. Acta Neuropathol. *125*, 777–794.

Borovac, J., Bosch, M., and Okamoto, K. (2018). Regulation of actin dynamics during structural plasticity of dendritic spines: Signaling messengers and actin-binding proteins. Mol. Cell. Neurosci. *91*, 122–130.

Bourne, J.N., and Harris, K.M. (2008). Balancing structure and function at hippocampal dendritic spines. Annu. Rev. Neurosci. *31*, 47–67.

Bowie, D., and Mayer, M.L. (1995). Inward rectification of both AMPA and kainate subtype glutamate receptors generated by polyamine-mediated ion channel block. Neuron *15*, 453–462.

Boyer, P., Phillips, J.L., Rousseau, F.L., and Ilivitsky, S. (2007). Hippocampal abnormalities and memory deficits: New evidence of a strong pathophysiological link in schizophrenia. Brain Res. Rev. *54*, 92–112.

Braak, H., and Braak, E. (1991). Neuropathological stageing of Alzheimer-related changes. Acta Neuropathol. *82*, 239–259.

Bredt, D.S., and Nicoll, R.A. (2003). Review AMPA Receptor Trafficking at Excitatory Synapses Characterization of Silent Synapses A resolution came with the discovery of ‘silent syn-apses’ (Durand et al. Neuron *40*, 361–379.

Broadbent, N.J., Squire, L.R., and Clark, R.E. (2004). Spatial memory, recognition memory, and the hippocampus. Proc. Natl. Acad. Sci. *101*, 14515–14520.

Buchsbaum, B.R., Hickok, G., and Humphries, C. (2001). Role of left posterior superior temporal gyrus in phonological processing for speech perception and production. Cogn. Sci. *25*, 663–678.

Burke, K.A., Janke, A.M., Rhine, C.L., and Fawzi, N.L. (2015). Residue-by-

Residue View of In Vitro FUS Granules that Bind the C-Terminal Domain of RNA Polymerase II. Mol. Cell *60*, 231–241.

Cajal, S.R. y (1894). The Croonian lecture.—La fine structure des centres nerveux. Proc. R. Soc. London *55*, 444–468.

Camina, E., and Güell, F. (2017). The neuroanatomical, neurophysiological and psychological basis of memory: Current models and their origins. Front. Pharmacol. *8*, 1–16.

Von Campenhausen, S., Bornschein, B., Wick, R., Bötzel, K., Sampaio, C., Poewe, W., Oertel, W., Siebert, U., Berger, K., and Dodel, R. (2005). Prevalence and incidence of Parkinson's disease in Europe. Eur. Neuropsychopharmacol. *15*, 473–490.

Capauto, D., Colantoni, A., Lu, L., Santini, T., Peruzzi, G., Biscarini, S., Morlando, M., Shneider, N.A., Caffarelli, E., Laneve, P., et al. (2018). A Regulatory Circuitry Between Gria2, miR-409, and miR-495 Is Affected by ALS FUS Mutation in ESC-Derived Motor Neurons. Mol. Neurobiol. *55*, 7635–7651.

Chen, L. (2009). A global comparison between nuclear and cytosolic transcriptomes reveals differential compartmentalization of alternative transcript isoforms. Nucleic Acids Res. *38*, 1086–1097.

Citri, A., and Malenka, R.C. (2008). Synaptic plasticity: Multiple forms, functions, and mechanisms. Neuropsychopharmacology *33*, 18–41.

Clayton, N.S., and Dickinson, A. (1998). Episodic-like memory during cache recovery by scrub jays. Nature *395*, 272–274.

Collingridge, G. (1987). The role of NMDA receptors in learning and memory. Nature *330*, 604–605.

Collingridge, G.L., Isaac, J.T.R.R., Yu, T.W., and Wang, Y.T. (2004). Receptor trafficking and synaptic plasticity. Nat. Rev. Neurosci. *5*, 952–962.

Colombrita, C., Onesto, E., Megiorni, F., Pizzuti, A., Baralle, F.E., Buratti, E.,

Silani, V., and Ratti, A. (2012). TDP-43 and FUS RNA-binding proteins bind distinct sets of cytoplasmic messenger RNAs and differently regulate their post-transcriptional fate in motoneuron-like cells. J. Biol. Chem. *287*, 15635–15647.

Costa-Mattioli, M., Sossin, W.S., Klann, E., and Sonenberg, N. (2009). Translational control of long-lasting synaptic plasticity and memory. Neuron *61*, 10–26.

Cowan, N. (2008). What are the differences between long-term, short-term, and working memory? Prog. Brain Res. *169*, 323–338.

Crozat, A., Aman, P., Mandahl, N., and Ron, D. (1993). Fusion of CHOP to a novel RNA-binding protein in human myxoid liposarcoma. Nature *363*, 640–644.

Van Damme, P., Dewil, M., Robberecht, W., and Van Den Bosch, L. (2005). Excitotoxicity and amyotrophic lateral sclerosis. Neurodegener. Dis. *2*, 147–159.

Deng, H., Gao, K., and Jankovic, J. (2014). The role of FUS gene variants in neurodegenerative diseases. Nat. Rev. Neurol. *10*, 337–348.

Deng, H.X., Zhai, H., Bigio, E.H., Yan, J., Fecto, F., Ajroud, K., Mishra, M., Ajroud-Driss, S., Heller, S., Sufit, R., et al. (2010). FUS-immunoreactive inclusions are a common feature in sporadic and non-SOD1 familial amyotrophic lateral sclerosis. Ann. Neurol. *67*, 739–748.

Deng, J., Yang, M., Chen, Y., Chen, X., Liu, J., Sun, S., Cheng, H., Li, Y., Bigio, E.H., Mesulam, M., et al. (2015). FUS Interacts with HSP60 to Promote Mitochondrial Damage. PLoS Genet. *11*, 1–30.

Dingledine, R., Borges, K., Bowie, D., and Traynelis, S.F. (1999). The glutamate receptor ion channels. Pharmacol. Rev. *51*, 7–61.

Djinovic-Carugo, K., Young, P., Gautel, M., and Saraste, M. (1999). Structure of the-Actinin Rod: Molecular Basis for Cross-Linking of Actin Filaments-

Actinin is composed of an amino-terminal actin-binding region consisting of two calponin homology (CH) domains, a central rod containing four spectrin-like re. Cell *98*, 537–546.

Dong, H., O'Brien, R.J., Fung, E.T., Lanahan, A.A., Worley, P.F., and Huganir, R.L. (1997). GRIP: a synaptic PDZ domain-containing protein that interacts with AMPA receptors. Nature *386*, 279–284.

Dormann, D. (2016). FUS cinating insights into motor neuron degeneration . EMBO J. *35*, 1015–1017.

Dormann, D., and Haass, C. (2011). TDP-43 and FUS: A nuclear affair. Trends Neurosci. *34*, 339–348.

Dormann, D., and Haass, C. (2013). Fused in sarcoma (FUS): An oncogene goes awry in neurodegeneration. Mol. Cell. Neurosci. *56*, 475–486.

Dormann, D., Rodde, R., Edbauer, D., Bentmann, E., Fischer, I., Hruscha, A., Than, M.E., MacKenzie, I.R.A., Capell, A., Schmid, B., et al. (2010). ALS-associated fused in sarcoma (FUS) mutations disrupt transportin-mediated nuclear import. EMBO J. *29*, 2841–2857.

Dormann, D., Madl, T., Valori, C.F., Bentmann, E., Tahirovic, S., Abou-Ajram, C., Kremmer, E., Ansorge, O., MacKenzie, I.R.A., Neumann, M., et al. (2012). Arginine methylation next to the PY-NLS modulates Transportin binding and nuclear import of FUS. EMBO J. *31*, 4258–4275.

Douglas, R.M., and Goddard, G. V. (1975). Long-term potentiation of the perforant path-granule cell synapse in the rat hippocampus. Brain Res. *86*, 205–215.

Easton, A., Webster, L.A.D., and Eacott, M.J. (2012). The episodic nature of episodic-like memories. Learn. Mem. *19*, 146–150.

Ebrahimi, S., and Okabe, S. (2014). Structural dynamics of dendritic spines: Molecular composition, geometry and functional regulation. Biochim. Biophys. Acta - Biomembr. *1838*, 2391–2398.

Ederle, H., and Dormann, D. (2017). TDP-43 and FUS en route from the nucleus to the cytoplasm. FEBS Lett. *591*, 1489–1507.

Eichenbaum, H. (2004). Hippocampus: Cognitive Processes and Neural Representations that Underlie Declarative Memory. Neuron *44*, 109–120.

Erkkinen, M.G., Kim, M., and Geschwind, M.D. (2019). Major Neurodegenerative Diseases.

Farg, M.A., Soo, K.Y., Warraich, S.T., Sundaramoorthy, V., Blair, I.P., and Atkin, J.D. (2013). Ataxin-2 interacts with FUS and intermediate-length polyglutamine expansions enhance FUS-related pathology in amyotrophic lateral sclerosis. Hum. Mol. Genet. *22*, 717–728.

Farrawell, N.E., Lambert-Smith, I.A., Warraich, S.T., Blair, I.P., Saunders, D.N., Hatters, D.M., and Yerbury, J.J. (2015). Distinct partitioning of ALS associated TDP-43, FUS and SOD1 mutants into cellular inclusions. Sci. Rep. *5*, 1–14.

Finkel, A., Wittel, A., Yang, N., Handran, S., Hughes, J., and Costantin, J. (2006). Population patch clamp improves data consistency and success rates in the measurement of ionic currents. J. Biomol. Screen. *11*, 488–496.

Van Der Flier, W.M., and Scheltens, P. (2005). Epidemiology and risk factors of dementia. Neurol. Pract. *76*, 2–7.

Fu, H., Hardy, J., and Duff, K.E. (2018). Selective vulnerability in neurodegenerative diseases. Nat. Neurosci. *21*, 1350–1358.

Fujii, R., and Takumi, T. (2005). TLS facilitates transport of mRNA encoding an actin-stabilizing protein to dendritic spines. J. Cell Sci. *118*, 5755–5765.

Fujii, R., Okabe, S., Urushido, T., Inoue, K., Yoshimura, A., Tachibana, T., Nishikawa, T., Hicks, G.G., and Takumi, T. (2005). The RNA binding protein TLS is translocated to dendritic spines by mGluR5 activation and regulates spine morphology. Curr. Biol. *15*, 587–593.

Fujioka, Y., Ishigaki, S., Masuda, A., Iguchi, Y., Udagawa, T., Watanabe, H.,

Katsuno, M., Ohno, K., and Sobue, G. (2013). FUS-regulated region- and cell-type-specific transcriptome is associated with cell selectivity in ALS/FTLD. Sci. Rep. *3*.

Gallagher, M. (1997). Animal models of memory impairment. Philos. Trans. R. Soc. B Biol. Sci. *352*, 1711–1717.

Gan, L., Cookson, M.R., Petrucelli, L., and La Spada, A.R. (2018). Converging pathways in neurodegeneration, from genetics to mechanisms. Nat. Neurosci. *21*, 1300–1309.

Geiger, J.R.P., Melcher, T., Koh, D.S., Sakmann, B., Seeburg, P.H., Jonas, P., and Monyer, H. (1995). Relative abundance of subunit mRNAs determines gating and Ca2+ permeability of AMPA receptors in principal neurons and interneurons in rat CNS. Neuron *15*, 193–204.

Goedert, M., Clavaguera, F., and Tolnay, M. (2010). The propagation of prion-like protein inclusions in neurodegenerative diseases. Trends Neurosci. *33*, 317–325.

Golde, T.E., and Miller, V.M. (2009). Proteinopathy-induced neuronal senescence: a hypothesis for brain failure in Alzheimer's and other neurodegenerative diseases. Alzheimers. Res. Ther. *1*, 5.

Golpich, M., Amini, E., Mohamed, Z., Azman Ali, R., Mohamed Ibrahim, N., and Ahmadiani, A. (2017). Mitochondrial Dysfunction and Biogenesis in Neurodegenerative diseases: Pathogenesis and Treatment. CNS Neurosci. Ther. *23*, 5–22.

Gomez-Pastor, R., Burchfiel, E.T., Neef, D.W., Jaeger, A.M., Cabiscol, E., McKinstry, S.U., Doss, A., Aballay, A., Lo, D.C., Akimov, S.S., et al. (2017). Abnormal degradation of the neuronal stress-protective transcription factor HSF1 in Huntington's disease. Nat. Commun. *8*, 1–17.

Greger, I.H., Watson, J.F., and Cull-Candy, S.G. (2017). Structural and Functional Architecture of AMPA-Type Glutamate Receptors and Their Auxiliary Proteins. Neuron *94*, 713–730.

Gregory, R.I., Yan, K.P., Amuthan, G., Chendrimada, T., Doratotaj, B., Cooch, N., and Shiekhattar, R. (2004). The Microprocessor complex mediates the genesis of microRNAs. Nature *432*, 235–240.

Guerrero, E.N., Wang, H., Mitra, J., Hegde, P.M., Stowell, S.E., Liachko, N.F., Kraemer, B.C., Garruto, R.M., Rao, K.S., and Hegde, M.L. (2016). TDP-43/FUS in motor neuron disease: Complexity and challenges. Prog. Neurobiol. *145–146*, 78–97.

Guo, L., Kim, H.J., Wang, H., Monaghan, J., Freyermuth, F., Sung, J.C., O'Donovan, K., Fare, C.M., Diaz, Z., Singh, N., et al. (2018). Nuclear-Import Receptors Reverse Aberrant Phase Transitions of RNA-Binding Proteins with Prion-like Domains. Cell *173*, 677-692.e20.

Haass, C., and Selkoe, D.J. (2007). Soluble protein oligomers in neurodegeneration: Lessons from the Alzheimer's amyloid β-peptide. Nat. Rev. Mol. Cell Biol. *8*, 101–112.

Hebb, D.O. (1949). The organization of behavior; a neuropsychological theory. (Oxford, England: Wiley).

Hee Jung Chung, Xia, J., Scannevin, R.H., Zhang, X., and Huganir, R.L. (2000). Phosphorylation of the AMPA receptor subunit GluR2 differentially regulates its interaction with PDZ domain-containing proteins. J. Neurosci. *20*, 7258–7267.

Hely, M.A., Reid, W.G.J., Adena, M.A., Halliday, G.M., and Morris, J.G.L. (2008). The Sydney Multicenter Study of Parkinson's disease: The inevitability of dementia at 20 years. Mov. Disord. *23*, 837–844.

Henriksen, E.J., Colgin, L.L., Barnes, C.A., Witter, M.P., Moser, M.B., and Moser, E.I. (2010). Spatial representation along the proximodistal axis of CA1. Neuron *68*, 127–137.

Hering, H., and Sheng, M. (2001). Dentritic spines: structure, dynamics and regulation. Nat. Rev. Neurosci. *2*, 880–888.

Hicks, G.G., Singh, N., Nashabi, A., Mai, S., Bozek, G., Klewes, L., Arapovic, D., White, E.K., Koury, M.J., Oltz, E.M., et al. (2000). Fus deficiency in mice results in defective B-lymphocyte development and activation, high levels of chromosomal instability and perinatal death. Nat. Genet. *24*, 175–179.

Hideyama, T., and Kwak, S. (2011). When Does ALS Start? ADAR2?GluA2 Hypothesis for the Etiology of Sporadic ALS. Front. Mol. Neurosci. *4*, 1–11.

Higelin, J., Demestre, M., Putz, S., Delling, J.P., Jacob, C., Lutz, A.-K., Bausinger, J., Huber, A.-K., Klingenstein, M., Barbi, G., et al. (2016). FUS Mislocalization and Vulnerability to DNA Damage in ALS Patients Derived hiPSCs and Aging Motoneurons. Front. Cell. Neurosci. *10*, 1–21.

Hirokawa, N., and Takemura, R. (2005). Molecular motors and mechanisms of directional transport in neurons. Nat. Rev. Neurosci. *6*, 201–214.

Hjelmstad, G.O., Nicoll, R.A., and Malenka, R.C. (1997). Synaptic refractory period provides a measure of probability of release in the hippocampus. Neuron *19*, 1309–1318.

Ho, V.M., Lee, J.A., and Martin, K.C. (2011). The cell biology of synaptic plasticity. Science (80-.). *334*, 623–628.

Hock, E.M., Maniecka, Z., Hruska-Plochan, M., Reber, S., Laferrière, F., Sahadevan M.K., S., Ederle, H., Gittings, L., Pelkmans, L., Dupuis, L., et al. (2018). Hypertonic Stress Causes Cytoplasmic Translocation of Neuronal, but Not Astrocytic, FUS due to Impaired Transportin Function. Cell Rep. *24*, 987-1000.e7.

Hofweber, M., Hutten, S., Bourgeois, B., Spreitzer, E., Niedner-Boblenz, A., Schifferer, M., Ruepp, M.D., Simons, M., Niessing, D., Madl, T., et al. (2018). Phase Separation of FUS Is Suppressed by Its Nuclear Import Receptor and Arginine Methylation. Cell *173*, 706-719.e13.

Hogan, D.B., Jetté, N., Fiest, K.M., Roberts, J.I., Pearson, D., Smith, E.E., Roach, P., Kirk, A., Pringsheim, T., and Maxwell, C.J. (2016). The prevalence and incidence of frontotemporal dementia: A systematic review. Can. J.

Neurol. Sci. *43*, S96–S109.

Honda, D., Ishigaki, S., Iguchi, Y., Fujioka, Y., Udagawa, T., Masuda, A., Ohno, K., Katsuno, M., and Sobue, G. (2014). The ALS/FTLD-related RNA-binding proteins TDP-43 and FUS have common downstream RNA targets in cortical neurons. FEBS Open Bio *4*, 1–10.

Hotulainen, P., and Hoogenraad, C.C. (2010). Actin in dendritic spines: Connecting dynamics to function. J. Cell Biol. *189*, 619–629.

Hsien, L.C., Kaur, P., Teo, E., Lam, V., Zhu, F., Kibat, C., Mathuru, A., Gruber, J., and Tolwinski, N.S. (2019). Application of Optogenetic Amyloid-β Distinguishes Between Metabolic and Physical Damage in Neurodegeneration. BioRxiv 1–21.

Huang, E.J., Zhang, J., Geser, F., Trojanowski, J.Q., Strober, J.B., Dickson, D.W., Brown, R.H., Shapiro, B.E., and Lomen-Hoerth, C. (2010). Extensive FUS-immunoreactive pathology in juvenile amyotrophic lateral sclerosis with basophilic inclusions. Brain Pathol. *20*, 1069–1076.

Ichetovkin, I., Grant, W., and Condeelis, J. (2002). Cofilin produces newly polymerized actin filaments that are preferred for dendritic nucleation by the Arp2/3 complex. Curr. Biol. *12*, 79–84.

Ichiyanagi, N., Fujimori, K., Yano, M., Ishihara-Fujisaki, C., Sone, T., Akiyama, T., Okada, Y., Akamatsu, W., Matsumoto, T., Ishikawa, M., et al. (2016). Establishment of in Vitro FUS-Associated Familial Amyotrophic Lateral Sclerosis Model Using Human Induced Pluripotent Stem Cells. Stem Cell Reports *6*, 496–510.

Imamura, K., Sahara, N., Kanaan, N.M., Tsukita, K., Kondo, T., Kutoku, Y., Ohsawa, Y., Sunada, Y., Kawakami, K., Hotta, A., et al. (2016). Calcium dysregulation contributes to neurodegeneration in FTLD patient iPSC-derived neurons. Sci. Rep. *6*, 34904.

Ionescu-Zanetti, C., Shaw, R.M., Seo, J., Jan, Y.N., Jan, L.Y., and Lee, L.P. (2005). Mammalian electrophysiology on a microfluidic platform. Proc. Natl.

Acad. Sci. U. S. A. *102*, 9112–9117.

Irish, M., and Piguet, O. (2013). The pivotal role of semantic memory in remembering the past and imagining the future. Front. Behav. Neurosci. *7*, 1–11.

Isaac, J.T.R., Ashby, M., and McBain, C.J. (2007). The Role of the GluR2 Subunit in AMPA Receptor Function and Synaptic Plasticity. Neuron *54*, 859–871.

Ishigaki, S., and Sobue, G. (2018). Importance of functional loss of FUS in FTLD/ALS. Front. Mol. Biosci. *5*, 1–8.

Ishigaki, S., Fujioka, Y., Okada, Y., Riku, Y., Udagawa, T., Honda, D., Yokoi, S., Endo, K., Ikenaka, K., Takagi, S., et al. (2017). Altered Tau Isoform Ratio Caused by Loss of FUS and SFPQ Function Leads to FTLD-like Phenotypes. Cell Rep. *18*, 1118–1131.

Ito, D., and Suzuki, N. (2011). Conjoint pathologic cascades mediated by ALS/FTLD-U linked RNA-binding proteins TDP-43 and FUS. Neurology *77*, 1636–1643.

Jarrard, L.E. (1993). On the role of the hippocampus in learning and memory in the rat. Behav. Neural Biol. *60*, 9–26.

Jarsky, T., Roxin, A., Kath, W.L., and Spruston, N. (2005). Conditional dendritic spike propagation following distal synaptic activation of hippocampal CA1 pyramidal neurons. Nat. Neurosci. *8*, 1667–1676.

Jia, Z., Agopyan, N., Miu, P., Xiong, Z., Henderson, J., Gerlai, R., Taverna, F.A., Velumian, A., MacDonald, J., Carlen, P., et al. (1996). Enhanced LTP in mice deficient in the AMPA receptor GluR2. Neuron *17*, 945–956.

Jonas, P., and Burnashev, N. (1995). Molecular mechanisms controlling calcium entry through AMPA-type glutamate receptor channels. Neuron *15*, 987–990.

Jucker, M., and Walker, L.C. (2011). Pathogenic protein seeding in

Alzheimer disease and other neurodegenerative disorders. Ann. Neurol. *70*, 532–540.

Jung, M.W., Wiener, S.I., and McNaughton, B.L. (1994). Comparison of spatial firing characteristics of units in dorsal and ventral hippocampus of the rat. J. Neurosci. *14*, 7347–7356.

Kamelgarn, M., Chen, J., Kuang, L., Jin, H., Kasarskis, E.J., and Zhu, H. (2018). ALS mutations of FUS suppress protein translation and disrupt the regulation of nonsense-mediated decay. Proc. Natl. Acad. Sci. U. S. A. *115*, E11904–E11913.

Kameoka, S., Duque, P., and Konarska, M.M. (2004). P54Nrb Associates With the 5′ Splice Site Within Large Transcription/Splicing Complexes. EMBO J. *23*, 1782–1791.

Kanai, Y., Dohmae, N., and Hirokawa, N. (2004). Kinesin Transports RNA. Neuron *43*, 513–525.

Kandel, E.R. (1976). Cellular basis of behavior: An introduction to behavioral neurobiology. (Oxford, England: W. H. Freeman).

Kang, J., Lim, L., Lu, Y., and Song, J. (2019). A unified mechanism for LLPS of ALS/FTLD-causing FUS as well as its modulation by ATP and oligonucleic acids.

King, A.E., Woodhouse, A., Kirkcaldie, M.T.K., and Vickers, J.C. (2016). Excitotoxicity in ALS: Overstimulation, or overreaction? Exp. Neurol. *275*, 162–171.

Kino, Y., Washizu, C., Kurosawa, M., Yamada, M., Miyazaki, H., Akagi, T., Hashikawa, T., Doi, H., Takumi, T., Hicks, G.G., et al. (2015). FUS/TLS deficiency causes behavioral and pathological abnormalities distinct from amyotrophic lateral sclerosis. Acta Neuropathol. Commun. *3*, 24.

Klausberger, T., and Somogyi, P. (2008). Neuronal diversity and temporal dynamics: The unity of hippocampal circuit operations. Science (80-.). *321*,

53–57.

Koganezawa, N., Hanamura, K., Sekino, Y., and Shirao, T. (2017). The role of drebrin in dendritic spines. Mol. Cell. Neurosci. *84*, 85–92.

Konorski, J. (1948). Conditioned reflexes and neuron organization. (New York, NY, US: Cambridge University Press).

Kosik, K.S., and Finch, E.A. (1987). MAP2 and tau segregate into dendritic and axonal domains after the elaboration of morphologically distinct neurites: an immunocytochemical study of cultured rat cerebrum. J. Neurosci. *7*, 3142–3153.

Kryndushkin, D., Wickner, R.B., and Shewmaker, F. (2011). FUS/TLS forms cytoplasmic aggregates, inhibits cell growth and interacts with TDP-43 in a yeast model of amyotrophic lateral sclerosis. Protein Cell *2*, 223–236.

Kullmann, D.M., and Nicoll, R.A. (1992). Long-term potentiation is associated with increases in quantal content and quantal amplitude. Nature *357*, 240–244.

Kumar, S.S., Bacci, A., Kharazia, V., and Huguenard, J.R. (2002). A developmental switch of AMPA receptor subunits in neocortical pyramidal neurons. J. Neurosci. *22*, 3005–3015.

Kuroda, M., Sok, J., Webb, L., Baechtold, H., Urano, F., Yin, Y., Chung, P., de Rooij, D.G., Akhmedov, A., Ashley, T., et al. (2000). Male sterility and enhanced radiation sensitivity in TLS(-/-) mice. EMBO J. *19*, 453–462.

Kwak, S., and Weiss, J.H. (2006). Calcium-permeable AMPA channels in neurodegenerative disease and ischemia. Curr. Opin. Neurobiol. *16*, 281–287.

Kwiatkowski, T.J., Bosco, D.A., Leclerc, A.L., Tamrazian, E., Vanderburg, C.R., Russ, C., Davis, A., Gilchrist, J., Kasarskis, E.J., Munsat, T., et al. (2009). Mutations in the FUS/TLS gene on chromosome 16 cause familial amyotrophic lateral sclerosis. Science *323*, 1205–1208.

Kwon, I., Kato, M., Xiang, S., Wu, L., Theodoropoulos, P., Mirzaei, H., Han, T., Xie, S., Corden, J.L., and McKnight, S.L. (2013). Phosphorylation-regulated binding of RNA polymerase II to fibrous polymers of low-complexity domains. Cell *155*, 1049–1060.

Lagier-Tourenne, C., and Cleveland, D.W. (2009). Rethinking ALS: The FUS about TDP-43. Cell *136*, 1001–1004.

Lagier-Tourenne, C., Polymenidou, M., and Cleveland, D.W. (2010). TDP-43 and FUS/TLS: Emerging roles in RNA processing and neurodegeneration. Hum. Mol. Genet. *19*, 46–64.

Van Langenhove, T., Van Der Zee, J., and Van Broeckhoven, C. (2012). The molecular basis of the frontotemporal lobar degeneration-amyotrophic lateral sclerosis spectrum. Ann. Med. *44*, 817–828.

Lanson, N.A., and Pandey, U.B. (2012). FUS-related proteinopathies: Lessons from animal models. Brain Res. *1462*, 44–60.

Lattante, S., Conte, A., Zollino, M., Luigetti, M., Del Grande, A., Marangi, G., Romano, A., Marcaccio, A., Meleo, E., Bisogni, G., et al. (2012). Contribution of major amyotrophic lateral sclerosis genes to the etiology of sporadic disease. Neurology *79*, 66–72.

Law, W.J., Cann, K.L., and Hicks, G.G. (2006). TLS, EWS and TAF15: A model for transcriptional integration of gene expression. Briefings Funct. Genomics Proteomics *5*, 8–14.

Leal, S.S., and Gomes, C.M. (2015). Calcium dysregulation links ALS defective proteins and motor neuron selective vulnerability. Front. Cell. Neurosci. *9*, 225.

Lee, S.H., Liu, L., Wang, Y.T., and Sheng, M. (2002). Clathrin adaptor AP2 and NSF interact with overlapping sites of GluR2 and play distinct roles in AMPA receptor trafficking and hippocampal LTD. Neuron *36*, 661–674.

Lenzi, J., De Santis, R., de Turris, V., Morlando, M., Laneve, P., Calvo, A.,

Caliendo, V., Chiò, A., Rosa, A., and Bozzoni, I. (2015). ALS mutant FUS proteins are recruited into stress granules in induced pluripotent stem cell-derived motoneurons. Dis. Model. Mech. *8*, 755–766.

Li, D.-P., Byan, H.S., and Pan, H.-L. (2012). Switch to glutamate receptor 2-lacking AMPA receptors increases neuronal excitability in hypothalamus and sympathetic drive in hypertension. J. Neurosci. *32*, 372–380.

Li, Y.R., King, O.D., Shorter, J., and Gitler, A.D. (2013). Stress granules as crucibles of ALS pathogenesis. J. Cell Biol. *201*, 361–372.

Ling, S., Albuquerque, C.P., Han, J.S., Lagier-Tourenne, C., Tokunaga, S., Zhou, H., and Cleveland, D.W. (2010). ALS-associated mutations in TDP-43 increase its stability and promote TDP-43 complexes with FUS/TLS. Proc. Natl. Acad. Sci. U. S. A. *107*, 13318–13323.

Ling, S.C., Polymenidou, M., and Cleveland, D.W. (2013). Converging mechanisms in als and FTD: Disrupted RNA and protein homeostasis. Neuron *79*, 416–438.

Liu, B., Liao, M., Mielke, J.G., Ning, K., Chen, Y., Li, L., El-Hayek, Y.H., Gomez, E., Zukin, R.S., Fehlings, M.G., et al. (2006). Ischemic insults direct glutamate receptor subunit 2-lacking AMPA receptors to synaptic sites. J. Neurosci. *26*, 5309–5319.

Liu, S.H., Lau, L., Wei, J.S., Zhu, D.Y., Zou, S., Sun, H.S., Fu, Y.P., Liu, F., and Lu, Y.M. (2004). Expression of Ca2+-permeable AMPA receptor channels primes cell death in transient forebrain ischemia. Neuron *43*, 43–55.

Loebel, A., Jean-Vincent, L.B., Richardson, M.J.E., Markram, H., and Herz, A.V.M. (2013). Matched pre-and post-synaptic changes underlie synaptic plasticity over long time scales. J. Neurosci. *33*, 6257–6266.

López-Erauskin, J., Tadokoro, T., Baughn, M.W., Myers, B., McAlonis-Downes, M., Chillon-Marinas, C., Asiaban, J.N., Artates, J., Bui, A.T., Vetto, A.P., et al. (2018). ALS/FTD-Linked Mutation in FUS Suppresses Intra-

axonal Protein Synthesis and Drives Disease Without Nuclear Loss-of-Function of FUS. Neuron *0*, 1–15.

Lu, W., Shi, Y., Jackson, A.C., Bjorgan, K., During, M.J., Sprengel, R., Seeburg, P.H., and Nicoll, R.A. (2009). Subunit Composition of Synaptic AMPA Receptors Revealed by a Single-Cell Genetic Approach. Neuron *62*, 254–268.

Luk, K.C., Kehm, V., Carroll, J., Zhang, B., O'Brien, P., Trojanowski, J.Q., and Lee, V.M.-Y. (2012). Pathological α-synuclein transmission initiates Parkinson-like neurodegeneration in nontransgenic mice. Science *338*, 949–953.

Lüscher, C., and Malenka, R.C. (2012). NMDA receptor-dependent long-term potentiation and long-term depression (LTP/LTD). Cold Spring Harb. Perspect. Biol. *4*, 3.

Lüthi, A., Chittajallu, R., Duprat, F., Palmer, M.J., Benke, T.A., Kidd, F.L., Henley, J.M., Isaac, J.T.., and Collingridge, G.L. (1999). Hippocampal LTD Expression Involves a Pool of AMPARs Regulated by the NSF–GluR2 Interaction. Neuron *24*, 389–399.

Lynch, M.A. (2004). Long-Term Potentiation and Memory. Physiol. Rev. *84*, 87–136.

Machamer, J.B., Woolums, B.M., Fuller, G.G., and Lloyd, T.E. (2018). FUS causes synaptic hyperexcitability in Drosophila dendritic arborization neurons. Brain Res. *1693*, 55–66.

Mackenzie, I.R.A., Neumann, M., Bigio, E.H., Cairns, N.J., Alafuzoff, I., Kril, J., Kovacs, G.G., Ghetti, B., Halliday, G., Holm, I.E., et al. (2010a). Nomenclature and nosology for neuropathologic subtypes of frontotemporal lobar degeneration: an update. Acta Neuropathol. *119*, 1–4.

Mackenzie, I.R.A., Rademakers, R., and Neumann, M. (2010b). TDP-43 and FUS in amyotrophic lateral sclerosis and frontotemporal dementia. Lancet Neurol. *9*, 995–1007.

MacKenzie, I.R.A., Munoz, D.G., Kusaka, H., Yokota, O., Ishihara, K., Roeber, S., Kretzschmar, H.A., Cairns, N.J., and Neumann, M. (2011). Distinct pathological subtypes of FTLD-FUS. Acta Neuropathol. *121*, 207–218.

Makino, H., and Malinow, R. (2011). Compartmentalized versus global synaptic plasticity on dendrites controlled by experience. Neuron *72*, 1001–1011.

Malenka, R.C., and Bear, M.F. (2004). LTP and LTD: an embarrassment of riches. Neuron *44*, 5–21.

Malinow, R., and Tsien, R.W. (1990). Presynaptic enhancement shown by whole-cell recordings of long-term potentiation in hippocampal slices. Nature *346*, 177–180.

Marrone, L., Qamar, S., Mannini, B., St George-Hyslop, P., and Vendruscolo, M. (2020). P525L promotes the aggregation of FUS by altering its biochemical and biophysical properties. Matters *6*, e202004000008.

Martel, M.A., Wyllie, D.J.A., and Hardingham, G.E. (2009). In developing hippocampal neurons, NR2B-containing N-methyl-d-aspartate receptors (NMDARs) can mediate signaling to neuronal survival and synaptic potentiation, as well as neuronal death. Neuroscience *158*, 334–343.

Martel, M.A., Ryan, T.J., Bell, K.F.S., Fowler, J.H., McMahon, A., Al-Mubarak, B., Komiyama, N.H., Horsburgh, K., Kind, P.C., Grant, S.G.N., et al. (2012). The Subtype of GluN2 C-terminal Domain Determines the Response to Excitotoxic Insults. Neuron *74*, 543–556.

Martin, S.J., Grimwood, P.D., and Morris, R.G. (2000). Synaptic plasticity and memory: an evaluation of the hypothesis. Annu. Rev. Neurosci. *23*, 649–711.

Mastrocola, A.S., Kim, S.H., Trinh, A.T., Rodenkirch, L.A., and Tibbetts, R.S. (2013). The RNA-binding protein fused in sarcoma (FUS) functions downstream of poly(ADP-ribose) polymerase (PARP) in response to DNA damage. J. Biol. Chem. *288*, 24731–24741.

Masuda, A., Takeda, J. ichi, and Ohno, K. (2016). FUS-mediated regulation of alternative RNA processing in neurons: Insights from global transcriptome analysis. Wiley Interdiscip. Rev. RNA *7*, 330–340.

Masurkar, A. V (2018). Towards a Circuit-Level Understanding of Hippocampal CA1 Dysfunction in Alzheimer's Disease Across Anatomical Axes. J. Alzheimer's Dis. Park. *08*, 1–6.

Mattson, M.R. (2007). Calcium and neurodegeneration. Aging Cell *6*, 337–350.

Mayeux, R., and Stern, Y. (2012). Epidemiology of Alzheimer disease. Cold Spring Harb. Perspect. Med. *2*.

Mayford, M., Siegelbaum, S.A., and Kandel, E.R. (2012). Synapses and memory storage. Cold Spring Harb. Perspect. Biol. *4*, 1–18.

McAllister, A.K. (2000). Biolistic Transfection of Neurons. Sci. Signal. *2000*, pl1–pl1.

McKay, S., Ryan, T.J., McQueen, J., Indersmitten, T., Marwick, K.F.M., Hasel, P., Kopanitsa, M. V., Baxter, P.S., Martel, M.A., Kind, P.C., et al. (2018). The Developmental Shift of NMDA Receptor Composition Proceeds Independently of GluN2 Subunit-Specific GluN2 C-Terminal Sequences. Cell Rep. *25*, 841-851.e4.

Miglio, G., Varsaldi, F., and Lombardi, G. (2005). Human T lymphocytes express N-methyl-D-aspartate receptors functionally active in controlling T cell activation. Biochem. Biophys. Res. Commun. *338*, 1875–1883.

Mitchell, J.C., McGoldrick, P., Vance, C., Hortobagyi, T., Sreedharan, J., Rogelj, B., Tudor, E.L., Smith, B.N., Klasen, C., Miller, C.C.J., et al. (2013). Overexpression of human wild-type FUS causes progressive motor neuron degeneration in an age- and dose-dependent fashion. Acta Neuropathol. *125*, 273–288.

Mochizuki, Y., Isozaki, E., Takao, M., Hashimoto, T., Shibuya, M., Arai, M.,

Hosokawa, M., Kawata, A., Oyanagi, K., Mihara, B., et al. (2012). Familial ALS with FUS P525L mutation: two Japanese sisters with multiple systems involvement. J. Neurol. Sci. *323*, 85–92.

Morris, R.G., Garrud, P., Rawlins, J.N., and O'Keefe, J. (1982). Place navigation impaired in rats with hippocampal lesions. Nature *297*, 681–683.

Morris, R.G., Anderson, E., Lynch, G.S., and Baudry, M. (1986). Selective impairment of learning and blockade of long-term potentiation by an N-methyl-D-aspartate receptor antagonist, AP5. Nature *319*, 774–776.

Morrison, B.M., Hof, P.R., and Morrison, J.H. (1998). Determinants of neuronal vulnerability in neurodegenerative diseases. Ann. Neurol. *44*, S32-44.

Moser, M.-B., Rowland, D.C., and Moser, E.I. (2015). Place cells, grid cells, and memory. Cold Spring Harb. Perspect. Biol. *7*, a021808.

Mulkey, R.M., Endo, S., Shenolikar, S., and Malenka, R.C. (1994). Involvement of a calcineurin/inhibitor-1 phosphatase cascade in hippocampal long-term depression. Nature *369*, 486–488.

Murakami, T., Yang, S.-P., Xie, L., Kawano, T., Fu, D., Mukai, A., Bohm, C., Chen, F., Robertson, J., Suzuki, H., et al. (2012). ALS mutations in FUS cause neuronal dysfunction and death in Caenorhabditis elegans by a dominant gain-of-function mechanism. Hum. Mol. Genet. *21*, 1–9.

Murakami, T., Qamar, S., Lin, J.Q., Schierle, G.S.K., Rees, E., Miyashita, A., Costa, A.R., Dodd, R.B., Chan, F.T.S., Michel, C.H., et al. (2015). ALS/FTD Mutation-Induced Phase Transition of FUS Liquid Droplets and Reversible Hydrogels into Irreversible Hydrogels Impairs RNP Granule Function. Neuron *88*, 678–690.

Murthy, A.C., Dignon, G.L., Kan, Y., Zerze, G.H., Parekh, S.H., Mittal, J., and Fawzi, N.L. (2019). Molecular interactions underlying liquid−liquid phase separation of the FUS low-complexity domain. Nat. Struct. Mol. Biol. *26*, 637–648.

Nadel, L., and Hardt, O. (2011). Update on memory systems and processes. Neuropsychopharmacology *36*, 251–273.

Nagy, Z., Jobst, K.A., Esiri, M.M., Morris, J.H., King, E.M., MacDonald, B., Litchfield, S., Barnetson, L., and Smith, A.D. (1996). Hippocampal pathology reflects memory deficit and brain imaging measurements in Alzheimer's disease: clinicopathologic correlations using three sets of pathologic diagnostic criteria. Dementia *7*, 76–81.

Naujock, M., Stanslowsky, N., Bufler, S., Naumann, M., Reinhardt, P., Sterneckert, J., Kefalakes, E., Kassebaum, C., Bursch, F., Lojewski, X., et al. (2016). 4-Aminopyridine Induced Activity Rescues Hypoexcitable Motor Neurons from Amyotrophic Lateral Sclerosis Patient-Derived Induced Pluripotent Stem Cells. Stem Cells *34*, 1563–1575.

Naumann, M., Pal, A., Goswami, A., Lojewski, X., Japtok, J., Vehlow, A., Naujock, M., Günther, R., Jin, M., Stanslowsky, N., et al. (2018). Impaired DNA damage response signaling by FUS-NLS mutations leads to neurodegeneration and FUS aggregate formation. Nat. Commun. *9*.

Naumann, M., Peikert, K., Günther, R., van der Kooi, A.J., Aronica, E., Hübers, A., Danel, V., Corcia, P., Pan-Montojo, F., Cirak, S., et al. (2019). Phenotypes and malignancy risk of different FUS mutations in genetic amyotrophic lateral sclerosis. Ann. Clin. Transl. Neurol. *6*, 2384–2394.

Nelson, S.B., and Turrigiano, G.G. (2008). Strength through Diversity. Neuron *60*, 477–482.

Neumann, M., Sampathu, D.M., Kwong, L.K., Truax, A.C., Micsenyi, M.C., Chou, T.T., Bruce, J., Schuck, T., Grossman, M., Clark, C.M., et al. (2006). Ubiquitinated TDP-43 in Frontotemporal Lobar Degeneration and Amyotrophic Lateral Sclerosis. Science (80-.). *314*, 130–133.

Neumann, M., Rademakers, R., Roeber, S., Baker, M., Kretzschmar, H.A., and MacKenzie, I.R.A. (2009). A new subtype of frontotemporal lobar degeneration with FUS pathology. Brain *132*, 2922–2931.

Neumann, M., Bentmann, E., Dormann, D., Jawaid, A., Dejesus-Hernandez, M., Ansorge, O., Roeber, S., Kretzschmar, H.A., Munoz, D.G., Kusaka, H., et al. (2011). FET proteins TAF15 and EWS are selective markers that distinguish FTLD with FUS pathology from amyotrophic lateral sclerosis with FUS mutations. Brain *134*, 2595–2609.

Neumann, M., Valori, C.F., Ansorge, O., Kretzschmar, H.A., Munoz, D.G., Kusaka, H., Yokota, O., Ishihara, K., Ang, L.-C.C., Bilbao, J.M., et al. (2012). Transportin 1 accumulates specifically with FET proteins but no other transportin cargos in FTLD-FUS and is absent in FUS inclusions in ALS with FUS mutations. Acta Neuropathol. *124*, 705–716.

Neves, G., Cooke, S.F., and Bliss, T.V.P. (2008). Synaptic plasticity, memory and the hippocampus: a neural network approach to causality. Nat. Rev. Neurosci. *9*, 65–75.

Newcomer, J.W., Farber, N.B., and Olney, J.W. (2000). NMDA receptor function, memory, and brain aging. Dialogues Clin. Neurosci. *2*, 219–232.

Nichols, E., Szoeke, C.E.I., Vollset, S.E., Abbasi, N., Abd-Allah, F., Abdela, J., Aichour, M.T.E., Akinyemi, R.O., Alahdab, F., Asgedom, S.W., et al. (2019). Global, regional, and national burden of Alzheimer's disease and other dementias, 1990–2016: a systematic analysis for the Global Burden of Disease Study 2016. Lancet Neurol. *18*, 88–106.

Nicoll, R.A. (2017). A Brief History of Long-Term Potentiation. Neuron *93*, 281–290.

Nishimune, A., Isaac, J.T.R., Molnar, E., Noel, J., Nash, S.R., Tagaya, M., Collingridge, G.L., Nakanishi, S., and Henley, J.M. (1998). NSF binding to GluR2 regulates synaptic transmission. Neuron *21*, 87–97.

Niu, C., Zhang, J., Gao, F., Yang, L., Jia, M., Zhu, H., and Gong, W. (2012). FUS-NLS/Transportin 1 Complex Structure Provides Insights into the Nuclear Targeting Mechanism of FUS and the Implications in ALS. PLoS One *7*.

Noh, K.M., Yokota, H., Mashiko, T., Castillo, P.E., Zukin, R.S., and Bennett, M.V.L. (2005). Blockade of calcium-permeable AMPA receptors protects hippocampal neurons against global schemia-induced death. Proc. Natl. Acad. Sci. U. S. A. *102*, 12230–12235.

Nolan, M., Talbot, K., and Ansorge, O. (2016). Pathogenesis of FUS-associated ALS and FTD: insights from rodent models. Acta Neuropathol. Commun. *4*, 99.

Nover, L., Scharf, K.D., and Neumann, D. (1989). Cytoplasmic heat shock granules are formed from precursor particles and are associated with a specific set of mRNAs. Mol. Cell. Biol. *9*, 1298–1308.

Okada, T., Yamada, N., Kakegawa, W., Tsuzuki, K., Kawamura, M., Nawa, H., Iino, M., and Ozawa, S. (2001). Sindbis viral-mediated expression of Ca2+-permeable AMPA receptors at hippocampal CA1 synapses and induction of NMDA receptor-independent long-term potentiation. Eur. J. Neurosci. *13*, 1635–1643.

Okamoto, K.I., Narayanan, R., Lee, S.H., Murata, K., and Hayashi, Y. (2007). The role of CaMKII as an F-actin-bundling protein crucial for maintenance of dendritic spine structure. Proc. Natl. Acad. Sci. U. S. A. *104*, 6418–6423.

Okreglak, V., and Drubin, D.G. (2010). Loss of Aip1 reveals a role in maintaining the actin monomer pool and an in vivo oligomer assembly pathway. J. Cell Biol. *188*, 769–777.

Okuyama, T., Kitamura, T., Roy, D.S., Itohara, S., and Tonegawa, S. (2016). Ventral CA1 neurons store social memory. Science *353*, 1536–1541.

Olypher, A. V., Lytton, W.W., and Prinz, A.A. (2012). Input-to-output transformation in a model of the rat hippocampal CA1 network. Front. Comput. Neurosci. *6*, 1–8.

Orozco, D., Tahirovic, S., Rentzsch, K., Schwenk, B.M., Haass, C., and Edbauer, D. (2012). Loss of fused in sarcoma (FUS) promotes pathological Tau splicing. EMBO Rep. *13*, 759–764.

Osten, P., Khatri, L., Perez, J.L., Köhr, G., Giese, G., Daly, C., Schulz, T.W., Wensky, A., Lee, L.M., and Ziff, E.B. (2000). Mutagenesis reveals a role for ABP/GRIP binding to GluR2 in synaptic surface accumulation of the AMPA receptor. Neuron *27*, 313–325.

Pachernegg, S., Münster, Y., Muth-Köhne, E., Fuhrmann, G., and Hollmann, M. (2015). GluA2 is rapidly edited at the Q/R site during neural differentiation in vitro. Front. Cell. Neurosci. *9*, 1–14.

Palop, J.J., and Mucke, L. (2010). Amyloid-B-induced neuronal dysfunction in Alzheimer's disease: From synapses toward neural networks. Nat. Neurosci. *13*, 812–818.

Paoletti, P., Bellone, C., and Zhou, Q. (2013). NMDA receptor subunit diversity: impact on receptor properties, synaptic plasticity and disease. Nat. Rev. Neurosci. *14*, 383–400.

Park, P., Volianskis, A., Sanderson, T.M., Bortolotto, Z.A., Jane, D.E., Zhuo, M., Kaang, B.K., and Collingridge, G.L. (2014). NMDA receptor-dependent long-term potentiation comprises a family of temporally overlapping forms of synaptic plasticity that are induced by different patterns of stimulation. Philos. Trans. R. Soc. Lond. B. Biol. Sci. *369*, 20130131.

Park, P., Kang, H., Sanderson, T.M., Bortolotto, Z.A., Georgiou, J., Zhuo, M., Kaang, B.-K., and Collingridge, G.L. (2018). The Role of Calcium-Permeable AMPARs in Long-Term Potentiation at Principal Neurons in the Rodent Hippocampus. Front. Synaptic Neurosci. *10*, 1–11.

Park, P., Kang, H., Sanderson, T.M., Bortolotto, Z.A., Georgiou, J., Zhuo, M., Kaang, B.-K., and Collingridge, G.L. (2019). On the Role of Calcium-Permeable AMPARs in Long-Term Potentiation and Synaptic Tagging in the Rodent Hippocampus. Front. Synaptic Neurosci. *11*, 4.

Parron, C., Poucet, B., and Save, E. (2006). Cooperation between the hippocampus and the entorhinal cortex in spatial memory: A disconnection study. Behav. Brain Res. *170*, 99–109.

Patel, A., Lee, H.O., Jawerth, L., Maharana, S., Jahnel, M., Hein, M.Y., Stoynov, S., Mahamid, J., Saha, S., Franzmann, T.M., et al. (2015). A Liquid-to-Solid Phase Transition of the ALS Protein FUS Accelerated by Disease Mutation. Cell *162*, 1066–1077.

Pavlov, I.P. (1927). Conditioned reflexes: an investigation of the physiological activity of the cerebral cortex. (Oxford, England: Oxford Univ. Press).

Pchitskaya, E., Popugaeva, E., and Bezprozvanny, I. (2018). Calcium signaling and molecular mechanisms underlying neurodegenerative diseases. Cell Calcium *70*, 87–94.

Penfield, W., and Milner, B. (1958). Memory deficit produced by bilateral lesions in the hippocampal zone. AMA. Arch. Neurol. Psychiatry *79*, 475–497.

Perez, J.L., Khatri, L., Chang, C., Srivastava, S., Osten, P., and Ziff, E.B. (2001). PICK1 targets activated protein kinase Cα to AMPA receptor clusters in spines of hippocampal neurons and reduces surface levels of the AMPA-type glutamate receptor subunit 2. J. Neurosci. *21*, 5417–5428.

Pievani, M., Filippini, N., Van Den Heuvel, M.P., Cappa, S.F., and Frisoni, G.B. (2014). Brain connectivity in neurodegenerative diseases - From phenotype to proteinopathy. Nat. Rev. Neurol. *10*, 620–633.

Protter, D.S.W., and Parker, R. (2016). Principles and Properties of Stress Granules. Trends Cell Biol. *26*, 668–679.

Qamar, S., Wang, G.Z., Randle, S.J., Ruggeri, F.S., Varela, J.A., Lin, J.Q., Phillips, E.C., Miyashita, A., Williams, D., Ströhl, F., et al. (2018). FUS Phase Separation Is Modulated by a Molecular Chaperone and Methylation of Arginine Cation-π Interactions. Cell *173*, 720-734.e15.

Qiu, H., Lee, S., Shang, Y., Wang, W.Y., Au, K.F., Kamiya, S., Barmada, S.J., Finkbeiner, S., Lui, H., Carlton, C.E., et al. (2014). ALS-associated mutation FUS-R521C causes DNA damage and RNA splicing defects. J. Clin. Invest.

124, 981–999.

Rabbitts, T.H., Forster, A., Larson, R., and Nathan, P. (1993). Fusion of the dominant negative transcription regulator CHOP with a novel gene FUS by translocation t(12;16) in malignant liposarcoma. Nat. Genet. *4*, 175–180.

Rappsilber, J., Friesen, W.J., Paushkin, S., Dreyfuss, G., and Mann, M. (2003). Detection of arginine dimethylated peptides by parallel precursor ion scanning mass spectrometry in positive ion mode. Anal. Chem. *75*, 3107–3114.

Reber, S., Stettler, J., Filosa, G., Colombo, M., Jutzi, D., Lenzken, S.C., Schweingruber, C., Bruggmann, R., Bachi, A., Barabino, S.M., et al. (2016). Minor intron splicing is regulated by FUS and affected by ALS -associated FUS mutants . EMBO J. *35*, 1504–1521.

Regan, P., Whitcomb, D.J., and Cho, K. (2017). Physiological and Pathophysiological Implications of Synaptic Tau. Neuroscientist *23*, 137–151.

Riggi, N., Cironi, L., Suvà, M.-L., and Stamenkovic, I. (2007). Sarcomas: genetics, signalling, and cellular origins. Part 1: The fellowship of TET. J. Pathol. *213*, 4–20.

Rochefort, N.L., and Konnerth, A. (2012). Dendritic spines: From structure to in vivo function. EMBO Rep. *13*, 699–708.

Rowe, R.G., and Daley, G.Q. (2019). Induced pluripotent stem cells in disease modelling and drug discovery. Nat. Rev. Genet. *20*, 377–388.

Sahoo, P.K., Smith, D.S., Perrone-Bizzozero, N., and Twiss, J.L. (2018). Axonal mRNA transport and translation at a glance. J. Cell Sci. *131*.

Sama, R.R. anjit. K., Ward, C.L., and Bosco, D.A. (2014). Functions of FUS/TLS from DNA repair to stress response: implications for ALS. ASN Neuro *6*.

Sama, R.R.K., Ward, C.L., Kaushansky, L.J., Lemay, N., Ishigaki, S., Urano, F., and Bosco, D.A. (2013). FUS/TLS assembles into stress granules and is

a prosurvival factor during hyperosmolar stress. J. Cell. Physiol. *228*, 2222–2231.

Sama, R.R.K., Fallini, C., Gatto, R., McKeon, J.E., Song, Y., Rotunno, M.S., Penaranda, S., Abdurakhmanov, I., Landers, J.E., Morfini, G., et al. (2017). ALS-linked FUS exerts a gain of toxic function involving aberrant p38 MAPK activation. Sci. Rep. *7*, 115.

Sanz-Clemente, A., Nicoll, R.A., and Roche, K.W. (2013). Diversity in NMDA receptor composition: Many regulators, many consequences. Neuroscientist *19*, 62–75.

Scekic-Zahirovic, J., Sendscheid, O., El Oussini, H., Jambeau, M., Sun, Y., Mersmann, S., Wagner, M., Dieterlé, S., Sinniger, J., Dirrig-Grosch, S., et al. (2016). Toxic gain of function from mutant FUS protein is crucial to trigger cell autonomous motor neuron loss. EMBO J. *35*, 1077–1097.

Schacter, D.L., and Tulving, E. (1994). What are the memory systems of 1994? In Memory Systems 1994, D.L. Schacter, and E. Tulving, eds. (Cambridge: MIT Press), pp. 1–38.

Schlesinger, F., Tammena, D., Krampfl, K., and Bufler, J. (2005). Two mechanisms of action of the adamantane derivative IEM-1460 at human AMPA-type glutamate receptors. Br. J. Pharmacol. *145*, 656–663.

Schoen, M., Reichel, J.M., Demestre, M., Putz, S., Deshpande, D., Proepper, C., Liebau, S., Schmeisser, M.J., Ludolph, A.C., Michaelis, J., et al. (2016). Super-resolution microscopy reveals presynaptic localization of the ALS/FTD related protein FUS in hippocampal neurons. Front. Cell. Neurosci. *9*, 1–16.

Schwartz, J.C., Ebmeier, C.C., Podell, E.R., Heimiller, J., Taatjes, D.J., and Cech, T.R. (2012). FUS binds the CTD of RNA polymerase II and regulates its phosphorylation at Ser2. Genes Dev. *26*, 2690–2695.

Schwartz, J.C., Cech, T.R., and Parker, R.R. (2015). Biochemical Properties and Biological Functions of FET Proteins. Annu. Rev. Biochem. *84*, 355–379.

Seelaar, H., Klijnsma, K.Y., De Koning, I., Van Der Lugt, A., Chiu, W.Z., Azmani, A., Rozemuller, A.J.M., and Van Swieten, J.C. (2010). Frequency of ubiquitin and FUS-positive, TDP-43-negative frontotemporal lobar degeneration. J. Neurol. *257*, 747–753.

Sephton, C.F., and Yu, G. (2015). The function of RNA-binding proteins at the synapse: Implications for neurodegeneration. Cell. Mol. Life Sci. *72*, 3621–3635.

Sephton, C.F., Tang, A.A., Kulkarni, A., West, J., Brooks, M., Stubblefield, J.J., Liu, Y., Zhang, M.Q., Green, C.B., Huber, K.M., et al. (2014). Activity-dependent FUS dysregulation disrupts synaptic homeostasis. Proc. Natl. Acad. Sci. U. S. A. *111*, E4769-78.

Shang, Y., and Huang, E.J. (2016). Mechanisms of FUS mutations in familial amyotrophic lateral sclerosis. Brain Res. *1647*, 65–78.

Sheldon, A.L., and Robinson, M.B. (2007). The role of glutamate transporters in neurodegenerative diseases and potential opportunities for intervention. Neurochem. Int. *51*, 333–355.

Shelkovnikova, T.A., Robinson, H.K., Southcombe, J.A., Ninkina, N., and Buchman, V.L. (2014). Multistep process of FUS aggregation in the cell cytoplasm involves RNA-dependent and RNA-independent mechanisms. Hum. Mol. Genet. *23*, 5211–5226.

Shiihashi, G., Ito, D., Yagi, T., Nihei, Y., Ebine, T., and Suzuki, N. (2016). Mislocated FUS is sufficient for gain-of-toxic-function amyotrophic lateral sclerosis phenotypes in mice. Brain *139*, 2380–2394.

Shiihashi, G., Ito, D., Arai, I., Kobayashi, Y., Hayashi, K., Otsuka, S., Nakajima, K., Yuzaki, M., Itohara, S., and Suzuki, N. (2017). Dendritic Homeostasis Disruption in a Novel Frontotemporal Dementia Mouse Model Expressing Cytoplasmic Fused in Sarcoma. EBioMedicine *24*, 102–115.

Shin, Y., Berry, J., Pannucci, N., Haataja, M.P., Toettcher, J.E., and Brangwynne, C.P. (2017). Spatiotemporal Control of Intracellular Phase

Transitions Using Light-Activated optoDroplets. Cell *168*, 159-171.e14.

Skinner, B.F. (1938). The behavior of organisms: an experimental analysis. (Oxford, England: Appleton-Century).

Snowden, J.S., Hu, Q., Rollinson, S., Halliwell, N., Robinson, A., Davidson, Y.S., Momeni, P., Baborie, A., Griffiths, T.D., Jaros, E., et al. (2011). The most common type of FTLD-FUS (aFTLD-U) is associated with a distinct clinical form of frontotemporal dementia but is not related to mutations in the FUS gene. Acta Neuropathol. *122*, 99–110.

Soo, K.Y., Halloran, M., Sundaramoorthy, V., Parakh, S., Toth, R.P., Southam, K.A., McLean, C.A., Lock, P., King, A., Farg, M.A., et al. (2015). Rab1-dependent ER–Golgi transport dysfunction is a common pathogenic mechanism in SOD1, TDP-43 and FUS-associated ALS. Acta Neuropathol. *130*, 679–697.

Soto, C., and Estrada, L.D. (2008). Protein misfolding and neurodegeneration. Arch. Neurol. *65*, 184–189.

Squire, L.R. (2009). Memory and brain systems: 1969-2009. J. Neurosci. *29*, 12711–12716.

Starr, A., and Sattler, R. (2018). Synaptic dysfunction and altered excitability in C9ORF72 ALS/FTD. Brain Res. *1693*, 98–108.

Stoica, R., Paillusson, S., Gomez-Suaga, P., Mitchell, J.C., Lau, D.H., Gray, E.H., Sancho, R.M., Vizcay-Barrena, G., De Vos, K.J., Shaw, C.E., et al. (2016). ALS/FTD-associated FUS activates GSK-3β to disrupt the VAPB–PTPIP51 interaction and ER–mitochondria associations. EMBO Rep. *17*, 1326–1342.

Suárez-Calvet, M., Neumann, M., Arzberger, T., Abou-Ajram, C., Funk, E., Hartmann, H., Edbauer, D., Kremmer, E., Göbl, C., Resch, M., et al. (2016). Monomethylated and unmethylated FUS exhibit increased binding to Transportin and distinguish FTLD-FUS from ALS-FUS. Acta Neuropathol. *131*, 587–604.

Südhof, T.C., and Malenka, R.C. (2008). Understanding Synapses: Past, Present, and Future. Neuron *60*, 469–476.

Sun, Z., Diaz, Z., Fang, X., Hart, M.P., Chesi, A., Shorter, J., and Gitler, A.D. (2011). Molecular determinants and genetic modifiers of aggregation and toxicity for the als disease protein fus/tls. PLoS Biol. *9*.

Sundaramoorthy, V., Sultana, J.M., and Atkin, J.D. (2015). Golgi fragmentation in amyotrophic lateral sclerosis, an overview of possible triggers and consequences. Front. Neurosci. *9*, 1–11.

Svetoni, F., Frisone, P., and Paronetto, M.P. (2016). Role of FET proteins in neurodegenerative disorders. RNA Biol. *13*, 1089–1102.

Swanson, G.T., Kamboj, S.K., and Cull-Candy, S.G. (1997). Single-channel properties of recombinant AMPA receptors depend on RNA editing, splice variation, and subunit composition. J. Neurosci. *17*, 58–69.

Tai, H.C., Serrano-Pozo, A., Hashimoto, T., Frosch, M.P., Spires-Jones, T.L., and Hyman, B.T. (2012). The synaptic accumulation of hyperphosphorylated tau oligomers in alzheimer disease is associated with dysfunction of the ubiquitin-proteasome system. Am. J. Pathol. *181*, 1426–1435.

Takehara-Nishiuchi, K. (2014). Entorhinal cortex and consolidated memory. Neurosci. Res. *84*, 27–33.

Talbott, E.O., Malek, A.M., and Lacomis, D. (2016). Chapter 13 - The epidemiology of amyotrophic lateral sclerosis. In Neuroepidemiology, M.J. Aminoff, F. Boller, and D.F.B.T.-H. of C.N. Swaab, eds. (Elsevier), pp. 225–238.

Taylor, J.P., Brown, R.H., and Cleveland, D.W. (2016). Decoding ALS: from genes to mechanism. Nature *539*, 197–206.

Templer, V.L., and Hampton, R.R. (2013). Episodic memory in nonhuman animals. Curr. Biol. *23*, R801–R806.

Tischbein, M., Baron, D.M., Lin, Y.-C.C., Gall, K. V., Landers, J.E., Fallini, C.,

and Bosco, D.A. (2019). The RNA-binding protein FUS/TLS undergoes calcium-mediated nuclear egress during excitotoxic stress and is required for GRIA2 mRNA processing. J. Biol. Chem. *294*, jbc.RA118.005933.

Tønnesen, J., and Nägerl, U.V. (2016). Dendritic spines as tunable regulators of synaptic signals. Front. Psychiatry *7*.

Tradewell, M.L., Yu, Z., Tibshirani, M., Boulanger, M.C., Durham, H.D., and Richard, S. (2012). Arginine methylation by prmt1 regulates nuclear-cytoplasmic localization and toxicity of FUS/TLS harbouring ALS-linked mutations. Hum. Mol. Genet. *21*, 136–149.

Traynelis, S.F., Wollmuth, L.P., McBain, C.J., Menniti, F.S., Vance, K.M., Ogden, K.K., Hansen, K.B., Yuan, H., Myers, S.J., and Dingledine, R. (2010). Glutamate receptor ion channels: structure, regulation, and function. Pharmacol. Rev. *62*, 405–496.

Tulving, E. (1972). Episodic and semantic memory. In Organization of Memory., (Oxford, England: Academic Press), pp. xiii, 423–xiii, 423.

Tulving, E. (2002). Episodic memory: from mind to brain. Annu. Rev. Psychol. *53*, 1–25.

Tyzack, G.E., Luisier, R., Taha, D.M., Neeves, J., Modic, M., Mitchell, J.S., Meyer, I., Greensmith, L., Newcombe, J., Ule, J., et al. (2019). Widespread FUS mislocalization is a molecular hallmark of amyotrophic lateral sclerosis. Brain *142*, 1–9.

Udagawa, T., Fujioka, Y., Tanaka, M., Honda, D., Yokoi, S., Riku, Y., Ibi, D., Nagai, T., Yamada, K., Watanabe, H., et al. (2015). FUS regulates AMPA receptor function and FTLD/ALS-associated behaviour via GluA1 mRNA stabilization. Nat. Commun. *6*, 1–13.

Vance, C., Rogelj, B., Hortobágyi, T., De Vos, K.J., Nishimura, A.L., Sreedharan, J., Hu, X., Smith, B., Ruddy, D., Wright, P., et al. (2009). Mutations in FUS, an RNA processing protein, cause familial amyotrophic lateral sclerosis type 6. Science *323*, 1208–1211.

Vance, C., Scotter, E.L., Nishimura, A.L., Troakes, C., Mitchell, J.C., Kathe, C., Urwin, H., Manser, C., Miller, C.C., Hortobágyi, T., et al. (2013). ALS mutant FUS disrupts nuclear localization and sequesters wild-type FUS within cytoplasmic stress granules. Hum. Mol. Genet. *22*, 2676–2688.

Vandenberghe, W., Robberecht, W., and Brorson, J.R. (2000). AMPA receptor calcium permeability, GluR2 expression, and selective motoneuron vulnerability. J. Neurosci. *20*, 123–132.

Wang, W.Y., Pan, L., Su, S.C., Quinn, E.J., Sasaki, M., Jimenez, J.C., MacKenzie, I.R.A., Huang, E.J., and Tsai, L.H. (2013). Interaction of FUS and HDAC1 regulates DNA damage response and repair in neurons. Nat. Neurosci. *16*, 1383–1391.

Wang, X., Schwartz, J.C., and Cech, T.R. (2015). Nucleic acid-binding specificity of human FUS protein. Nucleic Acids Res. *43*, 7535–7543.

Ward, C.L., Boggio, K.J., Johnson, B.N., Boyd, J.B., Douthwright, S., Shaffer, S.A., Landers, J.E., Glicksman, M.A., and Bosco, D.A. (2014). A loss of FUS/TLS function leads to impaired cellular proliferation. Cell Death Dis. *5*, 1–12.

Washburn, M.S., Numberger, M., Zhang, S., and Dingledine, R. (1997). Differential dependence on GluR2 expression of three characteristic features of AMPA receptors. J. Neurosci. *17*, 9393–9406.

Watkins, J.C., and Jane, D.E. (2006). The glutamate story. Br. J. Pharmacol. *147*, 100–108.

Waugh, N.C., and Norman, D.A. (1965). Primary memory. Psychol. Rev. *72*, 89–104.

Weber, S.C., and Brangwynne, C.P. (2012). Getting RNA and protein in phase. Cell *149*, 1188–1191.

Weber, J.P., Andrásfalvy, B.K., Polito, M., Magó, Á., Ujfalussy, B.B., and Makara, J.K. (2016). Location-dependent synaptic plasticity rules by

dendritic spine cooperativity. Nat. Commun. *7*.

Whitcomb, D.J., Hogg, E.L., Regan, P., Piers, T., Narayan, P., Whitehead, G., Winters, B.L., Kim, D.H., Kim, E., St George-Hyslop, P., et al. (2015). Intracellular oligomeric amyloid-beta rapidly regulates GluA1 subunit of AMPA receptor in the hippocampus. Sci. Rep. *5*, 1–12.

Whitehead, G., Jo, J., Hogg, E.L., Piers, T., Kim, D.H., Seaton, G., Seok, H., Bru-Mercier, G., Son, G.H., Regan, P., et al. (2013). Acute stress causes rapid synaptic insertion of Ca2+ -permeable AMPA receptors to facilitate long-term potentiation in the hippocampus. Brain *136*, 3753–3765.

Whitlock, J.R., Heynen, A.J., Shuler, M.G., and Bear, M.F. (2006). Learning induces long-term potentiation in the hippocampus. Science (80-.). *313*, 1093–1097.

Wiegert, J.S., and Oertner, T.G. (2013). Long-Term depression triggers the selective elimination of weakly integrated synapses. Proc. Natl. Acad. Sci. U. S. A. *110*.

Wishart, T.M., Parson, S.H., and Gillingwater, T.H. (2006). Synaptic vulnerability in neurodegenerative disease. J. Neuropathol. Exp. Neurol. *65*, 733–739.

Wolozin, B. (2012). Regulated protein aggregation: stress granules and neurodegeneration. Mol. Neurodegener. *7*, 56.

Wright, A., and Vissel, B. (2012). The essential role of AMPA receptor GluA2 subunit RNA editing in the normal and diseased brain. Front. Mol. Neurosci. *5*, 1–13.

Wu, S., and Green, M.R. (1997). Identification of a human protein that recognizes the 3’ splice site during the second step of pre-mRNA splicing. EMBO J. *16*, 4421–4432.

Wu, H., Nash, J.E., Zamorano, P., and Garner, C.C. (2002). Interaction of SAP97 with minus-end-directed actin motor myosin VI: Implications for

AMPA receptor trafficking. J. Biol. Chem. *277*, 30928–30934.

Yamashita, T., and Kwak, S. (2014). The molecular link between inefficient GluA2 Q/R site-RNA editing and TDP-43 pathology in motor neurons of sporadic amyotrophic lateral sclerosis patients. Brain Res. *1584*, 28–38.

Yamashita, T., Hideyama, T., Hachiga, K., Teramoto, S., Takano, J., Iwata, N., Saido, T.C., and Kwak, S. (2012). A role for calpain-dependent cleavage of TDP-43 in amyotrophic lateral sclerosis pathology. Nat. Commun. *3*, 1307–1313.

Yamazaki, T., Chen, S., Yu, Y., Yan, B., Haertlein, T.C., Carrasco, M.A., Tapia, J.C., Zhai, B., Das, R., Lalancette-Hebert, M., et al. (2012). FUS-SMN Protein Interactions Link the Motor Neuron Diseases ALS and SMA. Cell Rep. *2*, 799–806.

Yang, L., Zhang, J., Kamelgarn, M., Niu, C., Gal, J., Gong, W., and Zhu, H. (2015). Subcellular localization and RNAs determine FUS architecture in different cellular compartments. Hum. Mol. Genet. *24*, 5174–5183.

Yasuda, K., Zhang, H., Loiselle, D., Haystead, T., Macara, I.G., and Mili, S. (2013). The RNA-binding protein Fus directs translation of localized mrnas in APC-RNP granules. J. Cell Biol. *203*, 737–746.

Yokoi, S., Udagawa, T., Fujioka, Y., Honda, D., Okado, H., Watanabe, H., Katsuno, M., Ishigaki, S., and Sobue, G. (2017). 3′UTR Length-Dependent Control of SynGAP Isoform α2 mRNA by FUS and ELAV-like Proteins Promotes Dendritic Spine Maturation and Cognitive Function. Cell Rep. *20*, 3071–3084.

Zhang, W., and Linden, D.J. (2003). The other side of the engram: experience-driven changes in neuronal intrinsic excitability. Nat. Rev. Neurosci. *4*, 885–900.

Zhang, P., Fan, B., Yang, P., Temirov, J., Messing, J., Kim, H.J., and Taylor, J.P. (2018). OptoGranules reveal the evolution of stress granules to ALS-FTD pathology. BioRχiv.

Zhou, Y., Liu, S., Liu, G., Öztürk, A., and Hicks, G.G. (2013). ALS-Associated FUS Mutations Result in Compromised FUS Alternative Splicing and Autoregulation. PLoS Genet. *9*.

Zhou, Z., Licklider, L.J., Gygi, S.P., and Reed, R. (2002). Comprehensive proteomic analysis of the human spliceosome. Nature *419*, 182–185.

Zhu, H., Pleil, K.E., Urban, D.J., Moy, S.S., Kash, T.L., and Roth, B.L. (2014). Chemogenetic inactivation of ventral hippocampal glutamatergic neurons disrupts consolidation of contextual fear memory. Neuropsychopharmacology *39*, 1880–1892.

Zieglgänsberger, W., Parsons, C.G., and Danysz, W. (2005). Excitatory Amino Acid Neurotransmission. In Anxiety and Anxiolytic Drugs, (Berlin/Heidelberg: Springer-Verlag), pp. 249–303.

Zinszner, H., Sok, J., Immanuel, D., Yin, Y., and Ron, D. (1997). TLS (FUS) binds RNA in vivo and engages in nucleo-cytoplasmic shuttling. J. Cell Sci. *110*, 1741–1750.

Zola-Morgan, S., Squire, L.R., Clower, R.P., and Rempel, N.L. (1993). Damage to the perirhinal cortex exacerbates memory impairment following lesions to the hippocampal formation. J. Neurosci. *13*, 251–265.

Zsurka, G., and Kunz, W.S. (2015). Mitochondrial dysfunction and seizures: The neuronal energy crisis. Lancet Neurol. *14*, 956–966.

Zucker, R.S., and Regehr, W.G. (2002). Short-term synaptic plasticity. Annu. Rev. Physiol. *64*, 355–405.

Appendix

Yi et al. *Cell Discovery* (2018)4:44
DOI 10.1038/s41421-018-0046-x

Cell Discovery
www.nature.com/celldisc

ARTICLE Open Access

Postsynaptic p47phox regulates long-term depression in the hippocampus

Jee Hyun Yi[1], Dong Hyun Kim[1], Thomas M. Piers[1], Seung Chan Kim[1], Daniel J. Whitcomb[1], Philip Regan[1] and Kwangwook Cho[1,2]

Abstract

It is well documented that reactive oxygen species (ROS) affects neurodegeneration in the brain. Several studies also implicate ROS in the regulation of synapse function and learning and memory processes, although the precise source of ROS generation within these contexts remains to be further explored. Here we show that postsynaptic superoxide generation through PKCζ-activated NADPH oxidase 2 (NOX2) is critical for long-term depression (LTD) of synaptic transmission in the CA1–Shaffer collateral synapse of the rat hippocampus. Specifically, PKCζ-dependent phosphorylation of p47phox at serine 316, a NOX2 regulatory subunit, is required for LTD but is not necessary for long-term potentiation (LTP). Our data suggest that postsynaptic p47phox phosphorylation at serine 316 is a key upstream determinant for LTD and synapse weakening.

Introduction

Synapse weakening is part of a group of physiological processes referred to as synaptic plasticity, which govern changes in synaptic function in response to neuronal activity, and are thought to represent the cellular and molecular mechanisms of learning and memory[1]. On the other hand, aberrant activation of synapse weakening signalling pathways has been reported in several Alzheimer's disease (AD) models[2–4], suggesting that these signalling pathways represent a crucial interplay between physiology and the onset of disease-associated pathophysiology. Mounting evidence suggests that apoptotic signalling cascades, including caspase-3 and glycogen synthase kinase 3β (GSK-3β) activation, are centrally involved in physiological and pathophysiological forms of synapse weakening, manifest through postsynaptic α-amino-3-hydroxy-5-methyl-4-isoxazolepropionic acid receptor (AMPAR) endocytosis and long-term depression (LTD) of synaptic transmission[4–6]. However, how these signals are first initiated is unknown.

Reactive oxygen species (ROS) are not only well-known upstream regulators of neuronal apoptosis[7] and neurodegenerative signals[8] but are also known to play important regulatory roles in aspects of neuronal physiology, including synaptic plasticity and synapse weakening[9–13]. ROS can originate from numerous sources to affect synaptic plasticity, including presynaptic neurons, postsynaptic neurons and microglia[11, 13]. However, to date there has been no characterization or elucidation of the precise mechanisms of ROS generation that regulate synaptic plasticity.

Here, we examined the production of postsynaptic ROS during LTD, revealing a key role for postsynaptic ROS production via NADPH oxidase 2 (NOX2). Crucially, we find that the activity of postsynaptic protein kinase C zeta (PKCζ) is also required for LTD and identify the phosphorylation of p47phox at serine 316 as a necessary step in this pathway. Therefore, our results uncover a role for a specific postsynaptic ROS production pathway in activity-dependent synapse weakening.

Correspondence: Philip Regan (anplr@bristol.ac.uk) or Kwangwook Cho (Kei.Cho@kcl.ac.uk)
[1]Henry Wellcome Laboratories for Integrative Neuroscience and Endocrinology, Bristol Medical School, Faculty of Health Sciences, University of Bristol, Whitson Street, Bristol BS1 3NY, UK
[2]UK-Dementia Research Institute, Department of Basic and Clinical Neuroscience, Maurice Wohl Clinical Neuroscience Institute, King's College London, London SE5 9NU, UK
These authors contributed equally: Jee Hyun Yi, Dong Hyun Kim, Thomas M. Piers

Results

Postsynaptic superoxide is required for LTD in the CA1 of the hippocampus

Superoxide ions are one of the primary forms of ROS and are known to be elevated in neurons following the activation of *N*-methyl-D-aspartate receptors (NMDARs)[14–16]. We therefore hypothesized that intra-neuronal superoxide radicals are upstream regulators of NMDAR-dependent forms of synaptic plasticity. To address this, we analysed the effects of superoxide dismutase (SOD), a class of endogenous enzymes that catalyse superoxide dismutation[17], on an NMDAR-dependent form of LTD in rat hippocampal acute slices[18]. Accordingly, whilst application of low-frequency electric stimulation (LFS) during whole-cell patch clamp recording readily induced LTD in CA1–Schaffer collateral synapses (52.8 ± 9.0% of baseline, $p = 0.002$ vs. control input, Fig. 1a), postsynaptic infusion of SOD (300 units/ml) through the patch pipette blocked LTD (89.5 ± 8.7% of baseline, $p = 0.115$ vs. control input, Fig. 1b). To determine whether the superoxide radicals involved in this form of LTD could originate from an extracellular source, such as microglia[13], we bath applied SOD. Given that SOD has poor membrane permeability[19], extracellular bath application of the enzyme will catalyse extracellular superoxide dismutation without affecting intracellularly generated superoxide. Extracellular SOD application had no effect on LTD (57.5 ± 9.9% of baseline, $p = 0.004$ vs. control input, Fig. 1c), suggesting that postsynaptic intracellular superoxide, specifically, is critical for LTD expression. Since hydrogen peroxide (H_2O_2), another ROS, can be a product of SOD catalysis of superoxide dismutation and is also implicated in synaptic plasticity[20], we tested whether H_2O_2 is required for LTD. Postsynaptic infusion of catalase (300 units/ml), an enzyme that catalyses the decomposition of H_2O_2 to water and oxygen, had no effect on LTD (66.8 ± 4.7% of baseline, $p = 0.002$ vs. control input, Fig. 1d). We also tested whether H_2O_2 may be inhibiting NMDAR-LTD, which could provide an alternative explanation for the inhibition of LTD induced by SOD injection. To test this, we postsynaptically injected SOD along with catalase, thereby scavenging the H_2O_2 product of the SOD reaction. In this experiment, LTD was also blocked (SOD+catalase, 90.1 ± 4.8% of baseline, $p = 0.150$ vs. baseline, Fig. 1e). In bath application experiments, SOD and catalase co-treatment did not affect LTD (SOD+catalase, 68.3 ± 1.2% of baseline, $p < 0.001$ vs. baseline, Fig. 1f). Together, these results suggest that postsynaptic intracellular superoxide is required for NMDAR-dependent hippocampal LTD and that H_2O_2 itself is neither required for nor an inhibitor of LTD.

NOX2 regulates LTD

While several ROS-inducing mechanisms are present in neurons, emerging evidence suggests that superoxide production post-NMDAR activation is catalysed by NADPH oxidase (NOX)[15, 16]. NOX is a membrane-bound enzymatic complex responsible for the production of ROS and is present in neurons where it can localize to synapses[21]. Specifically, NOX2, commonly known as the prototypical NOX, has been suggested as the primary regulator of NMDAR-activated superoxide generation[15]. While NOX1–4 are reported to be expressed in the brain, NOX3 constitutively generates superoxide without stimulation[22] and NOX4 constitutively produces H_2O_2[23], an ROS that appears not to be involved in LTD. We therefore predicted that postsynaptic NOX1 and 2 are the most likely candidates for superoxide production during LTD. To test a requirement for these NOX isoforms for LTD, we utilized postsynaptic infusion of NOX inhibitors. Postsynaptic infusion of AEBSF (20 μM), a non-selective inhibitor of NOX[24], blocked LTD expression in CA1 neurons of acute hippocampal slices (90.4 ± 6.0% of baseline, $p = 0.146$ vs. control input, Fig. 2a), whilst postsynaptic infusion of the specific NOX1 inhibitor ML-171 (3 μM)[25] had no effect on LTD (58.9 ± 8.6% of baseline, $p = 0.006$ vs. control input, Fig. 2b). Postsynaptic infusion of apocynin (100 μM), a putative but non-selective inhibitor of NOX2[26], significantly impaired LTD expression (88.7 ± 8.3% of baseline, $p = 0.583$ vs. control input, Fig. 2c). In contrast, bath perfusion of apocynin after LTD induction failed to reverse the expression of LTD, indicating that NOX2 is not required for LTD maintenance (apocynin perfusion: 68.8 ± 4.0% of baseline vs. control: 78.9 ± 3.4% of baseline, $p = 0.078$, Supplementary Fig. S1). Together, these data are suggestive of a specific role for the NOX2 isoform of NOX in the regulation of LTD induction.

Owing to the limited pharmacological selectivity and off-target effects of available NOX inhibitors, we next utilized short hairpin RNA (shRNA) to knockdown either NOX1 or 2 expression (Fig. 2d). Biolistic transfection of NOX1 or NOX2 shRNA into CA1 neurons of organotypic cultured hippocampal slices was performed. LTD was readily inducible in cells transfected with NOX1 shRNA (NOX1 shRNA: 54.9 ± 4.7% of baseline; untransfected cells: 61.7 ± 3.5% of baseline, $p = 0.280$, Fig. 2e). In contrast, LTD was abolished in neurons transfected with NOX2 shRNA (NOX2 shRNA: 87.3 ± 11.5% of baseline; untransfected cells: 50.7 ± 7.4% of baseline, $p = 0.028$, Fig. 2f). Neither NOX1 nor NOX2 shRNA influenced the basal state of glutamatergic synaptic transmission, as measured by AMPAR-mediated excitatory postsynaptic current ($EPSC_{AMPA}$; Supplementary Fig. S2a and S2c) and NMDAR-mediated EPSC ($EPSC_{NMDA}$; Supplementary Fig. S2b and S2d). Furthermore, transfection of a scrambled form of NOX2 shRNA had no effect on LTD (scrNOX2 shRNA: 54.9 ± 7.3% of baseline; untransfected cells: 49.3 ± 5.2% of baseline, $p = 0.541$, Supplementary Fig. S2e). Therefore, our data strongly suggest that ROS

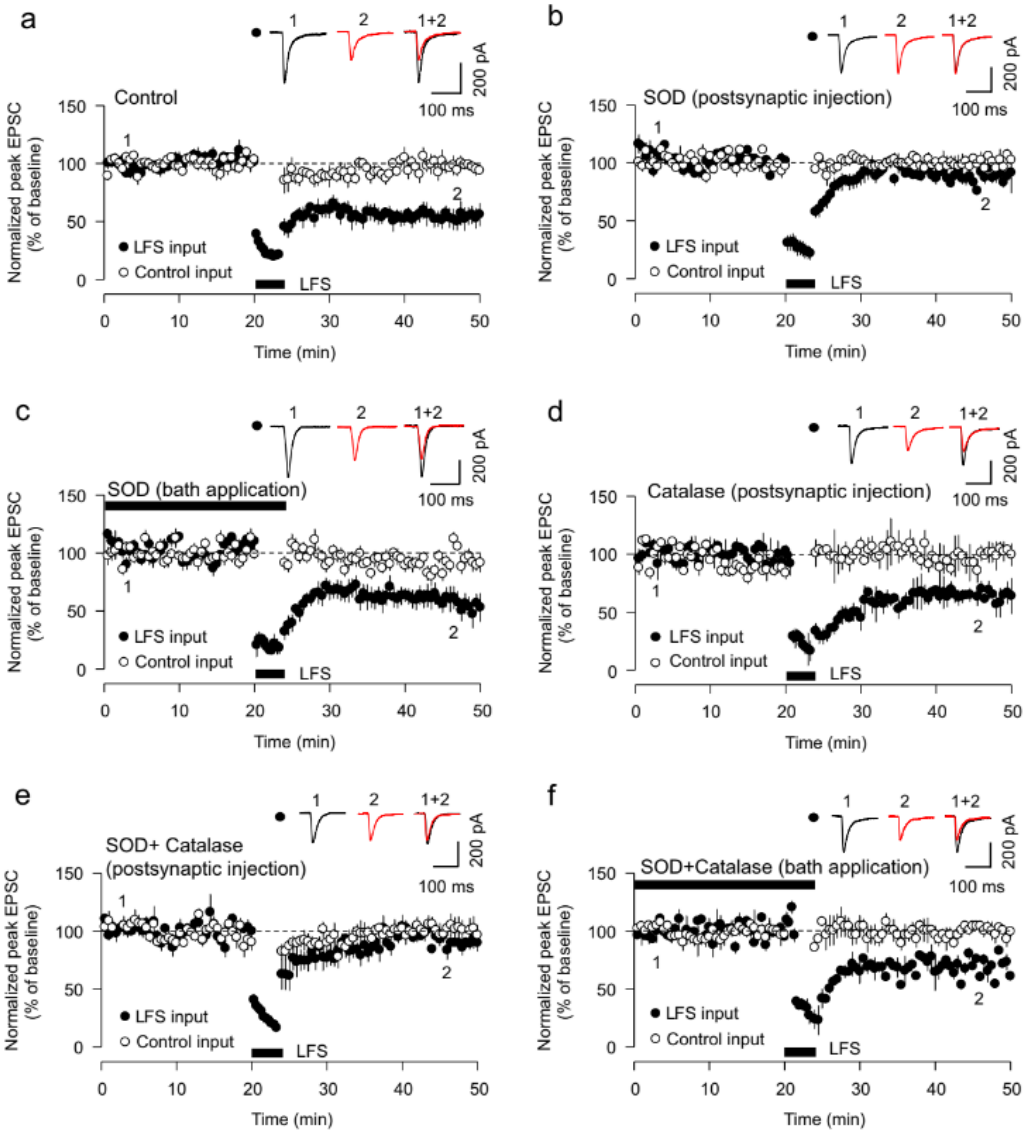

Fig. 1 Postsynaptic superoxide is required for LTD expression. a Low frequency stimulation (LFS) induces LTD in patch clamp recording mode in CA1–Schaffer collateral synapses in rat hippocampal acute slices ($n = 6$). **b** Postsynaptic injection of SOD (300 units/ml) blocked LTD ($n = 5$). **c** Bath application of SOD has no effect on LTD expression ($n = 5$). **d** Postsynaptic infusion of catalase (300 units/ml, 20 min) has no effect on LTD ($n = 5$). **e** Postsynaptic infusion of SOD and catalase inhibits LTD ($n = 6$). **f** Bath perfusion of SOD and catalase has no effect on LTD ($n = 6$). Symbols and error bars indicate mean ± SEM

production through postsynaptic NOX2 is involved in LTD regulation.

PKCζ and phosphorylation of p47phox is required for LTD

The function of NOX1/NOX2 is principally regulated through multi-site phosphorylation of the p47phox subunit of the complex by PKC isoforms, including the atypical PKCζ[27, 28]. Given the requirement for NOX2 in LTD, we hypothesized that phosphorylation of p47phox would also be required. To test this, we first utilized biolistic transfection of p47phox shRNA in CA1 neurons of organotypic hippocampal slices to knock down the expression of p47phox (Supplementary Fig. S3). Transfection of p47phox shRNA had no significant effect on basal $EPSC_{AMPA}$ compared with untransfected neighbouring cells (untransfected: 145.0 ± 15.1 pA, transfected: 162.1 ± 15.1 pA, $p = 0.594$, Fig. 3a). Consistent with our hypothesis, p47phox shRNA transfection significantly impaired LTD expression when compared to untransfected cells (p47phox shRNA-transfected cells: 87.2 ± 11.5% of baseline; untransfected cells: 50.6 ± 7.1% of baseline, $p = 0.0145$, Fig. 3b).

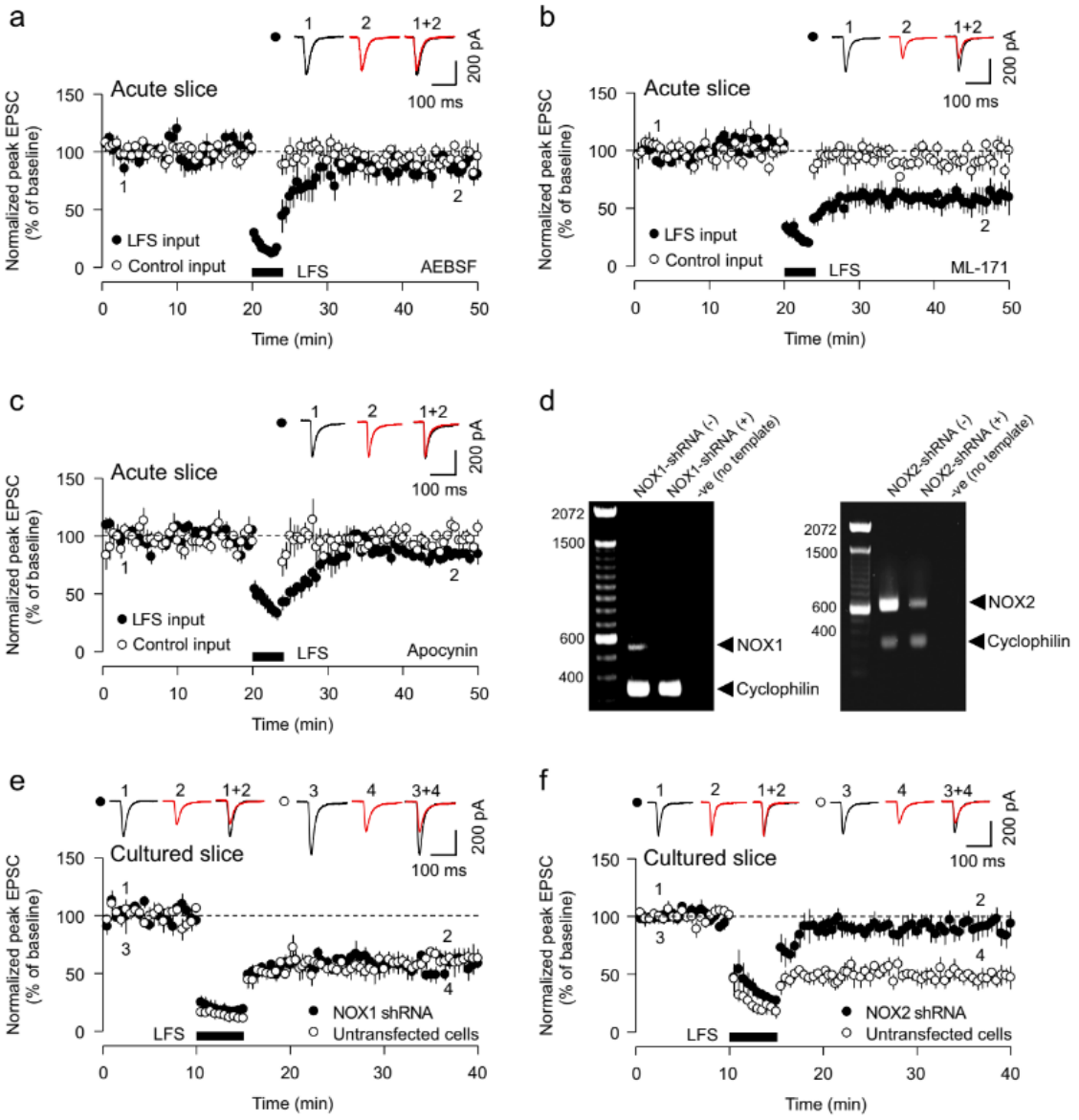

Fig. 2 Neuronal NADPH oxidase 2 (NOX2) is required for LTD expression. a Postsynaptic infusion of the NADPH oxidase inhibitor AEBSF (20 μM) blocks LTD ($n = 5$) in CA1 neurons from acute hippocampal slices. **b** Postsynaptic infusion of the NOX1 inhibitor ML-171 (3 μM) has no effect on LTD ($n = 5$). **c** Postsynaptic infusion of the NOX2 inhibitor apocynin (100 μM) blocks LTD ($n = 6$). **d** Single-cell PCR assays demonstrate efficient knockdown of NOX1 (left) and NOX2 (right) with their respective shRNAs in CA1 neurons of organotypic hippocampal slices. **e** LTD is readily inducible in both NOX1 shRNA-transfected cells (filled circle, $n = 5$) and untransfected control cells (open circle, $n = 6$). **f** LTD is abolished in neurons biolistically transfected with NOX2 shRNA (filled circle, $n = 5$), whilst LTD is induced in untransfected cells (open circle, $n = 5$). All data points represent mean ± SEM. Representative EPSC single traces are provided in inset from the time points indicated

Since phosphorylation of the p47phox subunit by the atypical PKCζ leads to superoxide generation[16, 27], we therefore used PKCζ shRNA (Supplementary Fig. S4) to examine whether PKCζ is also required for LTD. We found that transfection of PKCζ shRNA had no significant effect on basal $EPSC_{AMPA}$ (untransfected: 241.0 ± 33.2 pA, transfected 238.9 ± 22.6 pA, $p = 0.957$, Fig. 3c) but significantly impaired LTD (PKCζ shRNA: 90.6 ± 4.4% of baseline; untransfected cells: 50.4 ± 5.4% of baseline, $p = 0.0001$, Fig. 3d). Furthermore, the p47phox shRNA-mediated LTD deficit was rescued by co-expression of human p47phox (untransfected cells: 74.8 ± 8.9% of baseline; transfected cells: 69.2 ± 4.5% of baseline, $p = 0.583$; Fig. 3e).

To substantiate our hypothesis that PKCζ is an active component of LTD signalling, we tested whether LFS of hippocampal slices, which leads to NMDAR activation and LTD induction, regulates PKCζ activity. To do this,

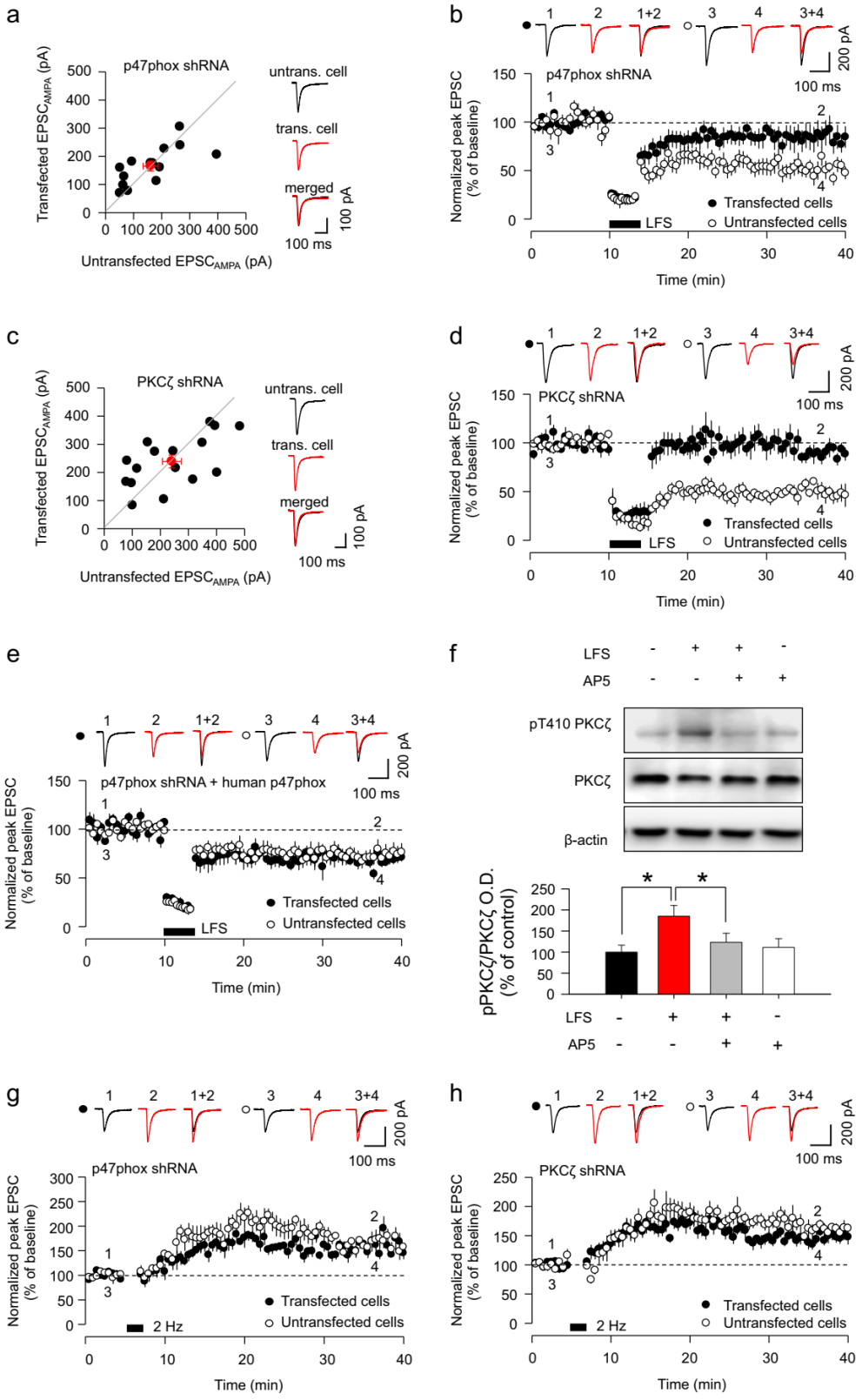

Fig. 3 (See legend on next page.)

(see figure on previous page)
Fig. 3 P47phox and PKCζ are necessary for LTD. a Synaptic AMPAR-mediated currents ($EPSC_{AMPA}$) are unchanged between p47phox shRNA-transfected cells and neighbouring untransfected cells ($n = 13$ pairs). Individual data points represent individual pairs of neurons. Red circles represent mean ± SEM. **b** LTD is abolished in neurons transfected with p47phox shRNA (filled circle, $n = 9$), whilst LTD is induced in untransfected cells (open circle, n = 8). **c** Synaptic AMPAR-mediated currents ($EPSC_{AMPA}$) are unchanged between PKCζ shRNA-transfected cells and neighbouring untransfected cells ($n = 16$ pairs). Individual data points represent individual pairs of neurons. Red circles represent mean ± SEM. **d** LTD is abolished in neurons transfected with PKCζ shRNA (filled circle, $n = 7$), whilst LTD is induced in untransfected cells (open circle, $n = 6$). **e** Co-transfection of human p47phox with p47phox shRNA rescues the expression of LTD (filled circles, $n = 7$) to levels similar to untransfected cells (open circles, $n = 7$). **f** Immunoblots showing LFS-induced enhanced PKCζ phosphorylation at threonine 410 residue (pT410PKCζ; $n = 5$) and AP5 inhibition of LFS-induced pT410PKCζ ($n = 5$). **g** LTP was present in p47phox shRNA-transfected cells (filled circle, $n = 7$) and untransfected cells (open circle, $n = 5$). **h** LTP was readily induced in both PKCζ shRNA-transfected cells (filled circle, $n = 7$) and untransfected cells (open circle, $n = 7$). Data represents mean ± SEM. Asterisk (*) indicates statistical significance ($p < 0.05$)

we utilized acutely prepared hippocampal slices prepared from 3-week-old rats. Since PKCζ activity depends on the phosphorylation of threonine 410 (pT410)[29, 30], we analysed whether LFS phosphorylates PKCζ at pT410. We found that LFS of Schaffer collateral afferents significantly increased phosphorylation of PKCζ at pT410, indicative of PKCζ activation, and this was blocked by AP5 (50 μM), an NMDAR antagonist (Control: 100 ± 16%; LFS: 185 ± 25%, $p < 0.05$ compared to control; LFS+AP5: 123 ± 21%, $p < 0.05$ compared to LFS; AP5: 111 ± 21%, Fig. 3f).

Interestingly, long-term potentiation (LTP) was readily inducible in cells expressing p47phox shRNA (p47phox shRNA: 154.2 ± 6.5% of baseline; untransfected cells: 167.1 ± 14.9% of baseline, $p = 0.416$, Fig. 3g). LTP was also intact in cells expressing PKCζ shRNA (PKCζ shRNA: 147.9 ± 9.4% of baseline; untransfected cells: 160.1 ± 10.0% of baseline, $p = 0.391$, Fig. 3h), indicating a selective role for p47phox and PKCζ in the LTD form of synaptic plasticity. Together, these data indicate that PKCζ activation downstream of NMDAR activation is a fundamental component of LTD signalling, regulating the activity of NOX2 via p47phox.

Phosphorylation of p47phox at serine 316 is required for LTD

Since both p47phox shRNA and PKCζ shRNA transfection resulted in a loss of LTD, it was of interest to determine the specific molecular mechanism surrounding the regulation of p47phox by PKCζ. We generated shRNA-resistant constructs of rat p47phox with differing combinations of site-specific mutations at four residues phosphorylated by PKCζ[27]. Consistent with our working hypothesis, LTD was blocked in cells co-transfected with p47phox shRNA and an shRNA-resistant mutant form of p47phox with all four residues mutated to alanine, to prevent their phosphorylation (after LFS: 95.1 ± 6.8%, $p = 0.725$ vs. control input, Fig. 4a). In cells expressing a triple phosphorylation mutant (S/T304/305/316A—residues notated as per rat p47phox), LTD was also impaired (after LFS: 88.0 ± 5.5%, $p = 0.087$ vs. control input, Fig. 4b). In comparison, LTD was readily inducible in cells transfected with a double S/T304/305A mutant (after LFS: 57.2 ± 4.1%, $p = 0.000117$ vs. control input, Fig. 4c). Notably, we found that LTD was also impaired in cells expressing the S316A mutant form of p47phox (after LFS: 98 ± 22.8%, $p = 0.73$ vs. control input, Fig. 4d) but the expression of S329A mutant form of p47phox had no effect on LTD induction (after LFS: 63.1 ± 7.0%, $p = 0.004$ vs. control input, Fig. 4e). Finally, we tested whether phosphorylation of p47phox at S316 is sufficient to induce synapse weakening, through paired recordings from neurons transfected with a S316 pseudo-phosphorylated form of p47phox (S316D) and neighbouring untransfected neurons. Our data showed significantly reduced AMPAR-mediated currents in S316D-transfected neurons (untransfected: 132.4 ± 12.9 pA vs. S316D transfected: 94.1 ± 9.4 pA, $p = 0.023$, Fig. 4f), indicating that phosphorylation at this residue is sufficient to reduce AMPAR-mediated synaptic transmission. This effect appears specific to AMPARs, as NMDAR-mediated currents were unchanged between the two cell types (untransfected: 131.1 ± 11.7 pA vs. S316D transfected: 118.7 ± 13.7 pA, $p = 0.495$, Fig. 4f). Taken together, these data suggest that phosphorylation at S316 of p47phox, likely by PKCζ, is a key regulator of a signalling cascade that governs LTD induction and synapse weakening.

Discussion

The notion that ROS production is a key element of synaptic plasticity has been well established[11–13, 20, 31]. However, the precise source of ROS and mechanisms by which it is regulated during synaptic plasticity have not been fully elucidated. Identification of these specific signalling pathways is necessary for our full understanding of its physiological and pathophysiological implications in synaptic function.

In the present study, we have shown that postsynaptic NOX2-mediated superoxide production, via PKCζ-mediated phosphorylation of p47phox at the serine 316 residue (pS316 p47phox), is pivotal for LTD expression and weakening of AMPAR-mediated synaptic transmission. Importantly, few studies have directly addressed the

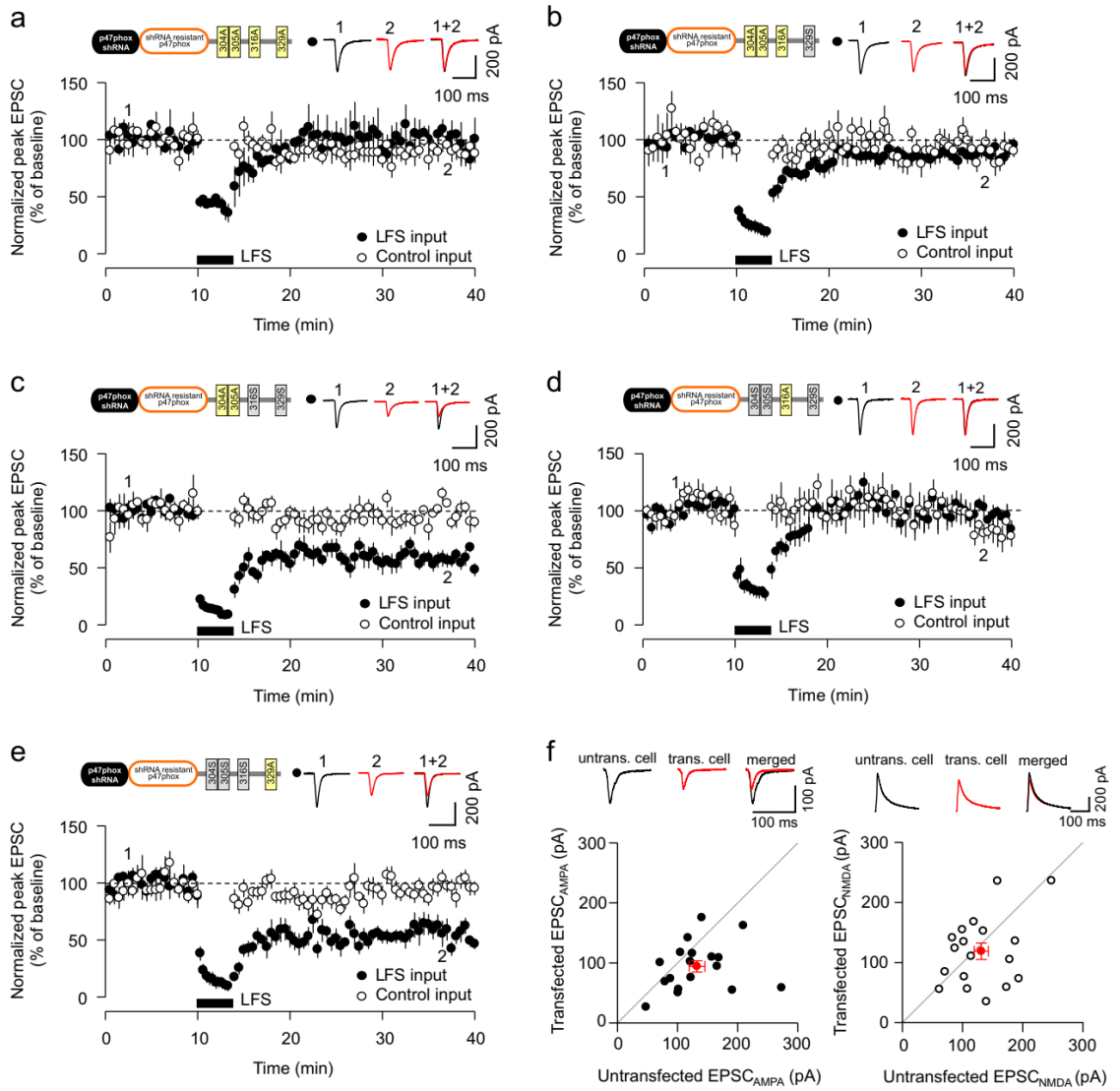

Fig. 4 Phosphorylation of p47phox at S316 is required for LTD. a LTD is impaired in cells co-transfected with p47phox shRNA and p47phox shRNA-resistant form of the S/T304/305/316/329A phosphorylation mutant p47phox ($n = 7$). **b** LTD is impaired in cells co-transfected with p47phox shRNA and p47phox shRNA-resistant form of the S304/305/316A triple phosphorylation mutant p47phox ($n = 7$). **c** LTD is inducible in cells co-transfected with the S304/305A double mutant form of p47phox ($n = 7$). **d** LTD is impaired in cells co-transfected with the S316A mutant form of p47phox ($n = 10$). **e** LTD is inducible in cells co-transfected with the S329A mutant form of p47phox ($n = 7$). Data represents mean ± SEM. **f** Synaptic AMPAR-mediated currents (EPSC$_{AMPA}$, filled circles), but not NMDAR-mediated currents (EPSC$_{NMDA}$, empty circles), are reduced in cells transfected with p47phox S316D compared to neighbouring untransfected cells ($n = 18$ pairs). Individual data points represent individual pairs of neurons. Red circles represent mean ± SEM. Representative single traces are provided in inset

source of ROS in the context of synaptic plasticity. Using our selective knockdown approach, in which we have specifically silenced or inhibited postsynaptic ROS production, we have now shown that postsynaptic NOX2 is a necessary hub for ROS production associated with LTD. Several research groups have shown a similar requirement for ROS during LTD or synapse weakening[9, 10, 12, 13] whilst evidence from other groups suggests that ROS can regulate LTP[12, 31, 32]. Quite how or why ROS can regulate both forms of synaptic plasticity is unclear, but it is possible that different ROS production sources and mechanisms may underpin different forms of synaptic plasticity.

NMDAR activation leads to PKCζ-mediated phosphorylation of the p47phox subunit, which is a critical activator signal for NOX2 mediated ROS production[15, 16]. In the present study, we show that low-frequency electrical stimulation of hippocampal slices, which induces an NMDAR-dependent form of LTD, also leads to the activation of PKCζ. This effect was blocked by D-AP5,

indicative of synaptic NMDAR-dependent activation of PKCζ that is associated with LTD induction. Importantly, through postsynaptic knockdown of PKCζ expression, we reveal an LTD-specific requirement for PKCζ with no observable contribution to LTP expression, consistent with other synapse weakening signals shown in previous studies[5, 6, 33–36]. Finally, our data show that constitutive phosphorylation of the PKCζ substrate, p47phox, at S316 is sufficient to induce weakening of AMPAR-mediated synaptic transmission, even in the absence of upstream activator signals. This single phosphorylation event, which induces NOX2 activation and ROS production, is therefore both necessary and sufficient for synapse weakening. It is not clear how postsynaptic ROS production is itself involved in the mechanisms of LTD signalling. One possibility is that postsynaptic ROS activates Bax protein to stimulate cytochrome *c* release from mitochondria[37]. Cytochrome *c* release induces caspase-3 activation[38], which in turn can affect synapse weakening signal cascades involving Akt-1 and GSK-3β[4, 39]. This possibility is supported by the observation that Bax is itself required for LTD signalling[33].

A growing list of molecules, including caspases, GSK-3β and tau, are now known to be involved in AMPAR endocytosis and LTD[5, 6, 33, 34]. Collectively, these molecules form what we have termed the synapse weakening pathway, encompassing molecules associated with apoptosis and synapse elimination in both physiological and pathophysiological circumstances[4, 36, 40]. It has been postulated that the balance between synapse weakening (caspase-3, GSK-3β and tau) and strengthening pathways (phosphoinositide-3 kinase and Akt-1) is critical to determine the direction of LTP and LTD and long-term fate of synapses[4–6, 35]. Indeed, models of neurodegenerative pathologies such as AD exhibit AMPAR endocytosis and facilitated LTD induction, concomitant with the inhibition of LTP in the hippocampus[2, 3, 39, 41, 42]. Aberrant activation of synapse weakening signals is therefore believed to be a central underlying molecular mechanism in the pathology and cognitive decline of numerous neurodegenerative diseases[4, 40, 43, 44]. Our results suggest that ROS, via a specific production mechanism, now form a part of this critical synapse weakening signalling cascade. Addressing whether aberrant LTD-like and/or AMPAR-mediated synapse weakening can be seen in human forms of neurodegenerative disease remains a key challenge to translating these findings into viable therapeutic targets.

Materials and methods

Animals

All procedures involving animals were carried out in accordance with the UK Animals (Scientific Procedures) Act, 1986. Male Wistar rats (Charles River, UK) were used to prepare organotypic (6–8 day-old rats) and acute hippocampal slices (2–4-week-old rats). Older rats were housed four or five per cage and allowed access to water and food ad libitum. The cages were maintained at a constant temperature (23 ± 1 °C) and relative humidity (60 ± 10%) under a 12-h light/dark cycle (lights on from 07:30 to 19:30).

Acute hippocampal slices

Rats were killed by cervical dislocation and decapitation. Following this, the brain was rapidly removed and placed into ice-cold artificial cerebrospinal fluid (aCSF; continuously bubbled with 95% O_2/5% CO_2) containing 124 mM NaCl, 3 mM KCl, 26 mM $NaHCO_3$, 1.25 mM NaH_2PO_4, 2 mM $CaCl_2$, 1 mM $MgSO_4$, and 10 mM D-glucose. Hippocampi were extracted and transverse hippocampal slices (400 µm thickness) were cut using a McIlwain tissue chopper. Following manual separation, the slices were then submerged in aCSF for a minimum of 1 h before experiments commenced.

Acute slices were placed in a recording chamber and perfused with warmed (28–29 °C) and carbogenated aCSF at 2 ml/min. Two independent stimulating electrodes were placed separately in the Schaffer collateral–CA1 input (test pathway) and subiculum–CA1 input (control pathway). For whole-cell patch experiments, 20 µM picrotoxin was included in the aCSF and CA1 neurons were blind-patched using a 4–6 MΩ borosilicate glass pipette containing 130 mM $CsMeSO_4$, 8 mM NaCl, 4 mM Mg-ATP, 0.3 mM Na-GTP, 0.5 mM EGTA, 10 mM HEPES, 6 mM QX-314, pH 7.2–7.3 and 280–290 mOsm/kg. For field excitatory postsynaptic potential (fEPSP) recordings, a glass pipette containing 3 M NaCl was placed in the *stratum radiatum* region of the CA1. LTD experiments during whole-cell patch were carried out as for cultured hippocampal slices (see below), except a 20-min baseline was used. For LTD of fEPSPs, a 30-min stable baseline at 70% of maximum stimulation intensity was followed by LFS, consisting of 900 pulses at 1 Hz, of the test pathway. This was followed by 60 min of post-conditioning recording. In some cases, slices were removed immediately after LFS for western blotting processing.

Hippocampal slice culture and whole-cell patch recording

Hippocampal slice cultures were prepared from 6–8-day-old male Wistar rats. Hippocampal slices (350 µm) were cut using a McIlwain tissue chopper and cultured on semipermeable membrane inserts (Millipore Corporation, Bedford, MA, USA) in a six-well plate containing culture medium (78.8% minimum essential medium, 20% heat-inactivated horse serum, 30 mM HEPES, 26 mM D-glucose, 5.8 mM $NaHCO_3$, 2 mM $CaCl_2$, 2 mM $MgSO_4$, 70 µM ascorbic acid, 1 µg/ml

insulin, pH adjusted to 7.3 and 320–330 mOsm). Slices were cultured for 6–8 days in vitro (DIV) with a change of medium every 2 days, without antibiotics. Neurons were transfected using a biolistic gene gun (Helios Gene-gun system, Bio Rad, USA) at DIV3–4 (100 µg DNA; 90% of the construct to test; 10% pEGFP-C1). Electrophysiological recordings were performed 3–4 days after transfection.

For whole-cell patch recordings, cultured slices were perfused with a warmed (28–29 °C) recording solution (119 mM NaCl, 2.5 mM KCl, 26 mM $NaHCO_3$, 1 mM NaH_2PO_4, 4 mM $MgCl_2$, 11 mM D-glucose, 4 mM $CaCl_2$, 10 µM 2-chloroadenosine and 20 µM picrotoxin). The recording solution was continuously bubbled with 95% O_2/5% CO_2 at source. The usual flow rate was 2 ml/min. In most recordings, two independent stimulating electrodes were placed separately in the Schaffer collateral–CA1 input and subiculum–CA1 input. Recordings were made from pyramidal neurons in the CA1 region, using glass pipettes containing $CsMeSO_4$ internal solution (as above) and neurons voltage clamped at −70 mV unless otherwise stated. To induce LTD, a 10-min baseline was followed by 1 Hz stimulation (200 stimuli) with recorded neurons voltage clamped at −40 mV. To induce LTP, a 5-min baseline was followed by a 2 Hz stimulation (200 stimuli) with recorded neurons voltage clamped at 0 mV. For quantification and comparisons between groups/inputs, the peak EPSC amplitude of the test input (relative to baseline) was averaged 15–20 min (cultured slice) or 20–25 min (acute slice) after conditioning was applied. $EPSC_{AMPA}$ was measured as the peak EPSC amplitude at a holding potential of −70 mV. $EPSC_{NMDA}$ was measured as the peak EPSC amplitude 90–100 ms after stimulus, at a holding potential of +40 mV.

Drugs and antibodies

The following drugs were dissolved in internal recording solution (for postsynaptic infusion) or aCSF (for bath perfusion) at concentrations based on previous studies: AEBSF (20 µM[45]; Sigma-Aldrich, MO, USA), apocynin (100 µM[46]; Abcam, Cambridge, UK), SOD (300 units/ml[47]; Sigma-Aldrich, MO, USA), catalase (300 units/ml[48]; Sigma-Aldrich, MO, USA), ML-171 (3 µM[49]; Tocris, Oxford, UK) and AP5 (Hello Bio, Bristol, UK). Primary antibodies used for western blotting were pT410 PKCζ (Cell Signaling, MA, USA), total PKCζ (Santa Cruz, Texas, USA) and total β-actin (Abcam, Cambridge, UK).

Expression/shRNA plasmids and single-cell PCR

Constructs for shRNA knockdown of target transcripts were generated using the Block-iT™ pENTR/U6 system, as per the manufacturer's instructions (Life Technologies, UK). The target sequences for rat NOX1 and NOX2 were GCAACTGTTCATACTCTTTCC and GGTCTTACTTT GAAGTGTTCT, respectively. NOX2 scrambled shRNA sequence was GGTAGTTACTCGTTAGTTTCT. PKCζ shRNA target sequence was GGCCATGAGCATCTCTG TTGT and for p47phox it was GCTCCTACCCTGCTT TAATGT. P47phox-rescue and mutation experiments were performed with co-transfection of the p47phox shRNA construct and a pCMV-SPORT6-p47phox cDNA clone (Source Bioscience, UK). Site-directed mutagenesis to generate S/T304/305A, S/T304/305/316A, S316A and S329A constructs was performed on the pCMV-SPORT6-p47phox construct using QuikChange™ technology, as per the manufacturer's instructions (Agilent Technologies, USA). All generated constructs were sequence verified via Sanger sequencing (Source Bioscience, UK).

Knockdown efficiencies of the generated shRNAs were verified by neuronal single-cell PCR. Briefly, transfected and non-transfected control cells were excised from cultured slices using low-resistance electrodes and then snap frozen. Cells were then subjected to OneStep™ RT-PCR (Qiagen, The Netherlands), as per the manufacturer's instructions, using specific exon-spanning primers: NOX1: sense 5′-AG AGGCTCCAGACCTCCATTT-3′, anti-sense, 5′-CGT GTGGTTGCAAAATGAGCA-3′; NOX2: sense 5′-AGCAC TTCACACGGCCATTC-3′, anti-sense 5′-AGAGGTCAG GGTGAAAGGGT-3′; PKCζ: sense 5′-GGACCTCTGTGA GGAAGTGC-3′, anti-sense, 5′-GGATGCTTGGGAAAAC GTGG-3′; PKMζ: sense 5′-CCTTCTATTAGATGCCTGC TCTCC-3′, anti-sense 5′-TGAAGGAAGGTCTACACCAT CGTTC-3′[50]; p47phox: sense 5′-CACCTTCATTCGCCAC ATCG-3′, anti-sense 5′-ATGTCCCTTTCCTGACCAC-3′; Cyclophilin: sense 5′-CCAAGACTGAGTGGCTGGA T-3′, anti-sense 5′- TCCTGCTAGACTTGAAGGGGA A-3′. Amplified PCR products were resolved on a 1% agarose/Midori Green gel and analysed under ultraviolet light.

Statistical analyses

Sample sizes, indicated by *n*, are indicated in the figure legends and represent the number of biological replicates. For experiments in acute slices, this reflects the number of individual animals from which the data were obtained. For cultured slices, this reflects the number of individual slices. Samples sizes for electrophysiology experiments were determined through empirical evidence obtained within our laboratory and are consistent with those found in existing literature. Data are expressed as mean ± standard error of the mean (SEM) and analysed using the SigmaPlot software (Systat Software, Chicago, USA). Significance was set at $p < 0.05$ and unpaired *t* tests were used to determine the statistical significance of effects vs. control inputs or untransfected cells, where appropriate, and paired *t* tests were used to compare to baseline values, when necessary.

Acknowledgements
This study was supported by a UK Wellcome Trust collaborative grant to K.C. and the BBSRC to K.C. and D.J.W. and the Korea-UK Alzheimer's disease Research Consortium grant to D.H.K. and J.H.Y. (Korean Ministry of Health and Welfare). K.C. was supported by the UK Dementia Research Institute.

Author details
[1]Henry Wellcome Laboratories for Integrative Neuroscience and Endocrinology, Bristol Medical School, Faculty of Health Sciences, University of Bristol, Whitson Street, Bristol BS1 3NY, UK. [2]UK-Dementia Research Institute, Department of Basic and Clinical Neuroscience, Maurice Wohl Clinical Neuroscience Institute, King's College London, London SE5 9NU, UK

Authors' contributions
The study was conceived and designed by K.C. Electrophysiological studies were conducted by D.H.K., J.H.Y., S.C.K. and P.R., constructs were produced by T.P. and biochemical assays were conducted by D.H.K. and J.H.Y. The manuscript was written by P.R., T.P., J.H.Y., D.J.W. and K.C.

Conflict of interest
The authors declare that they have no conflict of interest.

Supplementary Information accompanies the paper at (https://doi.org/10.1038/s41421-018-0046-x).

Received: 8 December 2017 Revised: 30 May 2018 Accepted: 31 May 2018
Published online: 28 August 2018

References

1. Citri, A. & Malenka, R. C. Synaptic plasticity: multiple forms, functions, and mechanisms. *Neuropsychopharmacology* **33**, 18–41 (2008).
2. Hsieh, H. et al. AMPAR removal underlies aβ-induced synaptic depression and dendritic spine loss. *Neuron* **52**, 831–843 (2006).
3. Shankar, G. M. et al. Amyloid-β protein dimers isolated directly from Alzheimer's brains impair synaptic plasticity and memory. *Nat. Med.* **14**, 837–842 (2008).
4. Jo, J. et al. Aβ(1-42) inhibition of LTP is mediated by a signaling pathway involving caspase-3, Akt1 and GSK-3β. *Nat. Neurosci.* **14**, 545–547 (2011).
5. Peineau, S., Taghibiglou, C., Bradley, C. & Liu, L. LTP Inhibits LTD in the hippocampus via regulation of GSK3β. *Neuron* **53**, 703–717 (2007).
6. Li, Z. et al. Caspase-3 activation via mitochondria is required for long-term depression and AMPA receptor internalization. *Cell* **141**, 859–871 (2010).
7. Greenlund, L. J., Deckwerth, T. L. & Johnson, E. M. Superoxide dismutase delays neuronal apoptosis: a role for reactive oxygen species in programmed neuronal death. *Neuron* **14**, 303–315 (1995).
8. Markesbery, W. R. Oxidative stress hypothesis in Alzheimer's disease. *Free Radic. Biol. Med.* **23**, 134–147 (1997).
9. Wang, Q., Rowan, M. J. & Anwyl, R. Beta-amyloid-mediated inhibition of NMDA receptor-dependent long-term potentiation induction involves activation of microglia and stimulation of inducible nitric oxide synthase and superoxide. *J. Neurosci.* **24**, 6049–6056 (2004).
10. Ma, T. et al. Amyloid β-induced impairments in hippocampal synaptic plasticity are rescued by decreasing mitochondrial superoxide. *J. Neurosci.* **31**, 5589–5595 (2011).
11. Massaad, C. A. & Klann, E. Reactive oxygen species in the regulation of synaptic plasticity and memory. *Antioxid. Redox Signal.* **14**, 2013–2054 (2011).
12. De Pasquale, R., Beckhauser, T. F., Hernandes, M. S. & Giorgetti Britto, L. R. LTP and LTD in the visual cortex require the activation of NOX2. *J. Neurosci.* **34**, 12778–12787 (2014).
13. Zhang, J. et al. Microglial CR3 activation triggers long-term synaptic depression in the hippocampus via NADPH oxidase. *Neuron* **82**, 195–207 (2014).
14. Bindokas, V. P., Jordan, J., Lee, C. C. & Miller, R. J. Superoxide production in rat hippocampal neurons: selective imaging with hydroethidine. *J. Neurosci.* **16**, 1324–1336 (1996).
15. Brennan, A. M. et al. NADPH oxidase is the primary source of superoxide induced by NMDA receptor activation. *Nat. Neurosci.* **12**, 857–863 (2009).
16. Brennan-Minnella, A. M., Shen, Y., El-Benna, J. & Swanson, R. A. Phosphoinositide 3-kinase couples NMDA receptors to superoxide release in excitotoxic neuronal death. *Cell Death Dis.* **4**, e580 (2013).
17. McCord, J. M., Keele, B. B. & Fridovich, I. An enzyme-based theory of obligate anaerobiosis: the physiological function of superoxide dismutase. *Proc. Natl Acad. Sci. USA* **68**, 1024–1027 (1971).
18. Dudek, S. M. & Bear, M. F. Homosynaptic long-term depression in area CA1 of hippocampus and effects of N-methyl-D-aspartate receptor blockade. *Proc. Natl Acad. Sci. USA* **89**, 4363–4367 (1992).
19. Rosenbaum, D. M., Kalberg, J. & Kessler, J. A. Superoxide dismutase ameliorates neuronal death from hypoxia in culture. *Stroke* **25**, 857–862 (1994). discussion 862–3.
20. Kamsler, A. & Segal, M. Paradoxical actions of hydrogen peroxide on long-term potentiation in transgenic superoxide dismutase-1 mice. *J. Neurosci.* **23**, 10359–10367 (2003).
21. Tejada-Simon, M. V. et al. Synaptic localization of a functional NADPH oxidase in the mouse hippocampus. *Mol. Cell. Neurosci.* **29**, 97–106 (2005).
22. Ueno, N., Takeya, R., Miyano, K., Kikuchi, H. & Sumimoto, H. The NADPH oxidase Nox3 constitutively produces superoxide in a p22phox-dependent manner: its regulation by oxidase organizers and activators. *J. Biol. Chem.* **280**, 23328–23339 (2005).
23. Martyn, K. D. et al. Functional analysis of Nox4 reveals unique characteristics compared to other NADPH oxidases. *Cell. Signal.* **18**, 69–82 (2006).
24. Diatchuk, V., Lotan, O., Koshkin, V., Wikstroem, P. & Pick, E. Inhibition of NADPH oxidase activation by 4-(2-aminoethyl)-benzenesulfonyl fluoride and related compounds. *J. Biol. Chem.* **272**, 13292–13301 (1997).
25. Gianni, D. et al. *Optimization and Characterization of an Inhibitor for NADPH Oxidase 1 (NOX-1)*. Probe Reports from the NIH Molcular Libraries Program [Internet] (National Center for Biotechnology Information (US), Bethesda, MD, 2010).
26. Jackman, K. A. et al. Reduction of cerebral infarct volume by apocynin requires pretreatment and is absent in Nox2-deficient mice. *Br. J. Pharmacol.* **156**, 680–688 (2009).
27. Fontayne, A., Dang, P. M.-C., Gougerot-Pocidalo, M. A. & El-Benna, J. Phosphorylation of p47phox sites by PKC alpha, beta II, delta, and zeta: effect on binding to p22phox and on NADPH oxidase activation. *Biochemistry* **41**, 7743–7750 (2002).
28. Bedard, K. & Krause, K.-H. The NOX family of ROS-generating NADPH oxidases: physiology and pathophysiology. *Physiol. Rev.* **87**, 245–313 (2007).
29. Chou, M. M. et al. Regulation of protein kinase C zeta by PI 3-kinase and PDK-1. *Curr. Biol.* **8**, 1069–1077 (1998).
30. Hirai, T. & Chida, K. Protein kinase Czeta (PKCzeta): activation mechanisms and cellular functions. *J. Biol. Chem.* **133**, 1–7 (2003).
31. Kishida, K. T. et al. Synaptic plasticity deficits and mild memory impairments in mouse models of chronic granulomatous disease. *Mol. Cell. Biol.* **26**, 5908–5920 (2006).
32. Thiels, E. et al. Impairment of long-term potentiation and associative memory in mice that overexpress extracellular superoxide dismutase. *J. Neurosci.* **20**, 7631–7639 (2000).
33. Jiao, S. & Li, Z. Nonapoptotic function of BAD and BAX in long-term depression of synaptic transmission. *Neuron* **70**, 758–772 (2011).
34. Kimura, T. et al. Microtubule-associated protein tau is essential for long-term depression in the hippocampus. *Philos. Trans. R. Soc. Lond. B. Biol. Sci.* **369**, 20130144–20130144 (2014).
35. Regan, P. L. et al. Tau phosphorylation at serine 396 residue is required for hippocampal LTD. *J. Neurosci.* **35**, 4804–4812 (2015).
36. Yi, J.-H. et al. Glucocorticoids activate a synapse weakening pathway culminating in tau phosphorylation in the hippocampus. *Pharmacol. Res.* **121**, 42–51 (2017).
37. Gomez-Lazaro, M. et al. Reactive oxygen species and p38 mitogen-activated protein kinase activate Bax to induce mitochondrial cytochrome c release and apoptosis in response to malonate. *Mol. Pharmacol.* **71**, 736–743 (2007).
38. Cai, J., Yang, J. & Jones, D. P. Mitochondrial control of apoptosis: the role of cytochrome c. *Biochim. Biophys. Acta* **1366**, 139–149 (1998).
39. Regan, P. L., Whitcomb, D. J. & Cho, K. Physiological and pathophysiological implications of synaptic tau. *Neuroscientist* https://doi.org/10.1177/1073858416633439 (2016).
40. Shipton, O. A. et al. Tau protein is required for amyloid β-induced impairment of hippocampal long-term potentiation. *J. Neurosci.* **31**, 1688–1692 (2011).

41. Kim, J. H., Anwyl, R., Suh, Y. H., Djamgoz, M. B. & Rowan, M. J. Use-dependent effects of amyloidogenic fragments of (beta)-amyloid precursor protein on synaptic plasticity in rat hippocampus in vivo. *J. Neurosci.* **21**, 1327–1333 (2001).
42. Shankar, G. M. et al. Natural oligomers of the Alzheimer amyloid-beta protein induce reversible synapse loss by modulating an NMDA-type glutamate receptor-dependent signaling pathway. *J. Neurosci.* **27**, 2866–2875 (2007).
43. Selkoe, D. J. Alzheimer's disease is a synaptic failure. *Science* **298**, 789–791 (2002).
44. Day, M. et al. Selective elimination of glutamatergic synapses on striatopallidal neurons in Parkinson disease models. *Nat. Neurosci.* **9**, 251–259 (2006).
45. Kovac, S. et al. Nrf2 regulates ROS production by mitochondria and NADPH oxidase. *Biochim. Biophys. Acta* **1850**, 794–801 (2015).
46. Lull, M. E., Levesque, S., Surace, M. J. & Block, M. L. Chronic apocynin treatment attenuates beta amyloid plaque size and microglial number in hAPP(751)(SL) mice. *PLoS ONE* **6**, e20153 (2011).
47. Preston, J. E., Hipkiss, A. R., Himsworth, D. T., Romero, I. A. & Abbott, J. N. Toxic effects of beta-amyloid(25-35) on immortalised rat brain endothelial cell: protection by carnosine, homocarnosine and beta-alanine. *Neurosci. Lett.* **242**, 105–108 (1998).
48. Yu, A. C., Gregory, G. A. & Chan, P. H. Hypoxia-induced dysfunctions and injury of astrocytes in primary cell cultures. *J. Cereb. Blood Flow Metab.* **9**, 20–28 (1989).
49. Cetinbas, N. et al. Loss of the tumor suppressor Hace1 leads to ROS-dependent glutamine addiction. *Oncogene* **34**, 4005–4010 (2015).
50. Marchand, F. et al. Specific involvement of atypical PKCζ/PKMζ in spinal persistent nociceptive processing following peripheral inflammation in rat. *Mol. Pain* **7**, 86 (2011).

COMMUNICATIONS BIOLOGY

ARTICLE

https://doi.org/10.1038/s42003-020-0792-9 OPEN

Beta amyloid aggregates induce sensitised TLR4 signalling causing long-term potentiation deficit and rat neuronal cell death

Craig Hughes[1,11], Minee L. Choi[2,3,11], Jee-Hyun Yi[4,9,11], Seung-Chan Kim[4,5], Anna Drews[1,10], Peter St. George-Hyslop[6], Clare Bryant[7], Sonia Gandhi[2,3], Kwangwook Cho[4,5] & David Klenerman[1,8]✉

The molecular events causing memory loss and neuronal cell death in Alzheimer's disease (AD) over time are still unknown. Here we found that picomolar concentrations of soluble oligomers of synthetic beta amyloid (Aβ42) aggregates incubated with BV2 cells or rat astrocytes caused a sensitised response of Toll-like receptor 4 (TLR4) with time, leading to increased production of TNF-α. Aβ aggregates caused long term potentiation (LTP) deficit in hippocampal slices and predominantly neuronal cell death in co-cultures of astrocytes and neurons, which was blocked by TLR4 antagonists. Soluble Aβ aggregates cause LTP deficit and neuronal death via an autocrine/paracrine mechanism due to TLR4 signalling. These findings suggest that the TLR4-mediated inflammatory response may be a key pathophysiological process in AD.

[1] Department of Chemistry, University of Cambridge, Lensfield Road, Cambridge CB2 1EW, UK. [2] Department of Clinical and Movement Neurosciences, UCL Queen Square Institute of Neurology, London WC1N 3BG, UK. [3] The Francis Crick Institute, 1 Midland Road, London NW1 1AT, UK. [4] Centre for Synaptic Plasticity, Faculty of Health Sciences, University of Bristol, Whitson Street, Bristol BS1 3NY, UK. [5] UK-Dementia Research Institute at King's College London, King's College, Department of Basic and Clinical Neuroscience, Institute of Psychiatry, Psychology and Neuroscience, London SE5 9NU, UK. [6] Cambridge Institute for Medical Research, University of Cambridge, Cambridge Biomedical Campus The Keith Peters Building Hills Road, Cambridge CB2 0XY, UK. [7] Department of Veterinary Medicine, University of Cambridge, Madingley Road, Cambridge CB3 0ES, UK. [8] UK Dementia Research Institute, University of Cambridge, Cambridge CB2 0XY, UK. [9] Present address: Center for Synaptic Brain Dysfunctions, Institute for Basic Science, Daejeon 34126, Republic of Korea. [10] Present address: The German Center for Neurodegenerative Diseases (DZNE), Sigmund-Freud-Str. 27, Venusberg-Campus, Gebäude 99, 53127 Bonn, Germany. [12] These authors contributed equally: Craig Hughes, Minee L. Choi, Jee-Hyun Yi. ✉email: dk10012@cam.ac.uk

Memory loss is a very common symptom of Alzheimer's disease (AD), however the molecular basis by which memory loss occurs is not understood[1]. This means it is currently challenging to develop treatments for AD. A synaptic correlate of memory is long-term potentiation (LTP). LTP is widely considered one of the major cellular mechanisms that underlies learning and memory. It has been found that soluble beta-amyloid (Aβ) aggregates from a variety of sources including soaked brain[2], brain homogenate, concentrated CSF and synthetic aggregates[3,4] can cause LTP deficit in brain slices. Significant efforts have been made to identify the nature of the aggregates that affect LTP deficit, so they can be targeted for potential therapy. Antibodies that bind the N-terminus of Aβ[4 4], knock-out of PrP or the use of PrP antibodies[5] have all been shown to be effective in preventing aggregate-induced LTP deficit. These results show that soluble Aβ aggregates initiate LTP deficit, but the mechanism by which this occurs and whether it is a result of the direct interaction of aggregates with synapses or occurs by a different mechanism has not been established to date. In vivo, Aβ can be post-translationally modified and interact with other proteins present, so that the aggregates present are heterogeneous in both size and composition. In contrast, synthetic aggregates made by aggregating Aβ42 in the test-tube are only heterogeneous in size not composition and still capable of causing LTP deficit[4]. In most experiments the aggregate concentration is not measured but only the total Aβ monomer concentration is known. This means that while it has been observed that brain-derived aggregates are more effective at causing LTP deficit than synthetic Aβ aggregates this could simply occur because the concentration of aggregates is higher in the preparations used. It is not possible to determine which type of aggregate is more effective at causing LTP without knowing the aggregate concentration.

Aβ aggregates can trigger the production of a number of proinflammatory cytokines, including TNF-α, from astrocytes and microglia[6,7], and the media from conditioned astrocytes is toxic to neurons[8] suggesting that neuronal cell death can occur via an inflammatory mechanism. One of the routes that pro-inflammatory cytokines are produced occurs via Toll-like receptors, pattern recognition molecules that recognize damaged molecules, particularly TLR2 and TLR4[9,10]. Our recent work shows that synthetic Aβ aggregates exist in a range of different sizes and structures with the longer protofibrils being the inflammatory species and signal via TLR4[11]. There is a crystal structure of TLR3, which is in the same family as TLR4, bound to an RNA dimer which is about 2 nm in diameter[12]. TLR3 signalling occurs when the RNA dimer is longer than 15 nm[13]. This suggests that long protofibrillar Aβ aggregates, which have a comparable diameter, initiate TLR4 signalling by forming a similar structure with a TLR4 dimers bound along the protofibril, providing a plausible explanation of both why they are the inflammatory species and how they initiate TLR4 signalling. However, to date, this experiment and many other experiments on aggregate induced inflammation have been performed at high aggregate concentrations in short time periods, typically 24 h. Therefore, there are important questions about the relevance of the results obtained at these high aggregate doses to AD. In particular, it is not clear how the response is altered at more relevant physiological concentrations of aggregates applied over longer times or if TLR4 signalling occurs at all. To address this issue, we first explored the response of BV2 microglial to extended doses of low concentrations of soluble aggregates, close to physiological levels, finding that this leads to sensitized response to these aggregates due to TLR4 signalling. We then explored if this aggregate-induced inflammatory response could lead to LTP deficit and neuronal cell death, cellular correlates of the symptoms associated with the development of AD, by performing experiments in the presence and absence of TLR4 antagonists.

Results

Pro-inflammatory response of macrophages to beta -amyloid. Experiments were firstly performed using synthetic oligomers of Aβ1-42, made by aggregating monomer and characterised by single molecule fluorescence, allowing us to estimate the soluble aggregate concentration[14,15], and hence be able to perform reproducible experiments. These soluble aggregates, oligomers, are predominantly trimers and tetramers although they range in size from dimer to 20mers[14] and are stable once formed allowing solutions of different initial aggregate concentrations to be made by serial dilution. This enables us to work at close to physiological concentrations of Aβ aggregates. Our initial experiments confirmed previous results that Aβ oligomers but not fibril or monomer lead to the production of TNF-α and IL-β in a BV2 microglial cell line and astrocytes in 24 h (Figs. 1 and 2). The synthetic Aβ monomer produced no TNF-α which confirmed that it contained no endotoxin contaminants. Using TLR4 and Myd88 knock-out cell lines we then showed that signalling was predominantly mediated by TLR4 and Myd88 (Fig. 1). We then performed experiments at lower aggregate concentrations for several days, close to the physiological concentration of 1–10 pM[16]. Control experiments showed that there was no significant change in the number of aggregates during the 24 hours' incubation with cells, before buffer exchange, for total monomer

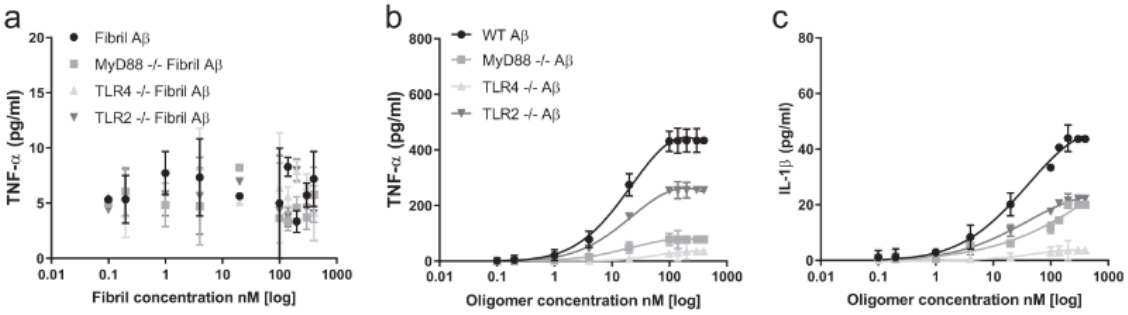

Fig. 1 Pro-inflammatory response of TLR4, MyD88 or TLR2 knockout macrophages to Abeta42(Aβ) oligomers and fibrils. Cells (WT: wild type, MyD88$^{-/-}$: MyD88 knockout, TLR4$^{-/-}$: TLR4 knock out and TLR2$^{-/-}$: TLR2 knockout) were stimulated with Aβ Fibrils (0.1–400 nM) and Aβ oligomers together with monomer (total monomer concentration 0.02–80 μM) for 24 h. The levels of the pro-inflammatory mediators TNF-α and IL-1β were measured. **a** TNF-α production remained unchanged at all concentrations with the addition of Fibrils ($n = 5$, ±sem). **b** TNF-α production significantly increases with increasing oligomer concentrations in all except the TLR4 knockout cells ($n = 5$, ±sem). **c** IL-1β levels production significantly increases with increasing oligomer concentrations in all except the TLR4 knockout cells ($n = 5$, mean ± sem).

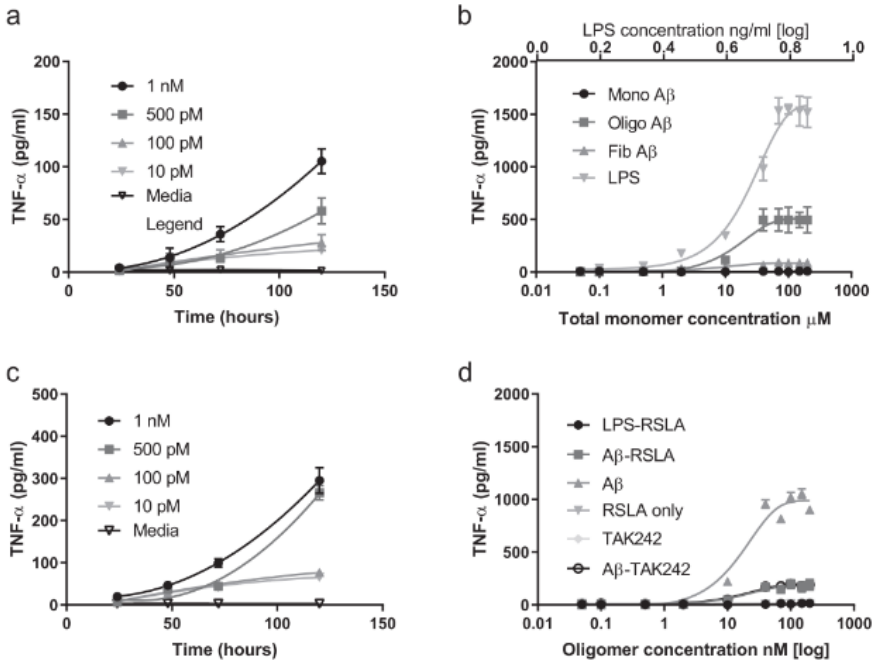

Fig. 2 Response of BV2 microglial cells and astrocytes to soluble Abeta42 (Aβ) aggregates (oligomers) and the blocking of the TNF-α production by TLR4 antagonists. a Time course of TNF-α production by BV2 cells in response to continual exposure to soluble Aβ oligomers (10 pM–1 nM) together with monomer (monomer concentration 0.002–0.2 μM) ($n = 4$, sem). **b** The response of astrocytes to Aβ monomers, Aβ oligomers together with monomer (oligomer concentration 0.25 to 1000 nM and total monomer concentration 0.05–200 μM) and Aβ fibrils (total monomer concentration) compared to LPS (0.05–200 ng/ml) stimulation for 24 h ($n = 4$, mean ± sem). The astrocyte preparation had <2% microglial. **c** Time course of TNF-α production by astrocyte cells in response to continual exposure to Aβ oligomers (10 pM–1 nM) together with monomer (total monomer concentration 0.002–0.2 μM) ($n = 4$, mean ± sem). **d** The response of astrocytes after a 24 h incubation with Aβ oligomers (0.05–200 nM oligomer) together with monomer (total monomer 0.01–40 μM)) only and together with the TLR4 antagonist RSLA (0.1 μg/ml), LPS and RSLA, RSLA only and the TLR4 antagonist TAK-242 (1 μM) alone and with Aβ oligomers and monomer ($n = 4$, mean ± sem).

concentrations below about 10 nM which is estimated to contain 350 pM soluble aggregates (Supplementary Fig. 1). Above 10 nM total monomer there is formation of additional aggregates, so the oligomer dose increases with time. There is also no significant cell death for total monomer concentrations below 40 nM (Supplementary Fig. 2). We found that both BV2 microglial cell line and astrocytes showed a sensitized response with time and this was significant at oligomer concentrations down to 10 pM (Fig. 2), but there was no measurable response in TLR4 and Myd88 knockout cell lines (Supplementary Fig. 3). The Aβ aggregate-induced TLR4 signalling can be effectively blocked by the TLR4 antagonists RSLA and TAK-242 (Fig. 2).

LTP deficit experiments. Next, we tested whether the Aβ-mediated LTP deficit involved TLR4 signalling. Using rat hippocampal slices Aβ aggregates were pre-incubated for a few hours before measurement of LTP. At 500 nM total Aβ monomer (~15 nM oligomers), 100 Hz electric stimulation-induced LTP in control slices (156.3 ± 5.3%, $n = 6$), this was inhibited in slices treated with Aβ oligomers (110.9 ± 3.1%, $n = 6$; Control vs. Aβ, $p = 0.0000228$). Treatment with RSLA prevented the Aβ-mediated inhibition of LTP (146.7 ± 3.2%, $n = 6$; RSLA with Aβ vs. Aβ, $p = 0.0000112$; control vs. RSLA with Aβ, $p = 0.155$; Fig. 3a). However, TAK-242 (100 ng–1 μg/ml) did not prevent Aβ-mediated inhibition of LTP (TAK-242 with Aβ (111.6 ± 8.2%, $n = 6$); TAK-242 with Aβ vs. Aβ, $p = 0.410$; Control vs. TAK-242 with Aβ, $p = 0.00414$; Fig. 3b). TAK-242 and RSLA had no effect on the magnitude of LTP induction compared with control (control: 155.9 ± 5.7%, $n = 7$; Tak-242: 153.2 ± 6.5%, $n = 6$; RSLA: 160.1 ± 8.1%, $n = 6$; Fig. 3c). RSLA directly blocks the TLR4-binding site[17] while TAK-242 binds an intracellular domain of TLR4[17,18] and hence may less effectively reach its binding site in the brain slice. An Elisa assay was performed which showed increased production of TNF-α in the hippocampus on addition of Aβ aggregates (Supplementary Fig. 4). These results together show that Aβ aggregate-induced LTP deficit can be reduced by blocking TLR4 signalling.

Neuronal cell death. The next set of experiments were designed to determine whether neuronal cell death was mediated by the direct action of aggregates acting on neurons and how much was mediated by cytokines produced by TLR4 signalling by a paracrine/autocrine mechanism. Rat neurons (E16–17), enriched astrocytes (purchased from Science Cell) and a co-culture of astrocytes and neurons (P2–P4) were exposed to 1 μM of aggregated Aβ containing ~15 nM oligomers in the absence or presence of specific inhibitors of TLR4 signalling, RSLA and TAK-242 (Fig. 4 and Supplementary Fig. 5). Addition of aggregated Aβ to enriched astrocyte cultures induced astrocytic cell death that was prevented by TLR4 antagonists. Addition of aggregated Aβ to enriched neuronal cultures induced neuronal cell death, and this was not significantly prevented by both TLR4 antagonists. Notably, addition of aggregated Aβ to neuron and astrocyte co-cultures induced significant cell death, which was prevented by TLR4 antagonists. Since it is not possible to perform reliable immunohistochemistry on dead cells we used a method developed previously, based on measurement of the nuclei size of live cells[19], to determine if there was a change in the proportion of surviving astrocytes and neurons in the co-culture, after treatment. The astrocytes and neurons have nuclei size in distinct size ranges with the neurons having smaller nuclei. Live cell imaging (Supplementary Fig. 6a, b) suggested that neurons were more

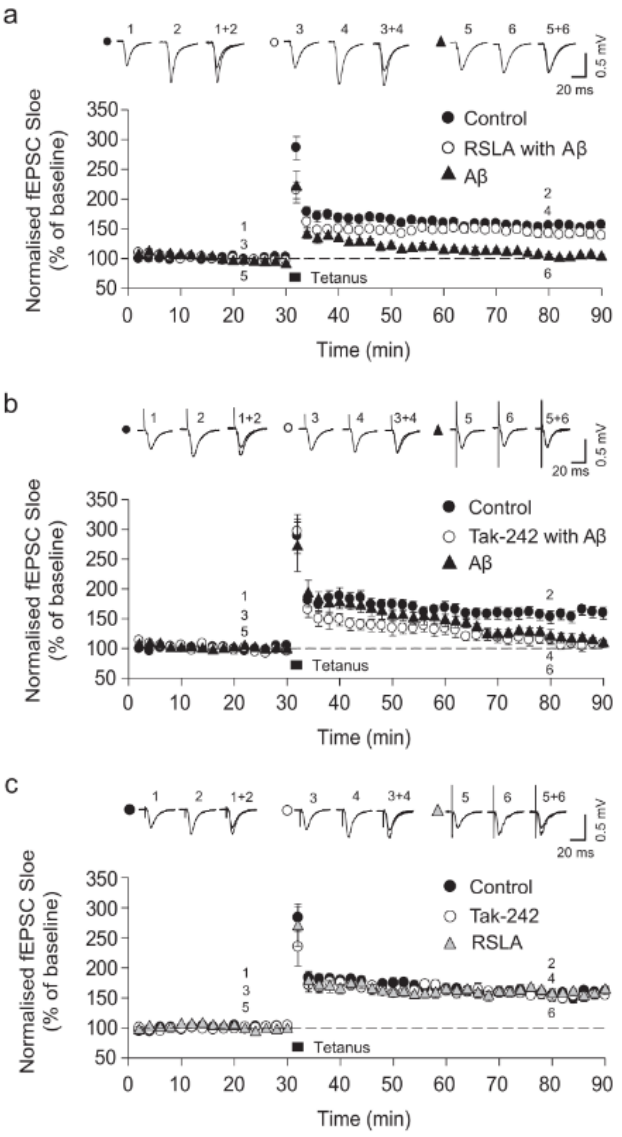

Fig. 3 Aβ42-mediated inhibition of LTP is rescued by RSLA but not TAK-242 treatment. Top: Example traces of fEPSPs from indicated time-points. Bottom: Mean fEPSP slope shown as percentage of the normalised baseline. **a** The inhibition of LTP by application of oligomerised Aβ42 (5 nM oligomers and 500 nM total monomer) was prevented by RSLA. **b** TAK-242 had no effect on Aβ-mediated inhibition of LTP. **c** TAK-242 and RSLA had no effect on the expression of LTP compared with control. All symbols represent the mean ± sem.

vulnerable in the co-culture, since we observed a significant increase in the average nuclei size of the surviving cells after treatment (attributable to a greater proportion of surviving astrocytes). We confirmed this result in an independent experiment where we performed immunocytochemistry on the co-culture, before and after addition of aggregated Aβ, and found that the proportion of surviving astrocytes increased and the proportion of neurons decreased (Supplementary Fig. 6c, d), consistent with predominantly neuronal cell death. Our data suggests that although both astrocytes and neurons exhibit reduced viability on exposure to aggregated Abeta, the glial cells are less vulnerable to cell death than the neurons. Overall our experiments show that the main cause of neuronal cell death in this acute dose experiment is caused by aggregate-initiated TLR4 signalling by glial cells, astrocytes and the small fraction of microglial present in the enriched astrocyte preparation. We cannot work out the relative contribution of astrocytes and microglia to this overall response, since although only 2% of the glial are microglia, they have higher expression of TLR4.

Discussion

Here we have shown using rat neuron and glial cells that Aβ aggregates cause LTP deficit and neuronal cell death predominantly by an autocrine/paracrine mechanism due to the production of pro-inflammatory cytokines, predominantly by TLR4 signalling by glial cells although we cannot rule out some contribution from neurons in the LTP deficit experiment. These experiments were performed with high doses of soluble aggregates but we also showed that physiological doses of aggregates over longer timespan also lead to the production of pro-inflammatory cytokines due to a sensitized response, as observed previously with alpha synuclein aggregates[19]. The concentration of TNF-α produced after several days approaches that observed in the CSF of individuals with AD, 400 pg/ml[20] and the concentration produced by larger doses of aggregates in the LTP-deficit experiments, 250 pg/ml.

There is a body of work that supports inflammation and aggregation occur concurrently in the development of the pathology of AD in both animal models and in humans, suggesting positive feedback between aggregation and inflammation[21]. Furthermore, acute doses of aggregates can lead to cognitive dysfunction[22] mediated by the TNF receptor[23] and involving activation of P38 MAP kinase[24]. However, the relevance of these observations to AD, which takes decades to develop, and the mechanism by which cognitive dysfunction occurs in AD has not been established. Our data suggests that sensitized aggregate-induced inflammation over time leads to LTP deficit and neuronal death, via TLR4 signalling, providing a molecular basis for the memory loss observed in the progression of AD, supported by the previous in vivo studies[22,23]. While our experiments suggest that the TLR4 signalling is predominantly from glial cells we cannot rule out a contribution from neurons and in addition TLR4 expression has been shown to increase as neurons age[25], suggesting that the neuronal contribution may increase with age in AD. Importantly our results point to an autocrine/paracrine mechanism due to secreted pro-inflammatory cytokines rather than direct binding of aggregates to receptors on neurons. In terms of the relevance of our finding to disease, we have recently found that the CSF from AD patients is significantly more inflammatory than control CSF when applied to BV2 cells over 5 days[26]. This shows that increased low levels of inflammatory aggregates occurs with the development of AD and in combination with the results in this paper that aggregate-induced inflammation could contribute significantly to the memory loss observed in these individuals. This inflammatory response is mediated by Aβ containing aggregates in the CSF, via TLR4 signalling, and correlates with the presence of protofibrils. Our recent work also shows that synthetic Aβ aggregates exist in a range of different size and structures with the longer protofibrils being the inflammatory species[11]. Selectively targeting these protofibrils rather than the fibrils, smaller aggregates or monomer is challenging, so that blocking sensitized TLR4 signalling seems an attractive alternative therapeutic strategy in AD. Memory loss is an early symptom of AD and continues throughout the disease, so this strategy could be used at all stages of disease and TLR4 antagonists could potentially be given intermittently, given the nature of the priming response observed in this work.

Methods

Protein preparation. The Aβ was purchased from American peptide (Aβ 1–42, 1.0 mg). 1 mg of amyloid pure peptide was dissolved in 100% 1, 1, 1, 3, 3, 3-Hexafluoro-2-propanol (HFIP) to a concentration of 2 mg/ml and incubated at

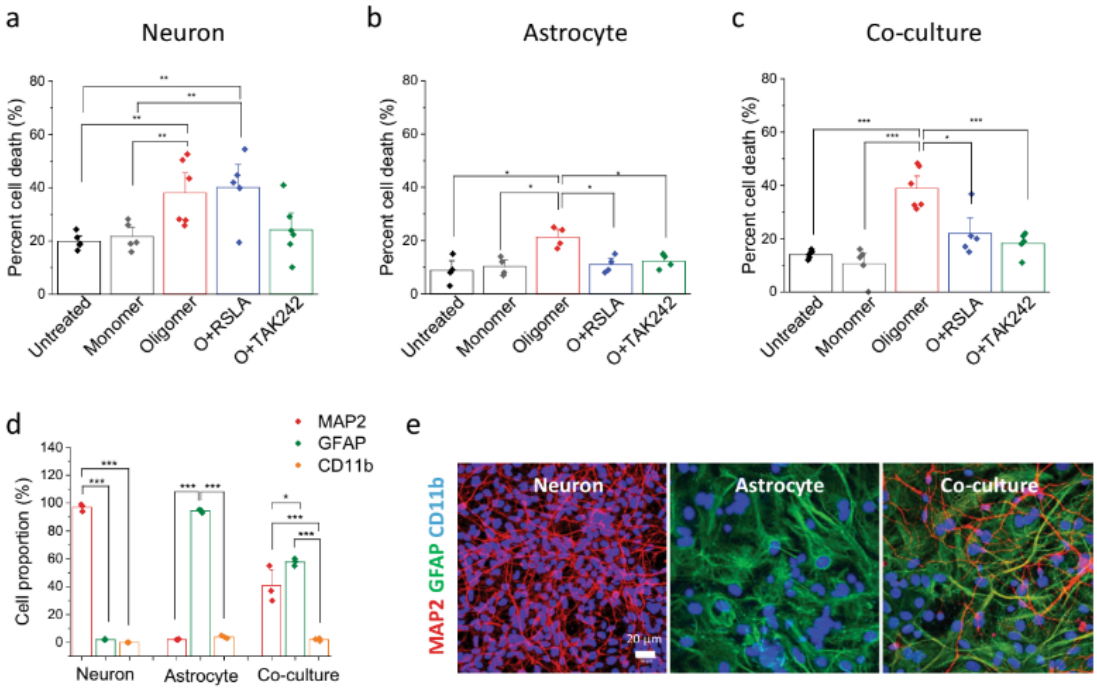

Fig. 4 Neuronal cell death caused by Aβ42 oligomers is mediated by initiating TLR4 signalling by glial cells. Cell death assay was performed using Sytox green on a live-cell imaging platform. **a** TLR4 inhibitors (0.1 µg/ml RSA, 1 µM TAK242) did not prevent Aβ42 oligomer-induced cell death in pure neuronal culture (5 nM oligomer and 1 µM total monomer). **b**, **c** Oligomer-induced astrocyte cell death was protected by TLR4 inhibitors. **d**, **e** Composition of the co-culture assessed using MAP2 (neuronal marker) and GFAP (astrocytic marker) immunocytochemistry together with representative images of a neuronal, astrocyte and co-culture. 97 ± 1.6% are MAP2-positive cells in neuronal prep, 92.2 ± 0.1% are GFAP-positive cells in astrocytic prep. 55.3 ± 7.1% MAP2 (+) and 44.1 ± 1.3% GFAP (+) are found in co-culture prep. The proportion of CD11b-positive cells is 3.8 ± 0.4% and 1.3 ± 0.5% in the astrocytic and co-culture preparations, respectively. ($n = 5$–6 from two independent experiments, mean ± sem).

room temperature until a clear solution was formed. The solution was then dried under a nitrogen stream before dissolved once more in HFIP and sonicated. 100 µl of solution was then aliquoted into an eppendorf and stored at −80 °C. When required the solution was thawed and left open in a fume hood overnight to evaporate the HFIP, leaving a peptide pellet. The peptide was dissolved in 10 µl of 100%DMSO and then transferred to a new eppendorf with DMEM.

Protein aggregation. Aβ oligomers were prepared by first diluting in DMEM buffer (DMEM + 1% FCS + 2 mM L-glutamine). The aggregation mixture was incubated for 6 h at 37 °C with constant shaking of 200 r.p.m (New Brunswick Scientific Innova 43, 25 mm orbital diameter) and centrifuged for 10 min at 14,200 r.p.m. to remove any fibrillar pellets. Aβ fibrils were formed by aggregation for 60 h. Aggregated Aβ was then stored at 4 °C until incubated with cells. Using ThT assays protein oligomers and fibrils were found to remain stable for 1 week after removal from the shaking incubator however aggregates were always used within 24 h.

ThT assay. The time course of the aggregation was monitored using thioflavin-T (ThT) assays. ThT (Sigma-Aldrich) stocks were prepared in DMSO (Sigma-Aldrich) and diluted into pre-filtered PBS (0.02 µm filter, Whatman) to a final concentration of ~100 µM. Aβ was added to 1 ml of ThT solutions and binding monitored by exciting the sample at 440 nm and recording the emission fluorescence spectrum from 460 to 560 nm (slit width 5 nm). Measurements were carried out on a Cary Eclipse spectrofluorometer with a Peltier-controlled holder (Varian, Mulgrave, Australia).

ThT imaging. ThT imaging utilised a method previously described[27]. Briefly glass cover-slides (VWR international, 20 × 20 mm) were cleaned using an argon plasma cleaner (PDC-002, Harrick Plasma) for at least 1 h to remove any residual that fluoresce. 50 µL of poly-L-lysine (70,000–150,000 molecular weight, Sigma-Aldrich) was added to the cover slides and incubated for 1 h before being gently washed with filtered PBS. Imaging was performed on a custom-built total internal reflection fluorescence microscope.

Cell culture. The BV2 cell lines were derived from immortalized murine neonatal microglia. They were grown in Dulbecco's modified Eagle's (DMEM) supplemented with 10% foetal bovine serum and 1% L-glutamine (Life Technologies) and incubated at 37 °C in a humidified atmosphere of 5% CO_2 and 95% air, until ~1.6×10^6 cell/ml. Immortalized MyD88$^{-/-}$, TLR2$^{-/-}$ and TLR4$^{-/-}$ murine cells had previously been generated[19] and grown from frozen stock samples under same conditions as BV2. Astrocyte cells were from a rat mixed glial preparation, cultured for 14 days with DMEM medium supplemented with 10% foetal bovine serum and 1% L-glutamine in a humidified atmosphere containing 5% CO_2 at 37 °C. This protocol minimizes the microglial contamination to <2%[28]. Astrocytes were cultured to 70% confluence. For long duration experiments the media was exchanged every 24 h.

ELISA assays. To determine cumulative TNF-α and Il-1β production, supernatants were obtained after incubation with the Aβ over viable time frames and stored at −80 °C until analysed. TNF-α, and Il-1β were analysed using the Duoset® enzyme-linked immunosorbent assay (ELISA) development system (R&D Systems, Abingdon, Oxfordshire, UK).

Animals. Electrophysiology experiments were conducted in accordance with the UK Animals Scientific Procedures Act, 1986. Male Wistar rats (Charles River, UK) were used to prepare acute hippocampal slices (4- to 5-week-old rats).

Electrophysiology. Brains were quickly removed into ice-cold artificial cerebrospinal fluid (ACSF; 124 mM NaCl, 3 mM KCl, 26 mM $NaHCO_3$, 1.25 mM NaH_2PO_4, 2 mM $CaCl_2$, 1 mM $MgSO_4$, 10 mM D-glucose, carbogenated with 95% O_2/5% CO_2). Transverse hippocampal slices (400 µm) were cut using a McIlwain tissue chopper (Mickle Laboratory Engineering) and allowed to recover in a submersion-type bath filled with ACSF for at least 60 min. Before recording, hippocampal slices were incubated in ACSF with pharmacological compounds at room temperature. Evoked field excitatory postsynaptic potentials (fEPSPs) were recorded in the CA1 region using glass electrodes containing NaCl (3 M). Twisted-tungsten wire stimulating electrodes were positioned in the CA2 region (Schaffer collateral pathway) and subiculum, and electric stimuli were delivered alternatively to the two electrodes (0.066 Hz). After 30 min of stable baseline, high-frequency tetanic stimulation (2 × 100 pulses; 100 Hz, 30 s interval) was used as the LTP induction protocol. Long-term synaptic plasticity was gauged as the change of fEPSP slope relative to the preconditioning baseline. Both control and experimental recordings were collected using slices prepared from the same animal. Data were captured and analysed using LTP114j software. Data are expressed relative to a normalized baseline. For analyses, the baseline was defined as five time-points before tetanic stimulation and the post-conditioning time was set at 75–80 min

following recording commencement. The difference between baseline and post-conditioning time-points was expressed as a percentage of baseline ± standard error of the mean (SEM), and was used to make comparisons between treatment groups. Statistical significance of observed effects between groups was analysed using unpaired *t*-tests.

Aβ preparation for LTP experiments. The Aβ (1–42) peptide (Stratech, A-1163, 0.5 mg) was initially dissolved at a concentration of 1 mg/ml in 100% (HFIP [Sigma-Aldrich]). This solution was incubated at room temperature for 1 h with vortexing every 10 min. Next, the solution was sonicated for 10 min in a water bath sonicator and then dried under a light stream of nitrogen gas. DMSO was added to the peptide, which was incubated at room temperature for 10 min with gentle mixing. Finally, this solution was aliquoted and stored at −80 °C. For a working solution, D-PBS (Invitrogen, UK) was added to the peptide stock solution and incubated for 2 h at room temperature for peptide oligomerisation. 500 nM oligomerised amyloid-beta was applied to hippocampal slices in ACSF for 2 h. Previous experiments show this protocol results in a solution containing 1–5 nM oligomers smaller than 10-mers[15].

Rodent neuron and astrocyte culture. Cultures of cortical neurons and the co-culture of neuron and astrocyte were prepared as described previously[19]. Briefly, cortices of brain from either embryos (E16–17) or postnatal pups (day 2–4) of Sprague-Dawley (UCL breeding colony) were collected for neuron and co-culture preparations, respectively. The tissue was digested with EDTA–trypsin for 15 min and washed before collecting pellets in complete neurobasal medium (Neurobasal media supplemented with B27, 2 mM Glutamax and 50 I.U./ml Penicillin/50 µg/ml Streptomycin). Approximately 50,000 cells for 96-well plates (Falcon/Corning Cat. no.: 353219) and 100,000 cells for u-slide eight-well slide ibidi chamber (Thistle Scientific Ltd, Cat. no.: IB-80826) were plated. Cells were used at 12–14 days in vitro. Cortical astrocytes were purchased from Caltag Med Systems (Science Cell, Cat. no.: R1800) which was derived from postnatal day 2 rat cortex. 7–10 times sub-culture of cortical astrocytes were carried out until use. Cells were cultured in rodent astrocyte medium (Caltag Medsystem, Cat. no.: 1831). All cells were maintained in incubator at 37 °C (5% CO_2).

Cell death assay. Cells were pre-treated with either 0.1 µg RSLA or 1 µM TAK-242 30 min prior to oligomer treatment. Cells were incubated with soluble aggregates overnight and cell death was detected using Sytox green (Molecular Probes). Cells were loaded with 0.5 µM Sytox green in HEPES balanced HBSS (pH adjusted at 7.4 with NaOH) for 15 min. High-throughput images were acquired using an Opera Phenix High-Content Screening System (PerkinElmer). Sytox green staining was imaged by 488 and 405 nm laser for Hoechst-stained nuclei (17–22 fields of images were taken per wells). The percentage cell death was quantified by the ratio between the number of Sytox green-positive cells and the total number of Hoechst-expressing cells per image. The number of fluorescent cells was determined using the multi-wavelength cell scoring module of Columbus Studio™ Cell Analysis Software and each experiment utilised the same threshold settings (e.g. intensity and size). Nuclei size of live cells (Sytox negative) was automatically acquired using the same analysis software first in the neuron only culture, and the enriched astrocyte culture. These size ranges were then used to determine the culture composition of the co-culture before and after treatment with Abeta aggregates.

Immunohistochemistry. Cells were fixed in 4% paraformaldehyde and permeabilized with 0.2 Triton-X 100. Non-specific binding was blocked using 5% BSA. Cells were incubated with primary antibodies for 1 h (MAP2; ab11267, GFAP; ab4674, CD11b; ab133357) at room temperature and washed three times. Secondary antibodies (donkey anti rabbit 488; ab150073, donkey anti-mouse; ab150110, goat anti-chicken 647; ab150171) were incubated for 1 h at room temperature. Cells were washed three times and Hoechst was added in the second wash. Cells were imaged with ProLong Diamond Antifade Mountant (Thermo Fisher Scientific).

Statistics and reproducibility. For live cell imaging, there were total two independent experiment which include different animals, different cell batch purchased separately and cell preparation. Each set of independent experiments consists of three wells per condition and the figures represent data polled from two independent experiments. One-way ANOVA with Bonferroni or Tukey correction was used to test statistical significance. One-way ANOVA with post hoc test was used to test statistical significance in the production of TNF-α in the slice experiments.

Reporting summary. Further information on research design is available in the Nature Research Reporting Summary linked to this article.

Data availability

Source data underlying Figs. 1 and 2 are in the Supplementary Data 1 file, Fig. 4a–c in Supplementary Data 2 file and Supplementary Fig. 4d in Supplementary Data File 3. All other data are available upon request from the corresponding author.

Received: 12 June 2019; Accepted: 24 January 2020;
Published online: 18 February 2020

References

1. Shankar, G. M. et al. Amyloid-β protein dimers isolated directly from Alzheimer's brains impair synaptic plasticity and memory. *Nat. Med.* **14**, 837 (2008).
2. Hong, W. et al. Diffusible, highly bioactive oligomers represent a critical minority of soluble Aβ in Alzheimer's disease brain. *Acta Neuropathol.* **136**, 19–40 (2018).
3. Jo, J. et al. Aβ1–42 inhibition of LTP is mediated by a signaling pathway involving caspase-3, Akt1 and GSK-3β. *Nat. Neurosci.* **14**, 545 (2011).
4. Li, S. et al. Decoding the synaptic dysfunction of bioactive human AD brain soluble Aβ to inspire novel therapeutic avenues for Alzheimer's disease. *Acta Neuropathol. Commun.* **6**, 121 (2018).
5. Laurén, J., Gimbel, D. A., Nygaard, H. B., Gilbert, J. W. & Strittmatter, S. M. Cellular prion protein mediates impairment of synaptic plasticity by amyloid-β oligomers. *Nature* **457**, 1128 (2009).
6. Jin, J.-J., Kim, H.-D., Maxwell, J. A., Li, L. & Fukuchi, K.-I. Toll-like receptor 4-dependent upregulation of cytokines in a transgenic mouse model of Alzheimer's disease. *J. Neuroinflamm.* **5**, 23–23 (2008).
7. Maezawa, I., Zimin, P. I., Wulff, H. & Jin, L.-W. Amyloid-beta protein oligomer at low nanomolar concentrations activates microglia and induces microglial neurotoxicity. *J. Biol. Chem.* **286**, 3693–3706 (2011).
8. Garwood, C. J., Pooler, A. M., Atherton, J., Hanger, D. P. & Noble, W. Astrocytes are important mediators of Aβ-induced neurotoxicity and tau phosphorylation in primary culture. *Cell Death Dis.* **2**, e167–e167 (2011).
9. Reed-Geaghan, E. G., Savage, J. C., Hise, A. G. & Landreth, G. E. CD14 and toll-like receptors 2 and 4 are required for fibrillar A{beta}-stimulated microglial activation. *J. Neurosci.* **29**, 11982–92 (2009).
10. Udan, M. L., Ajit, D., Crouse, N. R. & Nichols, M. R. Toll-like receptors 2 and 4 mediate Abeta(1–42) activation of the innate immune response in a human monocytic cell line. *J. Neurochem.* **104**, 524–33 (2008).
11. De, S. et al. Different soluble aggregates of Aβ42 can give rise to cellular toxicity through different mechanisms. *Nat. Commun.* **10**, 1541 (2019).
12. Liu, L. et al. Structural basis of toll-like receptor 3 signaling with double-stranded RNA. *Science* **320**, 379–381 (2008).
13. Leonard, J. N. et al. The TLR3 signaling complex forms by cooperative receptor dimerization. *Proc. Natl Acad. Sci. USA* **105**, 258–263 (2008).
14. Drews, A. et al. Individual aggregates of amyloid beta induce temporary calcium influx through the cell membrane of neuronal cells. *Sci. Rep.* **6** (2016).
15. Whitcomb, D. J. et al. Intracellular oligomeric amyloid-beta rapidly regulates GluA1 subunit of AMPA receptor in the hippocampus. *Sci. Rep.* **5**, 10934 (2015).
16. Mehta, P. D. et al. Plasma and cerebrospinal fluid levels of amyloid beta proteins 1–40 and 1–42 in Alzheimer disease. *Arch. Neurol.* **57**, 100–5 (2000).
17. Irvine, K. L. et al. Identification of key residues that confer *Rhodobacter sphaeroides* LPS activity at horse TLR4/MD-2. *PLoS ONE* **9**, e98776 (2014).
18. Matsunaga, N., Tsuchimori, N., Matsumoto, T. & Ii, M. TAK-242 (resatorvid), a small-molecule inhibitor of Toll-like receptor (TLR) 4 signaling, binds selectively to TLR4 and interferes with interactions between TLR4 and its adaptor molecules. *Mol. Pharm.* **79**, 34–41 (2011).
19. Hughes, C. D. et al. Picomolar concentrations of oligomeric alpha-synuclein sensitizes TLR4 to play an initiating role in Parkinson's disease pathogenesis. *Acta Neuropathol.* **137**, 103–120 (2019).
20. Tarkowski, E., Andreasen, N., Tarkowski, A. & Blennow, K. Intrathecal inflammation precedes development of Alzheimer's disease. *J. Neurol. Neurosurg. Psychiatry* **74**, 1200–1205 (2003).
21. Janelsins, M. C. et al. Early correlation of microglial activation with enhanced tumor necrosis factor-alpha and monocyte chemoattractant protein-1 expression specifically within the entorhinal cortex of triple transgenic Alzheimer's disease mice. *J. Neuroinflamm.* **2**, 23–23 (2005).
22. Balducci, C. et al. Toll-like receptor 4-dependent glial cell activation mediates the impairment in memory establishment induced by beta-amyloid oligomers in an acute mouse model of Alzheimer's disease. *Brain Behav. Immun.* **60**, 188–197 (2017).
23. Lourenco, M. V. et al. TNF-alpha mediates PKR-dependent memory impairment and brain IRS-1 inhibition induced by Alzheimer's beta-amyloid oligomers in mice and monkeys. *Cell Metab.* **18**, 831–43 (2013).
24. Wang, Q., Wu, J., Rowan, M. J. & Anwyl, R. Beta-amyloid inhibition of long-term potentiation is mediated via tumor necrosis factor. *Eur. J. Neurosci.* **22**, 2827–32 (2005).
25. Calvo-Rodríguez, M. et al. Aging and amyloid β oligomers enhance TLR4 expression, LPS-induced Ca2+ responses, and neuron cell death in cultured rat hippocampal neurons. *J. Neuroinflamm.* **14**, 24 (2017).

26. De, S. et al. Soluble aggregates present in cerebrospinal fluid change in size and mechanism of toxicity during Alzheimer's disease progression. *Acta Neuropathol. Commun.* **7**, 120 (2019).
27. Horrocks, M. H. et al. Single-molecule imaging of individual amyloid protein aggregates in human biofluids. *ACS Chem. Neurosci.* **7**, 399–406 (2016).
28. Saura, J. Microglial cells in astroglial cultures: a cautionary note. *J. Neuroinflamm.* **4**, 26 (2007).

Acknowledgements

This work was supported by ARUK. A.D. was financed by a Herchel Smith Postdoctoral Fellowship. D.K. acknowledges funding from the Royal Society, an ERC Advanced Grant (669237) and the UK Dementia Research Institute. S.G. acknowledges funding by a Wellcome fellowship (100172/Z/12A), and the National Institute for Health Research University College London Hospitals Biomedical Research Centre. K.C. acknowledges funding by the UK Dementia Research Institute. C.B. acknowledges funding from a Wellcome Investigator award (108045/Z/15/Z).

Author contributions

All authors of this paper have read and approved the final version of the submitted manuscript. D.K., K.C., P.S.G.-H., C.B. and S.G. developed the original hypothesis and designed the experiments. A.D. prepared the astrocytes. C.H. performed all the astrocyte, BV2 and macrophage experiments and analysed the data. J.-H.Y. and S.-C.K. performed and analysed all the LTP experiments. M.L.C. performed and analysed all the neuronal cell death experiments. All authors wrote the paper.

Competing interests

The authors declare no competing interests.

Additional information

Supplementary information is available for this paper at https://doi.org/10.1038/s42003-020-0792-9.

Correspondence and requests for materials should be addressed to D.K.

Reprints and permission information is available at http://www.nature.com/reprints

Publisher's note Springer Nature remains neutral with regard to jurisdictional claims in published maps and institutional affiliations.